DTIC
S ELECTE D
JAN 0 3 1992
D

CRACK GROWTH RATE MODELING
OF A TITANIUM-ALUMINIDE ALLOY
UNDER THERMAL-MECHANICAL CYCLING

DISSERTATION

John J. Pernot, Captain, USAF

AFIT/DS/AA/91-3

Approved for public release; distribution unlimited

92 1

CRACK GROWTH RATE MODELING

OF A TITANIUM-ALUMINIDE ALLOY

UNDER THERMAL-MECHANICAL CYCLING

DISSERTATION

Presented to the Faculty of the School of Engineering

of the Air Force Institute of Technology

Air University

In Partial Fulfillment of the

Requirements for the Degree of

Doctor of Philosophy

John J. Pernot, B.S., M.S.
Captain, USAF

December 1991

CRACK GROWTH RATE MODELING
OF A TITANIUM-ALUMINIDE ALLOY
UNDER THERMAL-MECHANICAL CYCLING

John J. Pernot, B.S., M.S.
Captain, USAF

Approved:

(signature)	Dec 2, 91
(signature)	2 Dec 1991
Alan V. Lair	2 Dec 1991
(signature)	3 Dec 91

Accepted:

(signature) 3 Dec. 1991

Institute Senior Dean

Acknowledgments

Table of Contents

iii

v

List of Figures

List of Figures (continued)

List of Tables

Abstract

⌐ In this study, a model is developed to predict crack growth rates in a titanium-aluminide alloy under thermal-mechanical fatigue (TMF). This TMF crack growth rate prediction model, which requires only isothermal data to define its parameters, is distinguished from earlier models in two ways. First, it accounts for mechanical-fatigue and environmental crack growth rate contributions while it also considers a retardation mechanism thought to be caused by creep blunting of the crack tip. This is the first study to account for such a retardation mechanism during TMF. The second uniqueness of the model is that its general form can account for cycle-dependent crack growth rate contributions that are temperature dependent.

In addition, a series of isothermal-fatigue and hold-time tests are performed to generate the data base required for model parameters, and TMF tests are used to validate the modeling technique. The model predicts in-phase, as well as 180° and 270° out-of-phase crack growth rates extremely well, and underpredicts the 90° out-of-phase crack growth rates by a factor of two. Two other, more complex TMF cycles are studied, and the predicted crack growth rates correlate well with the experimental data.

CRACK GROWTH RATE MODELING OF A TITANIUM-ALUMINIDE ALLOY UNDER THERMAL-MECHANICAL CYCLING

I. Introduction

The aircraft industry continually strives to improve the thrust and fuel efficiency of gas turbine engines for future aircraft. These improvements require lightweight engine components that must sustain higher temperatures and rotational speeds [1, 2]. In answer to these needs, new engine materials are being developed to sustain higher thermal and mechanical loading. Along with increasing the gas turbine engine's overall performance, designers also are placing more emphasis on improving the durability of such engine components, since these new materials are very expensive. Understanding a material's behavior under thermal and mechanical loading will enable the components to be kept in service for as long as they retain useful life. The objective of this dissertation is to model such behavior for a intermetallic compound that is being considered for future engine component applications.

During regular missions, components of gas turbine engines are subjected to complex thermal and mechanical cycling. The resulting thermal and mechanical stresses (or strains) can lead to fatigue damage and finally

1

failure of the component [3]. This form of fatigue is commonly referred to as thermal-mechanical fatigue (TMF).

Until the mid-1970s useful life estimates of gas turbine engine components were very conservative. For example, the total fatigue life of turbine disks was statistically determined, and only one out of every 1,000 discarded disks had a critical-sized crack, while the other 999 had remaining useful life. Therefore, a philosophy called Retirement for Cause was proposed so that only components with critical-sized cracks would be discarded. Using this philosophy, engine components would be inspected and those with remaining useful life would be placed back into service [4]. A successful Retirement for Cause program requires fracture mechanics to estimate the rate of crack growth; in turn, these crack growth rates determine an interval of component inspection. Principles of fracture mechanics used to understand crack growth behavior also are required during engine design to meet damage tolerance requirements, such as those imposed by the Air Force's Engine Structural Integrity Program [5]. This program requires the testing of components to establish crack growth rates. Understanding this behavior not only ensures that initial detectable flaws will not grow to a critical size over the expected life of the engine, but also helps in determining inspection intervals for all engine components [6].

The understanding of high-temperature fracture mechanics is not limited to gas turbine component design. It also is considered in the design of

airframes for hypersonic vehicles, since these vehicles encounter thermal as well as mechanical loading. Previously, designs were based only on strength, endurance, and creep [7], but future designs must include more complete crack growth studies in order to get the most use out of high-cost materials, while producing safe vehicles.

To determine the service life and inspection intervals for the previously mentioned aircraft components, crack growth rate models are needed to predict the behavior of cracks under combined thermal and mechanical loading. Until recently [8], models could predict crack growth rates only for isothermal fatigue, [9, 10] and isothermal fatigue with superimposed load hold times [11, 12]. Since TMF crack growth rate models do not exist for the majority of materials, TMF crack growth rates are assumed to be the same as those obtained under isothermal conditions. Most often, these estimates are based on isothermal crack growth rates acquired at the maximum temperature of the thermal cycle, but this is not always a conservative estimate [8]. Nicholas et al. [8] recently reviewed the most current efforts in TMF crack growth rate modeling. These efforts involving TMF crack growth rate behavior emphasize the need for models to predict crack growth rates solely from isothermal data [8,13]. This is attributed to the low cost of isothermal crack growth experiments and the large isothermal crack growth rate data base that currently exists.

3

Isothermal-data-based models have been used to predict crack growth rates for the nickel-base superalloys under isothermal fatigue with load hold times [11, 12] as well as TMF [14, 15]. These superalloys represent the current high-temperature class of materials. The crack growth rate models that have been developed successfully for these alloys, estimate the total crack growth rate as the linear combination of cycle-dependent and time-dependent growth rates. The cycle-dependent contribution is caused by mechanical fatigue, which is dominant at low temperatures and (or) high loading frequencies. The time-dependent contribution results from the environmental attack that accelerates crack growth when a material is subjected to elevated temperatures.

The work presented in this dissertation involves the TMF crack growth modeling of an intermetallic compound of titanium and aluminum alloyed with niobium. Such compounds combine attractive properties such as low density and high specific strength with that of high temperature capability, and such characteristics allow these compounds to be considered for engine and airframe components for future applications [16, 17]. Titanium aluminides have adequate creep strength and are oxidation resistant to much higher temperatures than conventional titanium alloys [18, 19]. The alpha-2 based titanium aluminide alloyed with niobium, Ti-24Al-11Nb, is selected for this study. The alpha-2 titanium aluminide is selected because it is more ductile, stronger, and more dense than the other titanium aluminides, and shows potential for elevated-temperature applications [20].

A study by Mall et al. [21] has shown that the linear summation model, discussed earlier, did not adequately estimate crack growth rates in Ti-24Al-11Nb under fatigue loading with superimposed hold times at 750°C. They found that the hold at maximum load retarded the cycle-dependent contribution of crack growth, and that the fatigue cycle accelerated the time-dependent contribution of growth. Because of these characteristics of Ti-24Al-11Nb, the linear model could not account for the hold-time behavior. The reason for this behavior is thought to be attributed to blunting of a crack caused by creep, which was not previously observed in the nickel-base alloys [8, 11, 14].

The fatigue crack growth behavior of Ti-24Al-11Nb during combined thermal and mechanical cycling appears, in a general sense, to follow the same trends observed in tests on the nickel-base superalloys. However, the crack growth in this alloy seems to be influenced by more than the two components of the linear summation model. In addition to the cycle-dependent and time-dependent contributions typically seen in nickel-base alloys when exposed to elevated temperatures, crack growth in Ti-24Al-11Nb appears to be influenced by a retardation mechanism. This retardation possibly can be attributed to blunting of the crack tip caused by creep. As previously mentioned, this also had been observed in Ti-24Al-11Nb by Mall et al. [21] during hold-time tests at 750°C. This complex crack growth phenomenon in this alloy is unlike that in nickel-base superalloys where the total crack growth rate could be expressed

5

as a linear combination of growth rates. Thus, the linear summation modeling technique is not applicable to Ti-24Al-11Nb under TMF conditions. This linear model had not taken into account the contribution of creep blunting or any other mechanisms of crack retardation.

Obviously, a model to predict the crack growth rate under combined thermal and mechanical loading that will account for these additional crack growth mechanisms is needed. The objective of this study is to incorporate such mechanisms into a model that estimates TMF crack growth rates solely from isothermal data. Then this model is used successfully to predict crack growth rates for thermal and mechanical cycles of varying complexity in the titanium-aluminide alloy, Ti-24Al-11Nb.

This dissertation contains a review of previous TMF testing and modeling efforts, a complete description of the test equipment and techniques used in this study, a discussion of the results of the experiments completed during this effort, a description of the TMF crack growth rate model developed during this effort, comparisons of the predictions of growth rates using this model with those obtained from experiments, and the conclusions and recommendations that are drawn from this work.

II. Background

There are four main topics of this chapter. First, the terminology used in this dissertation is defined. Included are definitions of terms relating to isothermal and thermal-mechanical fatigue (TMF) testing, the correlation and comparison of test results, elevated temperature crack growth mechanisms, cycle-dependent and time-dependent crack growth, and the different methods of controlling experiments and correlating data. Second, previous TMF studies are reviewed, including the correlation of test data and the comparisons of test results. Third, the previous efforts of modeling crack growth rates for elevated temperature fatigue and TMF crack growth are discussed in a general way. (The most significant of these models, which relates to the current modeling effort, is discussed in Chapter V during the development of the TMF crack growth rate model for Ti-24Al-11Nb.) Fourth, a background on titanium aluminides is presented.

Terminology

Isothermal and Thermal-Mechanical Fatigue Cycles

Cracks can occur in a component when subjected to alternating (or cyclic) loads well below the component's critical design load; this is known as fatigue, or sometimes referred to more specifically as mechanical fatigue. Deterioration and cracking of a material by alternate heating and cooling

7

(thermal cycling) is referred to as thermal fatigue [22]. If cracks are forming in a material as a result of the simultaneous cycling of temperature and mechanical loads (or displacements), the material is experiencing thermal-mechanical fatigue (TMF). The propagation of cracks under thermal-mechanical cycling is referred to as TMF crack growth, and the rate at which such cracks propagate is referred to as the TMF crack growth rate.

Aircraft engine components, particularly those of fighter aircraft, experience complex thermal and mechanical cycles during typical missions. A schematic of these is shown in Figure 2.1. In order to model such conditions, some simplified test cycles must be examined, and this section includes an explanation of these. In the following explanations, only load and temperature cycles are discussed, but displacement can be substituted for load in the following definitions.

The most basic type of fatigue test is isothermal. An isothermal fatigue test is simply a test in which the specimen is mechanically cycled while under constant temperature. Isothermal tests are used to determine the fatigue crack growth rates as a function of temperature. Most often, these tests are performed at room temperature, at the minimum temperature of the thermal cycle, and at the maximum temperature of the thermal cycle. A load hold-time (or load-dwell) test is an isothermal test in which a load is held for a specific time during an otherwise pure fatigue cycle. The hold most often occurs at maximum load, but also can be at any other load. These tests are
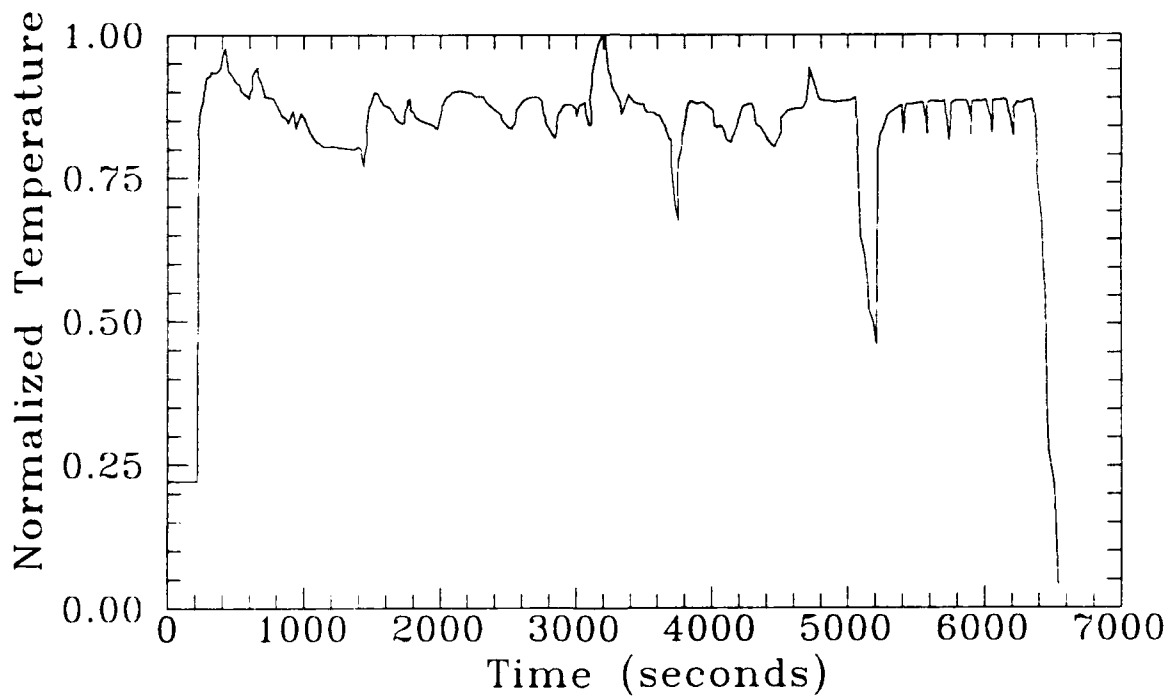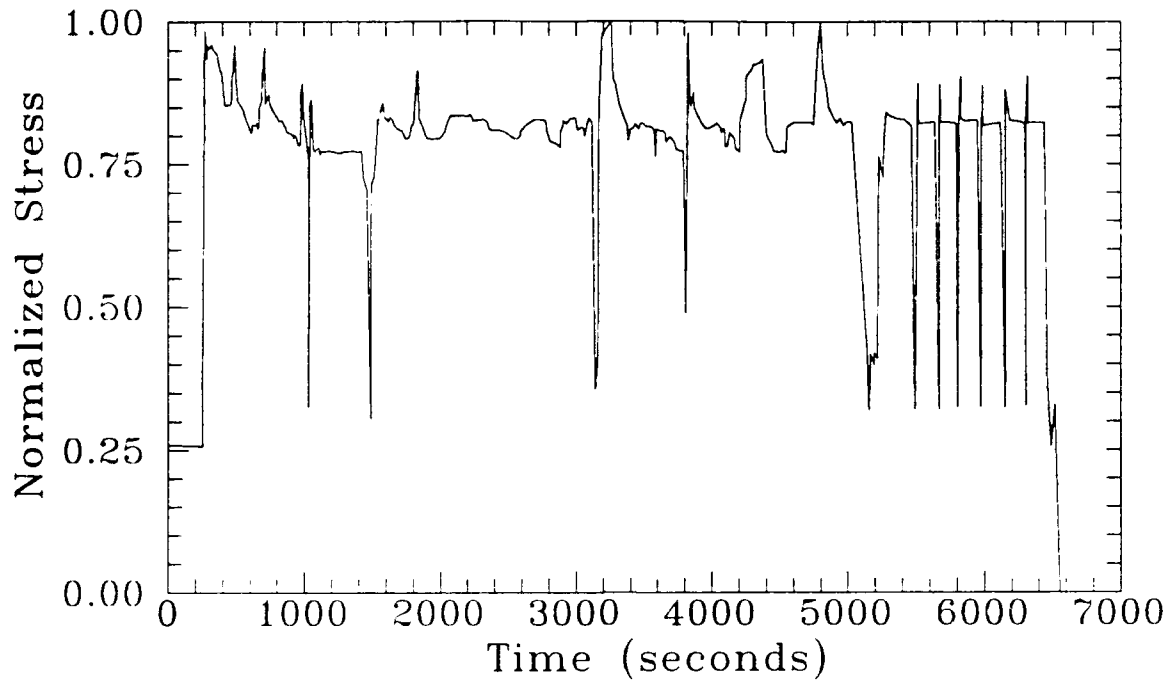
Figure 2.1 Schematic of Complex Thermal and Mechanical Cycles

9

used to understand the complex interaction of pure-fatigue and sustained-load conditions that contribute to crack growth.

The two most basic types of TMF tests are in phase and out of phase. Both temperature and load reach simultaneous maximum and minimum values during in-phase tests. For out-of-phase tests, the load (P) leads or lags the temperature (T) by some phase angle. In this study, the convention used to define the phase angle (ϕ) is P leads T. These TMF conditions are shown in Figure 2.2. In general, the cycles can be triangular (ramp), square, or sinusoidal, but triangular wave forms are used exclusively in the testing of Ti-24Al-11Nb in this study. The minimum and maximum temperature of a thermal cycle are called T_{min} and T_{max}, and the minimum and maximum loads of a mechanical load cycle are called P_{min} and P_{max}. The load ratio, R, is defined as:

$$R = \frac{P_{min}}{P_{max}} \qquad (2.1)$$

Most often, the crack growth rate data presented in the literature include the isothermal fatigue crack growth rates for T_{max} and T_{min}, the in-phase TMF crack growth rates, and the 180° out-of-phase TMF crack growth rates. Since the 180° out-of-phase test is the only type of out-of-phase test considered in this chapter, "out-of-phase" is used to denote the 180° out-of-phase test condition.

10

In–Phase TMF

Out–of–Phase TMF
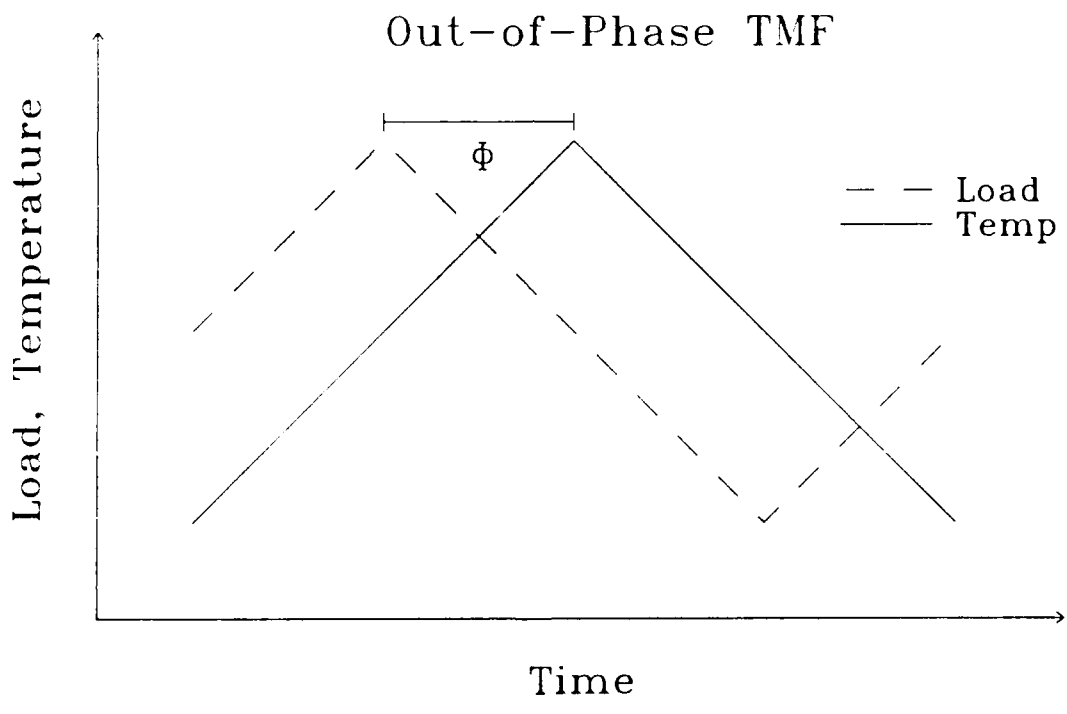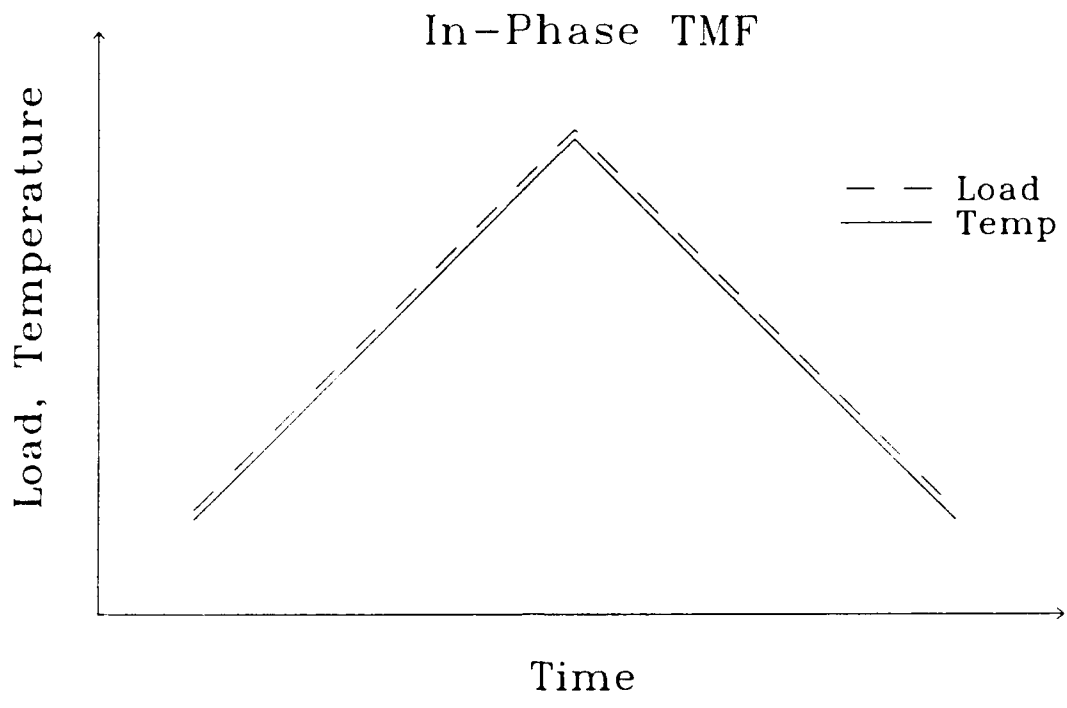
Figure 2.2 Simplified Thermal and Mechanical Cycles

11

Control of Experiments and Correlation of Data

TMF testing is performed with either displacement (strain) or load (stress) control. For a strain-controlled test, the strain of the specimen (or the displacement between two points) is monitored and used for feedback to control the loading. The results of these tests usually are correlated with the strain intensity range, ΔK_ϵ. ΔK_ϵ is expressed in functional form as:

$$\Delta K_\epsilon = f(\Delta \epsilon, a) \qquad (2.2)$$

where $\Delta \epsilon$ is the strain range, and a is the crack length. It is important to note that the stress in the material is not controlled, and the stress is dictated by the material's parameters [8].

A load-controlled test uses force (load) as feedback to the controller. The stress intensity factor, K, is a well established similitude parameter [23] and is used to correlate the data obtained from load-controlled tests. K can be expressed in functional form as:

$$K = f(\sigma, a) \qquad (2.3)$$

where σ is the applied stress and a is the crack length. The stress intensity range, ΔK is defined as:

$$\Delta K = K_{max} - K_{min} \tag{2.4}$$

where K_{min} and K_{max} are, respectively, the minimum stress intensity and maximum stress intensity of a fatigue cycle. In this study, ΔK is used to correlate all of the crack growth data.

There is an advantage of using ΔK instead of ΔK_ε. If ΔK has the same value for two cracked specimens, not necessarily of the same type, then the two cracks respond similarly [23]. This cannot be said about ΔK_ε since the strain range is a function of gauge length. There are variations in gauge length between different studies resulting in inconsistencies in the literature regarding TMF data correlated with ΔK_ε. This is discussed later in this chapter with the review of previous TMF studies. Since K can be expressed as a and σ as shown in Equation (2.3), and σ is a function of P and specimen area, the load ratio, R, shown previously in Equation (2.1), also can be expressed as:

$$R = \frac{K_{min}}{K_{max}} \tag{2.5}$$

In this dissertation, the total time of a fatigue cycle is referred to as t_{tot}, but is more commonly considered as the period, τ.

$$\tau = t_{tot} \tag{2.6}$$

13

The frequency (ν) of the cycle is defined as the inverse of the period.

$$\nu = \frac{1}{\tau} \tag{2.7}$$

Elevated Temperature Crack Growth Mechanisms

Before discussing the modeling of TMF crack growth rates, it is necessary first to understand the mechanisms of crack growth at elevated temperatures. In most cases, fatigue growth rates at elevated temperature are greater than those at room temperature. Lloyd [24] has studied this behavior and has noted that over the range 22-625°C growth rates in steels increase as much as 30 times at low values of K. When considering other materials for high-temperature applications, this increase could be much larger. In the case of superalloys, increases in growth rates as large as 1000 times have been observed for an increase from room temperature to 1000°C.

Three mechanisms of elevated temperature crack growth are considered here. They are mechanical fatigue, creep, and an environmental effect. The environmental effect is categorized separately from creep; however, they both are time-dependent processes that occur at elevated temperatures. Therefore, they are considered together in the following discussions.

Mechanical Fatigue

Fatigue is the degradation of a material from cyclic loading. The type of fatigue described here is mechanical fatigue. Mechanical fatigue damage can occur from 1) the formation and propagation of microcracks or 2) the cavitation of the grain boundaries over the entire cross section [25]. The first mechanism is dominant in most materials at room temperatures and can be present at elevated temperatures. This mechanism is dominant at higher temperatures only if the rate (frequency) of cycling is high enough not to allow oxygen diffusion and environmentally enhanced damage to occur. Further discussions pertaining to this effect of frequency are given in a later section.

Cyclic mechanical loads can cause crack formation even if the nominal loads are below the elastic limit of the material. Once the crack is formed, the crack can propagate under the process known as reverse slip. This process of mechanical fatigue can be described as follows: A sharp crack causes a high concentration of stresses at the crack tip, where slip can easily occur. During the rising portion of the mechanical loading cycle, flow occurs along favorable slip planes in the direction of maximum shear stress. This slip opens and extends the crack. Increased stress and work hardening activates parallel slip planes, which tend to blunt the crack tip. As the load decreases, the plastic deformation that has occurred in the small zone surrounding the crack tip can no longer fit into the elastic surroundings. The elastic region exerts compressive stresses on the plastic zone and subsequently closes and

15

resharpens the crack. This cyclic opening and closing of the crack surfaces causes a pattern of ripples, called striations, as the crack propagates, and the resulting fracture is transgranular [23, 26-29]

In the model development in this study, the mechanical fatigue contribution to crack growth is called cycle-dependent. The mechanisms that cause mechanical fatigue are not controlled by a rate process; therefore, this contribution to crack growth rate only is a function of stress intensity range (ΔK), load ratio (R), and possibly temperature (T). Cycle-dependent crack growth is discussed in a later section of this chapter.

Creep and Environmental Effects

Creep is a monotonic deformation process that can cause either crack-tip stress relaxation or crack extension [30, 31]. The first of these, stress relaxation, occurs by both crack-tip blunting and plastic deformation that can occur when a material is exposed to elevated temperature. This relaxation of stresses retards crack propagation, and in theory, totally inhibits crack extension in an ideally homogeneous material. In the current effort, crack-tip blunting is thought to cause retardation of crack growth rates in the titanium-aluminide alloy, Ti-24Al-11Nb, when it is simultaneously exposed to load hold times and elevated temperatures. This crack growth rate retardation phenomenon is discussed in greater detail in Chapters IV and V.

16

The second effect of creep is crack extension. Because of inhomogeneities that exist in materials, cavities can form and grow to extend an existing crack [32]. This crack extension is described in more detail here, but to eliminate confusion between these two effects of creep, crack extension caused by creep is referred to as creep crack growth, and most often, creep is used to describe crack-tip blunting and plastic deformation.

Creep crack growth can be considered as the extension of macroscopic cracks at elevated temperature [33] when a material is subjected to sustained loads. Note that environmental effects (interactions) that cause crack extension sometimes are considered in this category, since they also are time-dependent processes. The time-dependent crack growth mechanisms are divided into three categories, and the first two are forms of creep crack growth.

First, creep crack growth can occur by the forming and joining of the voids on the grain boundaries [25]. At low stress levels, void growth is usually controlled by the diffusion of the material along its surface. The material then flows along the grain boundaries. Second, creep crack growth can occur from the degradation of the microstructure of a material [34]. Riedel [25] has pointed out that many alloys contain second-phase particles that inhibit dislocation motion. Some examples of these second-phase particles are γ′ in the superalloys, intermetallics in aluminum alloys, and carbides in steels [35]. Over extended periods, the effectiveness of these particles decreases; therefore, so does the alloy's creep resistance.

17

A third possible cause of time-dependent crack growth is corrosive damage from aggressive gases [35]. This type of crack growth is sometimes referred to as environmentally-induced creep or environmental degradation [36]. This damage can occur on or below the surface of a material. One of the best examples of this is internal oxidation along grain boundaries, as is the case for some steels and superalloys [25].

Therefore, the main mechanisms for crack growth at elevated temperatures are mechanical fatigue, creep crack growth (grain boundary cavitation), and environmental effects (degradation), as elaborated above.

Fatigue-Creep-Environment Interaction

Fatigue-creep-environment interaction involves the application of cyclic loads at high enough temperatures where time-dependent, thermally activated processes occur along with the mechanical fatigue mechanisms [37]. The interaction between fatigue and creep crack growth is most often observed during testing when a load hold time (load dwell) is superimposed on a pure fatigue cycle. These types of cycles often are referred to as creep-fatigue cycles, but in this study, they are called hold-time cycles.

To understand the mechanisms of fatigue-creep interaction, it is helpful first to consider the micro-structural characteristics of: fatigue, which occurs from crack damage, and creep, which is caused by cavitation damage [38]. These mechanisms have been described in the two previous sections. When

18

creep and fatigue conditions occur simultaneously, they can be dominated by either cavitation damage or crack damage. Cavitation accelerates crack growth and the failure path, which was initially transgranular, becomes intergranular. Pure fatigue usually is characterized by a transgranular mode, but with an increase in temperature, the mode may change to intergranular, which is typically characteristic of creep failure [37, 38].

The introduction of an aggressive environment complicates the matter further. Crack growth rates from fatigue cycles with hold times usually are much larger in the presence of oxygen or sulfur than in an inert environment (inert gas or vacuum). But there is uncertainty as to whether the creep effect (considering bulk cavitation) or the environmental (corrosive) effect is the dominant mechanism at elevated temperature. It has been shown [36] during elevated-temperature mechanical fatigue testing, that if relatively low stress levels are introduced in the cycles for short hold times, environmental degradation is dominant. During fatigue cycling, if a material is subjected to high stresses for long hold times, the crack growth damage usually is caused by creep.

In a few cases, the oxide layer produced by the exposure of a material to oxygen reduces crack propagation. A corrosion product forms on the crack surfaces and enhances the crack-closure effect. This retards crack growth and at low loading levels can even stop crack growth. This has been observed for some superalloys exposed to high temperatures [25].

19

Frequency Dependence of Crack Growth

As discussed earlier, there are three mechanisms that most often contribute to crack growth at elevated temperatures. These include mechanical fatigue, creep, and environmental interaction. Mechanical fatigue is a cycle-dependent process, and environmental interaction and creep are time-dependent. Studies have shown that when a material experiences high frequency fatigue, the crack growth rates are not significantly influenced by the temperature or environment [39]. This condition is commonly referred to as cycle-dependent crack growth. When frequencies are low enough that the temperature and environment can contribute to crack growth, the growth rates increase. The growth rate is controlled by a combination of cycle-dependent and temperature-environment effects, referred to as mixed-mode crack growth [6]. At very low frequencies, the crack growth is totally dominated by the temperature and environment. This condition is referred to as pure-time dependent crack growth [40]. Under such conditions, the crack growth rate increases proportionally with increases in cycle time (or decreases in frequency). These three crack growth conditions are shown in Figure 2.3, where the crack growth rate is plotted as a function of frequency. The three conditions are described by the slope of the crack growth curve when plotted in this manner. A power-law equation can be used to define the slopes in each crack growth region. The equation is expressed:
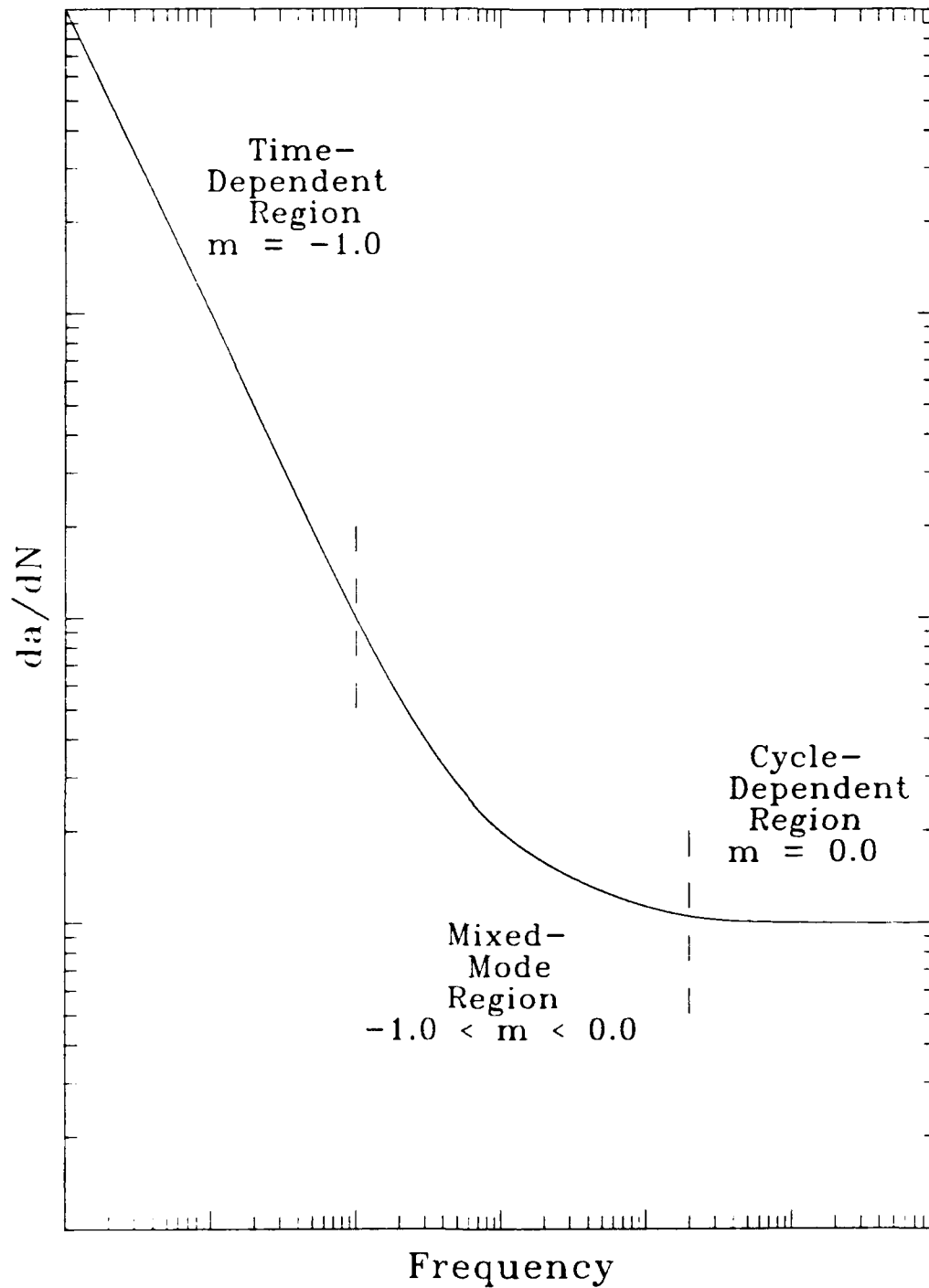
Figure 2.3 Effect of Frequency on Crack Growth Rates

21

$$\frac{da}{dN} = C_f \, v^m \tag{2.8}$$

where C_f is a constant that defines the crack growth rate at 1 Hz, v is the

loading frequency, and m is the exponent that defines the slope of the line. In

the cycle-dependent region, $m = 0$, since da/dN is not a function of frequency,

and in the time-dependent region, $m = -1$, which implies that da/dN increases

the same magnitude as v decreases. In the mixed-mode region, the tangent

slope of the curve will be greater than -1 and less than 0. In summary, the

slope, m is defined for each of the regions as:

$$
\begin{aligned}
m &= 0 \quad &&; \quad cycle\ dependent \\
-1 < m &< 0 \quad &&; \quad mixed\ mode \\
m &= -1 \quad &&; \quad time\ dependent
\end{aligned}
\tag{2.9}
$$

Review of Thermal-Mechanical Fatigue Testing

This section is divided into two categories: correlation of the test data

(which fracture mechanics parameters are used), and the comparison of test

results. The test control method (load-control or strain-control) and correlating

parameters used by the researchers are discussed first. This is followed by

comparisons of isothermal crack growth rate data and thermal-mechanical

fatigue (TMF) crack growth rate data of different phases (i.e. in phase and out

of phase) for various high-temperature structural materials. Later in this

chapter, the methods that have been used for predicting crack growth rates are

described, with particular emphasis on the TMF crack growth rate models.

Correlation of Test Data

As previously mentioned, two common ways of correlating TMF crack

growth rate data are to use either stress or strain intensity factors, ΔK or ΔK_ϵ .

The use of these and other parameters to correlate elevated-temperature

fatigue and TMF crack growth rate data are discussed in this section.

Sadananda and Shahinian [26] studied the possibility of using linear-

elastic fracture mechanics to characterize elevated-temperature crack growth.

The materials included in their study were aluminum alloys, low-alloy steels,

austenitic steels, and the superalloys. They concluded that, in general, ΔK is a

valid parameter as long as gross plasticity due to creep does not occur.

Pedron and Pineau [41] tested Inconel 718 at 650°C under load-controlled

conditions to study pure fatigue, creep, and creep-fatigue (hold-time)

interactions. They correlated the fatigue and hold-time crack growth rate data

(da/dN) with ΔK and the sustained-load crack growth rate data (da/dt) with K.

Saxena and Bassani [42] used ΔK to characterize da/dN at elevated-temperature

fatigue. They have presented data for Cr-Mo-V, 304 SS, and Inconel 718.

Larsen and Nicholas [43] used ΔK to model elevated-temperature crack growth

in the superalloys Waspaloy and IN 100. They also presented the crack

growth rates in terms of ΔK.

Among the earliest TMF crack propagation studies were those of Rau et al. [44]. They performed cyclic strain and temperature tests on cobalt-base and nickel-base superalloys. These superalloys were of the conventionally cast and directionally solidified type. They successfully correlated their crack growth rate data using ΔK_ε. Gemma et al. [45] further studied directionally solidified nickel-base superalloys by performing strain-controlled TMF tests. They also used ΔK_ε to correlate the crack growth rates.

Jordan and Meyers [13] used ΔK, ΔK_ε, and the J-integral range (ΔJ) to express strain-temperature cycling data for Hastelloy-X. They concluded that all three parameters correlated the da/dN data within a factor of two. Pelloux and Marchand [46] explored the possibility of using ΔK, ΔK_ε, ΔJ, crack-tip opening displacement range ($\Delta CTOD$), and Tomkin's model to analyze TMF data from tests on Inconel X-750, Hastelloy-X, and B-1900 + hafnium. They were successful in predicting TMF crack growth rates to within a factor of five with all the parameters except $\Delta CTOD$. Their investigations also were performed under strain-controlled conditions.

More recently Marchand et al. [47, 48] found that the most effective way to correlate their strain-controlled TMF crack growth rate data was to use a modified stress intensity factor. Marchand et al. [46] found that the Harris' [49] K solutions for single edge notch specimens overestimated K values. They proposed corrections to the stress intensity that accounted for the decreasing

24

load amplitude as the crack extends and the reduction of crack dr ving force caused by the closing bending moment.

Most of the TMF testing discussed previously was performed under strain-controlled conditions. Heil [6] and Nicholas et al. [8] correlated their load-controlled TMF test data in terms of ΔK. These studies are relevant to the current work since they also used this parameter for the modeling of TMF crack growth rates in Inconel 718. This model is discussed later in this chapter and is described in detail in Chapter V with the current model development.

Comparison of Test Results

In this section, the crack growth rates of TMF tests of various load-temperature (or strain-temperature) phase angles are discussed, and comparisons of TMF and isothermal fatigue crack growth rates are made in the cases where they were available in the literature. Note that a 180° out-of-phase test is referred to only as an out-of-phase test, since no other phase angle tests are discussed.

It is difficult to find general trends in the strain-controlled TMF crack growth rate data reported in the literature. Different researchers have even found opposite trends in crack growth behavior for the same material. Also, stress-controlled TMF test results do not always show the same trends as strain-controlled TMF experiments. To clarify some of this conflicting data, the strain-controlled and load-controlled TMF test results are considered

25

separately. The strain-controlled test results are discussed first and the load-controlled results are considered second.

Rau et al. [44] studied strain-temperature cycling of three superalloys: MAR-M 509, B-1900 + hafnium (Hf), and MAR-M200 + Hf. They concluded that at low growth rates, da/dN depends only on ΔK_ε. Out-of-phase TMF tests produced higher growth rates than in-phase tests, even at low strain amplitudes. All TMF tests produced higher crack growth rates than did the T_{min} isothermal tests.

Gemma et al. [45] performed strain-controlled TMF tests on directionally solidified MAR-M200 + Hf and conventionally cast B-1900 + Hf. Their main objective was to determine the effect of grain orientation on growth, but they also showed a correlation between modulus and growth rate. In stress-controlled tests, a lower modulus material tends to have higher crack growth rates than that of a higher modulus material of the same alloy. They found from their strain-controlled tests that the opposite is true.

Gemma et al. [50] studied the effect of varying mean strain during TMF cycles for directionally solidified MAR-M200 + Hf and conventionally cast B-1900 + Hf. They simulated creep/TMF conditions by increasing the mean strain by a fixed amount at T_{max} for each 20th TMF cycle. These creep/TMF growth rates were higher than those of pure TMF.

Marchand and Pelloux [51] observed from the data available in the literature that conventionally cast (CC) cobalt-base, CC nickel-base, and

26

directionally solidified nickel-base superalloys have higher growth rates under TMF conditions than under isothermal fatigue at T_{max}. Out-of-phase crack growth rates generally are greater than in-phase growth rates. For 12 Cr-Mo-V-W steel the growth rates for TMF and isothermal fatigue were very similar and 304 SS had higher growth rates under in-phase than out-of-phase cycling. Their results for Inconel X-750 showed higher rates at thermal-mechanical cycling (360-650°C) than isothermal fatigue at T_{max} (650°C). Out-of-phase cycling produced higher growth rates than in-phase cycling. They also have shown a noticeable effect of compressive cycling. Growth rates during tests with $R = -1$ were higher than those at $R = 0.05$.

Jordan and Meyers [13] used strain-controlled TMF tests to compare in-phase and out-of-phase cycling of Hastelloy-X. They have shown that cracks grew faster under in-phase cycling at low growth rates and grew faster under out-of-phase cycling at high growth rates. Marchand et al. [47] also studied Hastelloy-X under strain-temperature cycling, but considered low and high cases of strain separately. For elastic straining, the out-of-phase crack growth rates were higher than the crack growth rates of isothermal tests at T_{max} and the crack growth rates of in-phase TMF tests. For fully plastic straining, the isothermal growth rates were higher than TMF growth rates. Using ΔK_{eff} they found T_{max} and T_{min} provided upper and lower bounds for growth rates, respectively, for all their TMF crack growth rate data. Marchand et al. [48] have continued testing on the Hastelloy-X and B-1900 + hafnium alloys. Their

findings were consistent with their earlier studies [47].

In most strain-controlled TMF tests, the out-of-phase cycles produce higher crack growth rates than do the in-phase cycles. TMF growth rates are almost equal to those obtained under isothermal conditions at T_{max} . Nicholas et al. [8] have observed that, in some cases, TMF crack growth rates are higher than isothermal fatigue crack growth rates at T_{max} for low strain ranges and lower for high strain ranges. They also have found the opposite to be true for other cases. These test results were correlated using the strain intensity factor, which has no physical significance. The strain intensity factor is usually a function of the mechanical strain, which is obtained by subtracting the thermal strain from the total strain.

Stress-controlled TMF tests are presented in the following discussions. The results from these studies are more consistent among the different researchers than those of the strain-controlled tests discussed previously.

Gemma et al. [50] studied the effect of stress hold times during TMF cycles for directionally solidified MAR-M200 + hafnium (Hf) and conventionally cast B-1900 + Hf. When a hold-time was added at maximum load during in-phase TMF, the growth rates were higher than those for pure TMF conditions. Saxena and Bassani [42] also studied the effects of hold times at maximum load during isothermal tests, but their studies included Cr-Mo-V steel, 304 SS, and Inconel 718. For all the materials, the hold time increased the growth rate over that obtained under pure isothermal fatigue conditions.

DeLuca and Cowles [52] conducted TMF testing of a single crystal nickel-base alloy (Pratt & Whitney alloy 1480). In-phase cycling produced greater growth than out-of-phase cycling. Their tests have shown behavior that is inconsistent with most other TMF data. At high stress intensities, the in-phase TMF conditions produced growth rates that were larger than those at isothermal T_{max}.

Wilson and Warren [53] studied the IN 100 alloy under thermal-mechanical cycling. In-phase growth rates were similar to those at T_{max} isothermal and out-of-phase results were similar to those at T_{min} isothermal. Wright et al. [2] found that for Rene' N4 alloy, the thermal-mechanical cycling produced slightly higher rates than isothermal at T_{min} but much lower than isothermal at T_{max}.

Nicholas et al. [8] found that the isothermal crack growth rate tests at T_{max} and T_{min} were, respectively, upper and lower bounds for the TMF data for Inconel 718. The in-phase growth rates were slightly less than isothermal T_{max} and the out-of-phase rates were slightly greater than isothermal T_{min}. Initial studies of Ti-24Al-11Nb have produced TMF crack growth rate trends that appear to be consistent with those of Inconel 718 [54, 55].

Most load-controlled TMF crack growth studies show that growth rates for TMF are bounded by growth rates found for isothermal tests at T_{max} and T_{min}. These studies also show that in-phase cycling usually is more damaging than out-of-phase cycling.

29

Some cases that are inconsistent with these findings should be noted. When Marchand and Pelloux [51] tested Inconel X-750, they found the following three significant features: 1) crack growth rates under thermal-mechanical cycling were greater than those obtained during isothermal tests at T_{max}, 2) the growth rates obtained for load ratios (R) of -1 were higher than those for R = 0.05, and 3) under fully reversed stress (R = -1), out-of-phase cycling produced higher growth rates than in-phase cycling at high values of ΔK, and growth rates for both cases were nearly the same for low ΔK. Wilson and Warren [53] also performed out-of-phase TMF tests at load ratios of 0.01 and -1. The growth rates were nearly the same for both cases, unlike the earlier studies of Marchand and Pelloux [51]. Nicholas et al. [8] have attributed this apparent inconsistency to possibly oxide-induced closure and plasticity. Marchand and Pelloux [51, 56] consolidated their TMF data with an effective stress intensity factor, ΔK_{eff}, that considered closure. These are the only efforts, currently available in the open literature, that consider crack closure under combined thermal and mechanical loading.

Modeling Crack Growth Rates

Crack growth data typically are presented on a log-log plot of the crack growth rate, da/dN, vs. the stress intensity range, ΔK, as shown in Figure 2.4. There are three distinct regions of growth: Region I is the threshold crack growth region where the lower asymptote of the curve is the threshold stress
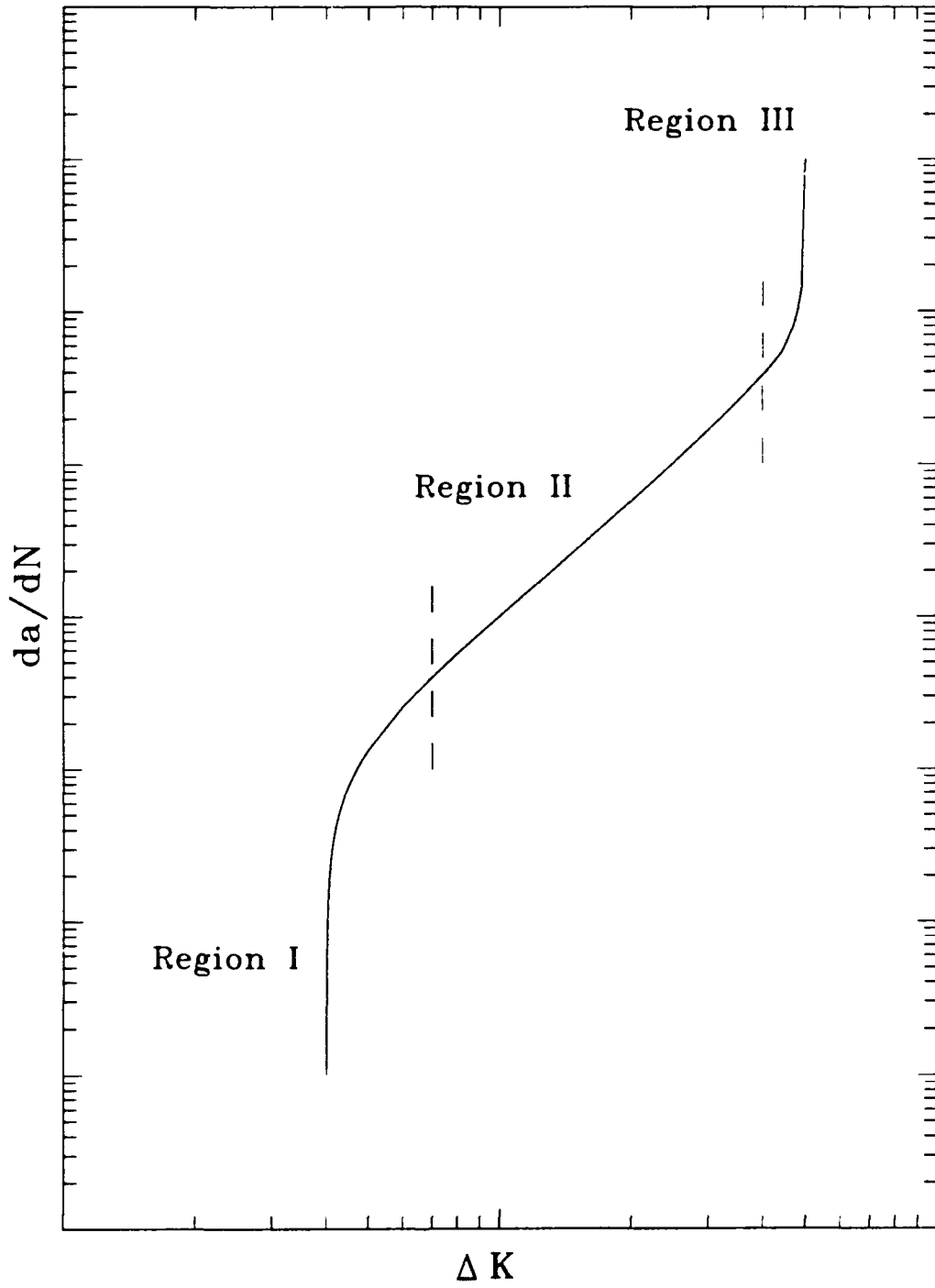
Figure 2.4 Typical da/dN vs. ΔK Curve

31

intensity range, ΔK_{th}. Region II defines the region of subcritical, stable crack growth. The discussions in this dissertation concentrate on data in this region. Region III describes the region of critical crack growth where the upper asymptote of the curve is the critical stress intensity range, ΔK_c.

Many relationships have been proposed to describe da/dN as a function of ΔK, and several of those relationships are discussed first in this section. The superposition expressions that model TMF crack growth rates are presented later in this section. Models that have been used to describe the retardation of crack growth rates are presented last.

Crack Growth Rate Relationships

Many proposed relationships have attempted to describe da/dN as a function of ΔK. The most basic of these relationships is the power law expression used by Paris [57] to describe the linear portion (region II) of the curve shown in Figure 2.4. This is expressed as:

$$\frac{da}{dN} = C_p \, (\Delta K)^n \tag{2.10}$$

Where the coefficient, C_p, and exponent, n, are material constants. There have been other attempts to modify Equation 2.10 to account for the effect of load ratio, R. These include work performed by Broek and Schijve [58], Erdogan [59], and Walker [60]. Forman et al. [61] modified Equation 2.10 to reflect the

behavior at the upper asymptote of the da/dN vs. ΔK curve. The equation they developed is expressed:

$$\frac{da}{dN} = \frac{C_f\,(\Delta K)^n}{(1 - R)(K_c - K_{max})} \tag{2.11}$$

where K_{max} is the maximum stress intensity of the fatigue cycle, K_c is the critical stress intensity (fracture toughness), and as before, C_f and n are constants. These expressions shown above are not general enough to apply to a wide range of materials over the full ranges of ΔK, nor could they accurately account for variations in load ratio, frequency, and temperatures. In order to create more general expressions, the hyperbolic sine (sinh) and sigmoidal crack growth relationships were developed at Pratt and Whitney [10] and General Electric [39], respectively.

The sinh crack growth model is expressed as:

$$\log\left(\frac{da}{dN}\right) = C_1 \sinh\left[C_2\,(\log \Delta K + C_3)\right] + C_4 \tag{2.12}$$

where the constants C_1 and C_2 scale the x and y axes, respectively, and C_3 and C_4 define the inflection point in the curve. C_1 is a material constant and C_2, C_3, and C_4 can be expressed as functions of temperature, frequency, hold-time, and load ratio [62-63].

33

The sigmoidal crack growth model is expressed as:

$$\frac{da}{dN} = \exp(B_{se}) \left(\frac{\Delta K}{\Delta K_{th}}\right)^{C} \left[\ln\left(\frac{\Delta K}{\Delta K_{th}}\right)\right]^{Q} \left[\ln\left(\frac{\Delta K_c}{\Delta K}\right)\right]^{D} \qquad (2.13)$$

where ΔK_{th} is the threshold stress intensity range (lower asymptote) and ΔK_c is the critical stress intensity range (upper asymptote). B_{se}, C, Q, and D are parameters that determine the shape of the curve. The parameters can be expressed in terms of temperature, frequency, and load ratio [64]. The advantages the sigmoidal model has over the sinh model are: 1) the lower and upper regions of the crack growth curve need not be symmetric since the shape of the lower and upper regions of the curve are defined independently, and 2) ΔK_{th} and ΔK_c appear explicitly in the sigmoidal expression. The modified sigmoidal equation (MSE), which is a variation of this sigmoidal equation, is used in the current modeling effort and is described in detail in Chapter V.

Crack Growth Rate Superposition Models

In this section, the previous attempts of modeling TMF crack growth rates using crack growth rate superposition techniques are discussed. This method first was used for estimating fatigue crack growth rates in materials exposed to aggressive environments (corrosion fatigue). Later efforts used

34

similar techniques to model crack growth rates in materials exposed to elevated temperatures, and finally for those experiencing TMF.

Wei and Landes [65] proposed a linear summation model for estimating crack growth rates for materials in an aggressive environment. They defined two components of crack growth: 1) mechanical and 2) environmental. In this case, the total crack growth rate can be expressed as:

$$\left(\frac{da}{dN}\right)_{tot} = \left(\frac{da}{dN}\right)_m + \left(\frac{da}{dN}\right)_e \tag{2.14}$$

where $(da/dN)_m$ and $(da/dN)_e$ are, respectively, the mechanical and environmental contributions to crack growth. The mechanical component is the fatigue crack growth rate obtained in an inert environment under the same mechanical loading conditions. The environmental component is obtained by integrating sustained-load crack growth data obtained in an identically aggressive environment.

Kim and Manning [66] proposed a three-term superposition model to define fatigue crack growth rates in aluminum alloys subjected to aggressive environments. The first term is the mechanical (inert) crack growth rate component, which is similar to those described above. The second term is the cycle-dependent contribution requiring synergistic fatigue-environment interaction. They theoretically determined this term based on 1) formation of hydrogens on the crack tip, 2) transfer of hydrogen to the microstructure, and

35

3) continuous accumulation of hydrogen at discontinuities. The third term is the sustained load crack growth per cycle (stress corrosion cracking during each cycle). They found for aluminum alloys the third term was negligible, and therefore, was not required. In addition, they successfully estimated crack growth rates, but only for a limited amount of test data.

Gebetta et al. [67] found that a load-environment interaction is better described by a three-term superposition model. The three contributions are: 1) a mechanical component, 2) a ΔK-dependent environmental component, and 3) a time-dependent environmental component. The model predicted crack growth rates in a reactor-pressure-vessel steel under corrosion fatigue.

It should be mentioned that these models [65-67] were not applied at elevated temperatures in these previous studies, but these concepts have been adopted by other researchers to model elevated-temperature crack growth, including TMF crack growth.

Winstone et al. [68] and Dimopulos et al. [69] used a two-term linear summation model to predict isothermal fatigue crack growth rates. Both studies used an approach similar to that shown in Equation (2.14). Winstone et al. [68] have found that when cycle-dependent (mechanical-fatigue) and time-dependent (environmental) processes occur simultaneously, they can be accounted for with a linear sum of terms that represent each contribution to crack growth. Using the same concept, Dimopulos et al. [69] have predicted crack growth rates in a nickel-base superalloy.

Nicholas and Weerasooriya [70] have shown that a linear-summation model can predict the total crack growth rate for hold-time tests of Inconel 718. They predicted the total crack growth rate as the sum of the fatigue contribution and the hold (environment) contribution. The model can be expressed as:

$$\left(\frac{da}{dN}\right)_{tot} = \left(\frac{da}{dN}\right)_f + t_h\left(\frac{da}{dt}\right)_{sl} \tag{2.15}$$

where $(da/dN)_f$ is the fatigue crack growth rate, $(da/dt)_{sl}$ is the sustained-load crack growth rate, and t_h is the length of the hold time. Larsen and Nicholas [43] used a similar technique for describing crack growth rates in IN 100 under hold-time conditions, and Nicholas et al. [71] also have used this technique to describe hold-time crack growth rates in nickel-base superalloys. Plumtree and Nai-yang Tang [72] suggest that in addition to the fatigue and environment terms shown in Equation (2.15), a fatigue-creep-environment interaction term is necessary in estimating crack growth rates under hold-time conditions in AISI type 304 stainless steel.

Haritos et al. [73] conducted sustained-load experiments under isothermal and non-isothermal conditions between 537-649°C. Then they used a linear cumulative-damage model to predict crack growth rates for the thermal-cycling condition using isothermal data. With this model, a complex thermal cycle is divided into linear segments and the average growth rate per

37

segment is calculated. The predicted growth rate for the entire cycle is then obtained by adding the components of each segment. This model can be expressed as:

$$\left(\frac{da}{dN}\right)_{tot} = \sum_i (da/dt)_{av} \, t_i \qquad (2.16)$$

where $(da/dt)_{av}$ is the average growth rate during segment i, and t_i is the time of segment i. Their predictions were in agreement with the experimental data within a factor of two.

Jordan and Meyers [13] predicted TMF crack growth rates from isothermal data. First, they developed an expression for the crack growth rate as a function of ΔK and temperature. They differentiated this expression to obtain the rate of change in growth rate with respect to ΔK. Next, they numerically integrated the new expression over the loading portion of the TMF cycle to obtain the total growth rate for the cycle (this integration is discussed in Chapter V with the current modeling effort). The predicted values of da/dN differ from the actual values by approximately a factor of two.

Heil [6] used a three-term superposition model to predict TMF crack growth rates for Inconel 718 during thermal-mechanical cycling. This model includes a cycle-dependent (mechanical-fatigue) contribution, a mixed-mode contribution, and time-dependent (environmental) contribution. The model can be expressed as:

38

$$\left(\frac{da}{dN}\right)_{tot} = \left(\frac{da}{dN}\right)_{cd} + \left(\frac{da}{dN}\right)_{mm} + \left(\frac{da}{dN}\right)_{td}$$ (2.17)

where $(da/dN)_{cd}$ is the cycle-dependent crack growth rate contribution, $(da/dN)_{mm}$ is the mixed-mode crack growth rate contribution, and $(da/dN)_{td}$ is the time-dependent crack growth rate contribution. He found that the mixed-mode term did not contribute significantly to the total crack growth rate; therefore, he suggested using only a two-term expression.

Heil et al. [74] developed a two-term superposition model resulting from the earlier work performed by Heil [6]. Their model could be expressed as that shown in Equation (2.17) with $(da/dN)_{mm}$ equal to zero. The cycle-dependent term is the mechanical-fatigue or inert term. By definition, it is independent of loading frequency, and in the case on Inconel 718, is also independent of test temperature. Cycle-dependent behavior is dominant in Inconel 718 below 538°C; therefore, they used existing fatigue data obtained at 427°C for this contribution of growth rate. The time-dependent term represents the crack growth rate contribution of environmental interaction. This contribution is obtained by integrating sustained-load growth rates (da/dt) during the mechanical loading portion of the fatigue TMF cycle when da/dt is an increasing function; therefore, the total crack growth rate could be expressed as:

39

$$\left(\frac{da}{dN}\right)_{tot} = \left(\frac{da}{dN}\right)_{cd} + \int_{loading} \left(\frac{da}{dt}\right)_{sl} dt \qquad (2.18)$$

where $(da/dN)_{cd}$ is the cycle-dependent crack growth rate contribution and $(da/dt)_{sl}$ is the sustained-load crack growth rate. Adding these two contributions shown in Equation (2.18) yields the total crack growth rate for the TMF cycle. Model predictions of TMF crack growth rates for cycles of various phase angles were accurate to within a factor of two of the experimental data. Harmon et al. [75] also used this type of model in a computer code to predict crack growth rates in both Inconel 718 and 6Al-2Sn-4Zr-2Mo titanium under general thermal-mechanical cycling.

The model developed by Heil et al. [74] is discussed in further detail in Chapter V. The model developed during the current study is similar in concept, but can be applied to a larger group of materials, since it does not only consider mechanical fatigue and environmental interaction, but also crack retardation effects. Retardation effects in the titanium-aluminide alloy studied in the current effort (Ti-24Al-11Nb) are thought to be caused by crack-tip blunting resulting from creep. (Creep is discussed earlier in this chapter). This retardation is discussed in Chapter IV with the isothermal and TMF crack growth behavior of Ti-24Al-11Nb.

In the following section, retardation models used in previous efforts are discussed.

Crack Growth Rate Retardation Models

A review of the literature [76, 77] indicates that retardation in crack growth rates most likely can be attributed to one of three mechanisms: 1) compressive residual stresses at the crack tip [78, 79], 2) a closure mechanism causing deformation behind the crack tip [80-85], and 3) crack-tip blunting [86, 87].

One of the most common examples of crack growth retardation is the application of an overload after constant amplitude fatigue cycling. Consider the case of a crack propagating at a constant growth rate under constant K_{max} conditions. When the overload is applied, the growth rates decrease. This decrease has been attributed to the enlarged plastic zone caused by the overload. When the crack is propagating through the enlarged zone the growth rates decrease, and after completely propagating through the enlarged plastic zone a normal growth rate condition resumes.

There are two ways to model such retardation: 1) by estimating an effective level of ΔK (i.e. ΔK_{eff}) during the retardation that would correspond to the crack growth rate observed during the retardation, or 2) by modeling the growth rates by reducing da/dN directly with a coefficient. Another method used to account for such retardation is to predict the number of delay cycles until the crack resumes unretarded propagation [39]. This method is not relevant to the application considered in this study since it does not model da/dN or ΔK explicitly; therefore, it is not discussed further in this dissertation.

41

A model to account for the effective level of ΔK was developed by Willenborg et al. [79], and this model was used to describe the retardation in the crack growth rate after the application of an overpeak load. The model could be expressed as:

$$\Delta K_{eff} = \Delta K_{app} + \Delta K_{res} \qquad (2.19)$$

where ΔK_{eff} is the effective value of ΔK, ΔK_{app} is the applied level of ΔK, and ΔK_{res} is the residual value of ΔK. For the overpeak condition, ΔK_{res} is negative to produce an effective value of ΔK (ΔK_{eff}) that is less than that applied (ΔK_{app}).

The effective value of ΔK also can be used to account for crack-closure effects. During fatigue cycles, the crack surfaces are not always open. Studies [80-85, 88] suggest that values of K less than that required to open a crack during a fatigue cycle (i.e. K_{op}) do not contribute to crack propagation. It has been proposed by Elber [81] that since K between K_{min} and K_{op} does not contribute to growth, K_{op} can be subtracted from K_{max} to obtain an effective range of K. The expression for the this effective value of ΔK (i.e. ΔK_{eff}) can be written:

$$\Delta K_{eff} = K_{max} - K_{op} \qquad (2.20)$$

where ΔK_{eff} is the effective value of ΔK, K_{max} is the maximum applied K, and K_{op} is the crack opening level of K. By comparing Equation (2.20) with

42

Equation (2.4), ΔK_{eff} is less than or equal to ΔK depending on whether K_{op} is greater than or equal to K_{min}. ΔK_{eff} has been used widely to account for variations in load ratio [81], and also to account for variations in load-temperature phase angle during TMF cycling [51, 56].

The second type of retardation model, the effective growth rate type, was used by Wheeler [78] to describe the overpeak retardation. The model is expressed as:

$$\left(\frac{da}{dN}\right)_{ret} = \Phi_{ol} \left(\frac{da}{dN}\right)_{lin} \tag{2.21}$$

where $(da/dN)_{ret}$ is the retarded crack growth rate, $(da/dN)_{lin}$ is the linear (unretarded) crack growth rate, and Φ_{ol} is the overload (overpeak) retardation coefficient.

This concept is used in this dissertation to account for the retardation of crack growth rates in the titanium-aluminide alloy, Ti-24Al-11Nb. The retardation in Ti-24Al-11Nb is believed to be caused by crack-tip blunting [89]. This crack growth rate retardation is discussed in Chapter IV with the crack growth results obtained during this study. The retardation model is discussed in Chapter V with the modeling of the crack growth rates of isothermal fatigue, isothermal fatigue with superimposed load hold times, and TMF. The titanium aluminides are discussed in the following section, and Ti-24Al-11Nb is described in Chapter IV.

43

Titanium Aluminides

The high-temperature materials used in current gas turbine engines consist of the nickel-base superalloys, cobalt-base superalloys, and conventional alpha-beta titanium alloys. Future engine designs dictate the need for lightweight materials that can operate at higher temperatures to meet thrust-to-weight ratio requirements, while meeting durability goals. These future engines require the development of a new class of materials than could operate at these higher temperatures while maintaining superior mechanical and corrosion properties [19]. Intermetallic compounds (ordered alloys) are being considered as possible candidate materials for future aircraft engine as well as high-temperature airframe applications [18, 19]. Two intermetallic compounds that have been studied extensively [16-21, 89-94], and found to exhibit favorable properties for high-temperature applications are the alpha-two and gamma titanium aluminides, Ti_3Al and $TiAl$, respectively.

High temperature material selection is based on two main criteria: mechanical properties and environmental resistance [20]. Intermetallic compounds of titanium and aluminum have attractive properties such as low density and high specific strength, along with high-temperature capability [16, 17]. The specific strength and stiffness of the titanium-aluminide alloys are competitive with those of the nickel superalloys up to 650°C; titanium aluminides could reduce the weight of components currently using nickel alloys.

44

The use of conventional titanium alloys is limited to approximately 600°C because of their inherent lack of oxidation resistance when exposed to higher temperatures. The titanium aluminides, on the other hand, are candidates for applications up to 750°C [20], and the titanium-aluminide compounds have adequate resistance to creep crack growth up to much higher temperatures than conventional titanium alloys [18]. Also, the gamma titanium aluminide is fire resistant, and the alpha-two alloy is more fire resistant than conventional titanium alloys; however, the alpha-two alloy will sustain combustion [17, 94].

The Ti_3Al alloy is more ductile, stronger, and more dense than the other titanium aluminide, TiAl, [18] and several studies [16-20] have shown its potential for elevated-temperature component applications. The alloy considered in the current investigation is the alpha-2 intermetallic alloyed with niobium, Ti-24Al-11Nb (shown as atomic percent). Further details about this alloy, including composition (weight percent), heat treatment, and tensile properties, are provided in Chapter III.

Limited data is available to characterize the fracture and fatigue crack growth behavior of this new class of advanced structural alloys at elevated temperatures. With the current unavailability of such understanding, the titanium aluminides are being considered solely for static components [17, 19]. It is the goal of this study, to provide the understanding of crack growth behavior under simultaneous mechanical and thermal-fatigue loading, and

then to develop a model to predict crack growth rates during such loading conditions. Since programs such as Retirement for Cause [4] and the Air Force Structural Integrity Program [5] require crack growth rate calculations for engine components under actual operating conditions, a model of this type is required for the titanium-aluminide alloys to be used to their full potential.

III. <u>Test Apparatus and Procedure</u>

In this chapter the material and specimen geometry are described along with the test equipment, testing procedure, and data analysis techniques. A summary of the tests completed during this effort and discussions of the results is presented in Chapter IV.

This chapter is divided into four sections: 1) material and specimen design, 2) test equipment, 3) testing procedure, and 4) data analysis techniques.

<u>Material and Specimen Description</u>

<u>Material Description</u>

The material used in this study is an alpha-2 based titanium-aluminide alloy whose nominal composition is Ti-24Al-11Nb (atomic %). The actual chemical composition (weight %) of the alloy is given in Table 3.1. (Atomic percent is the number of atoms of an element in a total of 100 representative atoms [95]. Atomic percent is related to weight percent using the atomic weight of the elements as given in reference [96].)

The material was triple melted, cast into ingot, and then forged to a slab 7.62 cm thick. The slab was cut into sheet bars, which were cross-rolled at 1038°C to a thickness of 4.06 cm. The resulting plates were beta annealed at 1177°C for 30 minutes and then cross-rolled to a thickness of 1.14 cm. The heat treatment of the alloy is summarized in Table 3.2. The resulting material

Table 3.1 Composition of the Ti-24Al-11Nb Alloy

Element	Ti	Al	Nb	Fe	O	N
Weight %	Bal	13.50	21.40	0.080	0.0084	0.003

Table 3.2 Heat Treatment of the Ti-24Al-11Nb Alloy

1 - 1149°C for 1 hr. in vacuum

2 - Fan-forced argon cooled at a rate of 1.67°C per sec.

3 - Age hardened at 760°C for 1 hr. in vacuum

4 - Air cooled to room temperature

was equiaxed and showed no preferred orientation. The prior beta grain size was approximately 1.0 mm in diameter.

The tensile properties of the alloy are presented in Table 3.3.

Table 3.3 Tensile Properties of the Ti-24Al-11Nb Alloy

Temperature	25°C	300°C	650°C
UTS (MPa)	669	707	504
0.2% YS (MPa)	555	412	337
Elongation (%)	1.6	6.1	16.3
Modulus (GPa)	91	86	55

Specimen Description

The material used in this study is high in cost and limited in supply; therefore, the specimens must be small. Compact tension (C(T)) specimens are used exclusively in this study, and machined according to ASTM Standard E 647 [97]. The nominal specimen width, W, is equal to 40.0 mm and H/W is equal to 0.6, where H is the specimen height as shown in Figure 3.1. A nominal thickness, B, equal to 2.54 mm is used to maximize the heating and cooling rates during thermal cycling and minimize the through-the-thickness variations in temperature. The specimens are polished to a 3 micron finish since visual crack length measurements need to be made. The stress intensity, K, for the C(T) geometry is expressed as:
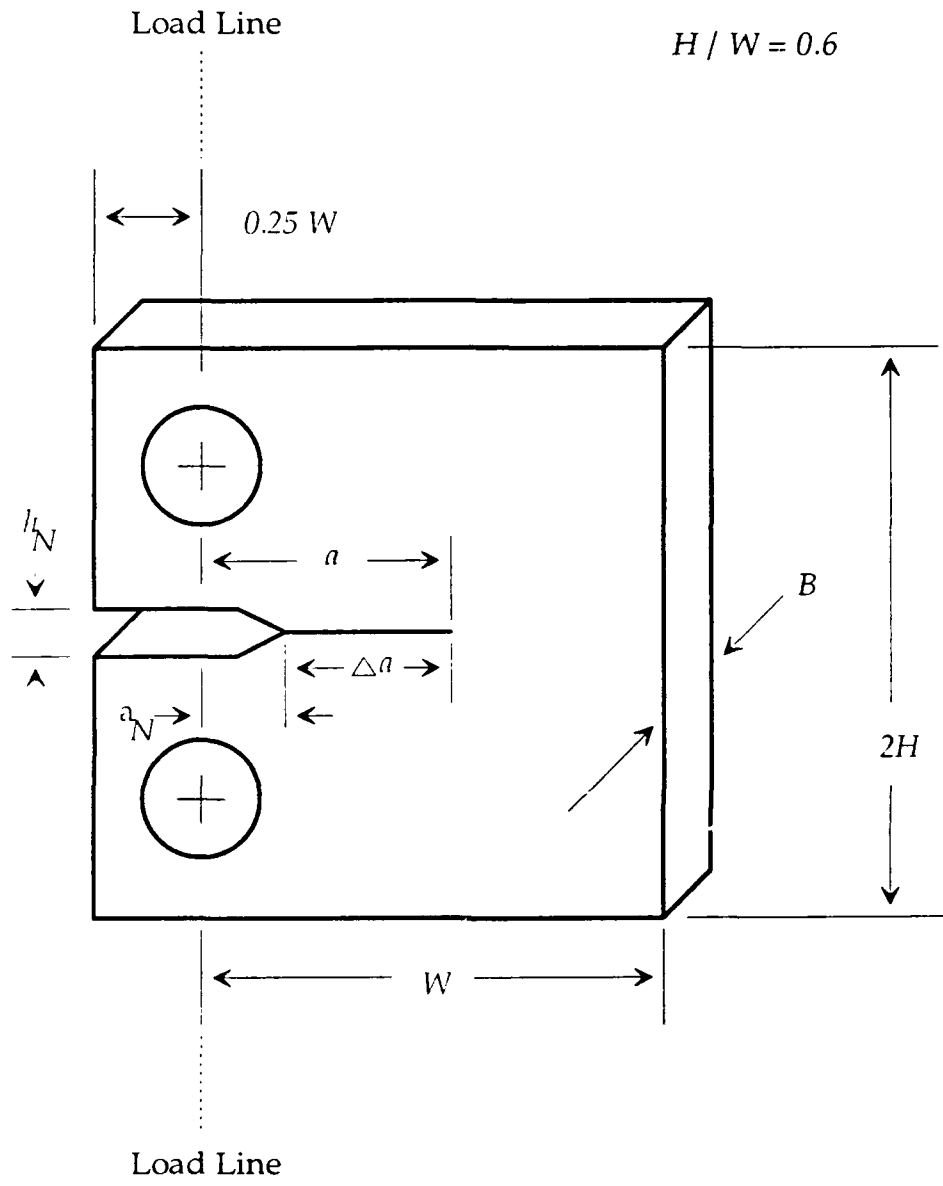
Figure 3.1 Compact Tension Specimen Dimensions

50

$$K = \frac{P(2 + \alpha)}{B \, W^{1/2} (1 - \alpha)^{3/2}} (0.886 + 4.64 \, \alpha - 13.32 \, \alpha^2$$

$$+ \; 14.72 \, \alpha^3 - 5.6 \, \alpha^4) \qquad (3.1)$$

where P is the appplied load, B is the specimen thickness, and W, is the specimen width [97]. The non dimensional crack length, α, is defined as:

$$\alpha = \frac{a}{W} \qquad (3.2)$$

where a is the crack length as shown in Figure 3.1.

Description of Test Equipment

The equipment used for the thermal-mechanical fatigue crack propagation study consists of devices that mechanically and thermally cycle the test specimen, and instruments that measure crack length. The mechanical loading is produced by a closed-loop servohydraulic loading system, and the temperature is maintained by both heating and cooling the specimen. The heating is provided by a radiant heating system consisting of four quartz lamp heaters, and cooling is produced by compressed air jets. The crack length is measured using an electrical potential drop technique, which is calibrated using visual measurements. A micro-computer is used to control each component of the system and acquire all the load, temperature, and crack

51

length data. All components are shown in Figure 3.2, and each system of components is discussed in more detail in the following sections. The components can be divided into four systems. These are:

1. mechanical loading system,

2. thermal loading system,

3. crack measurement system, and

4. computer control and data acquisition system.

The computer control and data acquisition system is discussed with the three other systems, since it is an integral part of these.

Mechanical Loading System

The major components of the system that mechanically load the specimen are shown in Figure 3.3. They include:

1) 44.48 kN MTS servohydraulic testing machine,

2) MTS 442 controller,

3) Wavetek model 75 programmable waveform generator, and

4) Zenith 248 micro-computer.
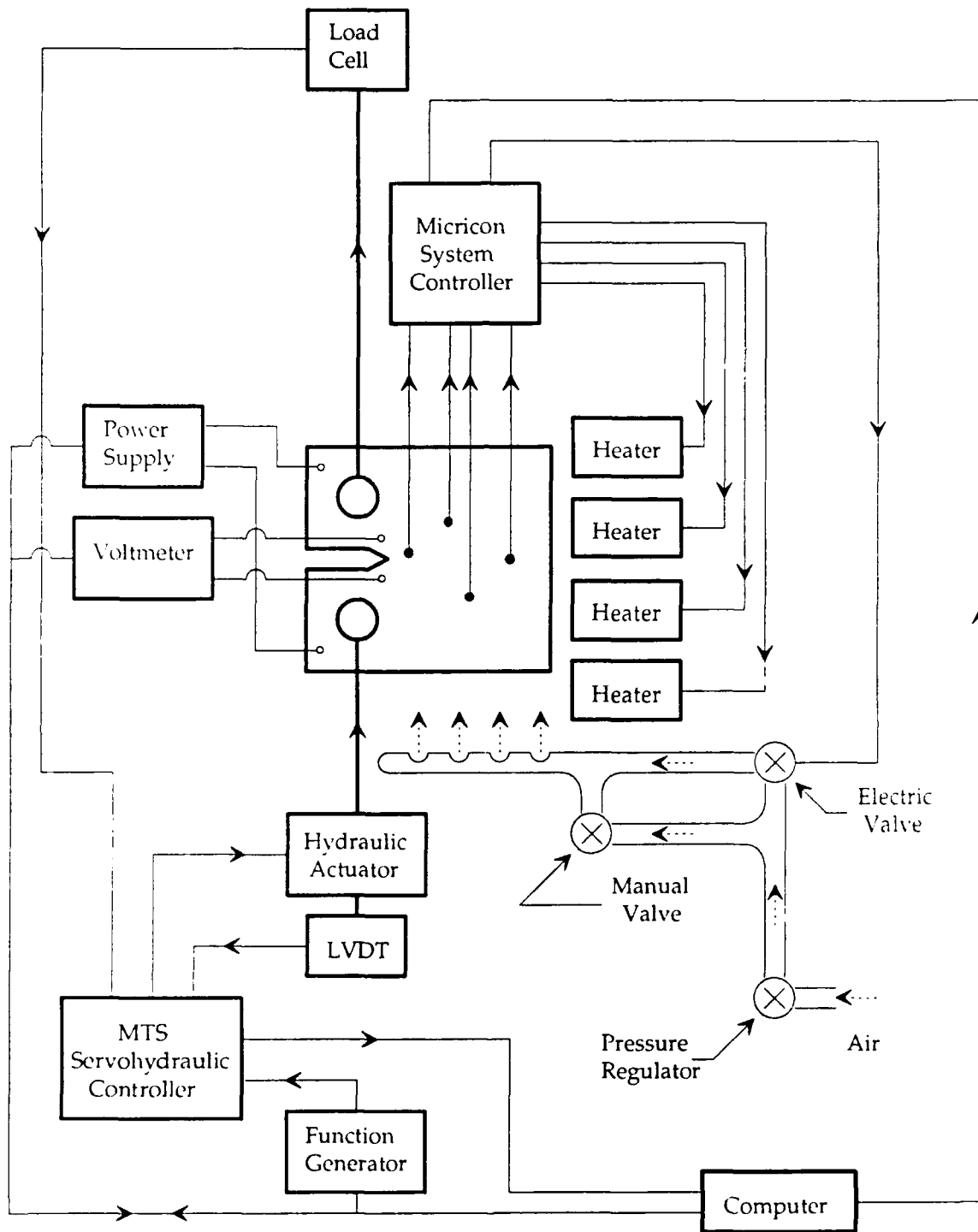
Figure 3.2 Thermal and Mechanical Loading Systems with
Computer Control and Data Acquisition

53

To load the specimen, the computer is programmed to send values of frequency, amplitude, offset, and wave shape to the waveform generator. Then the waveform generator transmits loading signals to the servohydraulic controller, and the controller loads the specimen in the servohydraulic testing machine. The MTS testing machine is operated in load control for all the tests performed in this study (i.e. the load cell signal is used for feedback to the controller); this type of control is discussed in Chapter II.

The load signal is used not only for feedback to the MTS controller, but also for computer control of the experiments. The computer uses the signal to adjust the load during a decreasing stress intensity test. This type of test is necessary to establish a crack in the specimen before the actual test is performed. These precrack tests are discussed later in this chapter. The computer uses the load signal also to maintain the required temperature-load phase. During tests that involve the cycling of both temperature and load, the computer checks and adjusts the phase of the cycle.

Modifications are made to the MTS load frame for high-temperature testing and electric potential crack length measurements. These include:

1) high-temperature clevises with clevis pin ceramic insulators,

2) water-cooled load frame extension rods,

3) water-cooled load cell heat shield, and

4) electric isolator.

54
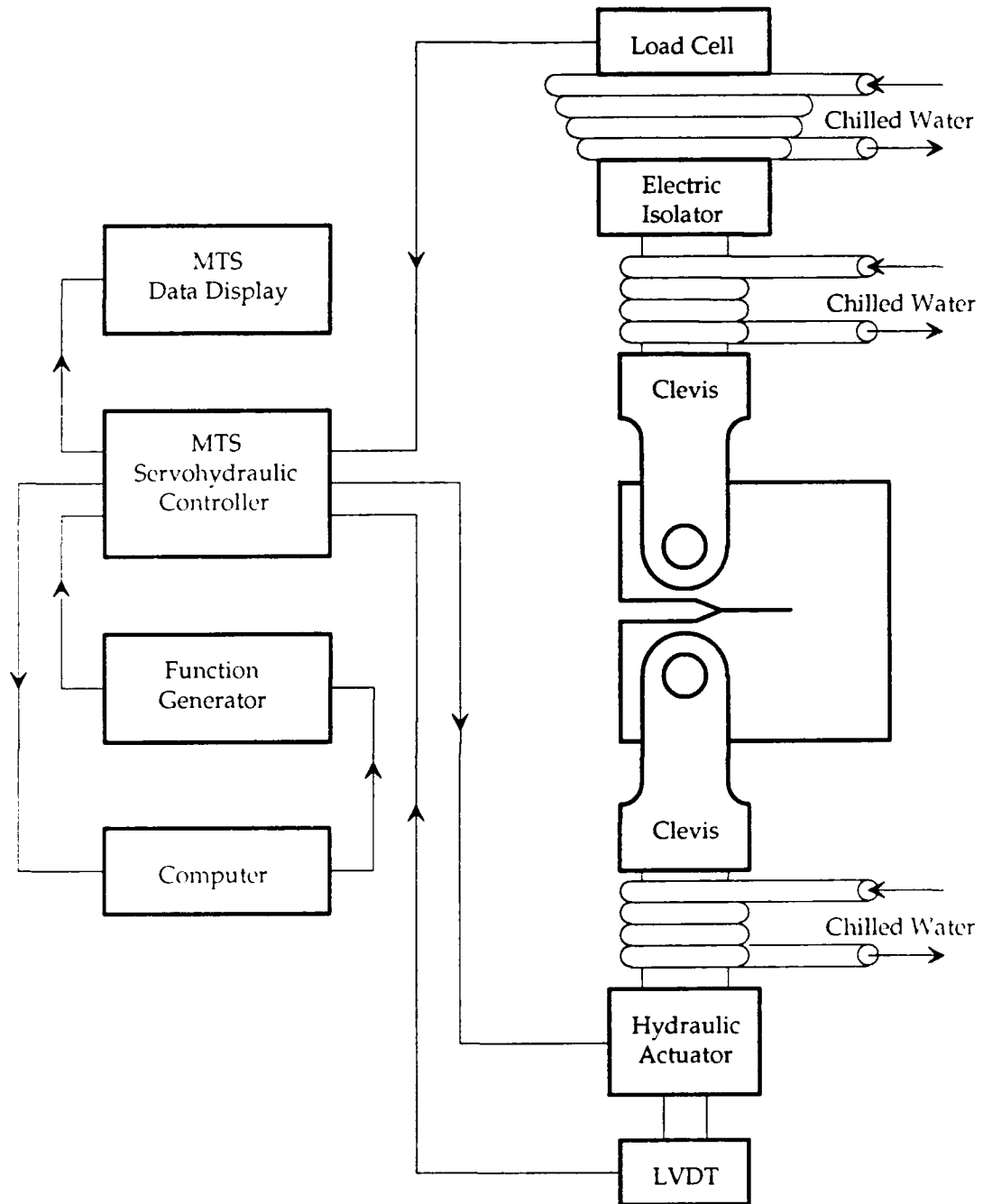
Figure 3.3 Mechanical Loading System

55

Initially, two clevises were manufactured according to the ASTM standard E 647 [97] using Rene' 41, a nickel-base alloy. The slot was then widened to allow for connection of the current leads that are used in the electric potential measurement of crack length. During preliminary experimentation involving thermal cycling of the specimen, the clevis, even with the slot modification, inhibited proper heating and cooling of the specimen. The slot in the clevis was not wide enough to allow the lamps to adequately cover the specimen, and this type of clevis acts as a heat sink and radiates energy back to the specimen during the cooling portion of the thermal cycle [54].

The clevis shown in Figure 3.4 is used to improve the temperature profile across the specimen [54]. The slot in new clevis is 10.16 mm wider and 32.77 mm longer than the modified ASTM-type clevis. This new type of clevis is machined from Inconel 718 according to the specifications shown in Figure 3.4, and allows for adequate heating and cooling of the specimens during thermal cycling. An actual thermal cycle is shown later in this chapter.

To reduce heating of the pins, ceramic insulators are utilized to prevent the lamp's direct radiant heat from contacting the clevis pins. These insulators, which are made from ceramic tubing, fit between the specimen and clevis, completely covering the pins. Since the insulators are of equal length, they also act as spacers, positioning the specimen in the center of the clevis slot.

30.48

40.64

34.29

95.25

50.8

5.08 R

5.08 R

Drill and
Tap Thru
(3/4 - 16 NF)

2 Holes
10.0076
Diam

10.16 R

5.08   20.32   5.08

5.08   30.48   5.08
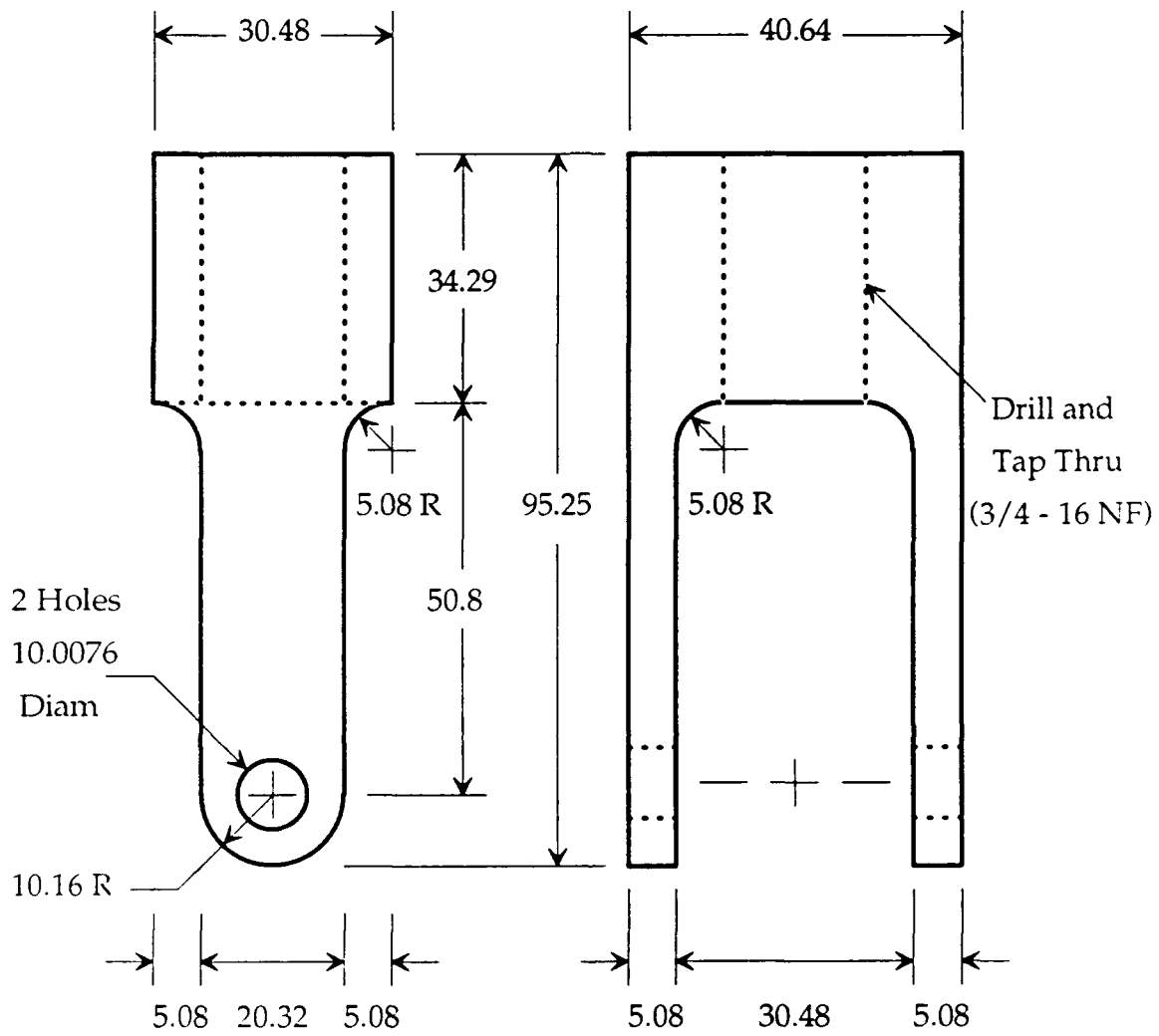
millimeters (inches)

Figure 3.4 Clevis Design Used in This Study

57

Two methods are used to reduce heating of the load cell: 1) the upper extension rod is cooled by passing chilled water through 6.35 mm (standard 0.25 in) copper tubing coiled around the rod to reduce conductive heat transfer, and 2) a water-cooled heat shield is mounted directly beneath the load-cell to reduce radiant and convective heat transfer. To protect the actuator piston from conductive heat, the lower extension rod also is water-cooled using the technique described above.

An electric isolator is connected between the load cell and upper extension rod to electrically isolate the upper portion of the specimen from the MTS load frame. This isolation is required for electric potential crack length measurement technique, which is discussed later in this chapter.

Temperature Control System

The components used for temperature control of the specimen are shown in Figure 3.5. The major components of the system are:

1) Four quartz lamp heaters,

2) Microprocessor-controlled and manually controlled cooling air,

3) Micricon 82300 process control system, and

4) Zenith 248 micro-computer.
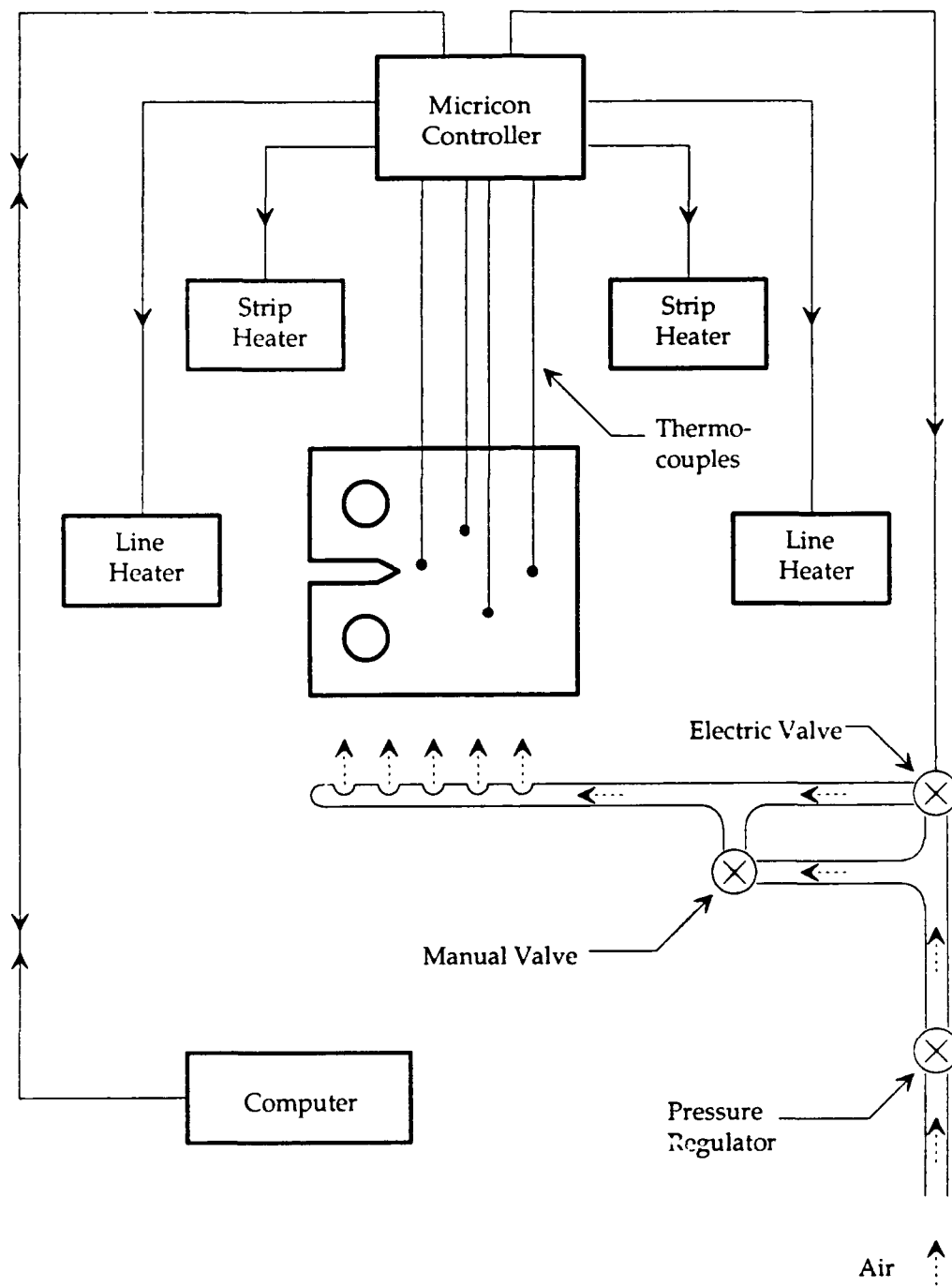
Figure 3.5 Temperature Control System

59

The specimen is heated with four quartz-lamp radiant heaters. The heaters use 1000-watt tungsten-filament quartz lamps that reflect radiant energy off a highly polished surface and onto the specimen. The specimen absorbs the infrared radiant energy and converts it to heat energy. A major advantage of this heating method is that the energy passes through the air without heating it; therefore, most of the energy is transmitted to the specimen. There is, however, a disadvantage in applying this heating method in the current study. In order for the lamps to operate most efficiently, the specimen should be dark and nonreflective to absorb more energy, but the specimens need to be highly polished for making visual crack length measurements [98]. These measurements are necessary for calibrating the electic potential technique to determine crack lengths, which is discussed later in this chapter.

The two front parabolic strip heaters are positioned horizontally and the two rear elliptical line heaters are positioned vertically. The regions of heat coverage are shown in Figure 3.6. The strip heaters produce a uniform heat distribution and are sufficient for regions one and two (Figure 3.6), but because of the geometry of the C(T) specimen, they are inadequate to heat regions three and four (Figure 3.6). A higher concentration of heat is needed near the clevis and near the outer edge of the specimen; therefore, line heaters are used to heat areas three and four to compensate for heat losses in these regions.

Back View

Zone 3 Zone 4

1.0
1.0

10.0 8.0

Front View

Zone 1

5.0

5.0

Zone 2

13.0

● thermocouple

(all dimensions in mm)
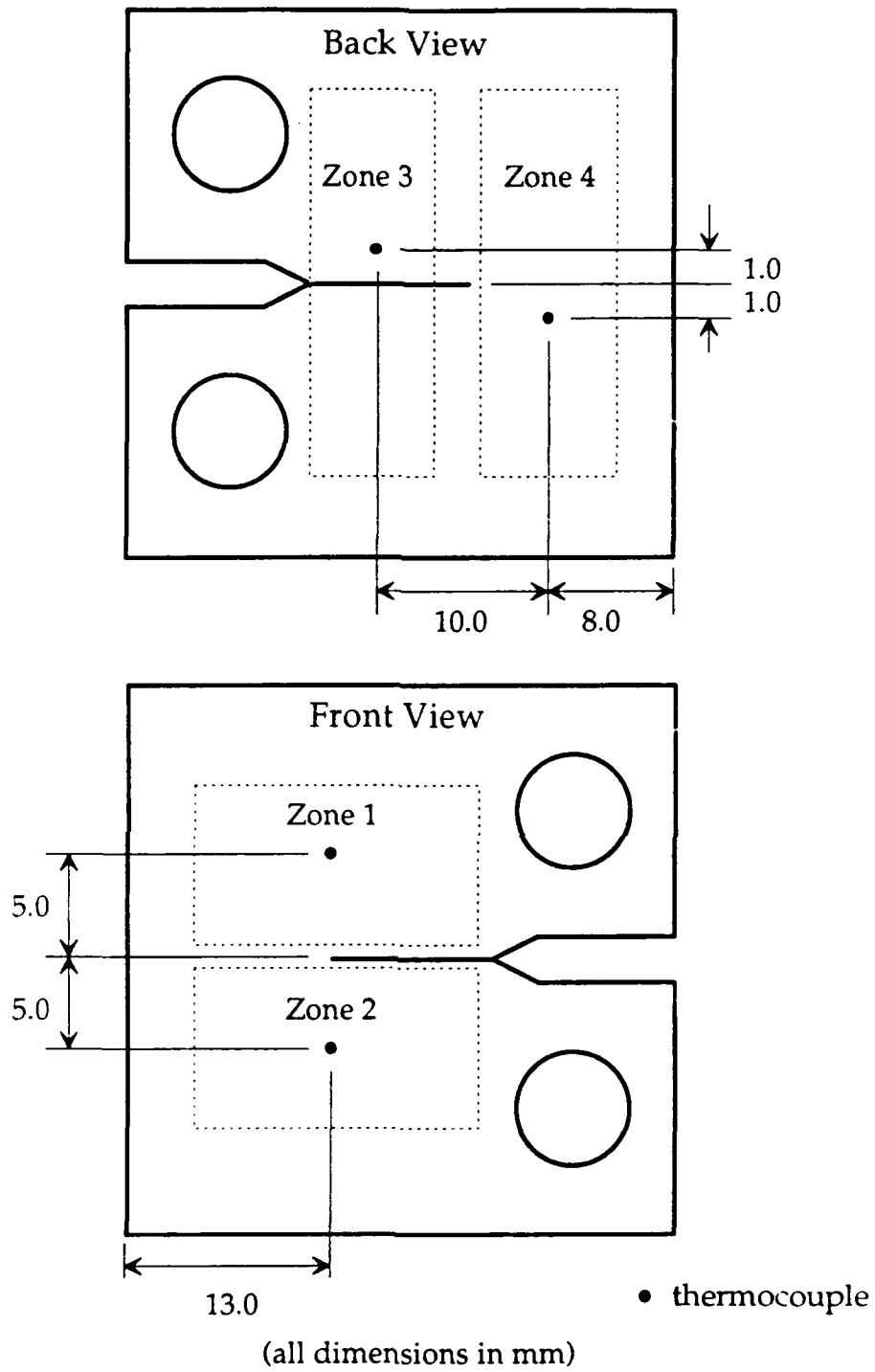
Figure 3.6 Areas of Coverage of Radiant Heaters and Thermocouple Locations

During temperature cycling, forced convective cooling is required to reduce specimen temperatures in the desired time. Jets of air are blown across the front and back of the specimen as illustrated in Figure 3.7. The airflow also is used during heating, since low levels of air flow during heating result in less temperature variation across the specimen. This two-level air flow is controlled by a combination of manual adjustments and microprocessor control. The system used to produce this air flow is shown in Figure 3.5. The manual valve is adjusted to achieve the desired level of air flow for the heating portion of the cycle, and during cooling, the microprocessor opens the electric valve, allowing secondary air flow to pass over the specimen. The air flow is regulated to provide consistent flow for the duration of the test. With this two-level cooling process, heating and cooling rates of 6.95°C per second are achieved (temperature ramps from 315°C to 649°C and back in 96 seconds).

A Micricon 82300 process control system is used to power the heating lamps and open and close the electric cooling-air value. Chromel-Alumel (type-K) thermocouples are used for feedback. The thermocouple wires are spot-welded to the specimen at the four locations as shown in Figure 3.6. The deviation between the actual and desired temperature is approximately equal to one percent during temperature cycling between 315°C and 649°C, and less than one percent during isothermal tests. A typical thermal cycle is shown in Figure 3.8. The temperature plotted here is obtained from a thermocouple located in the center of the four thermocouples used for feedback.
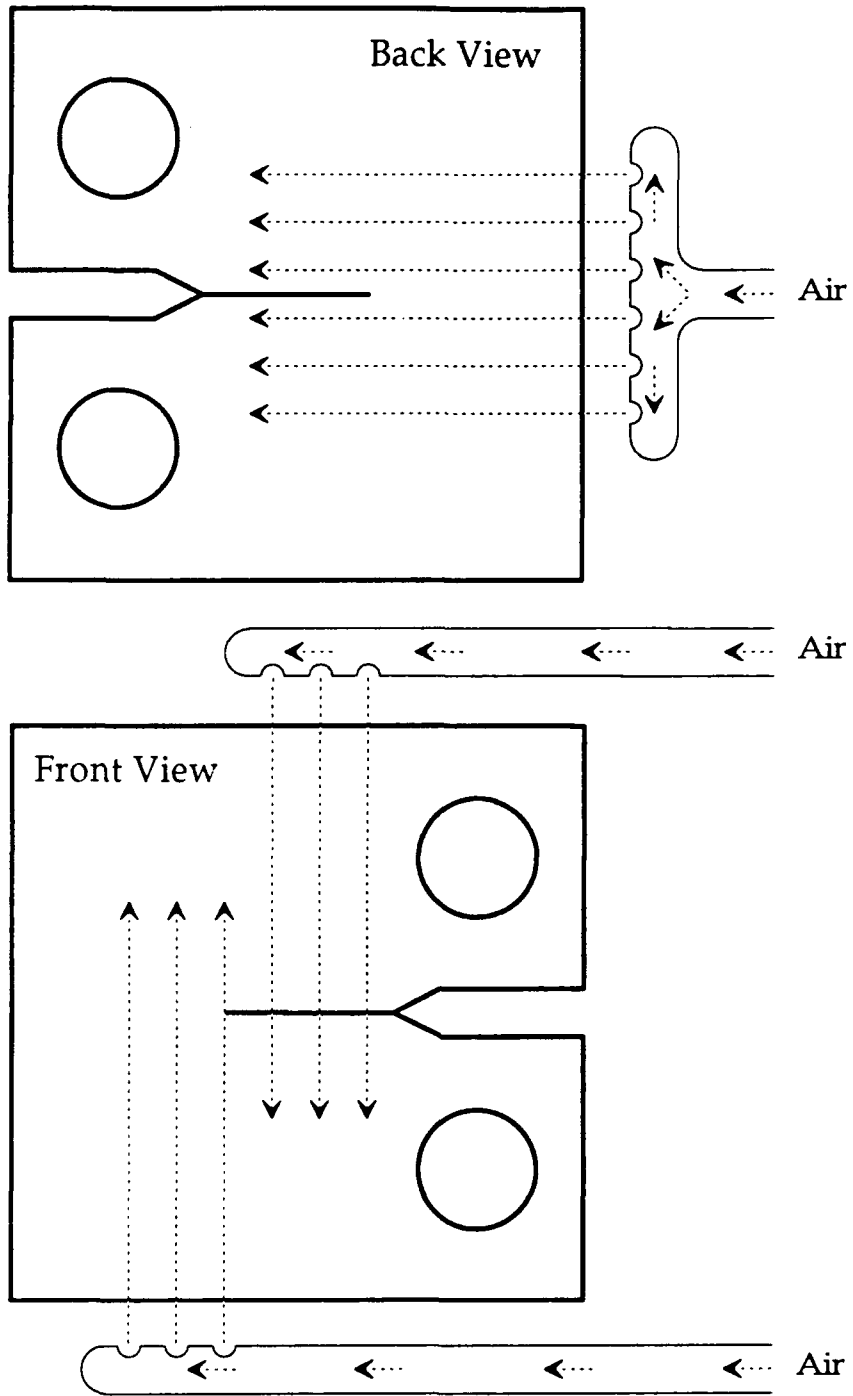
Figure 3.7   Air Jets for Specimen Cooling

63
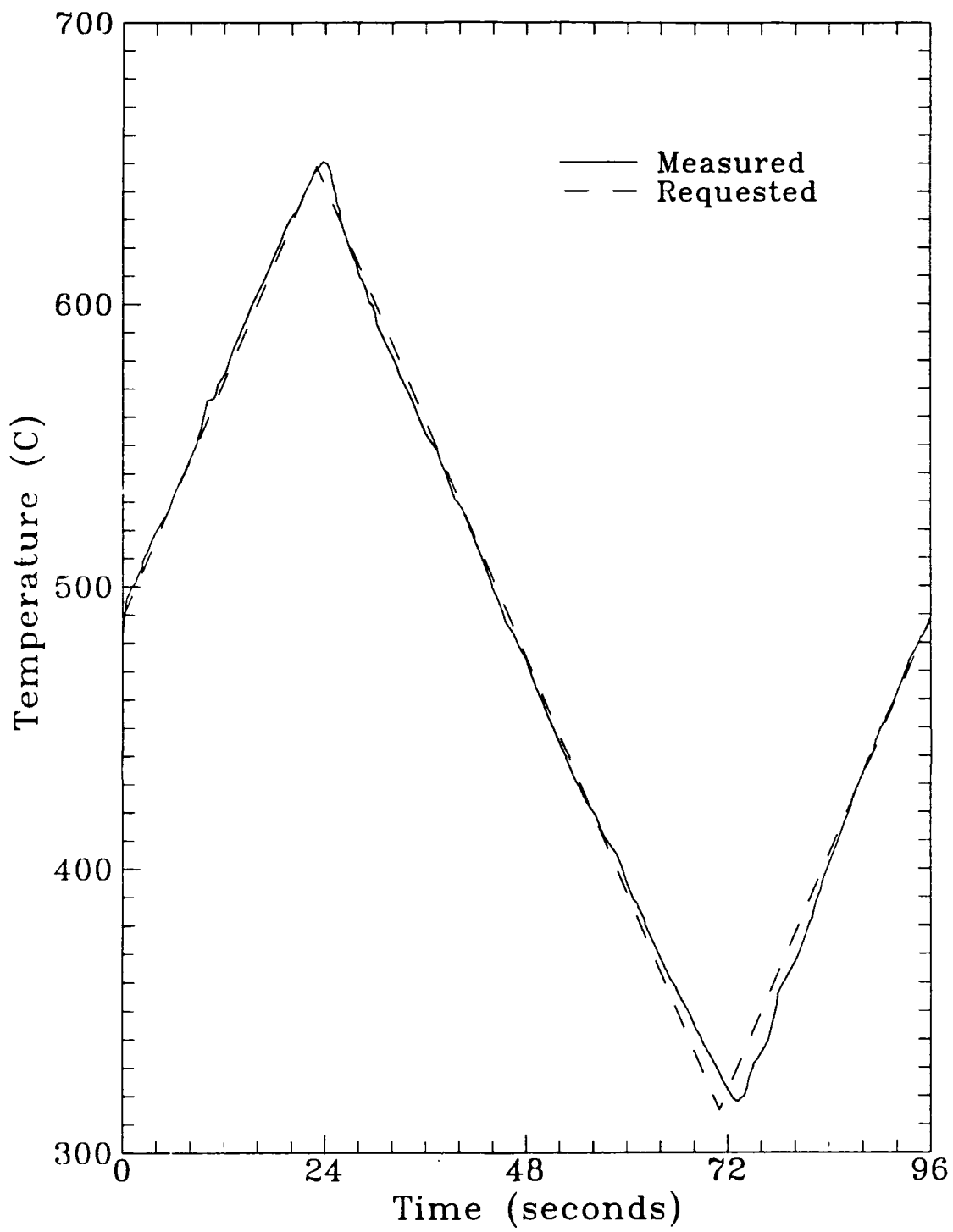
Figure 3.8 Typical Thermal Cycle Between 315 and 649°C

Crack Length Measurement System

Crack length is measured using the direct current (DC) electric potential drop method (also referred to as DC potential method). The devices used for DC potential crack length measurement are shown in Figure 3.9. Also, visual crack length measurements are needed to calibrate the electric potential crack length measurements. All components used in the measuring system are:

1) traveling telemicroscope with digital readout,

2) HP 6033A DC power supply,

3) HP 3456A digital voltmeter, and

4) Zenith 248 micro-computer.

In many previous studies, electric potential has been used to monitor crack length under isothermal conditions [99-103], and recently, this technique has been applied to thermal-mechanical fatigue studies [104]. The electric potential technique allows for continuous, accurate monitoring of crack length during testing at various temperatures and environmental conditions. This continuous monitoring is very useful for testing performed over long durations, which is the case for the current study; and is particularly important for tests involving the control of the stress intensity, K, instead of the load, P. K is not only a function of P, but also of crack length, a. The K-controlled testing is required for precracking specimens, and is discussed later in this chapter.

65
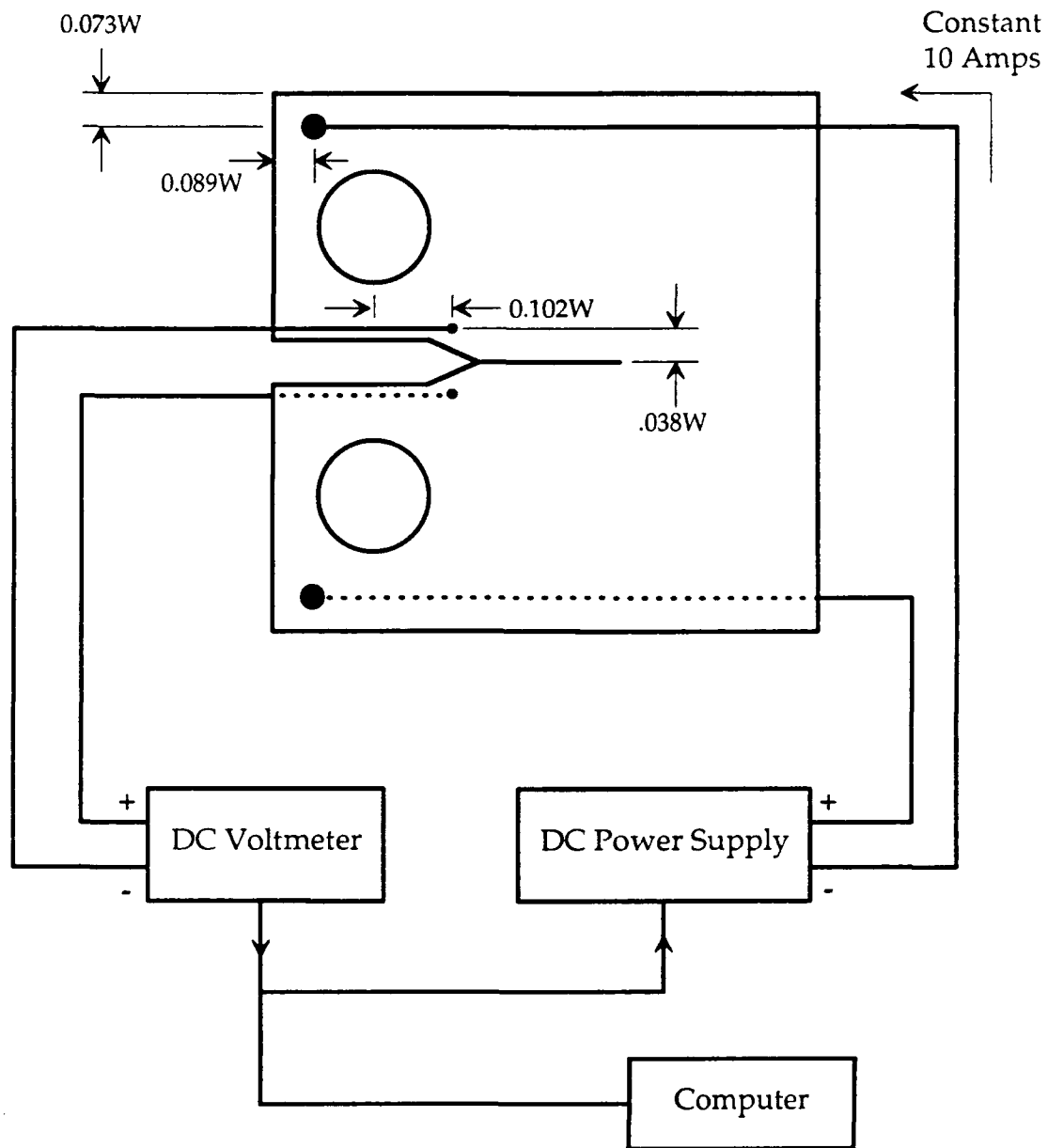
Figure 3.9 Electric Potential Crack Length Measurement System

66

Using the electric potential technique, crack length is measured by passing a constant current through a test specimen creating a potential field. In general, this field is a function of applied current, specimen geometry, material resistivity, current lead position, electric potential measurement lead position and crack length [101]. Then, as the crack in the specimen extends, the voltage drop across the crack region increases as a result of the increased resistance. This increase in resistance is a result of the reduction in remaining specimen area. The voltage (potential) across the crack is measured and related to crack length. The closed-form solutions for crack length exist for simple specimen geometry, such as the center-crack-tension specimen [99], but for a complex specimen geometry, such as the C(T) used in this study, an empirical relationship must be utilized. The calibration of the electric potential measurement technique with visual crack length measurements is discussed in the following section of this chapter.

For the C(T) specimen utilized in this study, the current and DC electric potential measurement leads are connected to the specimen as illustrated in Figure 3.9. The two current leads are bolted to the specimen in the upper and lower corners near the clevis pin holes, with the upper lead in front and the lower lead in back. 12-gauge solid copper wire is used for this purpose. Two nichrome-wire DC potential measurement leads are spot welded close behind the initial crack at the notch, with the upper lead in front and the lower lead in back (Figure 3.9).

67

This DC potential measurement lead placement is required to measure the potential drop in a controlled-temperature region on the specimen. The resistivity of the material is a function of temperature; therefore, errors could result if potential readings are not taken in a temperature-controlled region. This lead placement differs from the more typical way of measuring the voltage drop on the front face of the C(T) specimen [105-107].

The DC potential measurement lead placement shown in Figure 3.9 is advantageous since it not only reduces temperature effects, but also is more sensitive to crack extension than if the leads are placed on the front face [108, 109]. However, this placement creates an additional concern. The lines of constant potential are very concentrated near the notch; therefore, the measured voltage is very sensitive to lead placement in this region [108, 109]. This sensitivity in voltage measurement can result in crack length measurement errors if the DC potential lead placement changes from specimen to specimen. Since it is impossible to weld the leads in exactly the same place for every specimen, some errors do occur. To reduce the errors resulting from slight misplacement of the DC electric potential measurement leads, an offset expression [110] for crack length is used rather than the more-widely used ratio expression [111]. In functional form the ratio solution can be expressed as:

$$a/a_0 = f(V/V_0) \qquad\qquad (3.3)$$

and the offset solution can be expressed as:

$$a = g(V + V_0) \qquad\qquad (3.4)$$

where a is the instantaneous crack length corresponding to the DC electric potential measurement, V, and a_0 is the initial crack length corresponding to the initial potential, V_0. The calibration of this offset solution is discussed in the following section.

Before the calibration of the DC potential crack length measurement system is discussed, some additional concerns about using the electric potential system are considered here including: temperature dependence of material resistivity, crack closure effects, and thermal EMF effects.

As discussed previously, the resistivity of the material is dependent on temperature, and the electric potential measurement leads are placed within a temperature-controlled region to reduce temperature variations. Since temperature varies during the cycles, electric potential readings used for crack length measurements always are taken at the same temperature during the entire test. To prevent the effect of crack closure on the measured electric potential, readings are always taken near the maximum load, but slightly before any dramatic temperature variations.

69

The thermal EMF is subtracted from the electric potential measurements to reduce the error associated with EMF. Since thermal EMF remains when there is no current flowing through the specimen, the EMF can be measured easily. When the current is introduced into the specimen V_{tot} is read on the voltmeter, and when the current is removed, V_{emf} is measured. Then the corrected DC electric potential measurement is expressed as:

$$V = V_{tot} - V_{emf} \qquad (3.5)$$

where:

V is the value of potential that has been corrected for thermal EMF,

V_{tot} is the total potential (value of potential with the current on), and

V_{emf} is the EMF voltage (value of potential with the current off).

Calibration of DC Potential Crack Length Measurement

In this section, the process used to calibrate the electric potential crack length measurement system is discussed. As mentioned previously, there is no closed-form relationship between crack length and voltage (potential) for the C(T) specimen geometry. An offset voltage solution (i.e. $g(V+V_0)$) is used to define crack length. The function g is related to DC potential, material conductivity, specimen width, and applied current using the following expression:

$$g = \frac{\kappa \ W \ (V + V_0)}{I} \tag{3.6}$$

where:

κ is the material thermal conductivity,

W is the specimen width,

I is the applied current,

V is the instantaneous corrected DC potential, and

V_0 is the corrected DC potential corresponding to the initial

crack length, a_0 ,

An empirical expression was developed [110] that relates α to the function g

for the C(T) geometry and lead placement shown in Figure 3.9. This

expression is:

$$\alpha = 7.710 \times 10^{-3} + 2.214 \times 10^{-1} \ g + 2.641 \times 10^{-2} \ g^2 - 6.916 \times 10^{-3} \ g^3 \tag{3.7}$$

where α is the non-dimensional crack length (i.e. a/W). W, I, V, and V_0 in

Equation (3.6) are either known or measured during the experiment, and the

only parameter that needs to be determined is the material conductivity, κ. In

order to determine the value of κ at a given temperature, the following

iteration must be utilized. After a test is completed and various values of α

and corresponding values of V are known, an iteration of κ and V_0 is

performed to determine the best fit for the experimental data. The values of α

used in the iteration are determined using optical measurements obtained with

a Gaertner telemicroscope and a 0.001 mm resolution digital position readout.

These measurements are performed during a constant-load experiment, where

the crack length is not required for control. The DC potential readings are

converted to crack length for these calibration tests after the tests are

completed. For majority of the tests where data is sampled at 649^0C, κ is

approximately equal to 5.2×10^5 (Ohm-m)$^{-1}$. κ varies slightly with changes in

test temperature (i.e. κ is equal to 4.9×10^5 (Ohm-m)$^{-1}$ for a test where data is

sampled at 482^0C). Figure 3.10 shows a set of visual crack length and DC

potential data used to determine κ at 482°C for Ti-24Al-11Nb. In this figure, α

is plotted against the corrected DC potential, V, where the third-order

polynomial curve fit is obtained by substituting Equation (3.6) into Equation

(3.7) and V is the only independent variable, since κ, W, I, and V_0 are constant

throughout the test. This polynomial is expressed as:

$$\alpha = 4.597 \times 10^{-2} + 2.918 \times 10 \; V + 2.800 \times 10^2 \; V^2 - 1.172 \times 10^4 \; V^3 \qquad (3.8)$$

After κ is determined for these test conditions using the iteration

described above, the DC potential, V, versus cycle count, N, data are converted

to a versus N data using Equation (3.8). Figures 3.11 and 3.12 show,

respectively, the measured V versus N data from a 482°C test and the
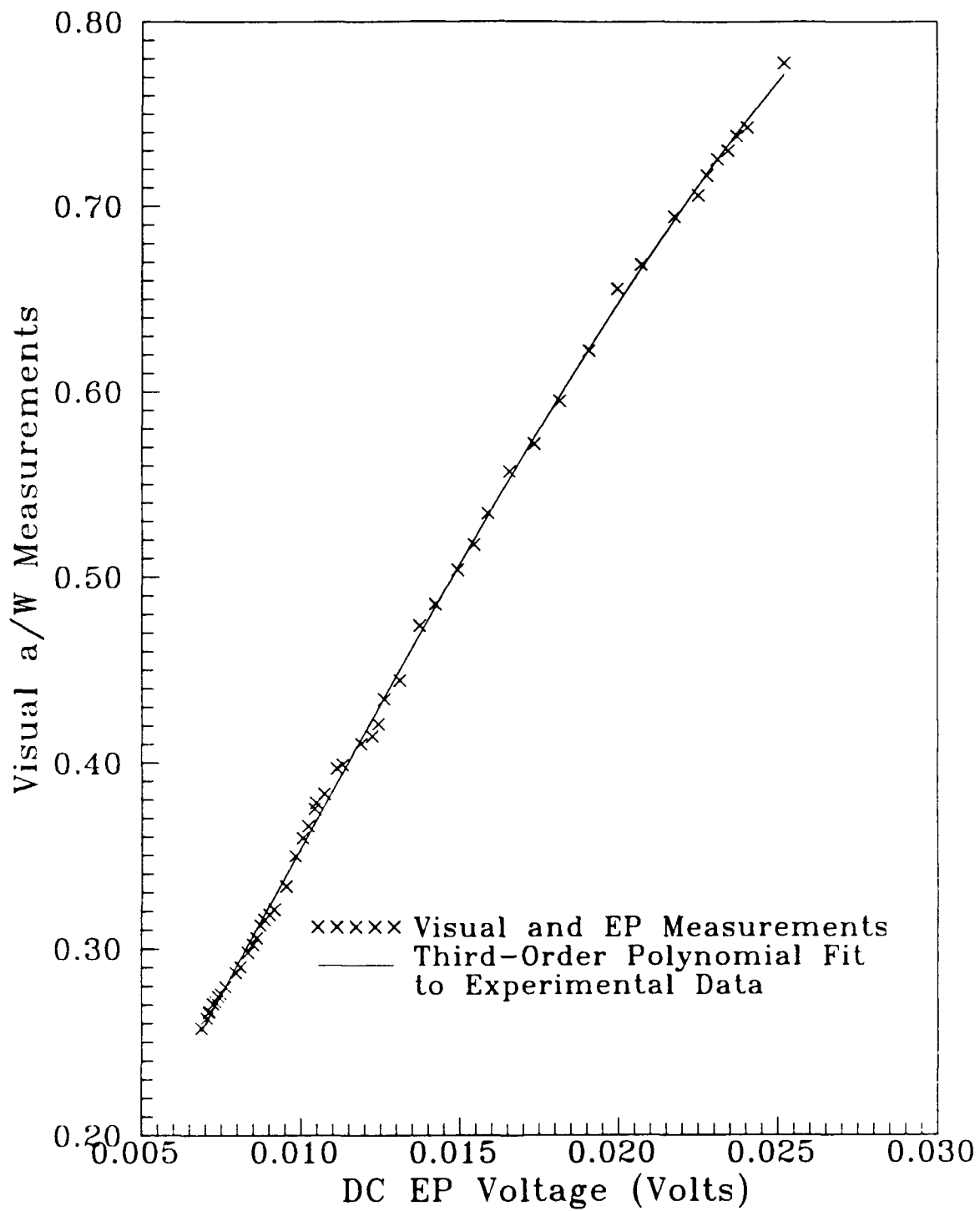
Figure 3.10 Visual a/W measurements and DC Potential Data
Used to Determine κ at 482°C for Ti-24Al-11Nb

73
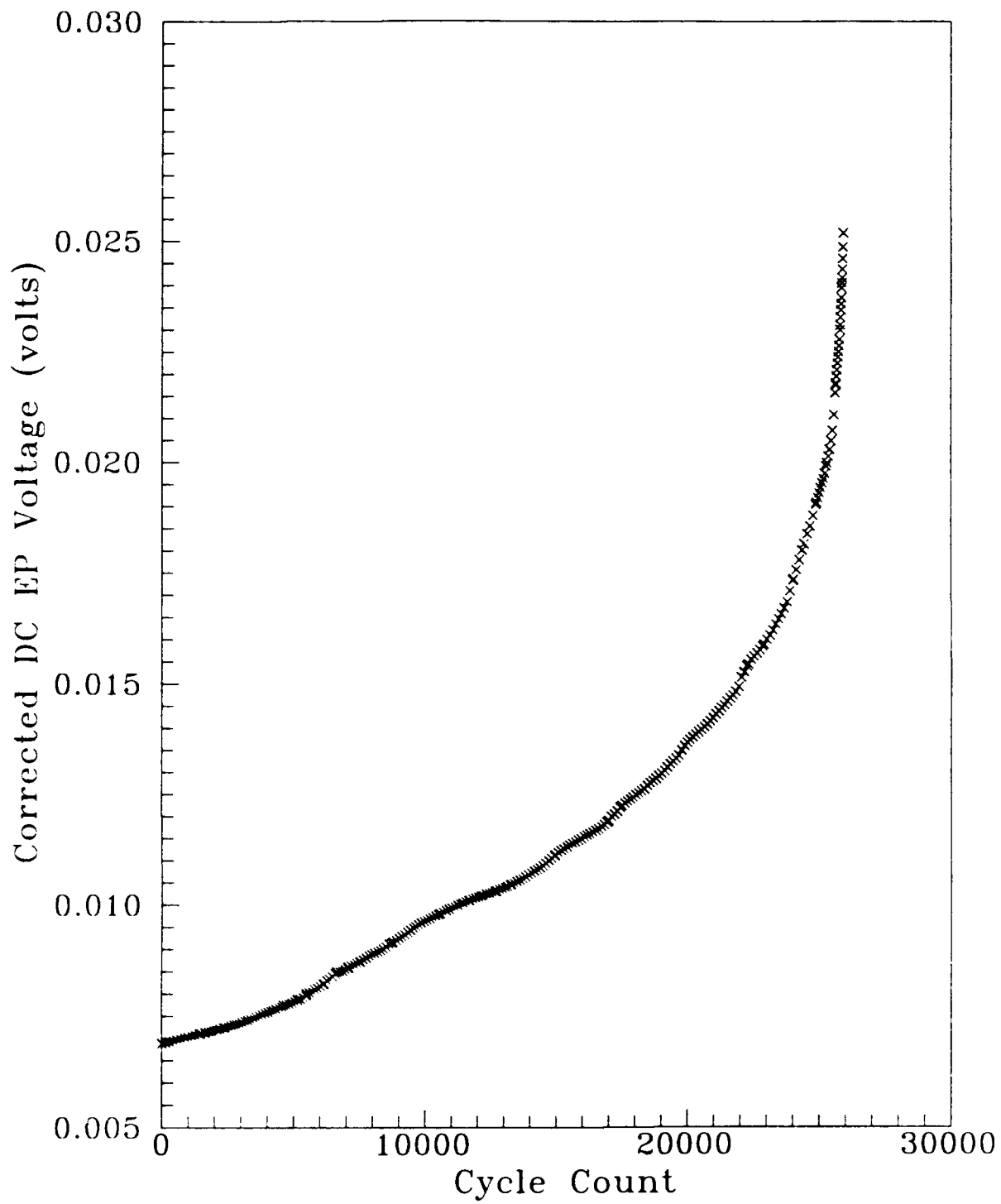
Figure 3.11 Corrected DC Potential Versus Cycle Count from a 482°C Test

74
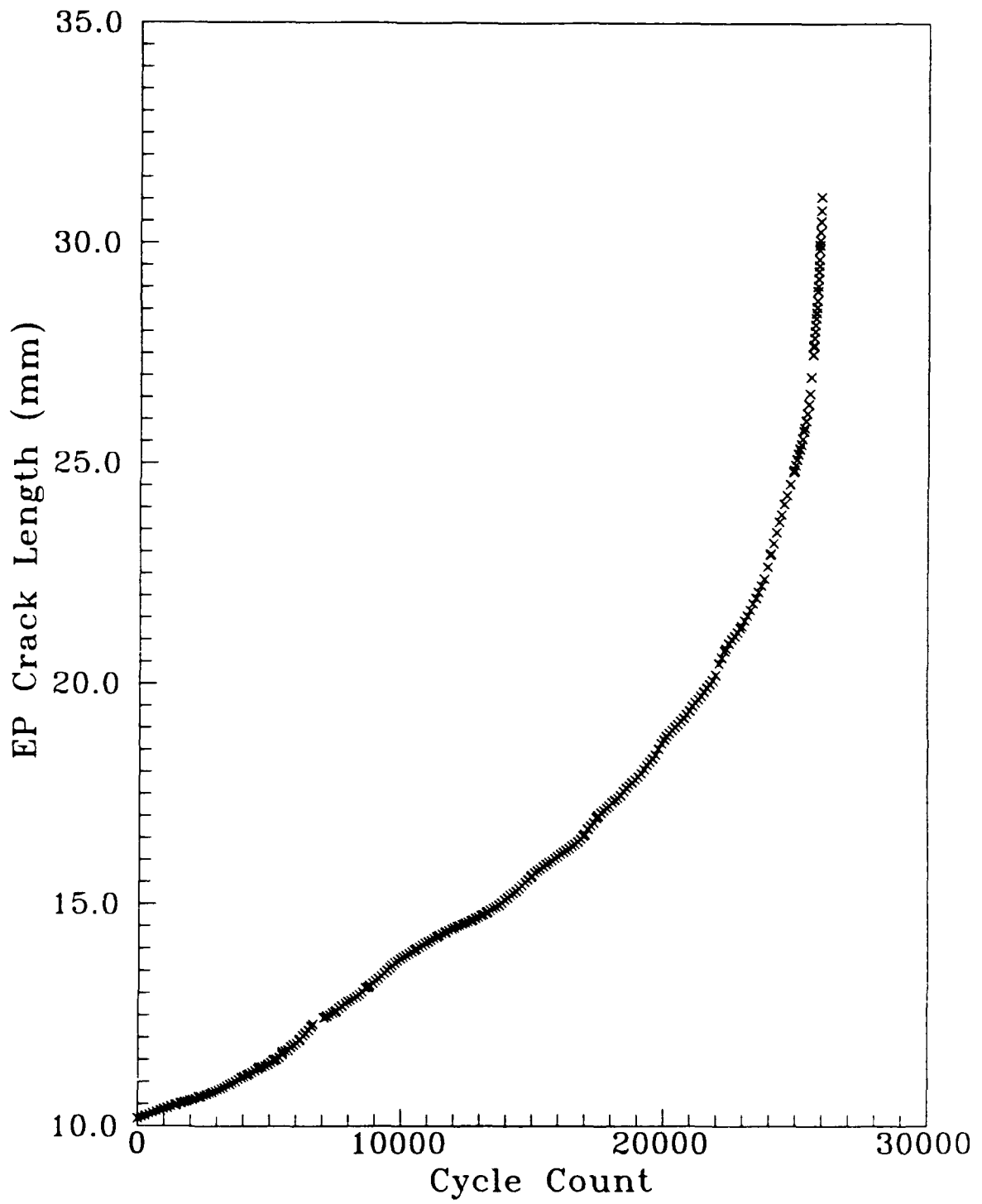
Figure 3.12 Crack Length Versus Cycle Count from a 482°C Test

corresponding converted a versus N data. After κ is known for a specific material (in this case, Ti-24Al-11Nb) at a given temperature, crack lengths are determined as the experiment proceeds, and a versus N data is obtained.

The a versus N crack growth rate data obtained during the tests is then reduced to the da/dN versus ΔK form for crack growth rate comparisons, and the technique used for this data reduction is discussed later in this chapter.

Procedure for Precracking Specimens

Before any crack growth test can be performed, a sharpened fatigue crack must be established in the specimen; this is referred to as precracking the specimen. Precracking the specimen insures that the effect of the starter notch is removed, and must be performed such that subsequent crack growth rate data is not effected by the precrack load history [97]. Precracking the specimen is performed by loading the specimen at high frequency with a maximum load large enough to initiate a crack; then reducing the maximum load to a level that is less than or equal to that of the experiment to be performed (i.e. the final K_{max} of precracking is less than or equal to the initial K_{max} of the test).

Precracking is performed on all the specimens in this study within the guidlines set by ASTM Standard E 647. The rate at which load is shed during precracking (from initial P_{max} to final P_{max}) is no more than 20 percent, and the final values of K_{max} and ΔK from precracking are equal to the initial values of

76

K_{max} and ΔK for the specified test. A typical plot of maximum load versus crack length for a precrack is shown in Figure 3.13. After the specimens are precracked, they are used for isothermal fatigue, isothermal fatigue with superimposed holds at P_{max}, and thermal-mechanical fatigue testing as described in Chapter IV.

Data Analysis Techniques

The crack length data sample intervals, which are used during the tests performed in this study, are discussed in this section. Also, the techniques used to reduce the crack length measurement and cycle count data to crack growth rates are presented here, including the data obtained from constant P_{max} and constant K_{max} tests.

Data Sampling Intervals

When the fatigue crack growth experiments are performed, ASTM E 647 [97] recommends the following crack length measurement intervals:

$$\Delta a \leq 0.04 \ W \ ; \ \textit{for } 0.25 \leq a/W \leq 0.40$$
$$\Delta a \leq 0.02 \ W \ ; \ \textit{for } 0.40 \leq a/W \leq 0.60 \quad (3.9)$$
$$\Delta a \leq 0.01 \ W \ ; \ \textit{for} \qquad a/W \geq 0.60$$

where Δa is the interval between crack length measurements. With the recommended intervals shown in Equation (3.9) the crack growth rates, da/dN,

77
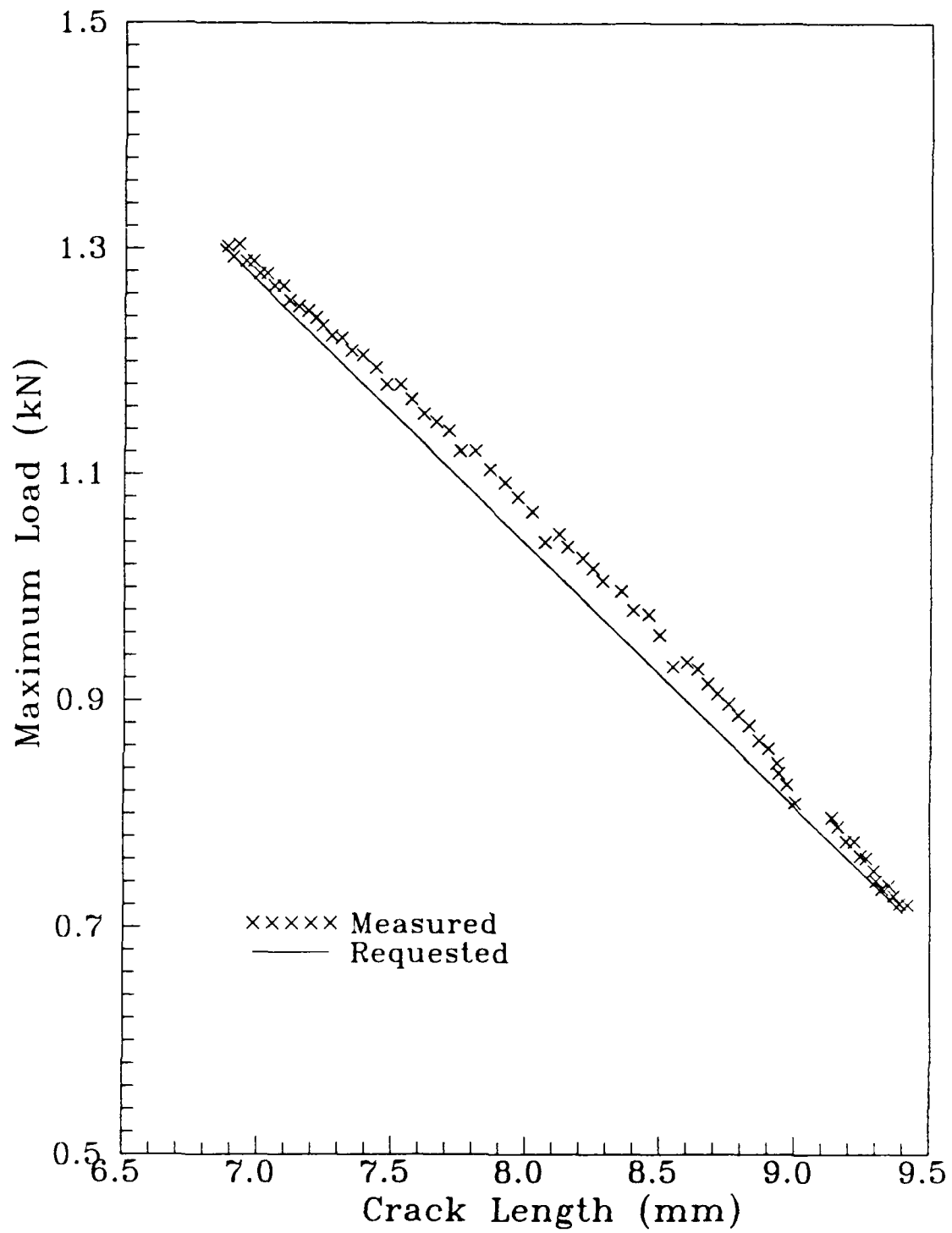
Figure 3.13 Plot of Maximum Load Versus Crack Length for a Precrack

are nearly evenly distributed with respect to ΔK [97]. Also, the minimum Δa must be ten times the precision of the measuring instrument.

During the thermal-mechanical fatigue experiments in this study, the a versus N data must be obtained much more often than recommended, particularly at low values of a/W. This excessive data sampling is required to maintain the proper phase angle between the temperature and load cycles, since every time data is acquired during the experiment, the load-temperature phase angle is checked, and adjusted if necessary. Data samples are taken at either a crack extension interval, Δa, equal to 0.05 mm or at a time interval, Δt, equal to 3,600 seconds, whichever is smaller. Early during a fatigue experiment, the growth rates, da/dN, are typically on the order of 1×10^{-7} meters. Since the total cycle time for the thermal-mechanical fatigue experiments in this study is 96 or 144 seconds, the Δt data sample interval is used during this portion of the test, and a large number of samples is obtained. When using standard methods of reducing the a versus N data, such as those recommended by ASTM [97], the growth rates are not spaced equally with respect to ΔK.

Constant Maximum Load Data Reduction

ASTM E 647 [97] recommends that the a versus N data from a constant P_{max} test be reduced to da/dN by either the secant method or incremental-polynomial method. The secant method calculates da/dN by fitting a straight

line between two consecutive points on the a versus N curve. The incremental-polynomial method, which is the more preferred method, calculates da/dN by fitting a second-order polynomial to consecutive sets of $(2n+1)$ data points on the a versus N curve. The value of n is typically equal to three, which provides seven consecutive data points for the calculation of da/dN; therefore, it is commonly referred to as a seven-point fit.

The standard seven-point data reduction scheme cannot be used effectively for the a versus N data obtained in this study, since large quantities of data are obtained, particularly for lower crack growth rates. Large errors could result from reducing a versus N data when no significant crack extension has occurred between data samples. Also, Δa is approximately constant at the intermediate-to-large crack growth rates, but since ΔK increases during constant P_{max} tests, the reduced data would not be spaced equally with respect to ΔK. Therefore, an alternate method is employed when reducing the data.

The alternate data reduction scheme used in this study was developed by Larsen [112]. This method of data reduction is referred to as a modified-incremental-polynomial approach [113]. A schematic representation of the modified-incremental-polynomial method for reducing crack growth data is shown in Figure 3.14. This method implements the recommendations of ASTM E 647 [97], with a significant modification. Instead of performing incremental regression to successive groups of data (i.e. typically seven data points) the modified-incremental-polynomial technique uses crack extension,

80
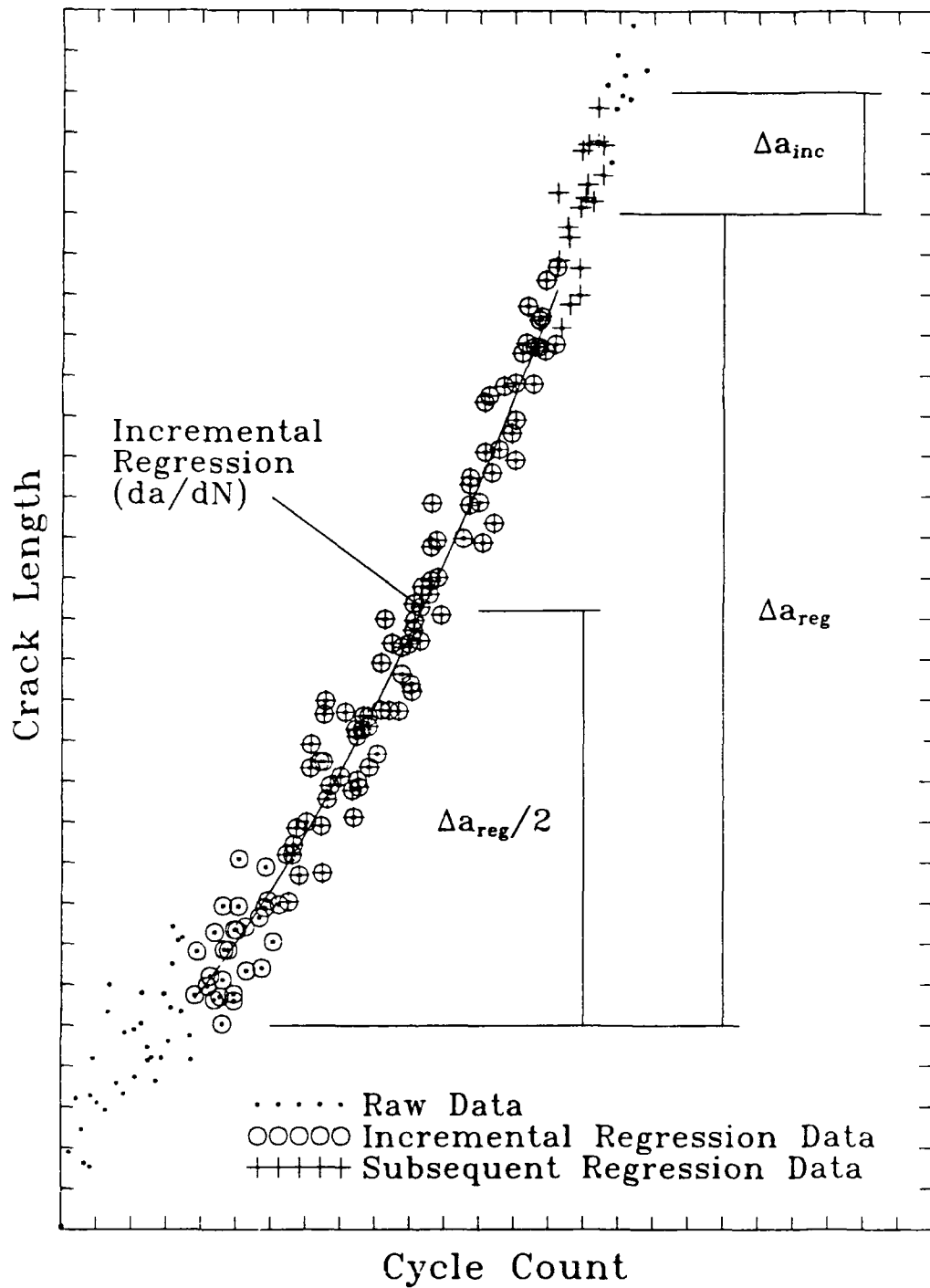
Figure 3.14 A Schematic Representation of the Modified-Incremental-Polynomial Method for Reducing Crack Growth Data

81

Δa_{reg} , when selecting data for regression analysis to obtain da/dN from the a versus N curve [113]. Successive regressions are incremented by Δa_{inc} , where Δa_{inc} is defined as:

$$\Delta a_{inc} = \frac{\Delta a_{reg}}{6} \qquad (3.10)$$

where Δa_{inc} is the increment between successive local regressions and Δa_{reg} is the crack length interval over which the regressions are performed. These local regressions are repeated over defined regions of Δa_{reg} unless the number of data points within that region is less that a prescribed value. In this case, seven is used as recommended by ASTM E 647 [97]. One of the main advantages of using this method over deleting a versus N data points to meet ASTM recommendations for data reduction is that the modified-incremental-polynomial technique uses all the acquired data during analysis [97].

The advantage of using the modified-incremental-polynomial method of data reduction as opposed to a standard seven-point fit is shown by comparing Figures 3.15 and 3.16. In Figure 3.15 a seven-point data reduction scheme is used according to ASTM E 647 [97]. There is large scatter in the data, particularly at the lower growth rates since there is a small Δa in this region. In Figure 3.16 the modified-incremental-polynomial data reduction method is used. The da/dN data in this figure are distributed evenly with respect to ΔK and there are less data points as a result of the process used to

82
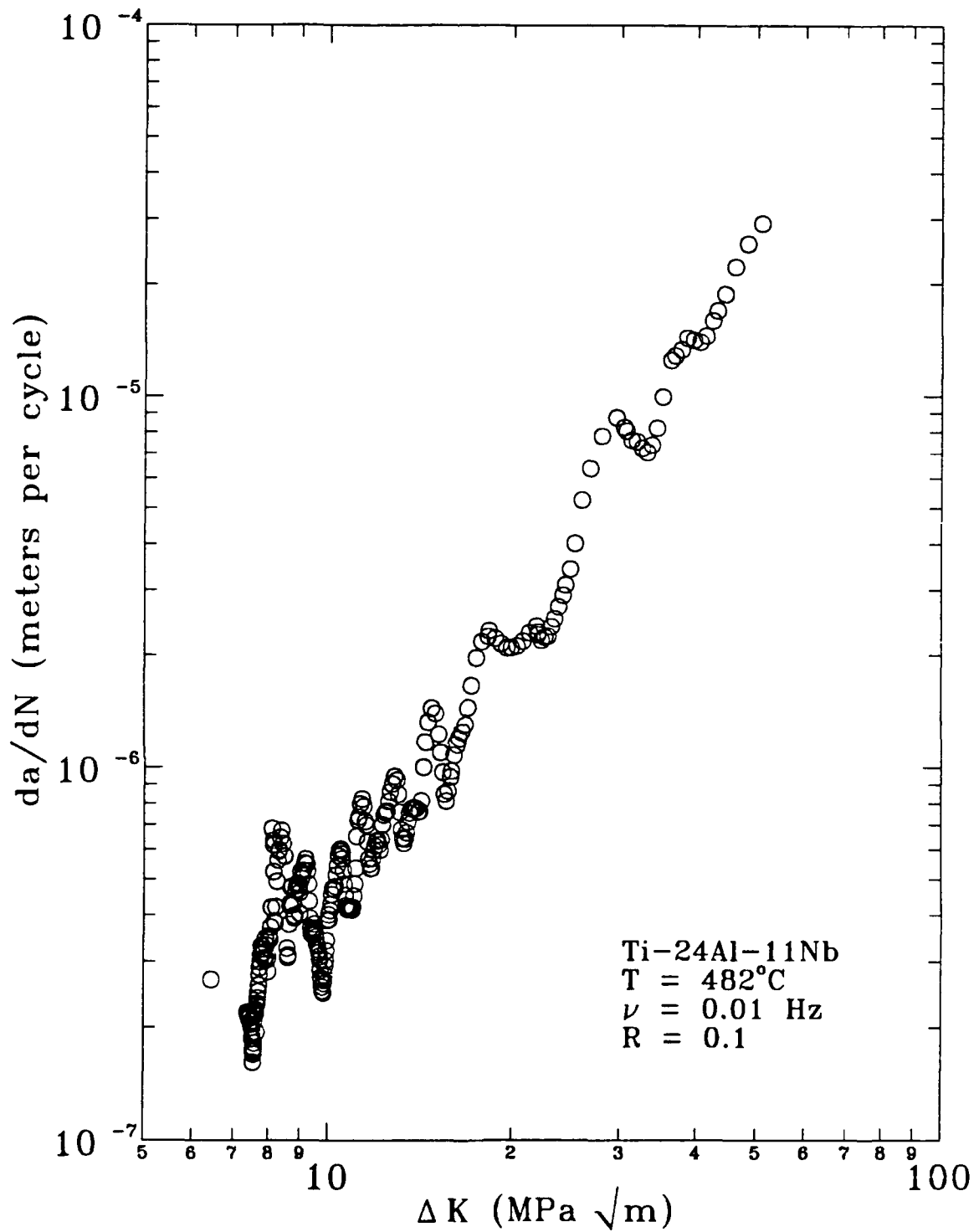
Figure 3.15 Data Reduced with the Standard Seven-Point Scheme

83
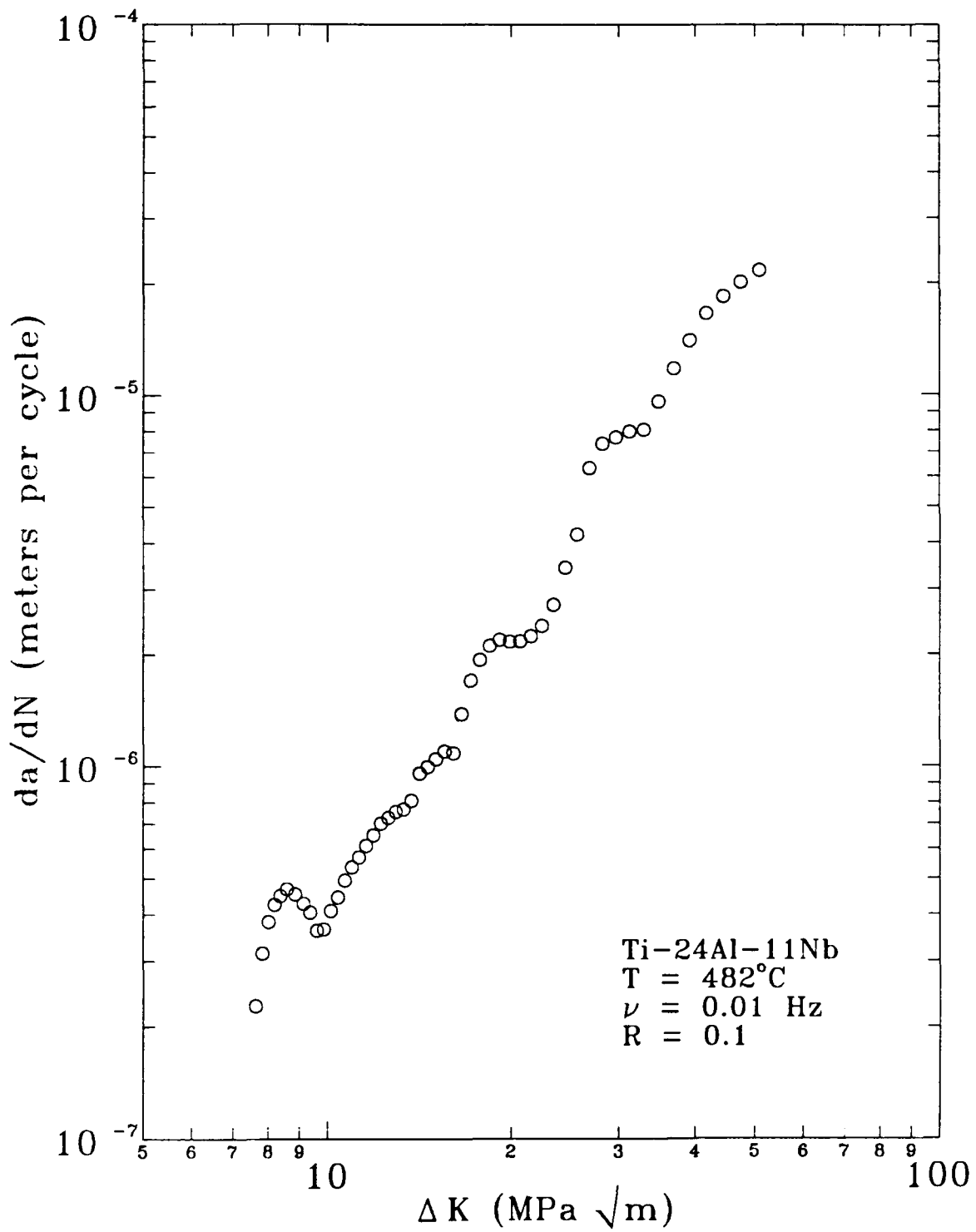
Figure 3.16 Data Reduced with the Modified-Incremental-Polynomial Scheme

select data for reduction. For all of the constant P_{max} tests performed during this study, this technique is employed with Δa_{reg} equal to 0.4 mm. These reduced data are presented in Chapter IV.

Constant Maximum Stress Intensity Data Reduction

In the experiments in which constant K_{max} control is utilized, the data samples are taken at crack extension intervals, Δa, which is approximately equal to 0.05 mm. These tests are performed for a total crack extension of at least 1.0 mm; therefore, at least 20 crack length measurements (data samples) are taken. The load is shed every time a measurement is taken to maintain a constant level of K_{max}. With the exception of the first few data points, the a versus N data form a straight line, which implies the crack growth rate, da/dN, (slope of the a versus N data) is approximately equal to a constant.

A fifteen-point polynomial, is employed to reduce these data. Using this method, da/dN is calculated by fitting a first-order polynomial to the last fifteen points of the data set. Therefore, a single value of da/dN is obtained from the data set. Figure 3.17 shows a fifteen-point polynomial fit applied to the last fifteen points of an a versus N data set.
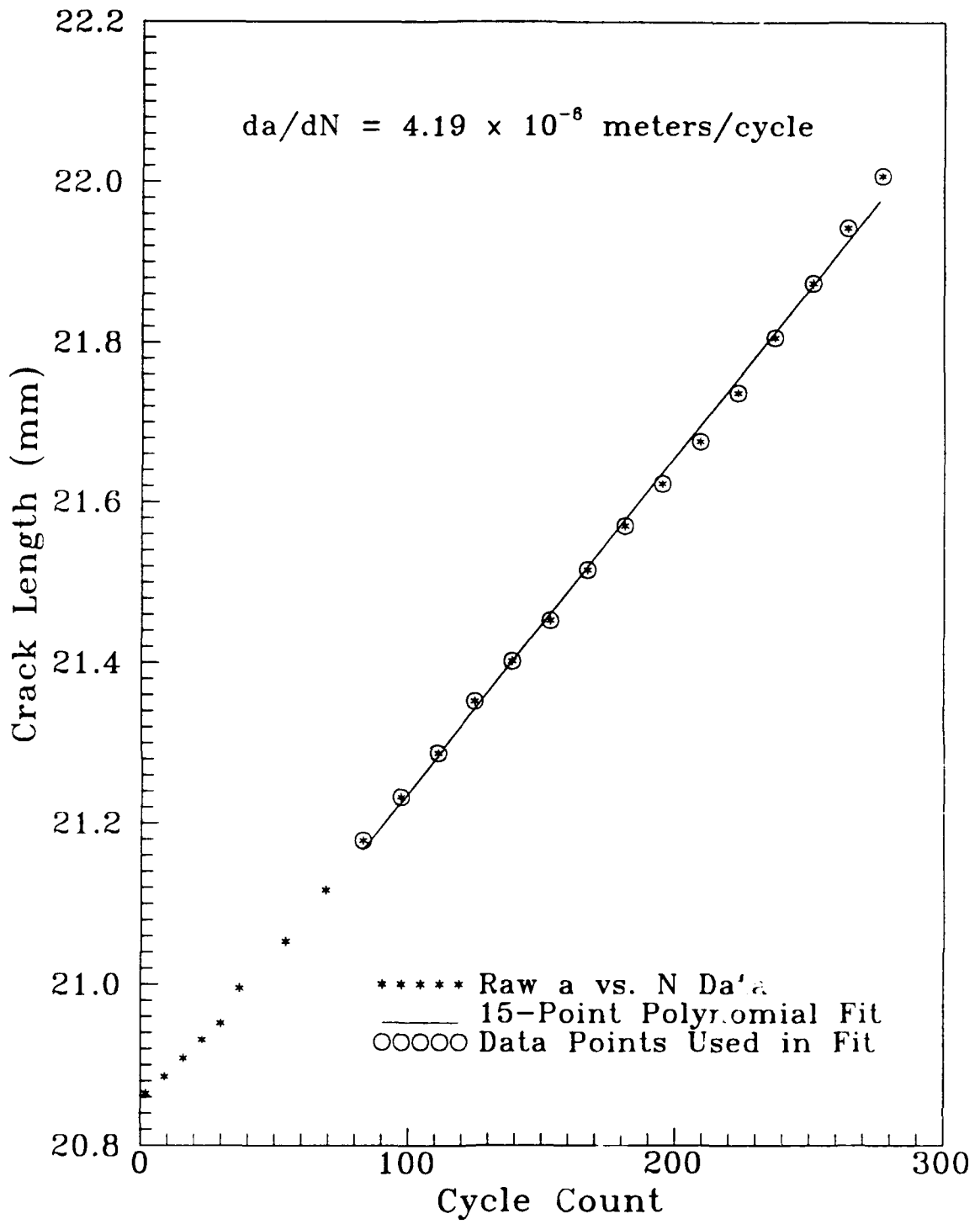
Figure 3.17 Constant K_{max} Test Data Reduced with the Fifteen-Point Scheme

86

IV. Test Results and Discussions

In this chapter, the complete thermal-mechanical fatigue (TMF) test results are presented and discussed, and these results are compared with previous TMF studies of nickel-base superalloys. In particular, the superalloy Inconel 718 is included in most discussions for two reasons. First, there have been extensive studies of that alloy, including many elevated-temperature isothermal fatigue and TMF tests. Second, and more importantly, crack growth rate modeling has been accomplished successfully for isothermal as well as TMF conditions for that alloy.

The TMF crack growth rate model development for Ti-24Al-11Nb is discussed in Chapter V of this dissertation, but before the model can be addressed, the behavior of this alloy under various isothermal and TMF conditions must be examined. The similarities, as well as the differences, between the crack growth rate behavior of this alloy and that of other alloys are discussed, and most importantly, these comparisons are shown in relation to the crack growth rate modeling. Specific aspects of the Ti-24Al-11Nb TMF crack growth behavior that make it impossible to use a linear-summation crack growth rate model are pointed out. Recall from Chapter II that a linear-summation model (Equation (2.18)) was used for the nickel-base superalloy, Inconel 718, to describe crack growth rates during thermal-mechanical cycling.

Summary of Tests Performed During This Study

A summary of all the experiments performed during this effort is presented in Tables 4.1 and 4.2. These tables include the identification number of the test specimen, the type of experiment performed on each specimen, the total cycle time of each test, and the temperature (or temperature range) used during the tests.

The majority of these tests are performed under constant maximum load, P_{max}, conditions. The tests that are performed under constant P_{max} conditions are summarized in Table 4.1. Isothermal and hold-time tests on specimens #88139 and #88140 are performed under constant maximum stress intensity, K_{max}, conditions, and these tests are summarized in Table 4.2. (Recall that K is not only a function of load, P, but also of crack length, a.) These experiments are used to generate the crack growth rate, da/dN, at a single value of ΔK, instead of the full range of ΔK, which would result from a constant P_{max} test.

Triangular wave forms are used for both load and temperature, and all experiments are performed with a load ratio, R, of 0.1. A representation of load vs. time and temperature vs. time for each test type is shown in Figure 4.1. When studying the load and temperature interaction during TMF cycles, the load vs. temperature relations are more useful; therefore, these traces are included in Figure 4.2.

88

Table 4.1 Summary of Tests Performed Under Constant P_{max} Conditions

Specimen ID #	Test Type	Total Cycle Time (Seconds)	Test Temperature (°C)
88129	Isothermal	96	649
88130	180° Out-of-Phase TMF	96	315-649
88131	In-Phase TMF	96	315-649
88133	270° Out-of-Phase TMF	96	315-649
88134	Isothermal	0.2	315
88135	Isothermal with 48 Second Hold	144	649
88136	Lower-Triangular-Phase TMF	144	315-649
88137	Isothermal with 10 Second Hold	110	649
88138	Isothermal with 100 Second Hold	200	649
88142	Isothermal	0.2	649
88143	Isothermal	10	649
88144	90° Out-of-Phase TMF	96	649
88145	Upper-Triangular-Phase TMF	144	315-649
88147	Isothermal	96	482
88148	Isothermal	96	593
88149	In-Phase TMF	96	315-649

Table 4.2 Summary of Tests Performed Under Constant K_{max} Conditions

Specimen ID #	Test Type	Total Cycle Time (Seconds)	Test Temperature (°C)
88139	Isothermal	1	649
	Isothermal with 10 Second Hold	11	
	Isothermal with 50 Second Hold	51	
88140	Isothermal	1	649
	Isothermal with 10 Second Hold	11	
	Isothermal with 50 Second Hold	51	
	Isothermal with 100 Second Hold	101	

As discussed in Chapter III, the two most basic types of experiments performed in this study are: 1) isothermal fatigue tests, and 2) isothermal fatigue tests with a superimposed hold at P_{max} , which are called hold-time tests. These experiments provide the basic understanding of temperature (environment) effects that are required for studying the more complex TMF experimental data. The temperature for all the TMF cycles studied here is cycled between 315°C (T_{min}) and 649°C (T_{max}). The TMF experiments discussed here are divided into two classes: baseline tests and proof tests. Four baseline TMF cycles are studied during this effort: 1) in phase, 2) 90° out of phase, 3) 180° out of phase, and 4) 270° out of phase.

Isothermal Fatigue
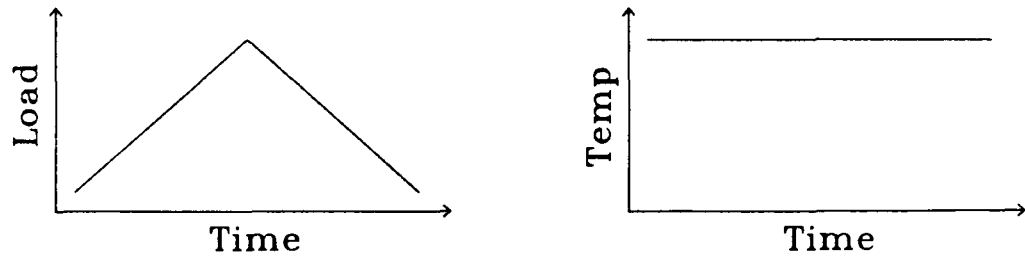
Isothermal Fatigue with Hold at P_{max}
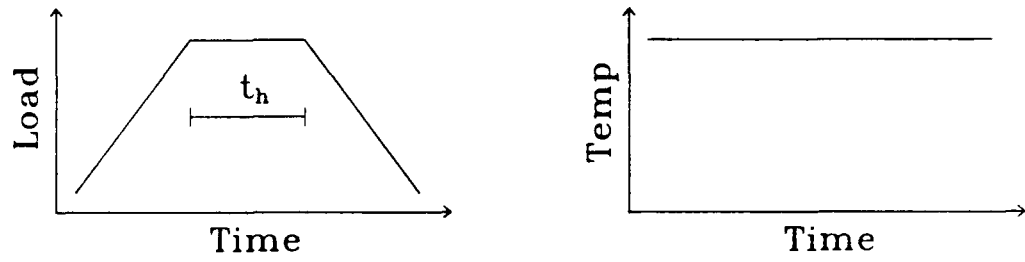
In-Phase TMF
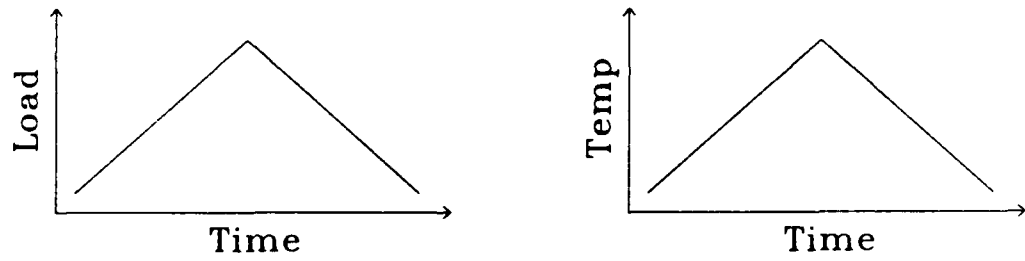
180° Out-of-Phase TMF
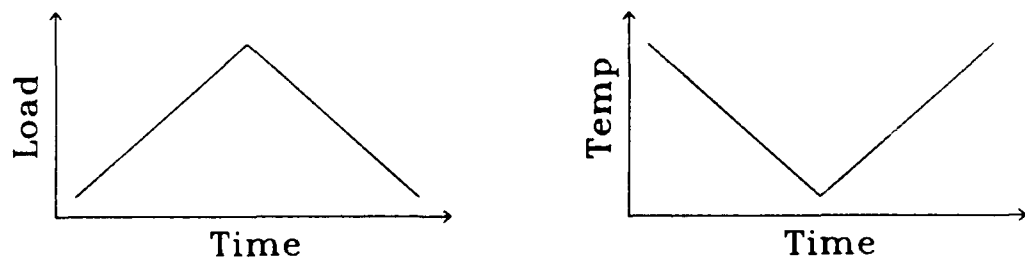
Figure 4.1 Load vs. Time and Temperature vs. Time Traces

270° Out-of-Phase TMF
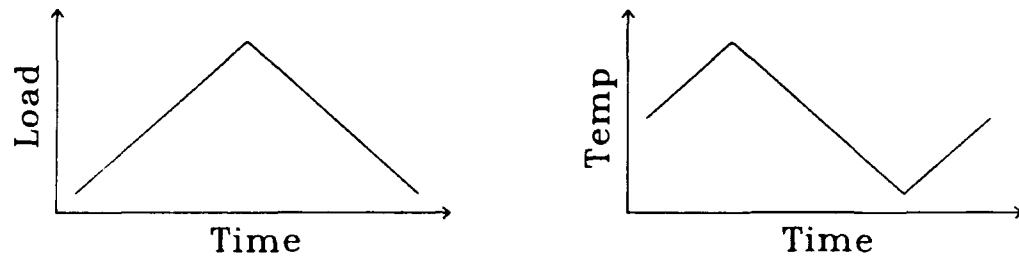
90° Out-of-Phase TMF
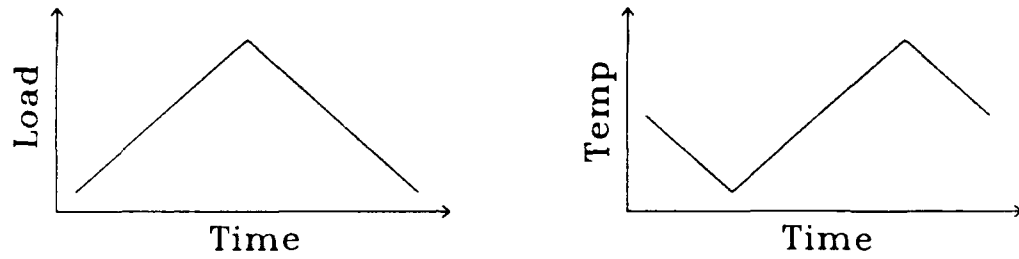
Upper-Triangular-Phase TMF
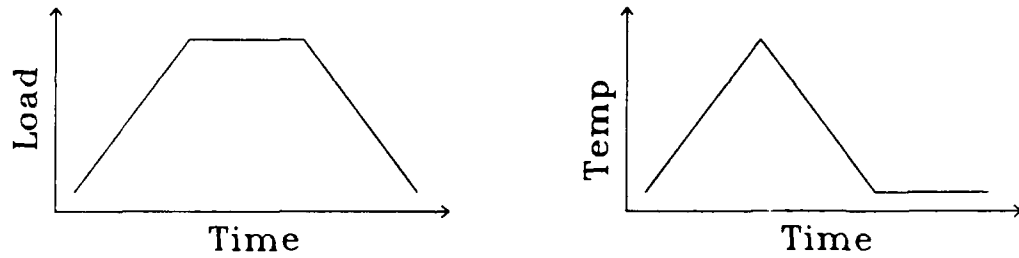
Lower-Triangular-Phase TMF
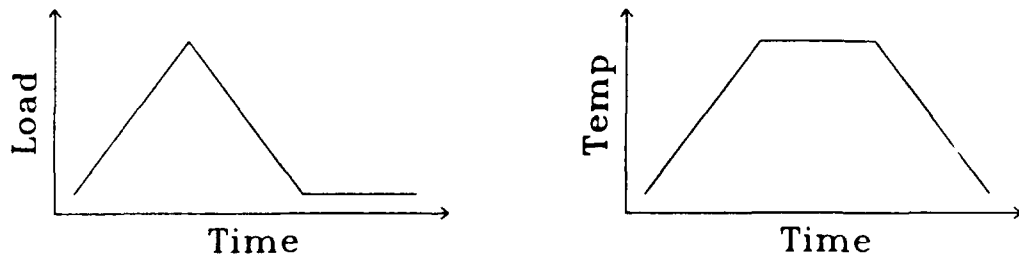
Figure 4.1 (continued) Load vs. Time and Temperature vs. Time Traces
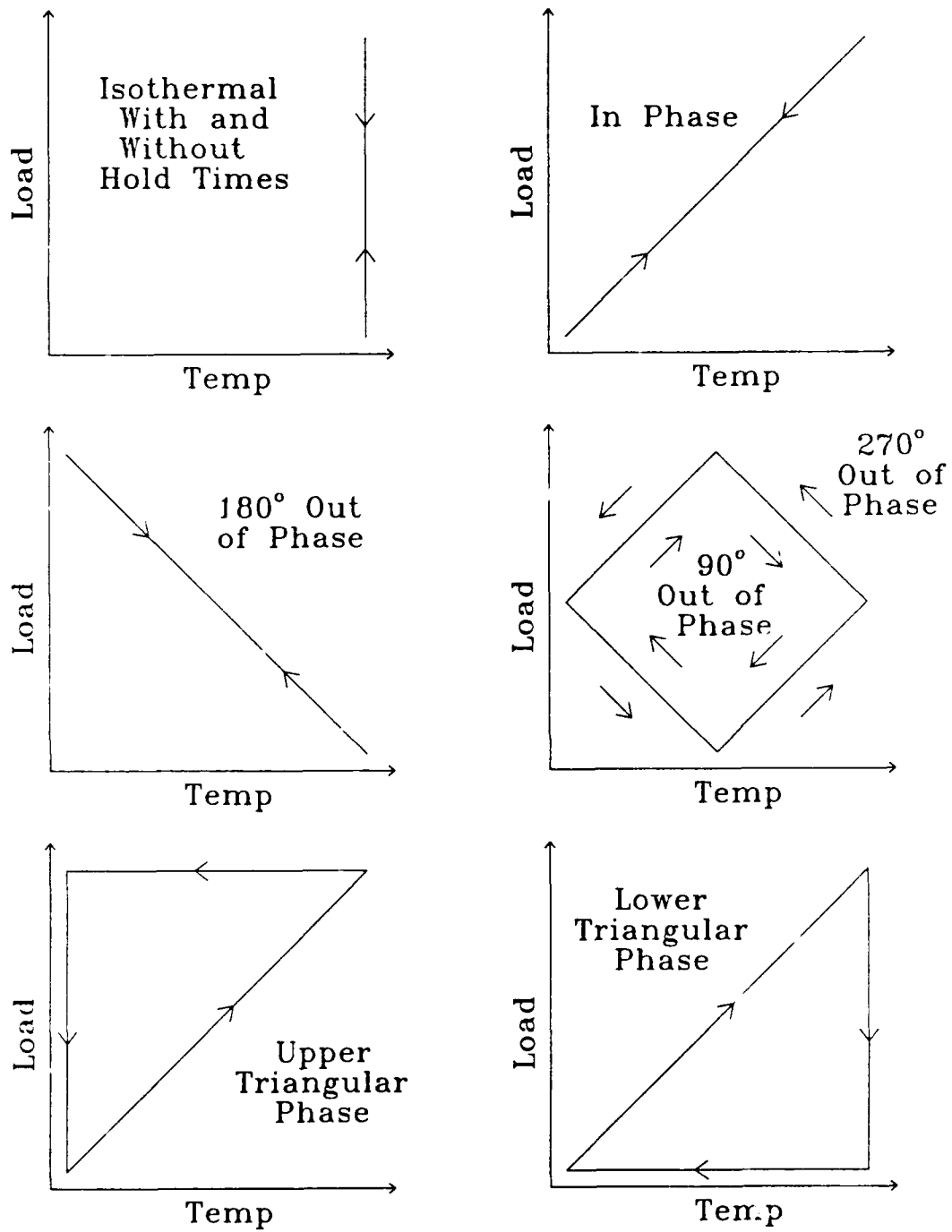
Figure 4.2 Load vs. Temperature Traces

93

These cycles have a loading frequency, v, approximately equal to 0.01 Hz. (The actual cycle period, τ, is 96 seconds.) The two types of proof tests studied in this dissertation are the upper-triangular-phase and lower-triangular-phase. The term "triangular" refers to the shape of the load vs. temperature relations, and the terms "upper" and "lower" refer to their relative position on a load vs. temperature plot (see Figure 4.2). These cycles have 48 second load and temperature ramps as the baseline TMF tests, but since load and temperature holds (see Figure 4.1) of 48 seconds are superimposed on the cycles, the total cycle time is 144 seconds. These cycles are used to validate the modeling technique developed during this study.

Other related experimental studies have provided significant data toward this effort. These experiments were not completed specifically for this study and are not included in Tables 4.1 or 4.2, but are discussed briefly here. Staubs [114] carried out sustained-load and hold-time tests on the Ti-24Al-11Nb alloy. These tests were performed at 700, 750, and 800°C. Although these temperatures are higher than those being considered in this study, the hold-time modeling concepts proposed by Mall et al. [21] are relevant to the current modeling effort and, therefore, the results of these tests are discussed. These test results show the limitations of cumulative-damage techniques that have been used in modeling Inconel 718 under similar loading conditions [8, 11]. Balsone et al. [115] and Parida and Nicholas [116, 117] also completed tests on the Ti-24Al-11Nb alloy that have aided in the modeling effort of the

94

present study. Balsone et al. [115] used constant K_{max} test conditions to perform isothermal tests at various temperatures and loading frequencies. They also tested the alloy under hold-time test conditions, and these data were very useful in the current modeling effort. Parida and Nicholas [117] provided isothermal-fatigue and hold-time data that are used during the TMF crack growth modeling. These results are discussed in more detail during the model development, which is presented in Chapter V.

Comparisons of Ti-24Al-11Nb and Inconel 718 Crack Growth Data

TMF Crack Growth Data

Prior to performing the first TMF test, a 650°C isothermal test with $v = 0.01$ Hz is performed to establish the material's crack growth behavior at T_{max} at the same frequency as the baseline TMF cycles. This isothermal test is followed by an in-phase TMF test to understand the effect that temperature cycling has on crack growth rates. Out-of-phase TMF tests of 90°, 180°, and 270° then are completed to understand the effect of varying load-temperature phase angle on the crack growth behavior of the material [54, 55]. The results of all these tests are presented in Figure 4.3. A 315°C isothermal fatigue test with $v = 0.01$ Hz also was attempted to establish crack growth behavior at the minimum TMF temperature, T_{min}, but the test could not be completed at this frequency because of the low crack growth rates under such conditions. Instead of plotting crack growth rate data over the entire ΔK range, one data
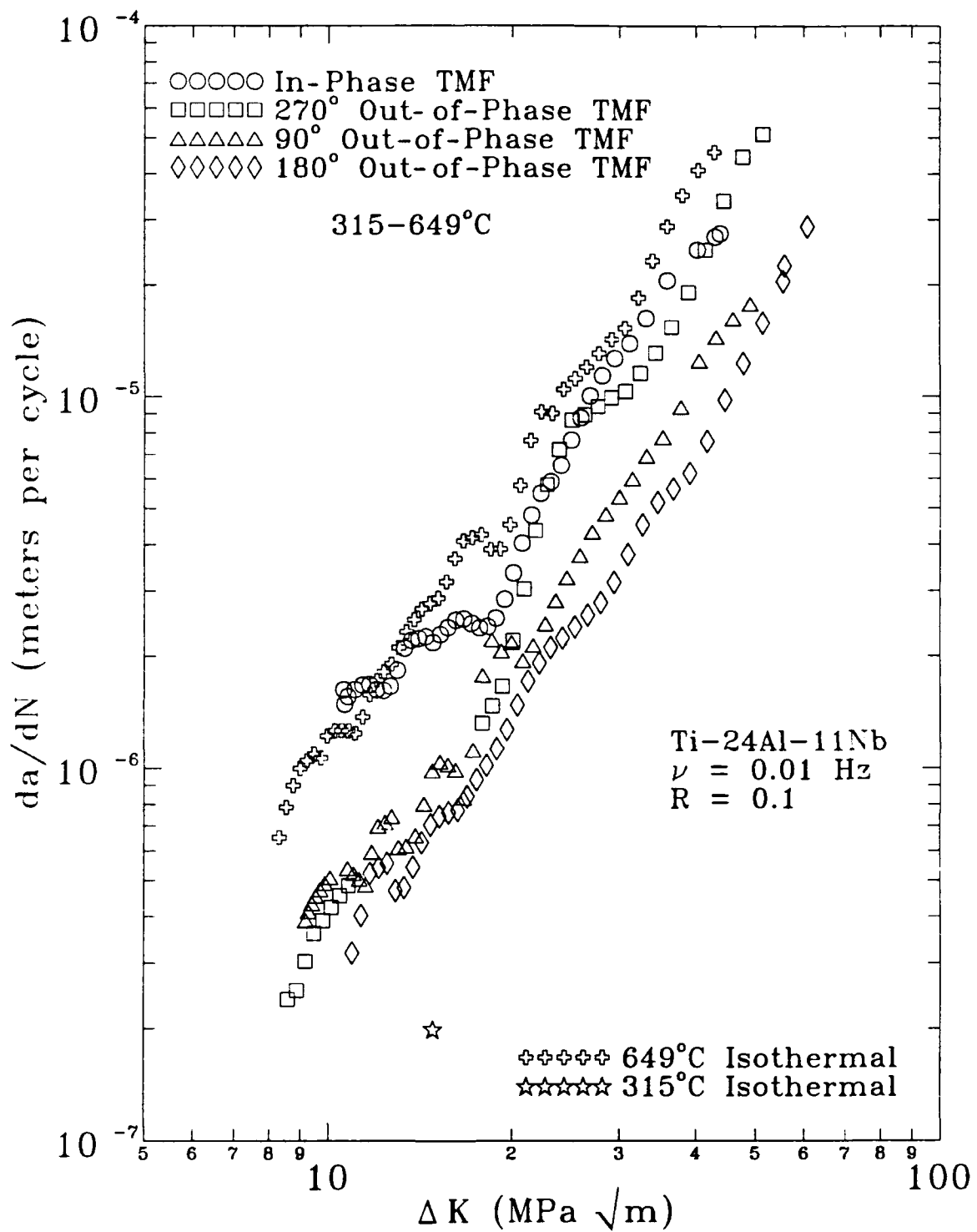
Figure 4.3 Summary of Ti-24Al-11Nb TMF Crack Growth Data

point has been plotted for the 0.01 Hz, 315°C isothermal case. This data point is generated using constant K_{max} tests instead of constant P_{max} tests in a previous study [115]. In that study [115], isothermal crack growth rates were generated under constant K_{max} conditions over the entire range of temperature and frequency that is considered in this study. These crack growth rate data are in agreement with those generated under constant P_{max} conditions in the present study; therefore, it is reasonable to assume that this data point is valid.

Similarities exist between the TMF crack growth behavior of Ti-24Al-11Nb shown in Figure 4.3 and that of Inconel 718 for the same baseline TMF cycles. Inconel 718 crack growth data for these cycles, obtained from Heil [6], are plotted in Figure 4.4. The TMF crack growth rates fall between the growth rates for fatigue under isothermal conditions at T_{max} and T_{min} . Out of these four types of TMF cycles, the in-phase test produces the highest growth rates in both materials. For Ti-24Al-11Nb there is very little difference, if any at all, between the T_{max} isothermal crack growth rates and the in-phase TMF crack growth rates (see Figure 4.3); whereas, in the case of Inconel 718, the difference is more dramatic (see Figure 4.4). The 90° out-of-phase and 180° out-of-phase TMF cycles produced similar crack growth rates in both the Ti-24Al-11Nb and Inconel 718 materials, and these cycles produced the lowest growth rates out of the four baseline TMF cycles. However, the difference in growth rates between these two conditions are more discernible in the titanium-aluminide alloy; and as shown in Figure 4.3, the growth rates for the 180° out-of-phase
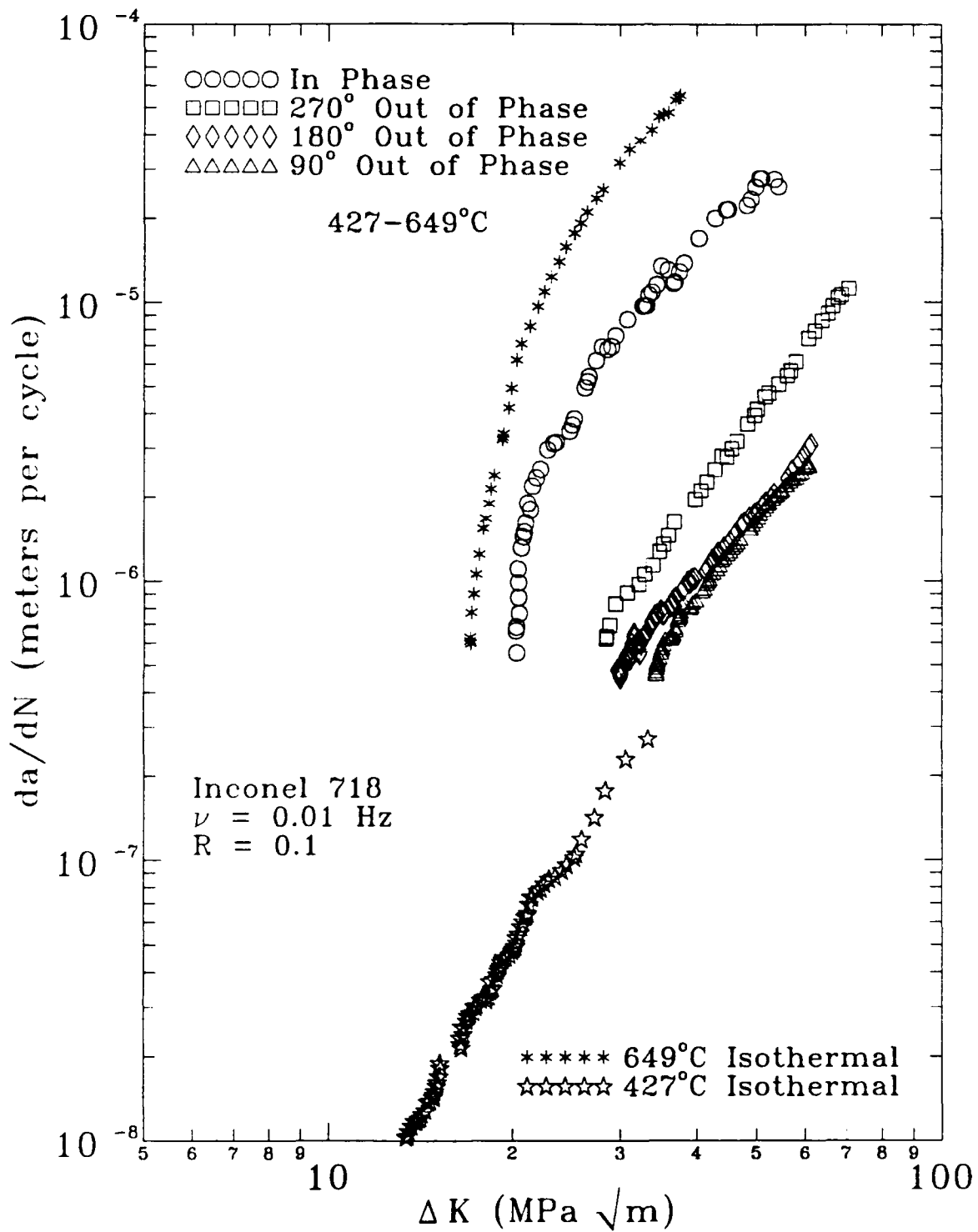
Figure 4.4 Summary of Inconel 718 TMF Crack Growth Data [6]

TMF cycle are slightly lower than those produced by the 90° out-of-phase TMF cycle for majority of the ΔK values.

Frequency Effects

Next, the effect that loading frequency has on growth rates in Ti-24Al-11Nb is discussed and compared with the frequency behavior of other materials, in particular, Inconel 718. Results from $649^\circ C$ isothermal tests (temperature is equal to T_{max} of the TMF tests) performed with loading frequencies of 0.01 Hz, 0.1 Hz, and 5 Hz are plotted in Figure 4.5. From these data, a general observation can be made that as the loading frequency increases, the growth rate decreases. Floreen and Kane [118] and Weerasooriya [119] found the same trend in Inconel 718, and James [120] saw the same effect of frequency on elevated-temperature isothermal crack growth rates in 304 SS. Saxena and Bassani [42] have observed similar behavior in Cr-Mo-V steels and nickel-base superalloys, and also note that the frequency dependence decreases as ΔK decreases. But this is not observed in the Ti-24Al-11Nb data shown in Figure 4.5.

To further study frequency effects at this temperature, additional experiments are performed with a constant K_{max} = 14.85 MPa(m)$^{1/2}$. These crack growth rate data, along with data obtained under constant P_{max} conditions (taken from Figure 4.5) and other data found in the literature [17, 115, 116], are plotted in Figure 4.6 This figure illustrates the frequency

99
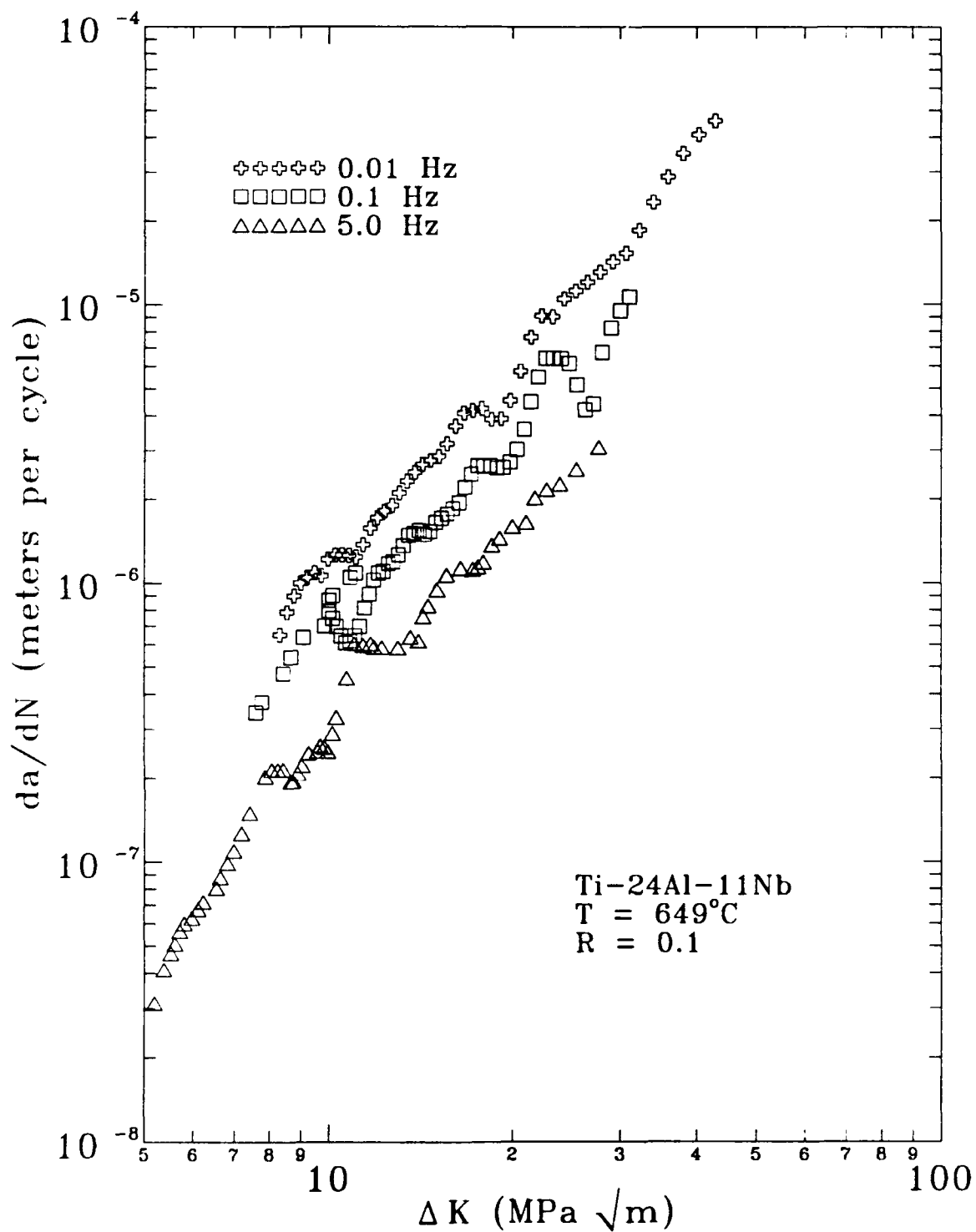
Figure 4.5 Effect of Frequency on Crack Growth Rates at 649°C
for a Range of ΔK Values
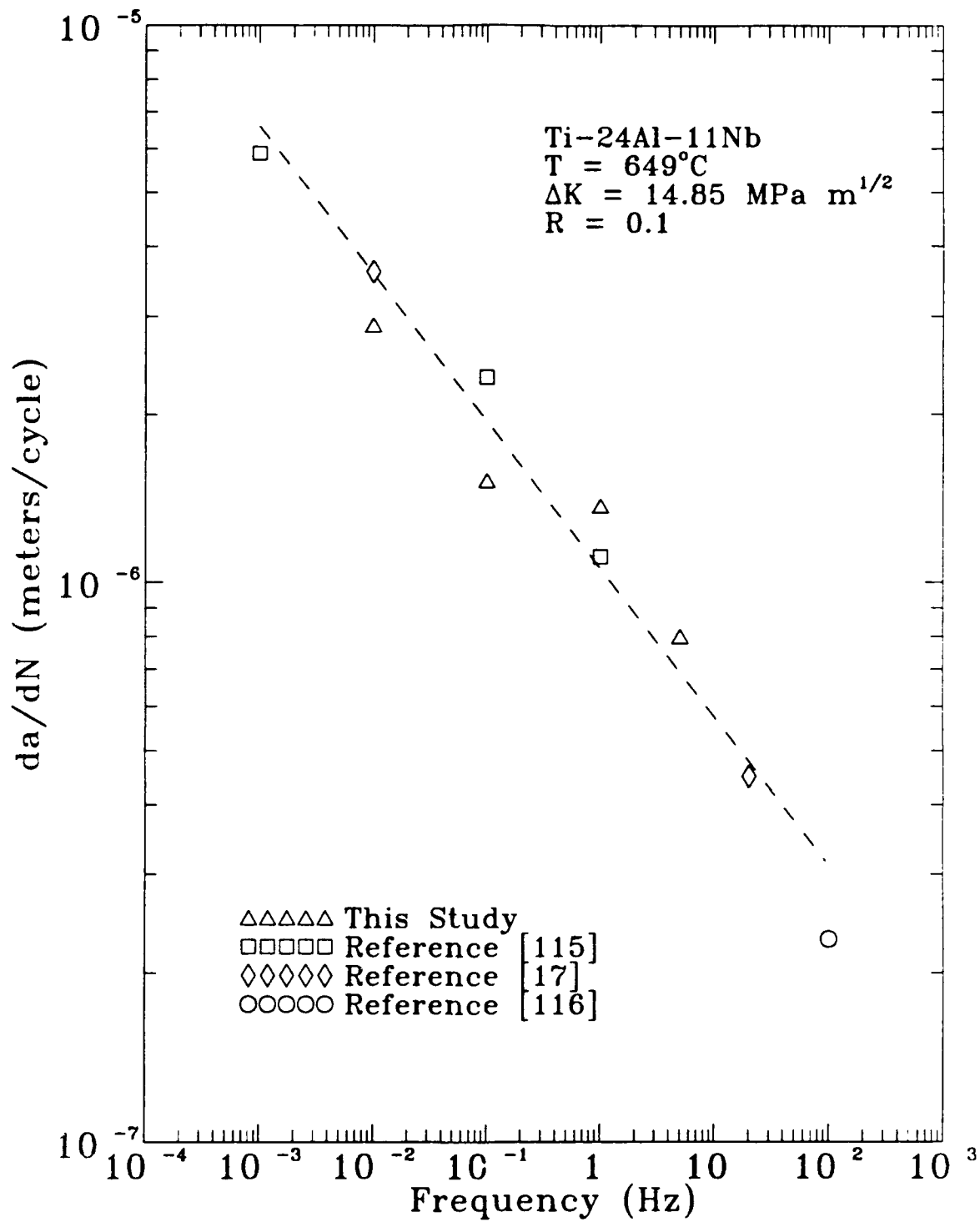
Figure 4.6 Effect of Frequency on Crack Growth Rates
at 649°C in Ti-24Al-11Nb

101

dependence of the crack growth rates at 649°C over a broad range of

frequency. The growth rates show a continual decrease from v = 0.001 Hz to

v = 100 Hz.

For the purpose of discussion, a power law is fit to these data, which is

of the form:

$$\frac{da}{dN} = C_f\, v^m \qquad\qquad (2.8)\ \text{repeated}$$

where C_f is a constant that defines the crack growth rate at 1 Hz, v is the

loading frequency, and m is the exponent that defines the slope of the line.

For the Ti-24Al-11Nb crack growth rate data shown in Figure 4.6, $m = -0.24$.

This implies that over the entire frequency range studied, the frequency must

decrease by four decades before the growth rate increases by one decade. This

type of behavior is defined in Chapter II as mixed-mode crack growth. Over

the entire frequency range studied at 649°C, the growth rates never become

completely time dependent or completely cycle dependent.

This frequency behavior of the titanium-aluminide alloy differs

dramatically from that of the superalloys, and for comparison, a plot of crack

growth rate versus frequency for Inconel 718 is presented in Figure 4.7. These

isothermal crack growth rates, taken from Weerasooriya [119], were obtained

at the same temperature ($T = 649°C$), load ratio ($R = 0.1$), and frequency range

(0.001 < v < 1,000 Hz) as shown in Figure 4.6. Two load conditions are
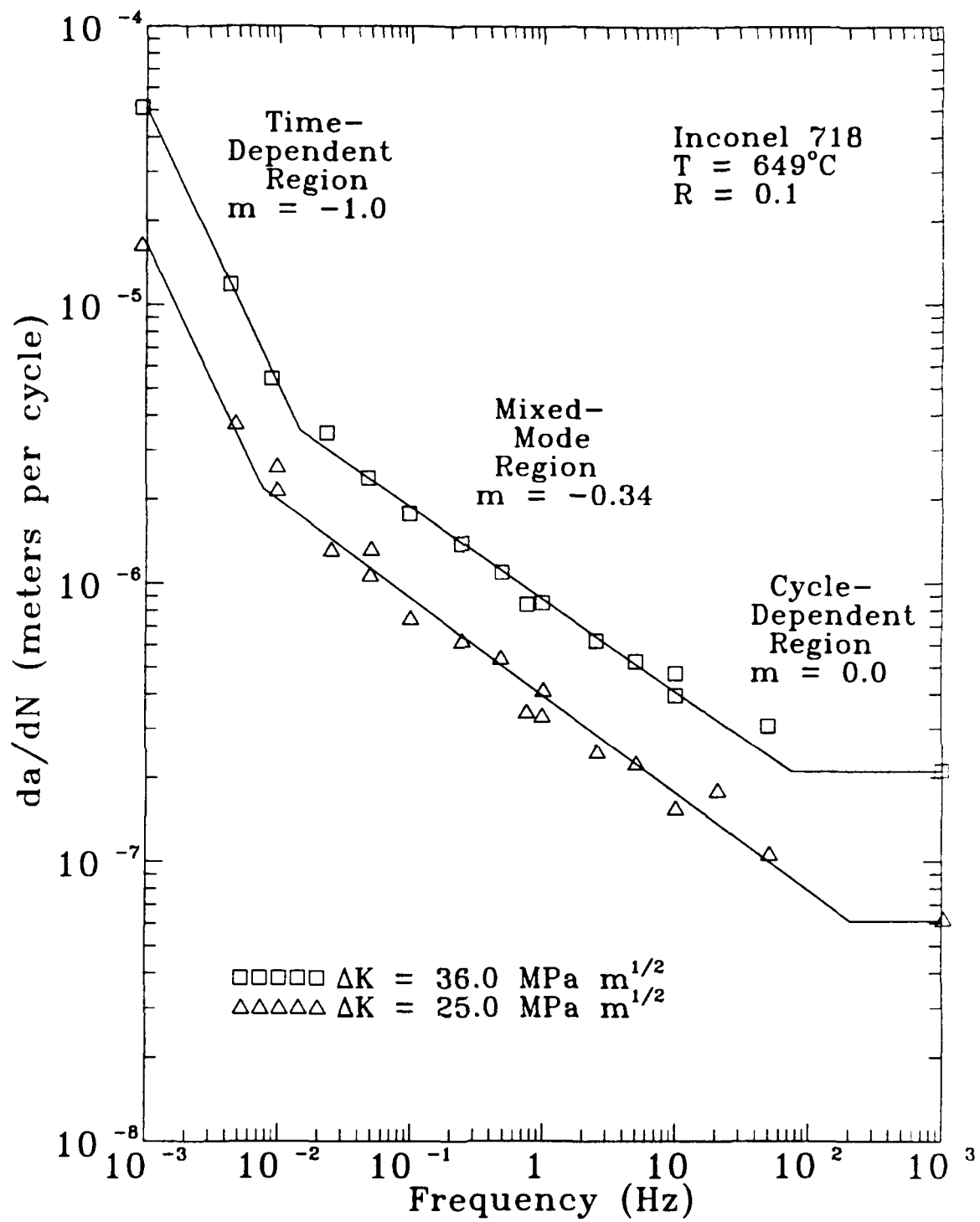
Figure 4.7 Effect of Frequency on Crack Growth Rates
at 649°C in Inconel 718 [119]

103

presented in Figure 4.7: ΔK = 27.8 and 40.0 MPa m$^{1/2}$. These crack growth data of Inconel 718 show distinct regions of cycle-dependent, mixed-mode, and time-dependent crack growth, as defined in Chapter II. (Note that 1 Hz crack growth data acquired at 38°C [40] and 10 Hz data acquired at 427°C [6] confirm the values for the cycle-dependent crack growth rates shown in Figure 4.7 for R = 0.1, ΔK = 27.8 MPa m$^{1/2}$ and R = 0.1, ΔK = 40.0 MPa m$^{1/2}$.)

For the superalloys at any given temperature (T), there appears to be a critical frequency above which the frequency no longer influences fatigue crack growth (FCG) behavior [42, 118 - 121]. When cycled at frequencies greater than this, the crack growth rate becomes frequency independent. This crack growth behavior, referred to as cycle-dependent crack growth, is shown in Figure 4.7 in the region where m = 0.0. In general, this cycle-dependent crack growth is a function of ΔK, R, and T. For Inconel 718, as is the case for most materials, the crack growth rate is not a function of T; therefore, the cycle dependent crack growth rate is identical to that observed at 25°C.

At 649°C, Ti-24Al-11Nb does not exhibit cycle-dependent crack growth behavior, even at frequencies as high as 100 Hz (see Figure 4.6). However, cycle-dependent crack growth behavior is observed between 25°C and 250°C, as is shown in a later section of this chapter. In this alloy, cycle-dependent crack growth is a function of not only ΔK and R, but also of T.

As frequency decreases, the crack growth rates in Inconel 718 eventually become a function of time and temperature, and at any given temperature, the

104

growth rate will increase with cycle time. As shown in Figure 4.7, this mixed-mode region is described by $m = -0.34$; i.e., it takes a reduction in frequency of approximately three decades to increase the growth rate by a single decade. As previously discussed, the titanium-aluminide alloy exhibits mixed-mode behavior over a wider frequency range where $m = -0.24$ (see Figure 4.6).

As frequency decreases further, the crack growth rates become time dependent, where this region is defined by $m = -1.0$. Under pure time-dependent conditions, when the frequency is reduced by one decade, the growth rate will increase by one decade. In Figure 4.7 this time-dependent behavior is observed in Inconel 718 at 649°C for frequencies less than 0.01 Hz. But in this study of Ti-24Al-11Nb, time-dependent crack growth is not observed at 649°C for frequencies even as low as 0.001 Hz.

Similarities and Differences in Crack Growth Behavior

The comparison of the crack growth behavior of Ti-24Al-11Nb and Inconel 718 under TMF as shown in Figures 4.3 and 4.4, and under isothermal fatigue at different frequencies as shown in Figures 4.6 and 4.7 may lead to speculation that the crack growth rates could be modeled in a similar way (although time-dependent behavior is not observed in the titanium-aluminide alloy under any of the conditions in this study). But, there is a key difference in behavior that makes it impossible to use the Inconel 718 crack growth rate model for the titanium-aluminide alloy. The model that was developed by

105

Heil, Nicholas, and Haritos (HNH) [15] uses the sum of cycle-dependent and time-dependent contributions of crack growth rates to estimate the total crack extension per cycle during elevated-temperature isothermal fatigue and TMF conditions. This model is shown in Chapter II and repeated here. The total crack growth rate, $(da/dN)_{tot}$, is expressed as:

$$\left(\frac{da}{dN}\right)_{tot} = \left(\frac{da}{dN}\right)_{cd} + \int_{loading} \left(\frac{da}{dt}\right)_{sl} dt \qquad \text{(2.18) repeated}$$

where $(da/dN)_{cd}$ is the cycle-dependent crack growth rate contribution and $(da/dt)_{sl}$ is the sustained-load crack growth rate. The cycle-dependent crack growth rate contribution is the growth rate that is observed during low-temperature and/or high-frequency cycling when the environment does not effect crack growth. This contribution, which is expressed as crack extension per cycle, can be obtained in the titanium-aluminide alloy, but the difficulty arises when trying to calculate the time-dependent contribution, which is the second term in Equation (2.18). For Inconel 718, this contribution was determined from the integration of crack growth rate data obtained from sustained-load elevated-temperature tests. These data are expressed as crack extension per time, and when integrated, they yield the crack extension per cycle resulting from the exposure of the material to elevated temperature. These sustained-load tests produce no measurable crack growth in Ti-24Al-11Nb [21, 114]; therefore, the HNH model would predict that the time-

106

dependent growth rate for Ti-24Al-11Nb is equal to zero. This, in turn, would suggest that the total crack growth rate would equal the cycle-dependent contribution of crack growth, and variations of temperature and frequency would have no effect on crack growth rates. This clearly is not the case, as seen from the test results presented in Figures 4.5 and 4.6.

Discussions of Isothermal Crack Growth in Ti-24Al-11Nb

The understanding of crack propagation under isothermal elevated-temperature conditions is necessary before TMF can be understood and subsequently modeled. Therefore, to further investigate the influence of temperature and time on the crack growth behavior of Ti-24Al-11Nb, the crack growth rate data obtained during experiments performed under isothermal conditions are examined. These tests include: first, isothermal fatigue tests performed at different temperatures and frequencies, and second, hold-time tests performed at 649°C.

Isothermal Fatigue

Before discussing the results of hold-time tests, additional isothermal data first are considered. An isothermal test at 0.01 Hz with $T = 482$°C is performed to supplement the data at T_{max} and T_{min}. These data from the three isothermal conditions are presented in Figure 4.8. The growth rates from the 482°C isothermal test are higher than those of the 315°C test, and this
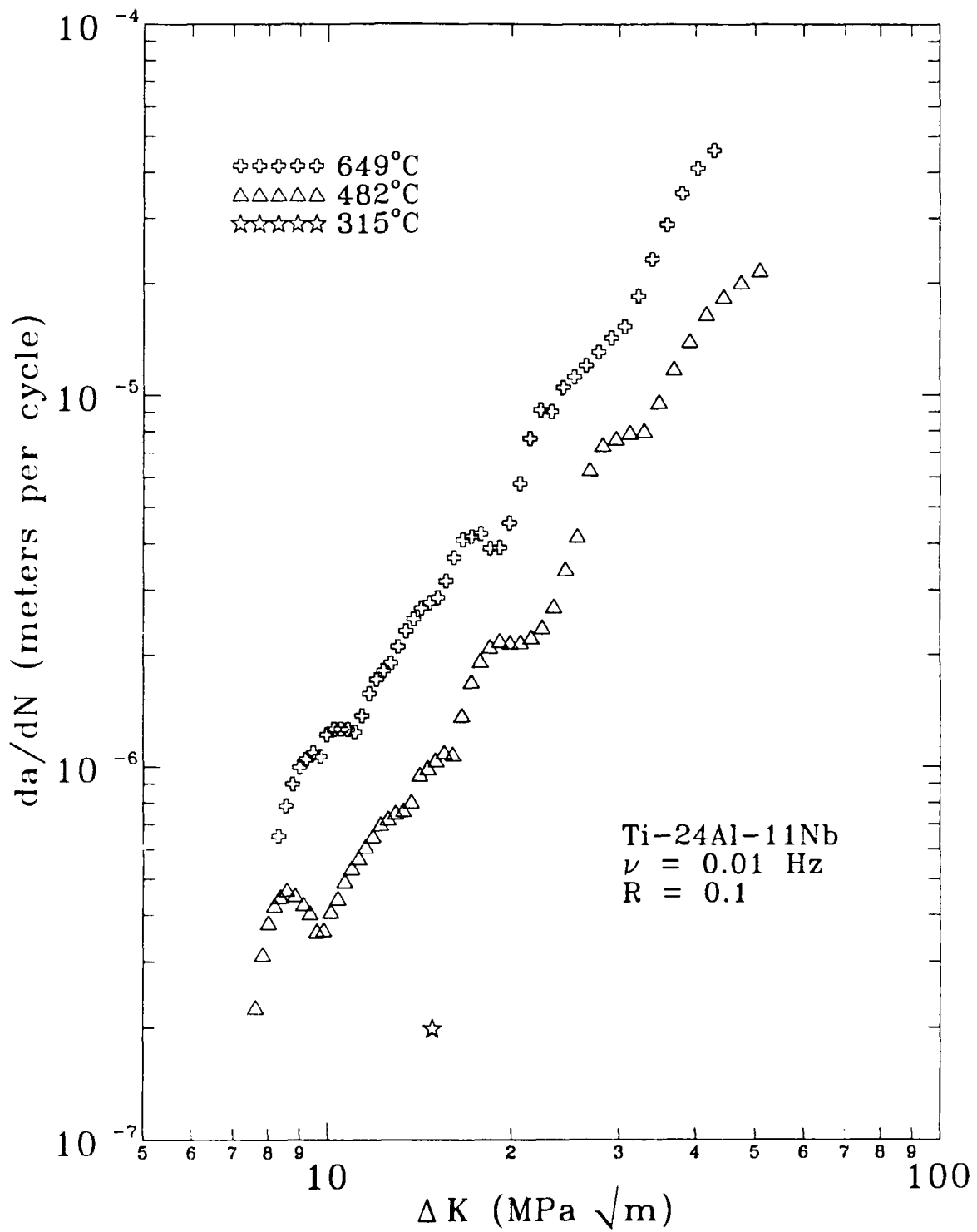
Figure 4.8 Isothermal Crack Growth Rate Data for 315, 482, and 649°C

108

behavior differs from that of Inconel 718. For that superalloy, the growth rates are purely cycle dependent below 538°C, and since these cycle-dependent crack growth rates are temperature independent [8], all crack growth rates obtained below 538°C would be equal to each other for any given combination of ΔK and R.

To further examine the influence of time and temperature on the crack growth behavior of the titanium-aluminide alloy, crack growth rates from experiments of 0.01 Hz and 1 Hz are plotted in Figure 4.9. These data are obtained over a temperature range of 25°C to 649°C for $\Delta K = 14.85$ MPa m$^{1/2}$ with $R = 0.1$. Dashed lines show the trends in the 0.01 Hz and 1 Hz data. In addition, 100 Hz isothermal fatigue crack growth rates at 25°C and 649°C are presented. Two observations can be made from the data shown in the figure.

First, at temperatures above 250°C, the crack growth rates are a function of frequency, and at temperatures below 250°C, the crack growth rates are cycle dependent (frequency independent). There are insufficient crack growth rate data at 100 Hz to show the trends as in the case of the 0.01 and 1.0 Hz data, but the available 100 Hz data are consistent with the trends at the other frequencies. To compare this behavior with that of Inconel 718, a similar plot of da/dN versus temperature for Inconel 718 is shown in Figure 4.10. This figure shows the crack growth rates for $\Delta K = 25.0$ MPa m$^{1/2}$ with $R = 0.1$ from 25°C to 649°C [6]. As mentioned in a previous discussion, the growth rates in Inconel 718 are independent of frequency below 538°C [8]. This temperature,
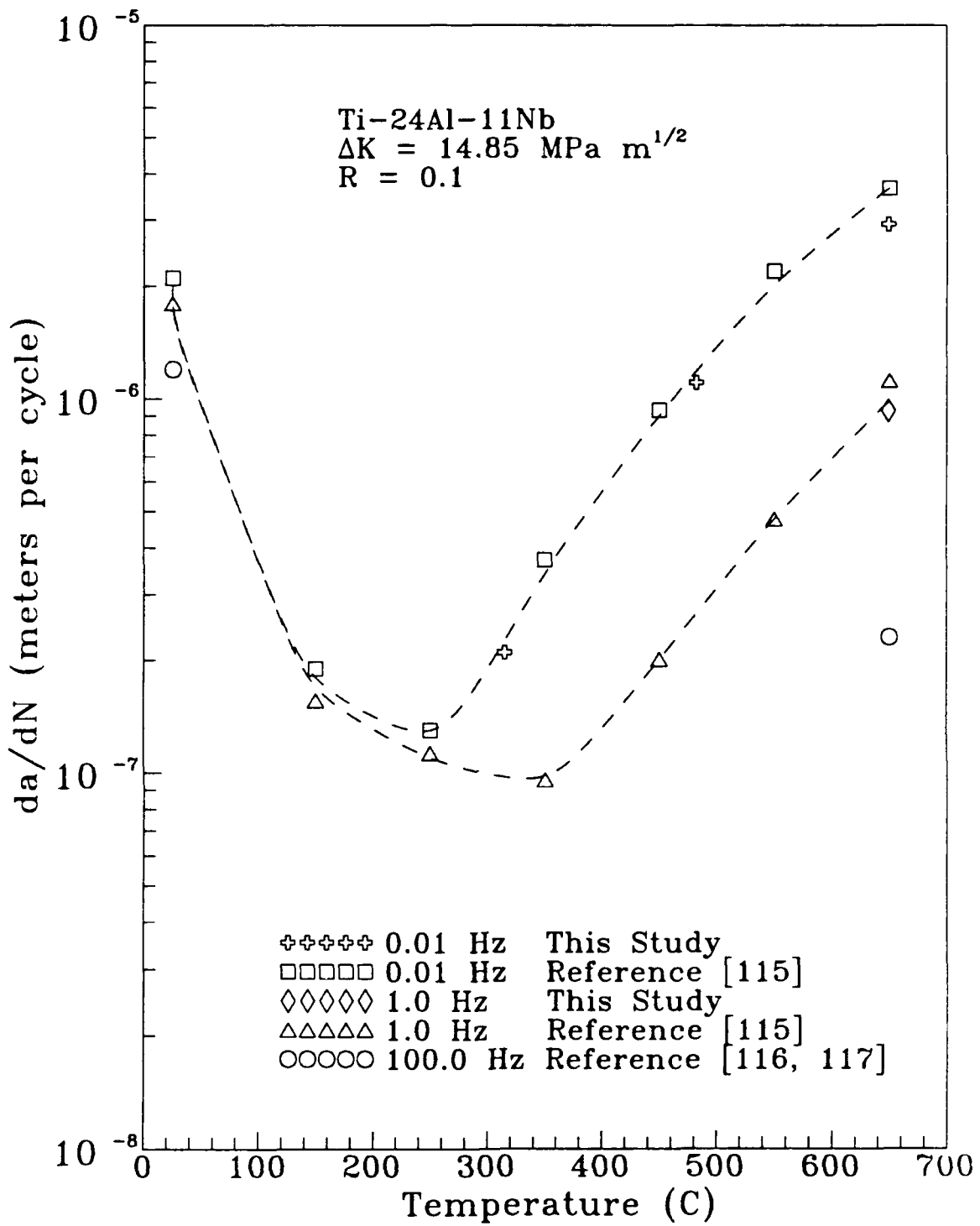
Figure 4.9 Isothermal Crack Growth Rates in Ti-24Al-11Nb
for Different Temperatures Ranging from 25°C to 650°C

110
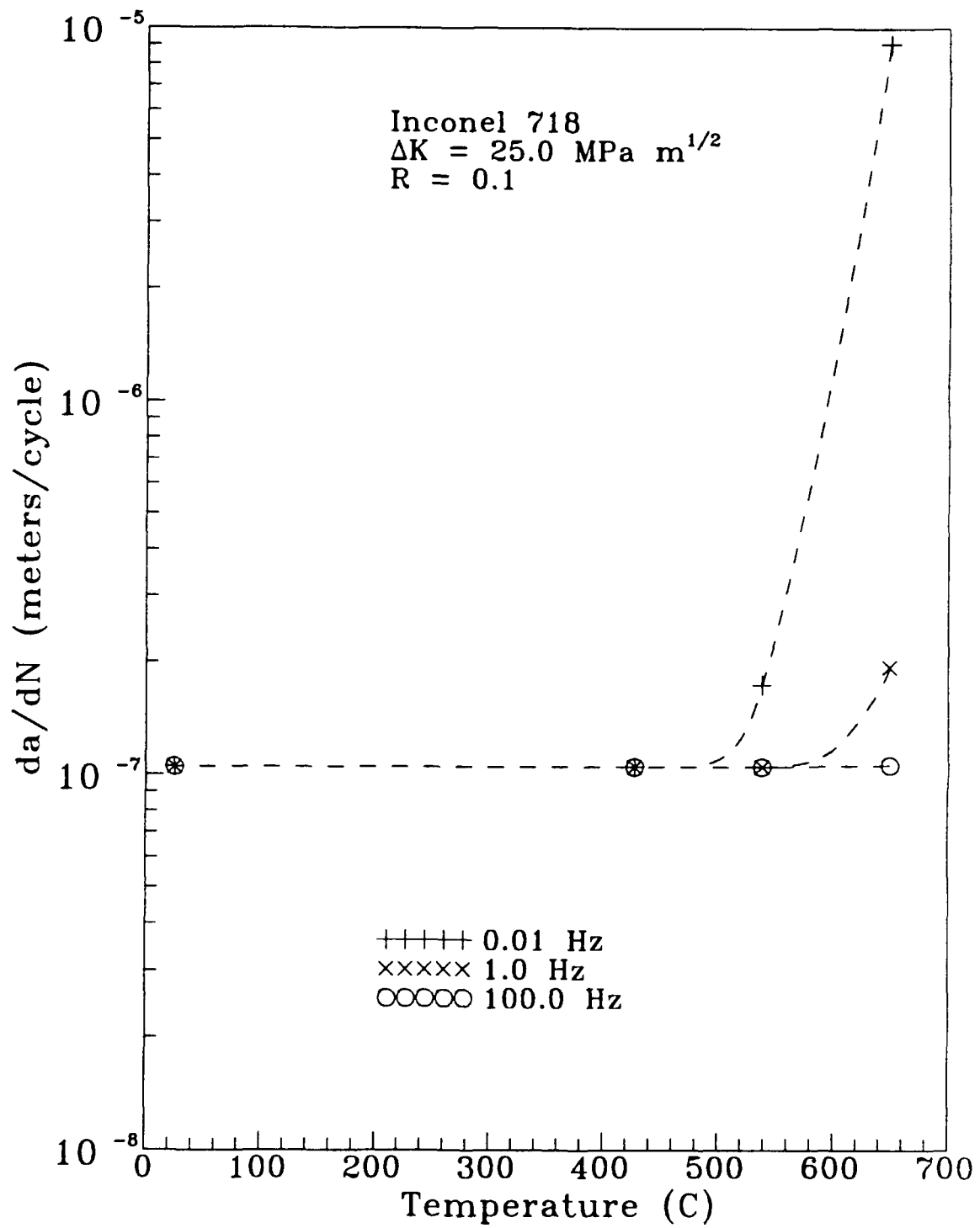
Figure 4.10 Isothermal Crack Growth Rates in Inconel 718
for Different Temperatures Ranging from 25°C to 650°C [6]

111

at which the crack growth rates in Inconel 718 change from cycle dependent to frequency dependent, is considerably higher than that observed in the titanium-aluminide alloy, Ti-24Al-11Nb.

The second observation made from the data presented in Figure 4.9 is that the cycle-dependent crack growth rate behavior that exists at and below 250°C is a function of temperature. This is dramatically different from the behavior in Inconel 718 (Figure 4.10); the cycle-dependent crack growth rates are are function of only ΔK and R from 25 to 650°C. Since the cycle-dependent crack growth rates in Ti-24Al-11Nb are a function of temperature, the form of the cycle-dependent term of the HNH model given in Equation (2.18) cannot be used to predict the growth rates in the titanium-aluminide alloy. Recall that Equation (2.18) was developed to model crack growth rates in Inconel 718, and the cycle-dependent crack growth rate in that model is equal to a constant for any given combination of ΔK and R.

Isothermal Fatigue with Superimposed Hold Times

The results of the second type of isothermal test considered in this study, the hold-time test, is now discussed. Hold-time tests are simply isothermal fatigue tests with a superimposed hold introduced at P_{max} , as shown previously in Figure 4.1, and the length of this hold is defined as t_h . Hold-time tests with fatigue cycles of 0.01 Hz and 1.0 Hz are performed during this investigation with t_h varying from 10 seconds to 1000 seconds.

Hold-Times Tests with 0.01 Hz Fatigue Cycles

The hold-time tests that are considered first consist of fatigue cycles of 96 or 100 seconds (approximately 0.01 Hz) and holds of t_h = 10, 48, and 100 seconds. A summary of these test results is presented in Figure 4.11 along with the results of a 0.01 Hz fatigue test performed at 649°C. As observed from this comparison, the addition of 10, 48, and 100 second hold times to 0.01 Hz fatigue cycles does not change the crack growth rates from the pure fatigue condition. To study more closely the effect of the addition of holds at P_{max}, the growth rates are plotted against the total cycle time for ΔK = 10, 14.85, 20, and 30 MPa m$^{1/2}$, and these data are presented in Figure 4.12. Dashed lines shown the trends in the data for each value of ΔK. At the larger values of ΔK, particularly ΔK = 30 MPa m$^{1/2}$, there is a slight increase in growth rate from data obtained under pure fatigue conditions to those obtained under fatigue with superimposed hold times. This is particularly noticeable in the data obtained from the test with t_h = 100 seconds (or total time, t_{tot}, = 200 seconds), but this increase is, for all practical purposes, negligible in comparison to the crack growth rate increases observed in the superalloys when hold times are added to fatigue cycles [70, 122]. The effect of a hold time added to fatigue cycles was negligible in previous studies of titanium alloys 6242S and 5621S at 450°C [123] and titanium alloy IMI 685 at room temperature [124]. However, other IMI 685 data [125] suggest a slight increase in growth rates when holds are added at elevated temperatures.

113
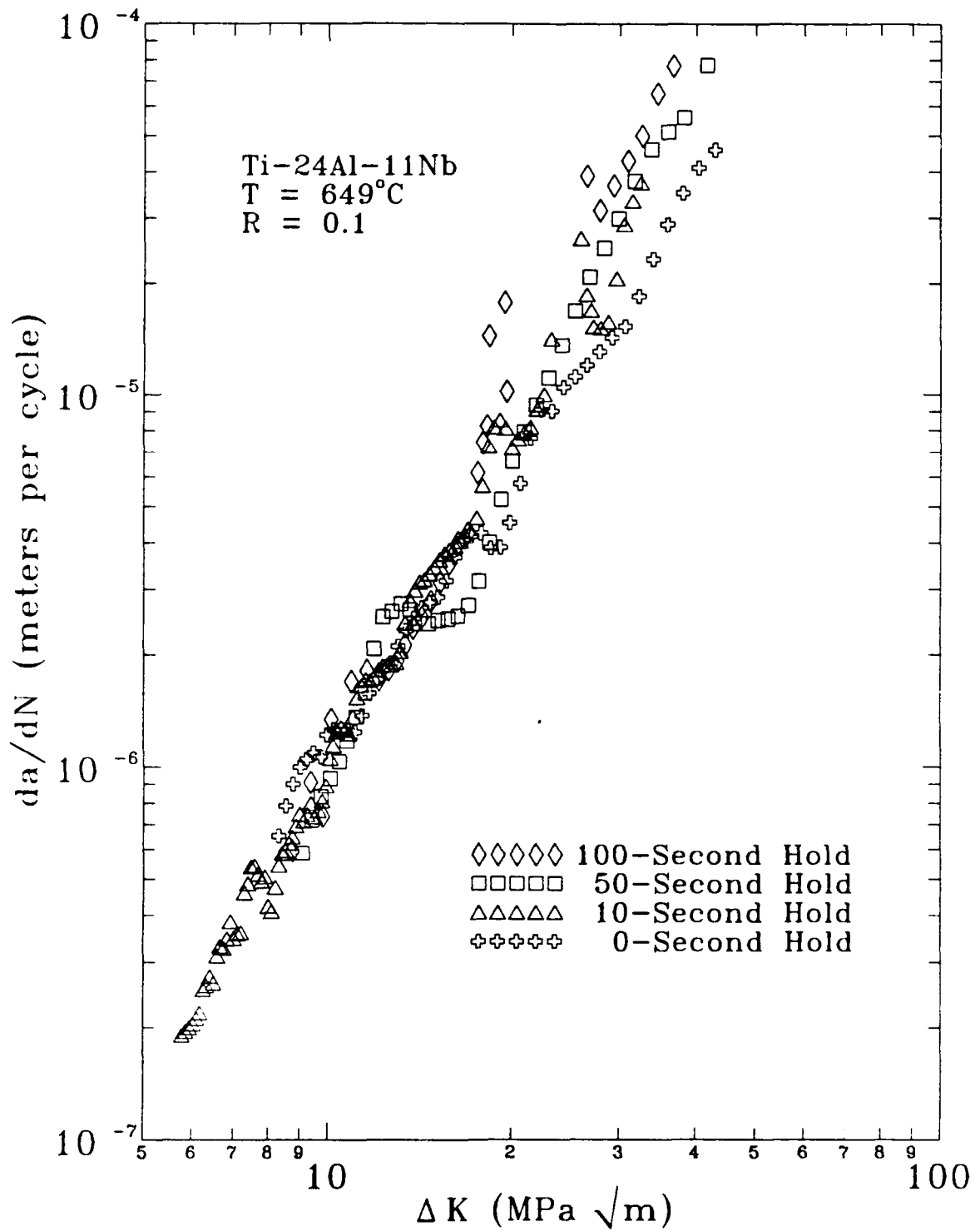
Figure 4.11 Comparison of 0.01 Hz, 649°C Isothermal Data with Data
Obtained with Superimposed Holds of 10, 48, and 100 Seconds

114
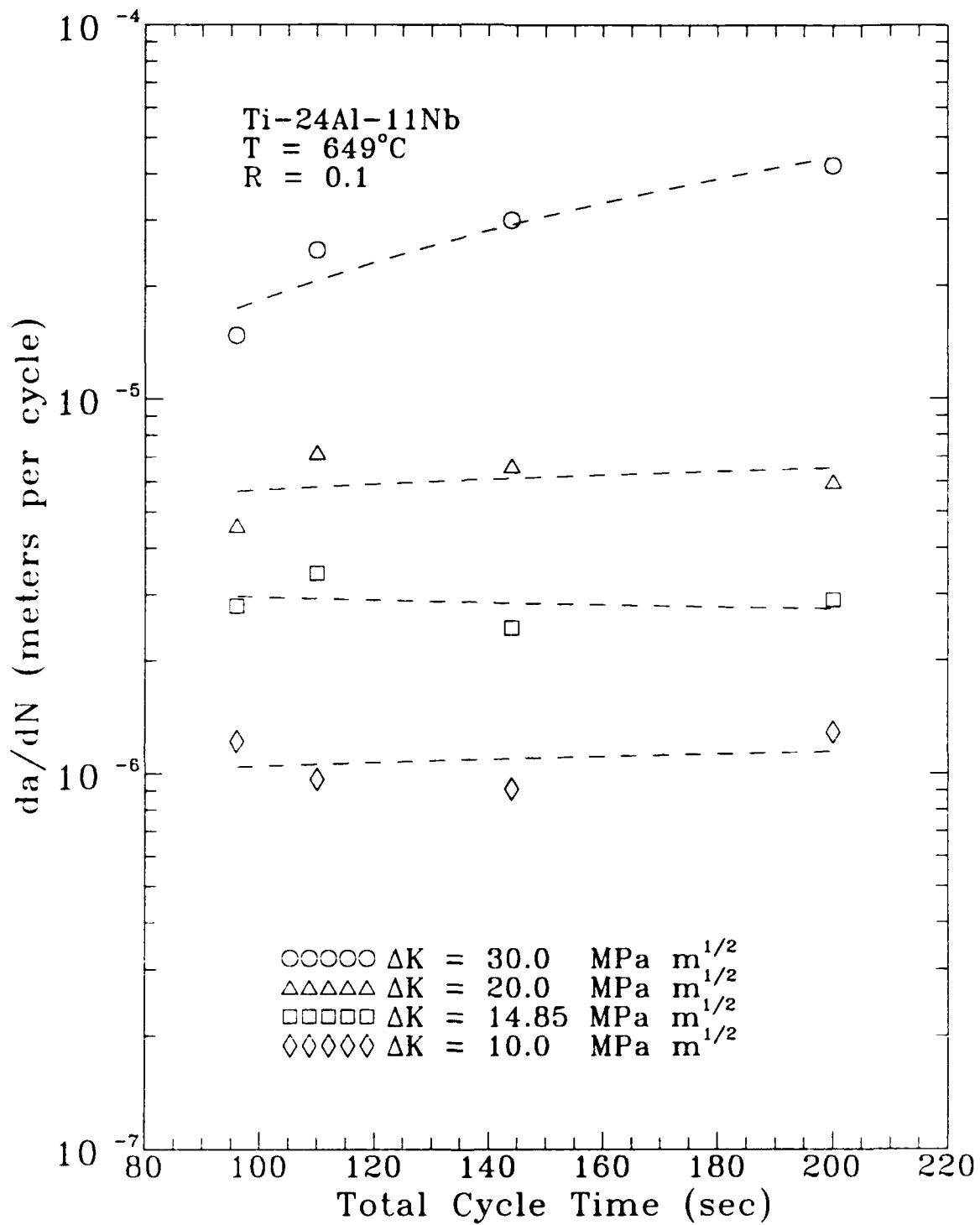
Figure 4.12 Comparison of 0.01 Hz, 649°C Isothermal Data with and
without Superimposed Holds Plotted Against Total Cycle Time

115

Nicholas and Weerasooriya [70] have shown that a linear summation of the crack growth contribution of the fatigue portion of the cycle and the contribution of the hold load could accurately predict the total growth rates for hold-time cycles in Inconel 718. Larsen and Nicholas [43] used this concept to model similar crack growth rate behavior in IN 100. The crack growth rate contribution of the hold time was obtained by multiplying t_h by the sustained-load crack growth rate. As shown in Chapter II, the total crack growth rate, $(da/dN)_{tot}$, is expressed as:

$$\left(\frac{da}{dN}\right)_{tot} = \left(\frac{da}{dN}\right)_f + t_h \left(\frac{da}{dt}\right)_{sl}$$

(2.15)
repeated

where $(da/dN)_f$ is the fatigue (cycle-dependent) crack growth rate contribution and $(da/dt)_{sl}$ is the sustained-load crack growth rate. This linear-summation model provided the basis for the HNH model, Equation (2.18), which was used to model TMF crack growth rates in the studies of the nickel-base superalloy, Inconel 718, discussed previously.

If a linear summation model were applicable in this case of the titanium-aluminide alloy, the 48 second hold would produce an increase in growth rate that is approximately five times that of the 10 second hold; additionally, the 100 second hold would produce an increase in growth rate that is an order of magnitude larger than obtained by the 10 second hold. This concept of linear summation would seem to be valid for predicting crack

116

growth rates in the titanium-aluminide alloy if the contribution of the hold were approximately equal to zero. This, in turn, suggests that the sustained-load crack growth rates in Ti-24Al-11Nb are approximately equal to zero, which is consistent with the findings of Mall et al. [21] discussed earlier. But this summation concept, which developed into the HNH model, still does not explain the frequency effect described earlier and presented in Figure 4.5.

Hold-Times Tests with 1.0 Hz Fatigue Cycles

To investigate further the effects of a hold at P_{max} during fatigue cycling, hold times of t_h = 10, 50, 100, and 1000 seconds are superimposed on 1.0 Hz fatigue cycles. These hold-time tests differ from those previously discussed since they introduce holds that are not of equal magnitude, but up to three orders of magnitude larger than the fatigue cycle. For these tests, constant K_{max} conditions were used to conserve time and material. The results of these tests are plotted with results from a previous investigation [115] in Figure 4.13. Power-law curves are fit to the data of equal hold times to group the data for presentation purposes, and these are shown as dashed lines in the figure. The crack growth rate data of equal K_{max} and t_h are averaged and plotted with respect to total cycle time in Figure 4.14. Dashed lines show the trends in the data.

These data shown in Figures 4.13 and 4.14 further emphasize the relatively small contributions that load holds have on growth rates in this

117
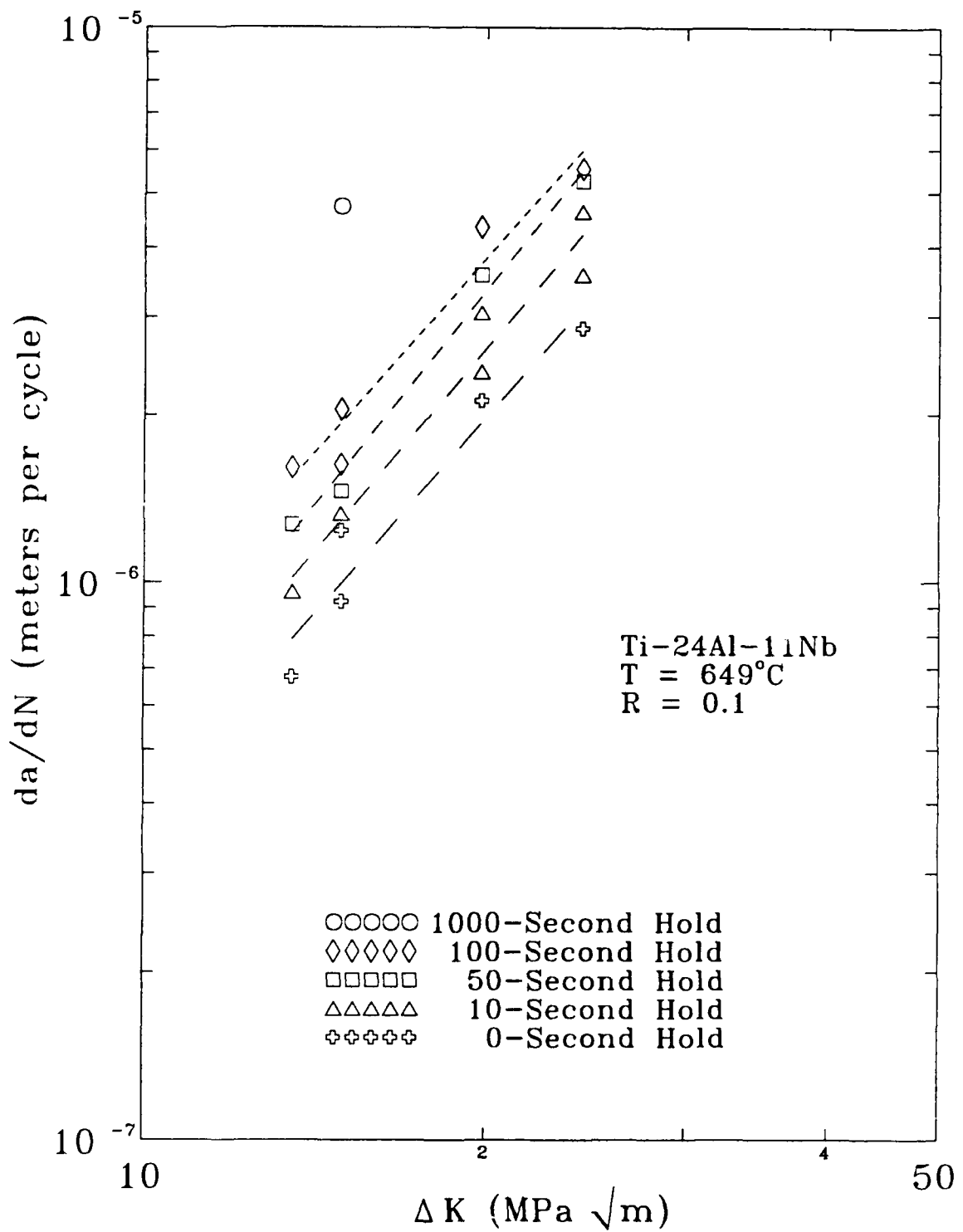
Figure 4.13 Comparison of 1.0 Hz, 649°C Isothermal Data with Data
Obtained with Superimposed Holds of 10, 50, 100, and 1000 Seconds

118
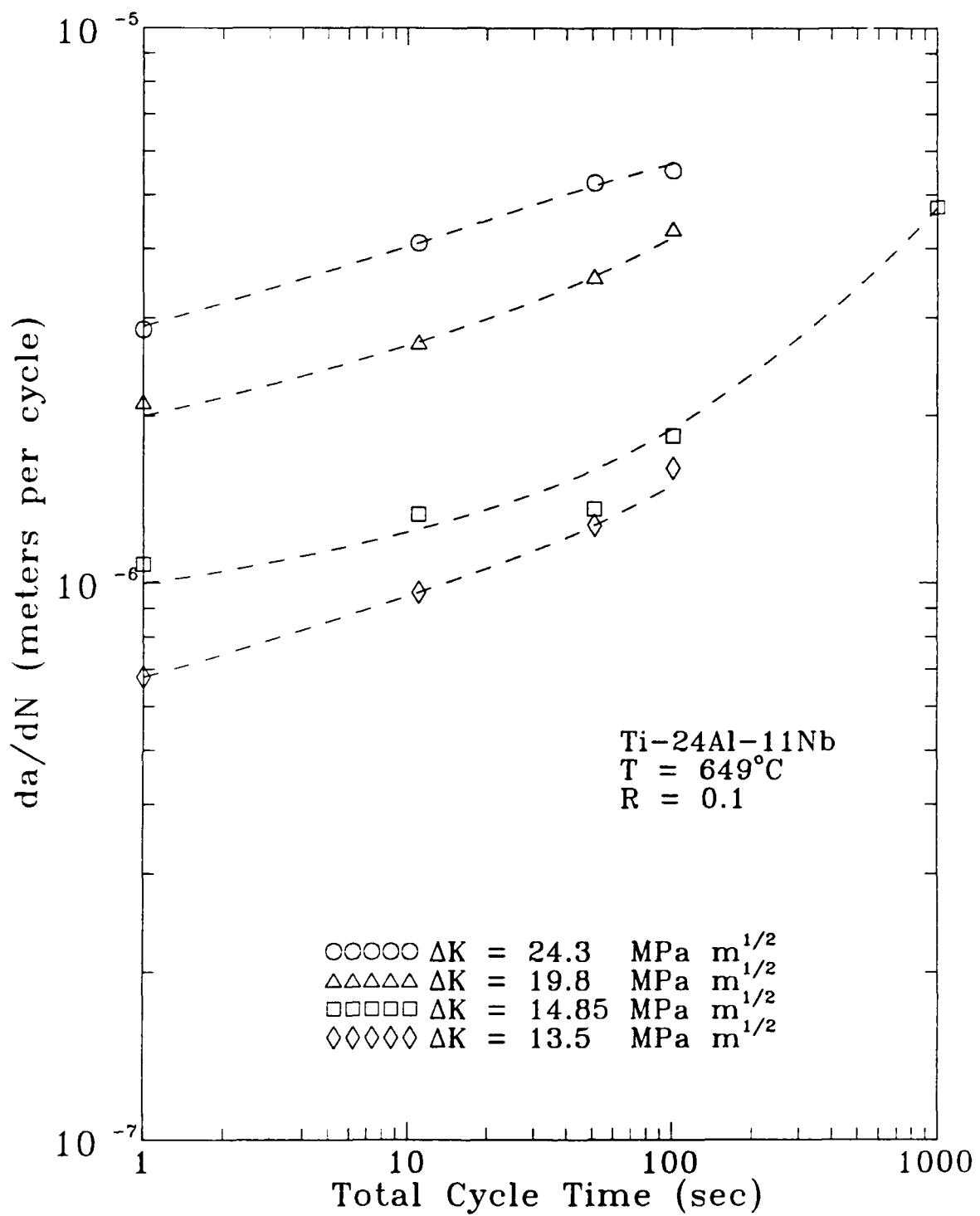
Figure 4.14 Comparison of 1.0 Hz, 649°C Isothermal Data with and
without Superimposed Holds Plotted Against Total Cycle Time

119

titanium-aluminide alloy. But unlike the data obtained from the hold-time studies with 0.01 Hz fatigue cycles, there is a distinguishable increase in growth rates as hold times are added to the 1.0 Hz fatigue cycles. However, adding a 100 second hold to a 1.0 Hz fatigue cycle does not even double the growth rate, and one could argue that this growth rate increase is not very significant. On the other hand, the 1000 second hold-time test produced a crack growth rate increase that is much more significant; however, in this case, the hold time increases the total cycle time by a factor of 1000, and the growth rate increases by a factor of approximately five. Thus, the data presented in Figures 4.13 and 4.14 show that effect of hold time is not as dramatic in this material as was found previously in many others, for example Cr-Mo-V steel [42], and Inconel 718 [119]. In Inconel 718 [119], a hold time at maximum load increases the growth rate proportionally to t_h . As shown in Equation (2.15), Nicholas and Weerasooriya [70] modeled the crack growth rate contribution of the hold time in Inconel 718 as t_h multiplied by the sustained-load crack growth rate. In that alloy, an increase in hold time of x times results in an increase in growth rate of x times. The growth rates in Ti-24Al-11Nb do not appear to follow such behavior, since the growth rate increase from no hold to t_h = 1000 seconds appears to be only five times greater than the increase from no hold to t_h = 100 seconds. Furthermore, the sustained-load crack growth rate in this material is approximately equal to zero. If Equation (2.15) were used to model the hold-time behavior in this alloy, the predictions would not

120

show any increase in crack growth rates as hold times were added to the fatigue cycles, and this is already pointed out in the discussions involving the 0.01 Hz fatigue cycles with hold times.

Another observation can be made by comparing the hold-time tests with fatigue cycles of 0.01 Hz with those of 1.0 Hz. From Figure 4.13 it appears that the addition of a 100 second hold shifts the entire da/dN vs. ΔK curve upward (increased growth rate for a given value of ΔK). The same value of t_h appears to have no effect on growth rates for the hold-time tests with 0.01 Hz fatigue cycles shown in Figure 4.11. The difference between these two tests is the length of the fatigue portion of the cycle. Therefore, it is postulated that the amount of crack propagation resulting from the hold-time is dependent upon the prior loading history (before the hold times are introduced), more specifically, the frequency of the fatigue portion of the loading cycle prior to the application of the hold.

Crack Growth Mechanisms

From the isothermal fatigue crack growth behavior and hold-time effects discussed previously in this chapter, it is postulated that the crack propagation in this material under the majority of the described conditions is entirely mixed mode. In addition, this mixed-mode crack growth can be described by both cycle-dependent and time-dependent contributions. The cycle-dependent contribution, by definition, is frequency independent. Pure cycle-dependent

121

behavior is shown in Figure 4.9 for temperatures between 25 and 250°C, and appears to be a function of temperature. At temperatures above 250°C the effects of the time-dependent contribution can be seen in Figure 4.9, where the crack growth is mixed mode. (Recall that pure time-dependent behavior is not observed in this alloy). It is postulated that this time-dependent crack growth contribution is caused by two competing mechanisms: an environmental mechanism (resulting in crack propagation) and a creep mechanism (resulting crack growth rate retardation).

The environmental mechanism, in the form of degradation, is thought to be caused by oxygen penetration ahead of the crack tip, causing the material to embrittle. The oxide buildup on the crack surfaces does not prevent the diffusion of oxygen near the crack tip [20], and these oxides are not sufficient to wedge the crack open and retard crack growth. This mechanism increases growth rates as frequency decreases (or cycle time increases), and this is observed in data obtained between 0.001 Hz and 100 Hz as shown in Figure 4.6. This mechanism is active even at temperatures as low as 315°C, as shown in Figure 4.9. Balsone et al. [115] have performed experiments that support the observation that there is a significant environmental effect present in this alloy at the temperatures considered in this study. They observed that the growth rates in an air environment are larger than those obtained in vacuum by an order of magnitude. Similar observations have been made in the titanium alloy, 6242S [126].

It is postulated that the second mechanism of time-dependent crack growth is creep near the crack tip, causing crack growth retardation. This mechanism is active when Ti-24Al-11Nb is held at an elevated temperature while under a sustained mechanical load. A subsequent fatigue cycle must overcome this retardation before the environment can attack the material and propagate the crack. The effects of this retardation are sh·wn in Figures 4.11 - 4.14; the addition of the hold times did not increase the growth rates dramatically. As previously mentioned, the effect of a hold time added to fatigue cycles was negligible in previous studies of titanium alloys 6242S and 5621S [123] and titanium alloy IMI 685 [124]. However, in previous investigations of nickel-base superalloys [43, 70] the crack propagation was purely time dependent for similar hold-time test conditions. This retardation observed in the Ti-24Al-11Nb crack growth rates is thought to be attributed to crack-tip blunting. Crack-tip blunting is observed visually during the experimentation, and is further confirmed by large crack opening displacements [89].

It also is postulated that this retardation in the titanium-aluminide alloy does achieve some steady-state condition. This steady-state behavior is observed in Figure 4.14 for hold times added to 1 Hz fatigue cycles. For the 10 second and 100 second hold-time conditions, the growth rate increase from the 1 Hz fatigue data is very small. But for the 1000 second hold, a more substantial increase is observed. Therefore, as the length of the hold time

increases, the contribution of the hold eventually becomes substantial. This implies that with increases in hold times, the retardation achieves some minimum level (lower limit), which is not equal to zero. Therefore, the crack growth rate contributions during the hold time are retarded, but are not equal to zero.

The mechanisms described above are discussed again in Chapter V when modeling of the TMF crack growth rates in Ti-24Al-11Nb is addressed, but the crack growth behavior of this alloy could be better understood by making a few additional comparisons, which involve the crack growth data from TMF experiments.

Discussions of TMF Crack Growth Data

The crack growth rates from the in-phase TMF test are compared to those of a 0.01 Hz, 649°C isothermal fatigue test. These crack growth rate data are shown in Figure 4.15. The total cycle time and mechanical loading profiles are identical in both cases (see Figure 4.1). The only difference is that the temperature is cycled between 315 and 649°C in the case of the in-phase TMF cycle and the temperature is held at 649°C in the case of the isothermal test. In general, the cycling of temperature does not show any effect on crack growth. In fact, the growth rates are nearly the same in both cases, with the exception of the low-to-intermediate regions of ΔK. These differences most likely could be attributed to scatter in the data. The similarities in crack
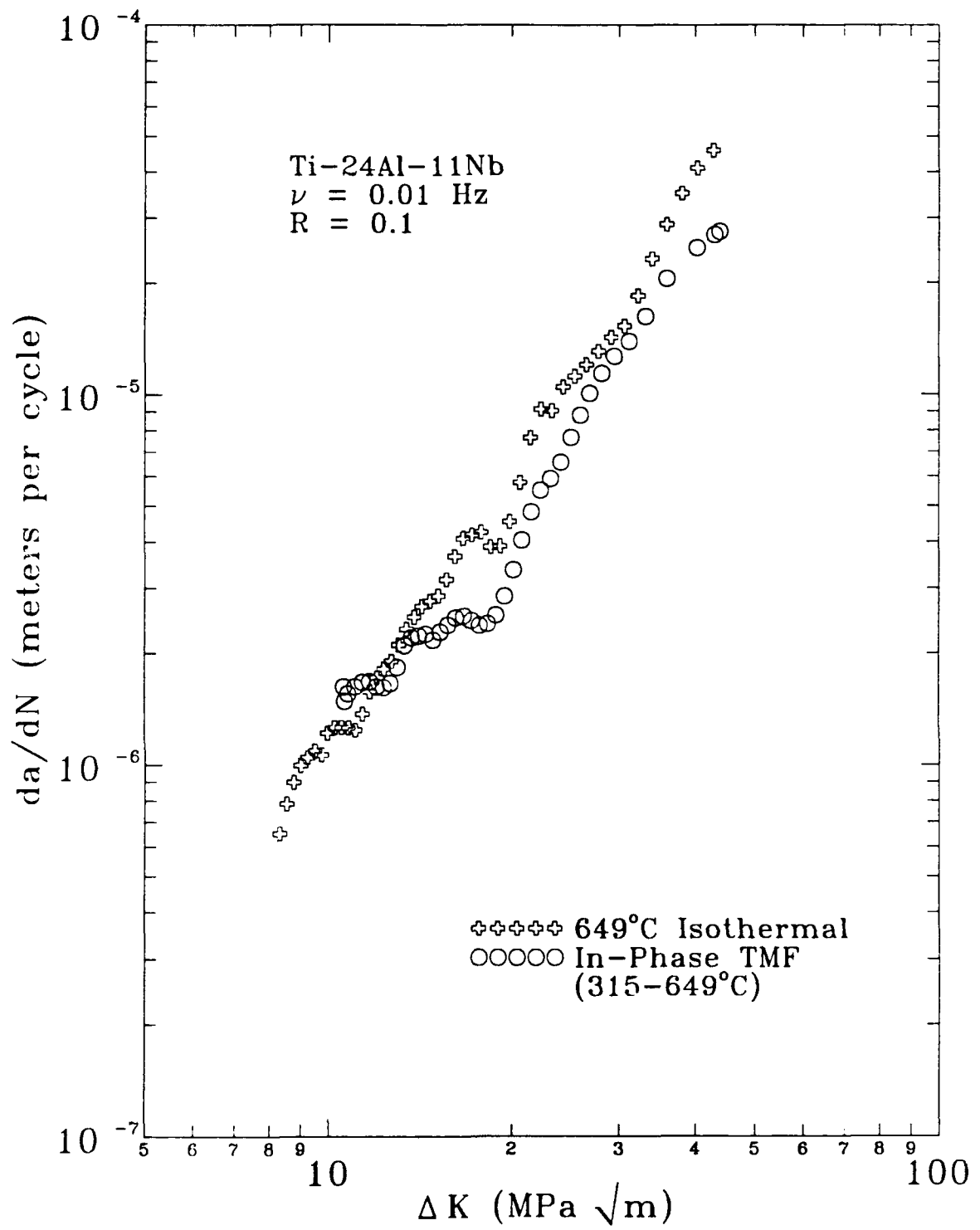
Figure 4.15 Comparison of In-Phase TMF Data with 649°C Isothermal Data

growth rates are probably best described by the competing crack growth mechanisms described earlier in this chapter.

From Figures 4.1 and 4.2 it is obvious that the temperature is equal to T_{max} during the entire isothermal fatigue cycle and the temperature is less than T_{max} for the majority of the in-phase TMF cycle. From the data presented in Figure 4.8, the isothermal test is expected to have a greater environmental (time-dependent) contribution to crack growth than the in-phase test; therefore, the isothermal test is expected to produce higher crack growth rates than the in-phase test. However, the TMF condition is expected to have less of a retardation effect, since the crack growth rate retardation (crack-tip blunting) has a strong dependence on temperature. The net result is that the growth rates for both cases are nearly the same. In the isothermal case, there is more of an environmental effect but also more crack growth rate retardation, and in the in-phase TMF condition, there is less of an environmental effect but also less retardation.

One more comparison can be made to determine what portions of the cycle influence the crack growth rate. Jordan and Meyers [13] had experimentally determined that under isothermal conditions, the growth rate is a function of only the loading portion of the cycle. Rogers and Nicholas [127] have demonstrated that the crack growth rates in Inconel 718 during TMF are not dependent upon what occurs during the unloading portion of the cycle, and this is important in defining when damage occurs. To examine this

126

behavior in the titanium-aluminide alloy, the results from the upper-triangular and lower-triangular-phase tests are compared with those of the in-phase test. The crack growth rate data from these three types of tests are presented in Figure 4.16.

The load and temperature traces for these three types of TMF cycles are presented in Figure 4.1. The lower-triangular-phase and upper-triangular-phase cycles are TMF cycles with in-phase loading from P_{min}, T_{min} to P_{max}, T_{max} and out-of-phase unloading as follows. For the lower-triangular-phase cycle, load is reduced to P_{min} while the temperature is held at T_{max}, and then the load is held at P_{min} while the temperature is reduced to T_{min}. For the upper-triangular-phase cycle, the load is held at P_{max} while temperature is reduced to T_{min}, and then the load is reduced to P_{min} while the temperature is held at T_{min}. Each portion of both cycles takes 48 seconds.

The loading portion of each of these TMF cycles is identical (i.e. 48 second ramp from P_{min} to P_{max}) and only the unloading portions differ. From previous TMF studies [13, 127], one would expect these three TMF cycles to produce similar crack growth rates. Comparing the three cycles shows that holding the load at P_{max} while the temperature is decreasing (upper-triangular-phase cycle) does not contribute to crack growth, but holding the temperature at T_{max} while the load is decreasing (lower-triangular-phase cycle) appears to contribute slightly to crack growth. This is particularly noticeable for ΔK values greater than 20.0 MPa $m^{1/2}$. This increase must be attributed to the

127
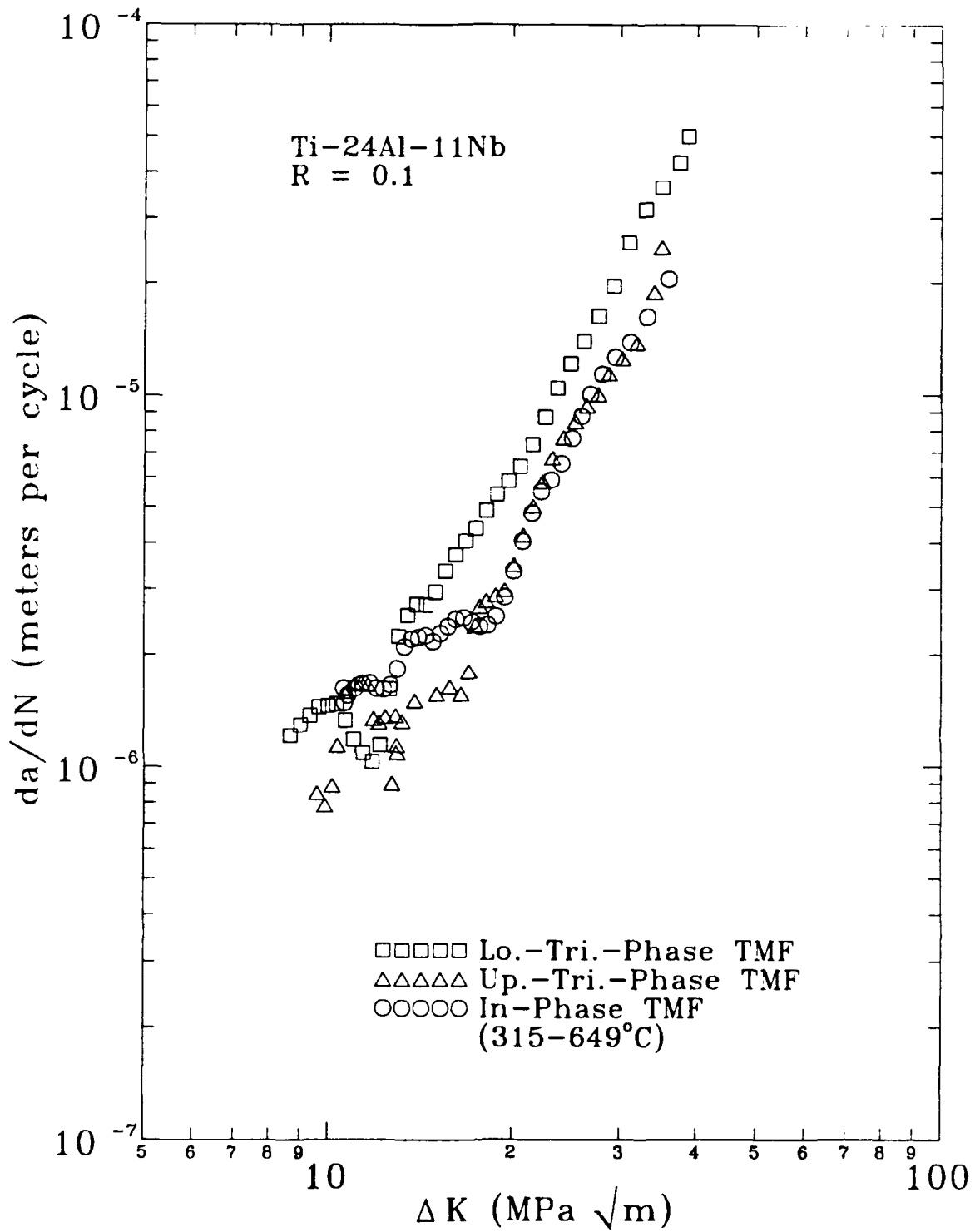
Figure 4.16 Comparison of Lower-Triangular-Phase and
Upper-Triangular-Phase TMF Data with In-Phase TMF Data

128

extended exposure at T_{max}. It should be noted, however, that this increase is not very significant and could possibly be attributed to scatter in the data. If this increase is not experimental scatter, this increased exposure at T_{max} may result in the environmental degradation being more dominant than the retardation mechanism, which is reduced since the load is reduced. It is speculated that in the case of the upper-triangular-phase cycle, the environmental contribution is reduced by the retardation mechanism; therefore, there is no net effect.

Summary of Crack Growth Mechanisms in Ti-24Al-11Nb

From the results presented in this chapter it can be summarized that in Ti-24Al-11Nb the crack growth rates appear to be mixed mode for majority of the test conditions studied. (Mixed-mode crack growth is described in Figure 2.3 and Equations (2.8) and (2.9).) This mixed-mode crack growth appears to be a result of cycle-dependent and time-dependent contributions of crack growth. The cycle-dependent contribution is temperature dependent. This is observed in the pure cycle-dependent crack growth behavior for temperatures less than 300°C (Figure 4.9). Also, there seems to be two competing time-dependent crack growth mechanisms. The first of these is an environmental degradation mechanism that enhances crack growth by oxygen diffusion, and the second, a retardation mechanism that inhibits crack growth rates when a crack is exposed to sustained loads and elevated temperatures. It is speculated

that this crack growth rate retardation is attributed to crack-tip blunting based on observations made during experimentation, but without further investigation, this is not conclusive. In Chapter V of this dissertation, a model is presented that accounts for this retardation of crack growth rates in the titanium-aluminide alloy based on the observed physical behavior discussed in this chapter.

V. Modeling TMF Crack Growth Rates in Ti-24Al-11Nb

Chapter IV is summarized briefly before discussing the crack growth

rate model. In Chapter IV, the isothermal fatigue and the thermal-mechanical

fatigue (TMF) behavior of the titanium-aluminide alloy, Ti-24Al-11Nb, are

presented and discussed. The behavior of this alloy is compared to the results

of previous studies involving other materials, particularly the superalloys. The

overall comparison of the crack growth rates of Ti-24Al-11Nb with those of the

superalloy, Inconel 718 shows that the crack growth behavior during elevated-

temperature fatigue and TMF are similar in both of these alloys.

The in-phase, 90° out-of-phase, 180° out-of-phase, and 270° out-of-phase

TMF crack growth rates are bounded by the T_{max} isothermal crack growth

rates (upper bound) and the T_{min} isothermal crack growth rates (lower bound).

Of these four TMF cycles, the in-phase cycle produces the highest growth

rates, and the 90° and 180° out-of-phase cycles produce the lowest, which are

nearly equal (see Figure 4.3 and 4.4). Also for both of the alloys, changes in

frequency at elevated temperatures produced similar trends in growth rates.

The crack growth rate increases as loading frequency (v) decreases at 649°C for

0.01 Hz < v < 100.0 Hz (see Figure 4.6 - 4.7).

From these results, one might conclude that the model developed by

Heil, Nicholas, and Haritos (HNH model) [15] and used to predict TMF crack

growth rates in Inconel 718 could be used in the case of Ti-24Al-11Nb; but

there are several differences in behavior that make the use of such a model impossible. Specifically, when testing the titanium-aluminide alloy at elevated temperatures, the addition of hold times at P_{max} to fatigue cycles leads to very minimal increases in growth rates (see Figures 4.11 - 4.14); however, if the cycle time of a pure fatigue cycle is increased, there is an increase in growth rate. The nickel-base superalloys (e.g. Inconel 718), on the other hand, exhibit nearly pure time-dependent behavior when hold times were added to fatigue cycles [12], i.e. for the superalloys, the increases in growth rate were proportional to the increases in cycle time. Also, the sustained-load crack growth rate data necessary for the HNH model could not be obtained for the titanium aluminide, since a crack does not propagate under such conditions [89]. These differences dictate a need for an alternative method of modeling TMF crack growth rates in the titanium aluminide, which is the objective of this study.

The topics discussed in this chapter are: first, the procedure that was used in a previous study to model the crack growth rates in Inconel 718 under TMF conditions and the limitations of such a model for use with Ti-24Al-11Nb; second, some previous attempts to model crack growth rates in Ti-24Al-11Nb under isothermal conditions and the limitations of these isothermal models for use under TMF conditions; third the development of a model to predict the crack growth rate behavior in Ti-24Al-11Nb and determination of the model parameters from experimental data; fourth, a description of the computer

program that is used to model the TMF behavior in Ti-24Al-11Nb. The crack growth rate predictions using this TMF crack growth rate model are presented in Chapter VI.

Modeling TMF Crack Growth Rates in Inconel 718

The crack growth rate model developed in the current study uses the concept that the total crack growth rate during TMF cycling can be represented as a combination of two crack growth rate components, a cycle-dependent contribution and a time-dependent contribution. This concept was used by Heil, Nicholas, and Haritos (HNH model) [15] to predict TMF crack growth rates in Inconel 718, but needs to be modified for use with Ti-24Al-11Nb. Before the details of this modified model are presented, the HNH model is discussed in more detail.

The HNH cumulative-damage crack growth rate model [8, 15] uses the linear sum of pure mechanical fatigue (cycle-dependent behavior) and environmental interaction (time-dependent behavior) to estimate the total crack growth rate. This model has been used to estimate crack growth rates during TMF cycling between 427 and 649°C with a loading frequency of 0.01 Hz. This model is expressed as:

$$\left(\frac{da}{dN}\right)_{tot} = \left(\frac{da}{dN}\right)_{cd} + \left(\frac{da}{dN}\right)_{td} \qquad (5.1)$$

133

where $(da/dN)_{tot}$ is the total crack growth rate, $(da/dN)_{cd}$ is the cycle-dependent crack growth rate, and $(da/dN)_{td}$ is the time-dependent crack growth rate. The data used to compute the cycle-dependent crack growth rate as a function of ΔK and R were obtained from 10 Hz isothermal fatigue tests at $427^{\circ}C$ with $R = 0.1$ and $R = 0.5$. At temperatures below $538^{\circ}C$, cycle-dependent damage dominated the growth rates and these were found to be temperature independent; therefore, to completely define the cycle-dependent crack growth rates it was sufficient to acquire data at only one temperature. The cycle-dependent crack growth rate was expressed in terms of ΔK and R:

$$\left(\frac{da}{dN}\right)_{cd} = f(\Delta K, R) \tag{5.2}$$

The time-dependent term was determined by integrating elevated-temperature sustained-load crack growth rate data, $(da/dt)_{sl}$, over the loading portion of the fatigue cycle, while $(da/dt)_{sl}$ is a non-decreasing function. This integration is expressed as:

$$\left(\frac{da}{dN}\right)_{td} = \int_{\substack{non- \\ decreasing}} \left(\frac{da}{dt}\right)_{sl} dt \tag{5.3}$$

The integration shown in Equation (5.3) starts when the load begins to increase $(t = 0)$, and ends when $(da/dt)_{sl}$ begins to decrease. Heil et al. [15] attempted to integrate $(da/dt)_{sl}$ from $t = 0$ to $t = t_{nd}$ (time of non-decreasing

134

load), but found these limits to be insufficient. Heil et al. [15] noted that under isothermal fatigue conditions, $(da/dt)_{sl}$ begins to decrease when the load begins to decrease (i.e. at $t = t_{nd}$), but when temperature is changing during a cycle, this is not necessarily the case. Therefore, they proposed to terminate the integration when $(da/dt)_{sl}$ begins to decrease. The term "non-decreasing" was used (instead of "increasing") in Equation (5.3) to include the conditions of a hold at P_{max} ; $(da/dt)_{sl}$ would remain constant under such conditions. Nicholas and Weerasooriya [70] found that contributions to crack growth continue during a hold time at P_{max} for the Inconel 718 alloy.

The sustained-load crack growth rate, $(da/dt)_{sl}$, was expressed in terms of the K and T:

$$\left(\frac{da}{dt}\right)_{sl} = f(K, T) \tag{5.4}$$

The integration of $(da/dt)_{sl}$ yields the time-dependent crack extension per cycle. The cycle-dependent contribution (Equation (5.2)) is then added to this growth rate to yield the total crack growth rate per cycle, $(da/dN)_{tot}$. For Inconel 718, the predicted $(da/dN)_{tot}$ for TMF cycles of various phase angles were within a factor of two of the experimental data [15].

Modeling Isothermal Crack Growth Rates in Ti-24Al-11Nb

In this section, previous efforts of modeling Ti-24Al-11Nb are discussed. The concepts used in those previous efforts are considered in the development of the TMF model, which is presented later in this chapter.

Mall et al. [21] attempted to model the crack growth behavior of the titanium-aluminide alloy, Ti-24Al-11Nb under hold-time conditions at 750°C using the linear-summation model (Equation (2.11)) developed by Nicholas and Weerasooriya [70] to predict crack growth rates in Inconel 718 under similar conditions. Sustained-load crack growth occurs in Ti-24Al-11Nb at 750°C; therefore, it was possible to obtain the required $(da/dt)_{sl}$ for such a model. Mall et al. [21] found that the linear-summation model could not predict crack growth rates in the titanium-aluminide alloy for 0.1 Hz fatigue cycles with superimposed holds at P_{max} of one-half, two, five, and ten minutes. The model underestimated growth rates for the experiments with one-half, two and five-minute holds and overestimated growth rates for the experiment with the ten-minute hold.

It is clear that an alternate method must be used in modeling the crack growth rate in the titanium-aluminide alloy, Ti-24Al-11Nb. The test results presented in Chapter IV suggest that when Ti-24Al-11Nb is subjected to elevated temperatures, the crack growth is controlled by two competing mechanisms: 1) an environmental mechanism, which tends to increase the growth rate, and 2) a retardation mechanism, which is believed to be blunting

136

of the crack tip. The linear-summation model used by previous investigators [15, 70] does not account for this creep mechanism. But in other previous studies, the crack growth rates in the titanium-aluminide under hold-time conditions were modeled using a coefficient (multiplier) in both the cycle-dependent and time-dependent contributions of crack growth. The coefficients were used to account for the retardation effects that have been attributed to crack-tip blunting [21, 128, 129]. Creep causes blunting of the crack tip, which in turn, causes a reduction in the crack growth rate. These retardation effects are discussed in further detail in Chapter IV. The coefficients used in previous crack growth studies of Ti-24Al-11Nb [21, 128, 129] create an effective value of crack growth rate similar to that used by Wheeler [78] to account for overload (overpeak) crack growth rate retardation, as discussed in Chapter II.

Based on the models used to account for the retardation of crack growth rates during hold-time experiments [21, 128, 129], a general expression for the total crack growth rate can be written as the sum of an effective cycle-dependent crack growth rate and an effective time-dependent crack growth rate. The effective values account for the creep effect. The total crack growth rate can be expressed as:

$$\left(\frac{da}{dN}\right)_{tot} = \beta_{cd}\left(\frac{da}{dN}\right)_{cd} + \beta_{td}\left(\frac{da}{dN}\right)_{td} \tag{5.5}$$

where β_{cd} and β_{td} are the retardation coefficients for the cycle-dependent and

137

time-dependent contributions to crack growth, respectively.

Using an expression similar to this, Mall et al. [21] have modeled the crack growth rate behavior for fatigue and hold-time tests of the Ti-24Al-11Nb alloy under isothermal conditions at 750°C, which is higher than those being considered in the current study. They expressed the total crack growth rate in the form of crack extension per time unlike Equation (5.5), which expresses the crack growth rates in extension per cycle. The time differential form is determined by dividing the total crack extension per cycle (i.e. da/dN) by the total time, t_{tot}. The total crack growth rate is expressed in this form as:

$$\left(\frac{da}{dt}\right)_{tot} = \frac{1}{t_{tot}} \left(\frac{da}{dN}\right)_{tot} = \frac{\beta_1}{t_{tot}} \left(\frac{da}{dN}\right)_f + \frac{\beta_2}{t_{tot}} \left(\frac{da}{dN}\right)_{ht} \tag{5.6}$$

where β_1 and β_2 account for the blunting and sharpening of the crack tip that occurs as a result of the load hold-time and fatigue portions of the cycle, $(da/dN)_f$ is the crack growth contribution of the fatigue portion of the cycle, and $(da/dN)_{ht}$ is the contribution of the hold-time portion of the cycle. These contributions also can be expressed in time-differential form by dividing each growth rate by the time of their respective portions of the cycle:

$$\left(\frac{da}{dN}\right)_f = t_f \left(\frac{da}{dt}\right)_f \tag{5.7}$$

where t_f is the period of the fatigue portion of the cycle, and:

138

$$\left(\frac{da}{dN}\right)_{ht} = t_h \left(\frac{da}{dt}\right)_{ht} \qquad (5.8)$$

where t_h is the length of the hold time at P_{max}. The total time is the sum of the period of the fatigue portion of the cycle and the hold time.

$$t_{tot} = t_f + t_h \qquad (5.9)$$

Substituting Equation (5.7) and (5.8) into Equation (5.6) yields:

$$\left(\frac{da}{dt}\right)_{tot} = \beta_1(t_h)\,\frac{t_f}{t_{tot}}\left(\frac{da}{dt}\right)_f + \beta_2(t_h)\,\frac{t_h}{t_{tot}}\left(\frac{da}{dt}\right)_{ht} \qquad (5.10)$$

The coefficients β_1 and β_2 are expressed as functions of hold time. β_1 accounts for the retardation of fatigue crack growth, which is assumed to be caused by crack-tip blunting. β_1 is expressed as:

$$\beta_1 = \exp(-\alpha_1\,t_h) \qquad (5.11)$$

where the constant, α_1, is determined from the experimental data. This empirical expression was developed to estimate the amount of retardation as a function of hold time. When t_h is equal to zero, β_1 is equal to unity, since this case represents pure fatigue cycling and the fatigue contribution of the model is not reduced. As t_h increases, the fatigue contribution of growth rate

139

decreases, and as t_h approaches infinity, the fatigue portion approaches zero, corresponding to a sustained-load condition.

β_2 accounts for the acceleration of the time-dependent crack growth rate contribution caused by the fatigue portion of the cycle. β_2 is expressed as:

$$\beta_2 = 1 + \alpha_2 \exp(-\alpha_1 t_h) \qquad (5.12)$$

where the empirical constant, α_2, was determined experimentally. β_2 increases as t_h decreases, since the crack is given less time to retard (blunt) under maximum load. When t_h is equal to zero, β_2 is equal to $1+\alpha_2$. Note that t_h appears in the numerator of the hold-time term in Equation (5.10) and this reduces the hold-time contribution to zero as t_h approaches zero. As t_h increases, β_2 decreases, and as t_h approaches infinity, β_2 reduces to unity, which implies steady-state sustained-load crack growth.

Nicholas and Mall [128] later proposed that the total crack growth under fatigue cycles with superimposed hold times could be expressed as the sum of a cyclic term, an environmentally enhanced fatigue term, and a load hold-time term. Using a retardation coefficient similar to that in the model proposed by Mall et al. [21] (the model is discussed above), the sum could be expressed as:

$$\left(\frac{da}{dN}\right)_{tot} = \beta_1'(t_h)\left(\frac{da}{dN}\right)_f + \beta_2'(t_h)\, t_{tot}^{\gamma-1}\left[\int_{\substack{fatigue \\ cycle}}\left(\frac{da}{dt}\right)_{sl} dt + \left(\frac{da}{dt}\right)_{sl} t_h\right] \quad (5.13)$$

where $(da/dN)_f$ is the cyclic contribution to crack growth, $(da/dt)_{sl}$ is the sustained-load crack growth rate, and β_1' and β_2' are the retardation coefficients. The two terms that contain $(da/dt)_{sl}$ represent the environmentally-enhanced fatigue and load hold-time contributions to crack growth. Nicholas and Mall [128] point out that since the environmentally-enhanced fatigue and sustained-load contributions are not purely time dependent in the titanium-aluminide alloy, the second term in Equation (5.13) needs to include a multiplication factor. The factor $t_{tot}^{\gamma-1}$ was used so that this contribution to crack growth would increase proportionally with t_{tot}^{γ} as opposed to t_{tot}, which would be the case if the crack were to propagate under purely time-dependent conditions [128]. For Inconel 718, the 650°C isothermal crack growth shown in Figure 4.7 is purely time-dependent at frequencies less than 0.01 Hz, where the slope, m, is equal to -1.0, but for the titanium-aluminide alloy (Figure 4.6), m is equal to -0.24, since the crack growth rates are mixed mode for equivalent temperatures and frequencies.

The second term in Equation (5.13) represents the integration of $(da/dt)_{sl}$ over the entire cycle. Since $(da/dt)_{sl}$ remains constant during the hold portion of the cycle, the integral could be simplified as shown in Equation (5.13), and the integration remains for only the fatigue portion of the cycle.

141

Nicholas [129] used the expression shown in Equation (5.13) to demonstrate the capability of such a model for hold-time conditions at 650 and 750°C. He used functions β_1' and β_2' of the form:

$$\beta_1' = (1 + \mu t_h)^{-\alpha} \tag{5.14}$$

and

$$\beta_2' = 1 + \rho (1 + \mu t_h)^{-\alpha} \tag{5.15}$$

where μ, α, and ρ are empirical constants that account for the crack-tip blunting. The retardation coefficients, β_1' and β_2', use a decreasing exponential, whereas β_1 and β_2 use a power expression. Although these are of slightly different forms, they have similar characteristics. For t_h equal to zero, β_1' is equal to unity and β_2' is equal to $1 + \rho$. As t_h increases, β_1' and β_2' decrease.

In the two models described above, the various empirical constants can be changed to model different materials, temperatures, frequencies and hold times. The major limitation of these models is that they cannot be used when temperature changes during a cycle (i.e. a TMF cycle). To model these conditions of a TMF cycle, an equation (model) must be developed that allows parameters to change during the cycle. This is the objective of the current investigation, and this model is developed in the remainder of this chapter.

142

Modeling TMF Crack Growth Rates in Ti-24Al-11Nb

This section focuses on the development of the TMF crack growth rate model for the titanium-aluminide alloy, Ti-24Al-11Nb. Topics include: first, the basic formulation of the TMF crack growth rate model; second, the development of the retarded cycle-dependent crack growth rate contribution; third, the development of the retarded time-dependent crack growth rate contribution; fourth, an explanation of the retardation coefficient; and fifth, a summary of the equations that describe the TMF model. Later in this chapter, the computer program that is used to predict the crack growth rates based on this model is discussed, and the crack growth rate predictions are presented in Chapter VI.

Basic Formulation of the Model

As shown previously, the concept of multiplying contributions of cycle-dependent and time-dependent crack growth by a retardation coefficient is sufficient for modeling isothermal hold-time tests at 650 and 750°C, as well as accounting for changes in frequency. In Equation (5.5), a general expression is shown that describes the total crack growth rate as the sum of retarded cycle-dependent and retarded time-dependent crack growth contributions. Equations (5.10) and (5.13) verify that this concept could be used under isothermal conditions [21, 129]. However, it is necessary to develop a technique that is more general to be used in isothermal fatigue, isothermal

143

fatigue with additions of load hold times, and most importantly, TMF conditions.

The model developed in this study combines concepts from the HNH linear-summation model (Equation (5.1)) with the concept of crack growth rate retardation. This model, which is used in this study to calculate TMF crack growth rates in Ti-24Al-11Nb, adds the contributions of crack extension during the cycle as loads and temperatures vary, while using a retardation effect that is a function of cycle time.

This modified TMF crack growth rate model differs from the HNH linear-cumulative damage model, described earlier, in two significant ways: 1) it utilizes a coefficient to account for the retarded crack growth behavior described in Chapter IV, which is thought to be caused by crack-tip blunting, and 2) it allows the cycle-dependent contribution to crack growth to be a function of temperature, which is observed in the isothermal crack growth rate results presented in Chapter IV.

The retardation coefficient, the first modification to the model, is introduced because the observed hold-time and frequency effects are inconsistent with the predictions of the HNH model. At elevated temperatures, growth rates in Ti-24Al-11Nb increase as fatigue cycle time increases (frequency decreases), as shown in Figure 4.6. However, crack growth rates do not increase significantly if the cycle time increases as a result of a hold time superimposed on a fatigue cycle, as shown in Figure 4.12 and

Figure 4.14. When considering the HNH formulation, one would expect that the addition of a hold time to a fatigue cycle would show a growth rate increase on the same order of magnitude as a decrease in frequency of a pure fatigue cycle. The retardation coefficient, introduced in the current modeling effort, decreases the crack growth rate contribution during a hold time to reflect the observed hold-time behavior of Ti-24Al-11Nb, while maintaining the frequency effect of the crack growth rates.

The second modification to the model is the temperature dependence of the cycle-dependent crack growth rate contribution. Figure 4.9 illustrates that as temperature decreases, the crack growth rates in Ti-24Al-11Nb become frequency independent (cycle dependent); however, the cycle-dependent crack growth rate still changes as a function of temperature. Since the cycle-dependent term is a function of temperature, its contribution to the total crack growth rate must be determined from an integration when temperature varies during a cycle, which is the case during a TMF cycle.

The model developed in this study, like that shown in Equation (5.5), describes the total crack growth rate as the sum of retarded cycle-dependent and retarded time-dependent contributions. However, the retardation coefficients in Equation (5.5) are functions of only hold-time duration, but the new model uses a retardation coefficient that can vary during the TMF cycle as a function of cycle time. Therefore, this retardation coefficient should appear inside the integral terms of retarded cycle-dependent and time-dependent

145

crack growth rates. The integral forms of these crack growth rate components are discussed in the sections that follow. Since the retardation effects are incorporated into each of the crack growth components, the new model is written in a form similar to the HNH model shown in Equation (5.1). This new model is expressed as:

$$\left(\frac{da}{dN}\right)_{tot} = \left(\frac{da}{dN}\right)_{\substack{ret \\ cd}} + \left(\frac{da}{dN}\right)_{\substack{ret \\ td}} \tag{5.16}$$

where the total crack growth rate, $(da/dN)_{tot}$, is shown as a linear combination of a retarded cycle-dependent crack growth rate and a retarded time-dependent crack growth rate, but it can be considered a nonlinear summation of cycle-dependent and time-dependent crack growth rates. These retarded crack growth rate terms are discussed in the following sections of this dissertation.

Development of the Cycle-Dependent Term

Formulation of the Cycle-Dependent Term

The cycle-dependent retarded growth rate shown in Equation (5.16) is expressed as:

$$\left(\frac{da}{dN}\right)_{\substack{ret \\ cd}} = \int_0^{t_{ul}} \beta(t)\left(\frac{da}{dt}\right)_{\substack{ur \\ cd}} dt \tag{5.17}$$

146

where β is the retardation coefficient used in this study and is a function of time; t_{ul} is the uploading time of the cycle; and $(da/dt)_{ur\ cd}$ is the unretarded cycle-dependent crack growth rate, which is a function of temperature.

In general, β is a continuously changing parameter, which changes as load (P) and temperature (T) change. Since load and temperature are changing continuously during a TMF cycle (i.e. $P(t)$, $T(t)$), β must remain inside the integral. The evolution equation, which provides the rate of change of β with time, is discussed later in this chapter. The uploading time of the cycle is the time required for the load to reach maximum load. The unretarded crack growth rate is considered as the growth rate of a crack that is not blunted by creep deformation near the crack tip.

The retarded cycle-dependent term is obtained by integrating the retardation coefficient, $\beta(t)$, multiplied by the unretarded cycle-dependent crack growth rates over the loading portion of the TMF cycle as shown in Equation (5.17). The integration is limited to the loading portion of the fatigue cycle to be consistent with previous modeling efforts [12, 13, 15], where it was shown that damage occurs only during loading. The unretarded crack growth rates are obtained from very high-frequency fatigue cycles, and these crack growth rates are expressed in crack extension per cycle, $(da/dN)_{ur\ cd}$. To convert to crack extension per time, $(da/dt)_{ur\ cd}$, the crack growth rate $(da/dN)_{ur\ cd}$ must be divided by the uploading cycle time of a fatigue cycle, which is equal to half the period. The unretarded $(da/dt)_{ur\ cd}$ is expressed as:

$$\left(\frac{da}{dt}\right)_{\substack{ur\\cd}} = \frac{\left(\frac{da}{dN}\right)_{\substack{ur\\cd}}}{\left(\frac{\tau}{2}\right)} \qquad\qquad (5.18)$$

where the cycle period, τ, is expressed as:

$$\tau = 1/\nu \qquad\qquad (5.19)$$

where ν is the frequency of the pure fatigue cycle. When using this model for alloys that maintain unretarded crack growth rate conditions, such as Inconel 718, β is equal to unity, and the retarded and unretarded crack growth rates are identical, as shown in Equation (5.20).

$$\left(\frac{da}{dN}\right)_{\substack{ret\\cd}} = \left(\frac{da}{dN}\right)_{\substack{ur\\cd}} \quad ; \quad for \ \beta = 1.0 \qquad\qquad (5.20)$$

For the Ti-24Al-11Nb alloy, these unretarded growth rates correspond to the lowest obtainable growth rate at any given temperature. That is, $(da/dN)_{ur\ cd}$ is assumed to be equal to the growth rate at the highest frequency tested, since the crack growth rates vary continuously with frequency between 315 and 649°C and never become purely cycle dependent. The pure cycle-dependent crack growth rate condition is defined as 100 Hz, since this is the highest

148

frequency data that are obtained either during this study or found in available literature [115-117]. Therefore, there is no basis for using this model above this frequency. The model is based on the assumption that further increases in frequency will not reduce the growth rate further.

At high frequencies, the retardation effect is reduced and β approaches unity (the totally unretarded crack growth rate condition). Therefore, β is assumed to be equal to unity when defining the parameters for the pure cycle-dependent crack growth condition, and the retarded growth rates are equal to the unretarded crack growth rates.

In general, the unretarded growth rate, $(da/dN)_{ur\ cd}$, is a function of ΔK, R, and T expressed here in functional form:

$$\left(\frac{da}{dN}\right)_{\substack{ur\\cd}} = f(\Delta K, R, T) \tag{5.21}$$

This unretarded crack growth rate is expressed in terms of the modified sigmoidal equation (MSE), which is a modified form of the six-parameter sigmoidal equation developed at General Electric [39, 64, 130]. The MSE that expresses $(da/dN)_{ur\ cd}$ as a function of ΔK and six independent parameters is:

$$\left(\frac{da}{dN}\right)_{\substack{ur\\cd}} = \exp(B_m)\left(\frac{\Delta K}{\Delta K_i}\right)^C \left[\ln\left(\frac{\Delta K}{\Delta K_{t\lambda}}\right)\right]^Q \left[\ln\left(\frac{\Delta K_c}{\Delta K}\right)\right]^D \tag{5.22}$$

149

where:

ΔK_{th} is the threshold stress intensity range, i.e. the value of ΔK at the

lower asymptote of the da/dN vs. ΔK curve,

ΔK_c is the critical stress intensity range, i.e. the value of ΔK at the upper

asymptote of the da/dN vs. ΔK curve,

ΔK_i is the value of ΔK at the curve's inflection point, and

Q and D are the lower and upper shaping coefficients, respectively.

B_m is defined as:

$$B_m = \ln\left(\frac{da}{dN}\right)_i - Q \ln\left[\ln\left(\frac{\Delta K_i}{\Delta K_{th}}\right)\right] - D \ln\left[\ln\left(\frac{\Delta K_c}{\Delta K_i}\right)\right] \tag{5.23}$$

where $(da/dN)_i$ is the value of da/dN at the curve's inflection point, and the

exponent, C, is defined as:

$$C = \left(\frac{da}{dN}\right)_i' - \frac{Q}{\ln(\Delta K_i / \Delta K_{th})} + \frac{D}{\ln(\Delta K_c / \Delta K_i)} \tag{5.24}$$

where $(da/dN)_i'$ is the slope of the curve at the inflection point when plotted as

$\log(da/dN)$ vs. $\log(\Delta K)$.

The MSE shown in Equation (5.22) differs slightly from the sigmoidal

equation shown in Chapter II (Equation (2.13)). The revised coefficient, B_m , is

used instead of B_{se} , which aids in relating the coefficients to test variables [64].

With this modified form, ΔK_i is substituted for ΔK_{th} in the denominator of the

second term in Equation (2.13), and ΔK at the inflection point, ΔK_i, is defined explicitly [64]. ΔK_i is a function of four independent parameters.

$$\Delta K_i = \exp\left[\frac{-(Q^{1/2})\ \ln(\Delta K_c) + (-D)^{1/2}\ \ln(\Delta K_{th})}{-(Q^{1/2}) + (-D)^{1/2}}\right] \tag{5.25}$$

It is more useful to express D as a dependent parameter instead of ΔK_i.

$$D = -\left[Q^{1/2}\ \frac{\ln(\Delta K_i/\Delta K_c)}{\ln(\Delta K_i/\Delta K_{th})}\right]^2 \tag{5.26}$$

Then the six independent parameters are ΔK_c, ΔK_{th}, ΔK_i, $(da/dN)_i$, $(da/dN)_i'$, and Q. The parameters are shown on a plot of da/dN vs. K in Figure 5.1.

The MSE can be simplified by making the da/dN vs. ΔK curve symmetric about the inflection point, and this is accomplished by setting:

$$D = -Q \tag{5.27}$$

Substituting Equation (5.27) into Equation (5.26) and solving for the non-trivial solution allows ΔK_c to be expressed as a function of ΔK_i and ΔK_{th}:

$$\Delta K_c = \frac{\Delta K_i^2}{\Delta K_{th}} \tag{5.28}$$

151
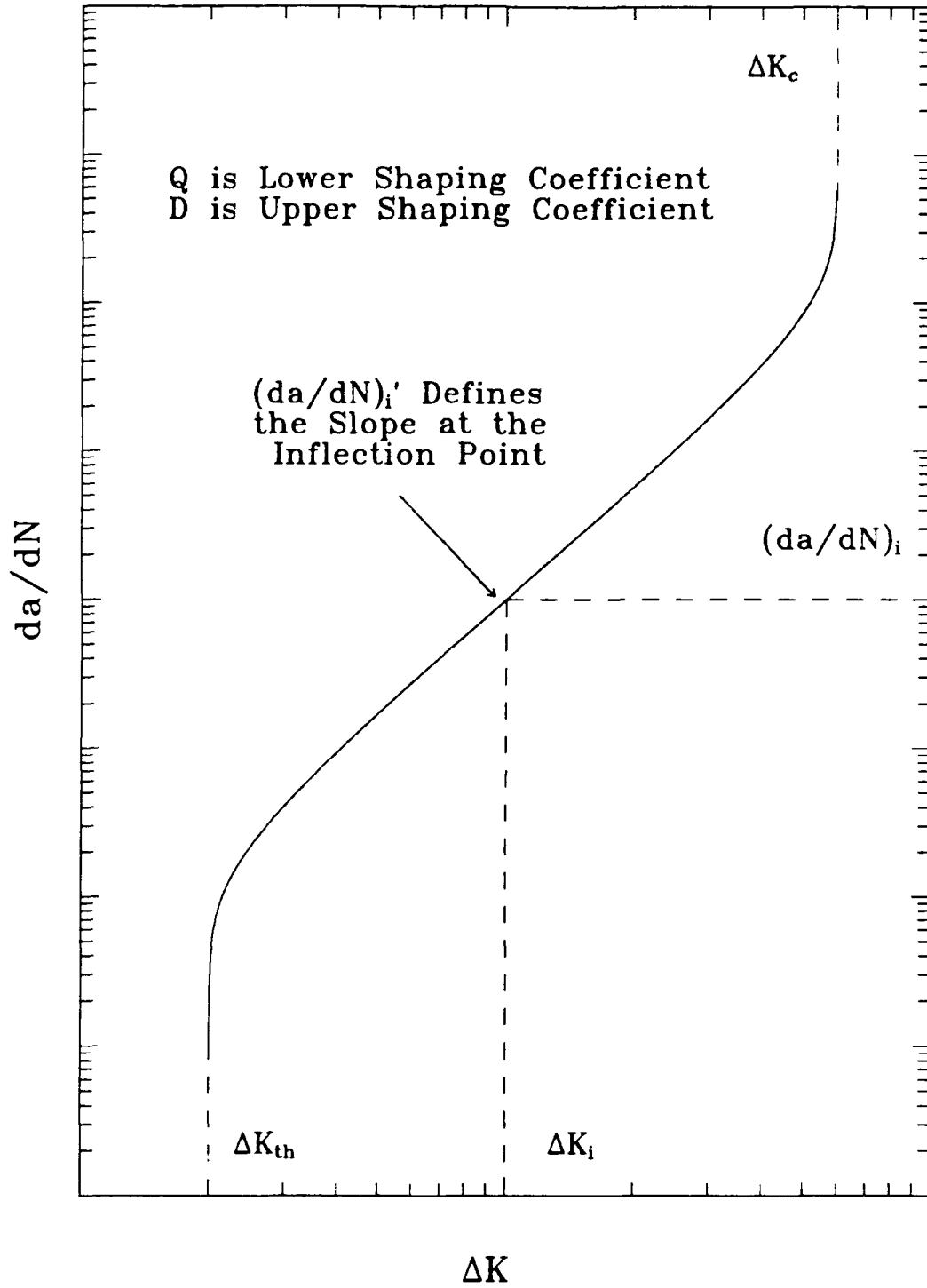
Figure 5.1 Definition of the MSE Parameters on a *da/dN* vs. Δ*K* Plot

152

With this simplification, the independent parameters that define the symmetric curve are reduced to five, which are ΔK_{th}, ΔK_i, $(da/dN)_i$, $(da/dN)_i'$, and Q. Subsequently, when the lower and middle regions of the da/dN vs. ΔK curve are defined, the upper region of the curve also is defined. This was used in a previous modeling effort involving the MSE [15], and it did not restrict the modeling since the region near the upper asymptote of the curve was not used. Similarly, in the current effort, the symmetric assumption is employed, and the upper asymptotic region of the crack growth curve is not modeled.

Previous studies involving the modeling of Inconel 718 data [6, 131] have shown that the lower shaping coefficient, Q, was not a function of frequency, load ratio, or temperature; therefore, assuming Q is equal to a constant did not impair the modeling process. In the current study, there are insufficient crack growth rate data in the threshold stress intensity region to properly model the behavior of Q for the range of frequencies and temperatures studied; therefore, this region of crack growth is not modeled. Q is fit to the data obtained from a 5 Hz, 649°C isothermal test, and Q is assumed not to be a function of R or T in Ti-24Al-11Nb, i.e. Q = constant. Even though the threshold regions were not modeled, the data from all other tests did not invalidate this assumption.

The cycle-dependent crack growth rate is expressed only as a function of ΔK, load ratio (R), and temperature (T) since the basic premise of cycle dependence is that the growth rates are frequency independent. The

153

expression used to define the MSE parameters for the unretarded cycle-dependent crack growth rate in terms of R and T is:

$$
\begin{bmatrix}
\log(\Delta K_{th}) \\
\log(\Delta K_i) \\
\log(da/dN)_i \\
(da/dN)_i'
\end{bmatrix}
=
\begin{bmatrix}
\log(\Delta K_{th}) \\
\log(\Delta K_i) \\
\log(da/dN)_i \\
(da/dN)_i'
\end{bmatrix}_{ref}
+
\begin{bmatrix}
A_{11} & A_{12} \\
A_{21} & A_{22} \\
A_{31} & A_{32} \\
A_{41} & A_{42}
\end{bmatrix}
\begin{bmatrix}
\log\left(\dfrac{1-R}{1-R_{ref}}\right) \\
(T-T_{ref})
\end{bmatrix}
\qquad (5.29)
$$

Ideally, a test at the reference condition (not to be confused with the unretarded crack growth rates) is performed first, and the reference parameters shown in Equation (5.29) are determined. Second, tests at different frequencies and load ratios are performed to establish the A_{ij} in Equation (5.29). The unretarded cycle-dependent growth rates then can be expressed as a function of stress intensity range, load ratio, and temperature. In the following discussions, the constants in Equation (5.29) are determined.

Determination of the Cycle-Dependent MSE Parameters

In the current effort, the reference condition for the MSE parameters that define the unretarded cycle-dependent crack growth rate, $(da/dN)_{ur\,cd}$, is taken as $T = 250^{\circ}C$ and $R = 0.1$. Complete da/dN vs. ΔK data are not available at this condition, but the following observations make it possible to use other fatigue data to completely define the curve at this reference condition. These observations also make it possible to reduce the A_{ij} coefficients.

154

Since modeling of the threshold of ΔK is not being considered in this study, a selection of ΔK_{th} is made such that the value is less than all the data being modeled. The 5 Hz, 649°C test produced crack growth rates for the lowest values of ΔK studied; therefore, the reference ΔK_{th} is selected based on this test.

$$[\Delta K_{th}]_{ref} = 4.0 \ MPa \ m^{1/2} \tag{5.30}$$

Also, since the regions near the threshold and critical values of ΔK are not modeled, ΔK_{th} and ΔK_c are held constant as temperature varies. Since ΔK_{th} is not a function of T:

$$A_{12} = 0 \tag{5.31}$$

Since, ΔK_{th} and ΔK_c are held constant as temperature varies and the da/dN vs. ΔK curve is symmetric ($D = -Q$), ΔK_i also is not a function of temperature (see Equation (5.28)), and this implies:

$$A_{22} = 0 \tag{5.32}$$

The reference value of ΔK_i is selected as:

$$[\Delta K_i]_{ref} = 30.0 \ MPa \ m^{1/2} \tag{5.33}$$

155

Therefore, the inflection point is described completely as a function of temperature by $(da/dN)_i$. In this case, $(da/dN)_i'$ is determined before $(da/dN)_i$, and in doing so, an additional simplification is made regarding the coefficient, A_{42}.

Isothermal test data obtained at 649 and 482°C indicate that the da/dN vs. ΔK curves shift as temperature varies but remain parallel. These data are presented in Figure 5.2. This observation indicates that the slope of the linear region of the curve is temperature independent. In turn, the slope at the inflection point, $(da/dN)_i'$, is not a function of temperature, therefore:

$$A_{42} = 0 \tag{5.34}$$

$(da/dN)_i'$ is the slope of the $\log(da/dN)$ vs. $\log(\Delta K)$ curve at the inflection point, but it also can be considered the exponent of a power fit to the data in the linear region.

$$\frac{da}{dN} = C_k (\Delta K)^n \tag{5.35}$$

where n is the power law exponent and C_k is a constant defined as the crack growth rate, da/dN, for $\Delta K = 1.0$ MPa m$^{1/2}$. $(da/dN)_i'$ is determined by fitting Equation (5.35) to the crack growth data at different temperatures, and then selecting an average value that best describes the data. These curve fits are

156
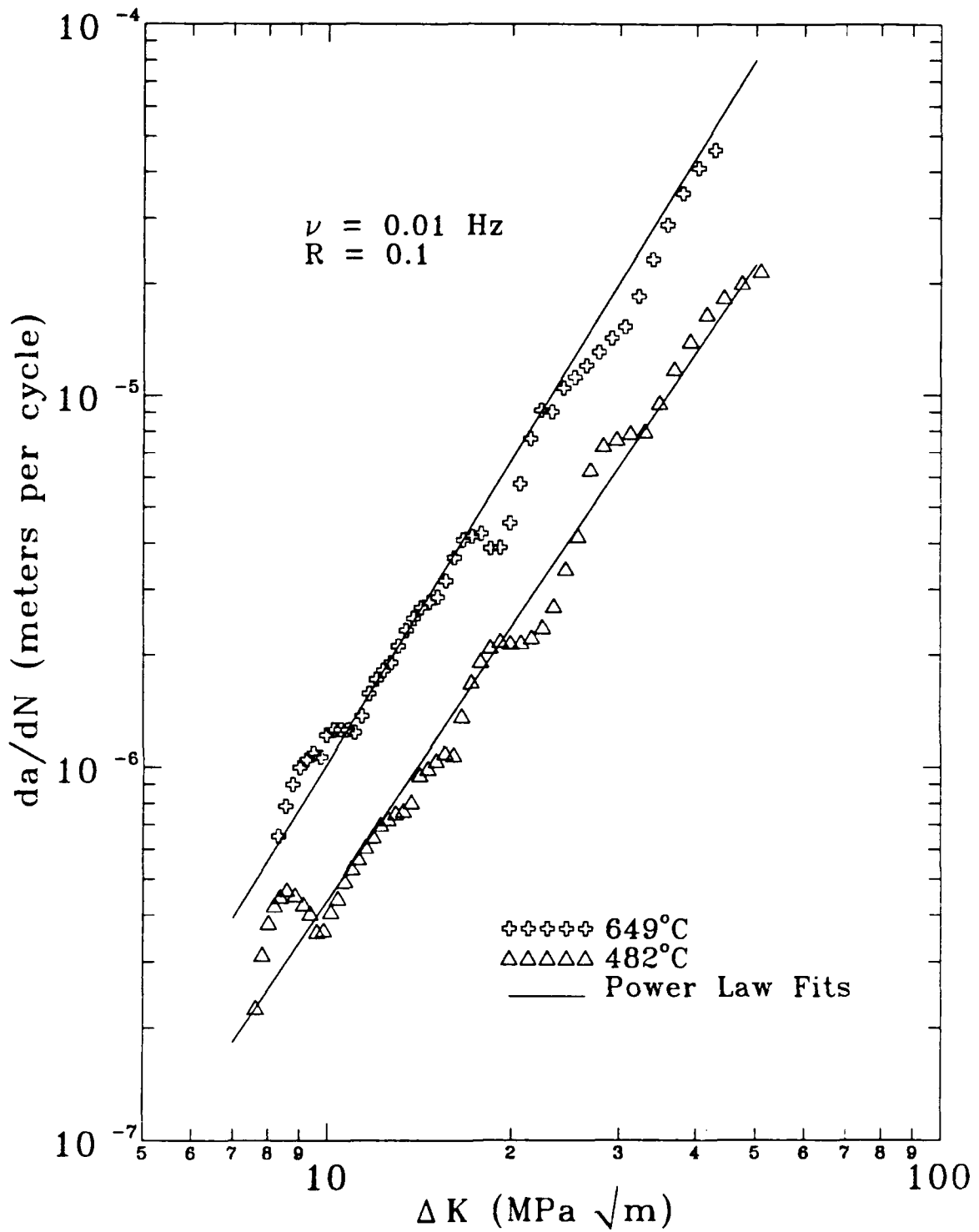
Figure 5.2 Crack Growth Variations with Temperature
Including Power Law Curve Fits to the Data

157

also shown in Figure 5.2. The data presented in Figure 5.2 are obtained from

0.01 Hz experiments, but the reference condition is determined at 100 Hz. No

data were acquired at 100 Hz since $(da/dN)_i'$ does not significantly vary with

frequency, as shown in Figure 5.3 where data of 0.01, 0.1, and 5.0 Hz are

plotted. The power law expression also is fit to these data and used in the

selection of $(da/dN)_i'$. A summary of these curve-fit results is presented in

Table 5.1.

Table 5.1 A Summary of Power Law Curve Fits

Temperature (°C)	Frequency (Hz)	C_k	n
482	0.01	1.57×10^{-9}	2.45
649	0.01	2.03×10^{-9}	2.70
649	0.1	2.67×10^{-9}	2.38
649	5.0	6.44×10^{-10}	2.64

From the data presented in Table 5.1, the reference value of $(da/dN)_i'$ is

selected as:
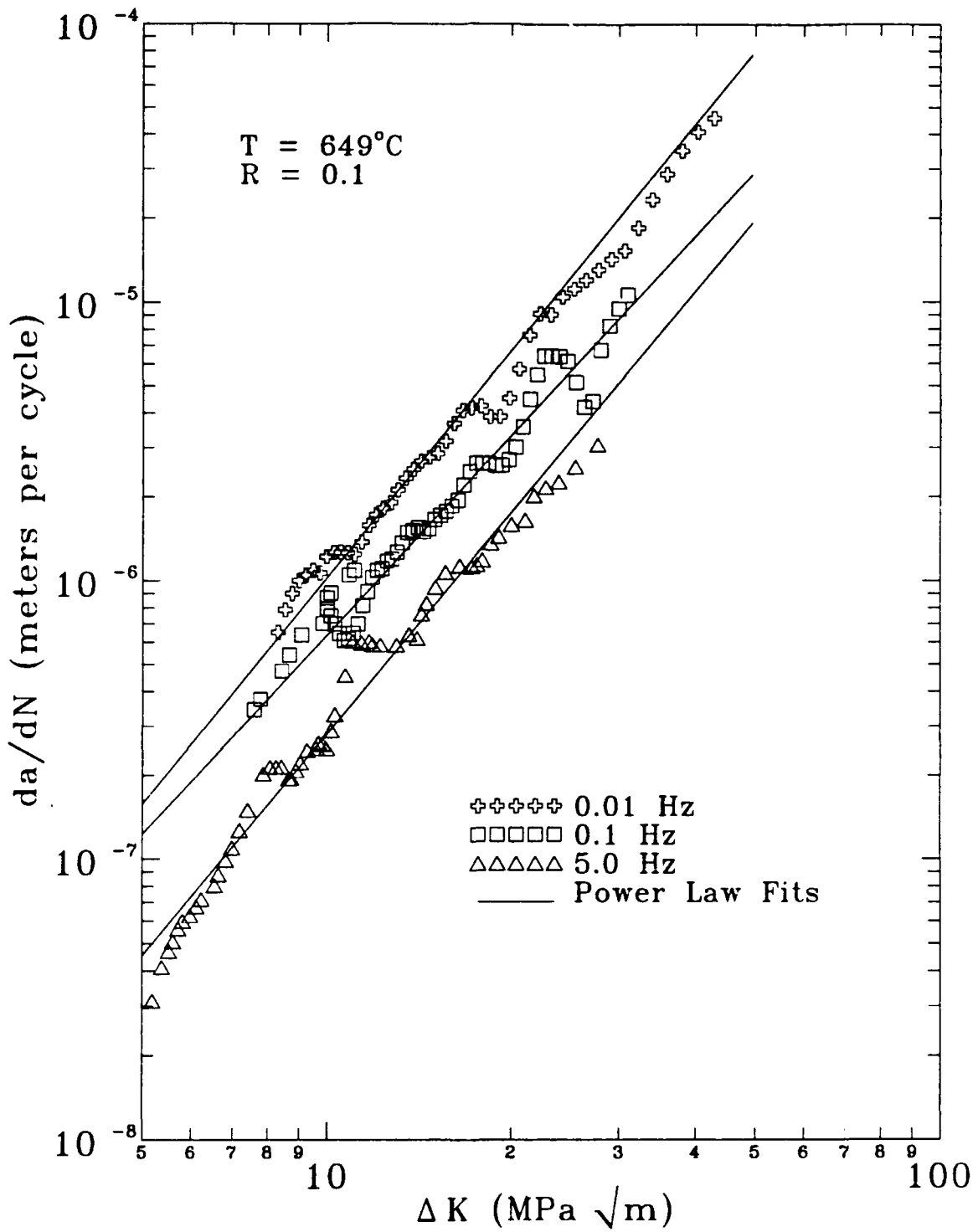
Figure 5.3 Crack Growth Variations with Frequency
Including Power Law Curve Fits to the Data

159

$$\left[(da/dN)_i\right]'_{ref} = 2.5 \tag{5.36}$$

The remaining reference parameter in Equation (5.29) that needs to be determined is $(da/dN)_i$, and it is now possible to determine the lower shaping coefficient, Q. A value of $(da/dN)_i = 4.5 \times 10^{-6}$ meters/cycle is selected to match the 5.0 Hz, 649°C isothermal fatigue data, and using these reference parameters described above, Q is defined as 0.4. The MSE curve fit to these data is shown in Figure 5.4. Since the da/dN vs. ΔK curves remain parallel with temperature, it is valid to use the 649°C data to define Q. Assuming Q is constant, $[(da/dN)_i]_{ref}$ and A_{32} can be defined. $[(da/dN)_i]_{ref}$ is adjusted to match the growth rates at 250°C and is:

$$\left[(da/dN)_i\right]_{ref} = 8.00 \times 10^{-7} \; meters/cycle \tag{5.37}$$

The parameters that define the reference condition are:

$$
\begin{bmatrix} \log(\Delta K_{th}) \\ \log(\Delta K_i) \\ \log(da/dN)_i \\ (da/dN)'_i \end{bmatrix}_{\substack{T = 250°C \\ R = 0.1}}
=
\begin{bmatrix} \log(4.00) \\ \log(30.0) \\ \log(8.00 \times 10^{-7}) \\ 2.50 \end{bmatrix}
=
\begin{bmatrix} 6.02 \times 10^{-1} \\ 1.48 \\ -6.10 \\ 2.50 \end{bmatrix}
\tag{5.38}
$$

A_{32} is determined by using 100 Hz data available at 25 and 650°C.
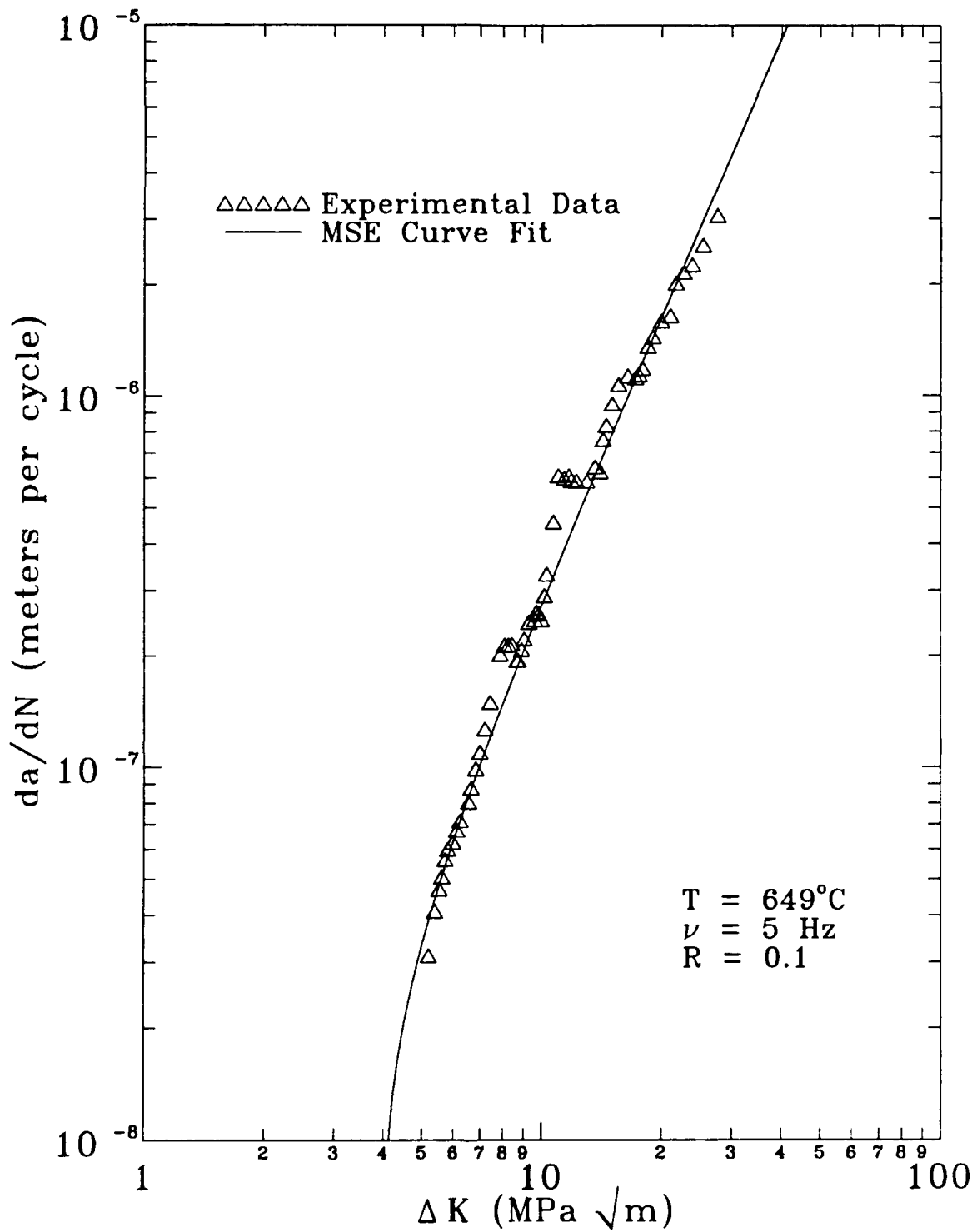
Figure 5.4 MSE Fit to 5 Hz, 649°C Isothermal Crack Growth Data

161

There is a considerable change in $(da/dN)_i$ for temperatures between 25 and 250°C, but $(da/dN)_i$ remains relatively constant for temperatures between 250 and 650°C. Nevertheless, Equation (5.29) is fit to the data, and A_{32} is determined separately for temperatures below and above 250°C. The R dependence of the MSE parameters appears in Equation (5.29) to maintain generality, but is not repeated here since all tests considered in this study are performed with $R = 0.1$. The MSE parameters that represent the unretarded cycle-dependent crack growth rate contribution at $R = 0.1$ are:

$$
\begin{bmatrix}
\log(\Delta K_{th}) \\
\log(\Delta K_i) \\
\log[(da/dN)_i] \\
(da/dN)_i'
\end{bmatrix}
=
\begin{bmatrix}
6.02 \times 10^{-1} \\
1.48 \\
-6.10 \\
2.50
\end{bmatrix}
+
\begin{bmatrix}
0.0 \\
0.0 \\
A_{32} \\
0.0
\end{bmatrix}
[T - 250°C]
\qquad (5.39)
$$

where:

$$
A_{32} =
\begin{cases}
-4.44 \times 10^{-3} \quad ; \quad T \leq 250°C \\
4.44 \times 10^{-4} \quad ; \quad T > 250°C
\end{cases}
\qquad (5.40)
$$

and Q is given as:

$$
Q = 0.4 \qquad (5.41)
$$

162

The MSE parameters that define the unretarded cycle-dependent crack growth rate are determined based on the assumptions that the crack growth rates at and below 250°C are purely cycle dependent and the retardation effects can be ignored at 100 Hz. Later in this chapter, the retardation effects are introduced into the cycle-dependent crack growth rate equations, but the parameters defined in this chapter are not changed.

Development of the Time-Dependent Term

Formulation of the Time-Dependent Term

The retarded time-dependent contribution to crack growth, the second term of the TMF crack growth rate model shown in Equation (5.16), is defined as:

$$\left(\frac{da}{dN}\right)_{\substack{ret \\ td}} = \int_0^{t_{nd}} \beta\,(t)\,\left(\frac{da}{dt}\right)_{\substack{ur \\ td}} dt \tag{5.42}$$

where β is the retardation coefficient, the upper limit of integration, t_{nd}, is the time when the load begins to decrease, and $(da/dt)_{ur\ td}$ is the unretarded time-dependent crack growth rate contribution.

As mentioned previously, the retardation coefficient changes with load and temperature and is expressed as a function of time. This coefficient is discussed in a later section of this chapter.

The time when the load begins to decrease, t_{nd} , is defined as:

$$t_{nd} = t_{ul} + t_h \tag{5.43}$$

where t_{ul} is the uploading time and t_h is load hold time. For pure fatigue

cycles, $t_h = 0$; therefore, $t_{nd} = t_{ul}$. When load holds are superimposed on a

fatigue cycle, the hold time is added to the uploading time to obtain t_{nd} . This

is illustrated further for TMF cycles by examining the load and temperature

cycles from the two proof tests presented in Figure 5.5. The cycles are

presented such that the load always begins to increase at t = 0. For the upper-

triangular-phase TMF cycle, the hold is added to the uploading time to

determine the non-decreasing load time, but for the lower-triangular-phase

TMF cycle the non-decreasing load time is equal to the uploading time. Even

though there is a hold (at P_{min}) in the load trace of the lower-triangular-phase

TMF cycle, it is not included in the non-decreasing load time since the load

decreases before this hold is encountered.

When a hold is superimposed on a fatigue cycle, this time is included in

the time-dependent integration; therefore, the upper limit on the time-

dependent integration is t_{nd} . As discussed in Chapter IV, Nicholas and

Weerasooriya [12] found that these integration limits of the time-dependent

crack growth contribution were sufficient to predict crack growth rates in

Inconel 718 under hold-time conditions. Recall that the upper limit of the

164
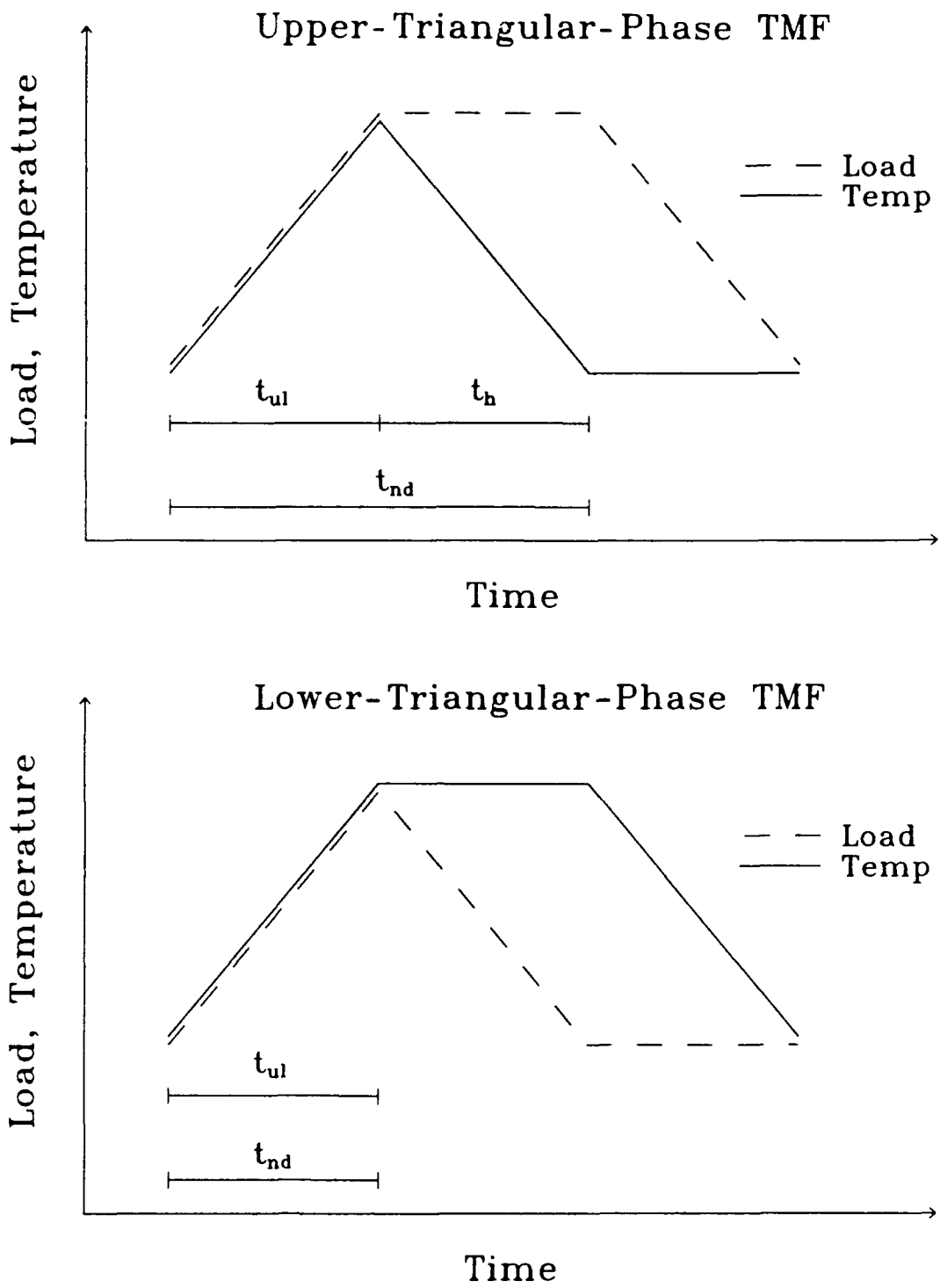
Figure 5.5 Limits of Integration Described on Upper-Triangular-Phase and Lower-Triangular-Phase TMF Load and Temperature Traces

165

cycle-dependent integration is t_{ul} , since the cycle-dependent crack growth contribution is assumed to occur only during the fatigue portion of the cycle.

Heil et. al [15] found that a slight modification to the limits of integration for the time-dependent term was necessary for TMF modeling using Equation (5.1). Under isothermal conditions the integrand of Equation (5.3) begins to decrease when the load begins to decrease, but when temperature and load are changing during a cycle, this is not necessarily the case. Therefore, in that study [15], the time-dependent integration was carried out while the integrand, $(da/dt)_{sl}$, was a non-decreasing function.

This additional restriction of the integration is not imposed in the current modeling effort, since the retardation coefficient, β, is multiplied by the unretarded time-dependent crack growth rate, and the integration in this case is carried out until $t = t_{nd}$ regardless to how $(da/dt)_{ur\ td}$ is changing. β is used to reduce the effect of $(da/dt)_{ur\ td}$ if it is necessary, which is the case for the load holds at P_{max} during hold-time tests. The form of β is described later in this chapter. The results of this study show that no other restriction on the integration is necessary to accurately predict crack growth rates of pure isothermal fatigue, isothermal fatigue with load hold times, and TMF experiments. These crack growth rate predictions are presented in Chapter VI.

The unretarded time-dependent crack growth rate in Equation (5.42) represents a growth rate of a crack if it experienced no retardation effects (i.e. $\beta = 1$) under a sustained load. This is similar to the unretarded cycle-

166

dependent crack growth rate, where it also represents a condition of no retardation. These crack growth rates cannot be measured directly as in the case of the HNH model since the sustained-load crack growth rates for the titanium-aluminide alloy are, for all practical purposes, equal to zero. Under sustained load, crack growth is totally retarded (the crack tip is assumed to blunt); therefore, the unretarded crack growth rates have to be determined indirectly using the results from isothermal-fatigue and hold-time tests. These unretarded crack growth rates are obtained from an iteration process, which will be discussed in detail after the formulation of β is discussed.

The unretarded time-dependent crack growth rate, $(da/dt)_{ur\ td}$, is a function of the stress intensity, K, and temperature, T.

$$\left(\frac{da}{dt}\right)_{\substack{ur \\ td}} = f(K,T) \tag{5.44}$$

This unretarded crack growth rate is expressed in terms of the K and T using the MSE:

$$\left(\frac{da}{dt}\right)_{\substack{ur \\ td}} = \exp(B_m)\left(\frac{K}{K_i}\right)^C\left[\ln\left(\frac{K}{K_{th}}\right)\right]^Q\left[\ln\left(\frac{K_c}{K}\right)\right]^D \tag{5.45}$$

where the parameters of this form of the MSE are defined similar to those of the cycle-dependent form (Equation (5.22)):

K_{th} is the threshold stress intensity, i.e., the value of K at the lower

asymptote of the da/dt vs. K curve,

K_c is the critical stress intensity, i.e., the value of K at the upper

asymptote of the da/dt vs. K curve,

K_i is the value of K at the curve's inflection point, and

Q and D are the lower and upper shaping coefficients, respectively.

The MSE parameters B_m and C are defined very similarly to those in Equations (5.23) and (5.24), except in this case, the growth rates are expressed as time differentials and stress intensity is used instead of stress intensity range. B_m is expressed as:

$$B_m = \ln\left[\left(\frac{da}{dt}\right)_i\right] - Q \ln\left[\ln\left(\frac{K_i}{K_{th}}\right)\right] - D \ln\left[\ln\left(\frac{K_c}{K_i}\right)\right] \tag{5.46}$$

where $(da/dt)_i$ is the value of da/dt at the inflection point of the da/dt vs. K curve. C is expressed as:

$$C = \left(\frac{da}{dt}\right)_i' - \frac{Q}{\ln(K_i/K_{th})} + \frac{D}{\ln(K_c/K_i)} \tag{5.47}$$

where $(da/dt)_i'$ is the slope of the curve at that inflection point when plotted as $\log(da/dt)$ vs. $\log(K)$. These parameters are depicted on a da/dt vs. K plot in Figure 5.6.

168
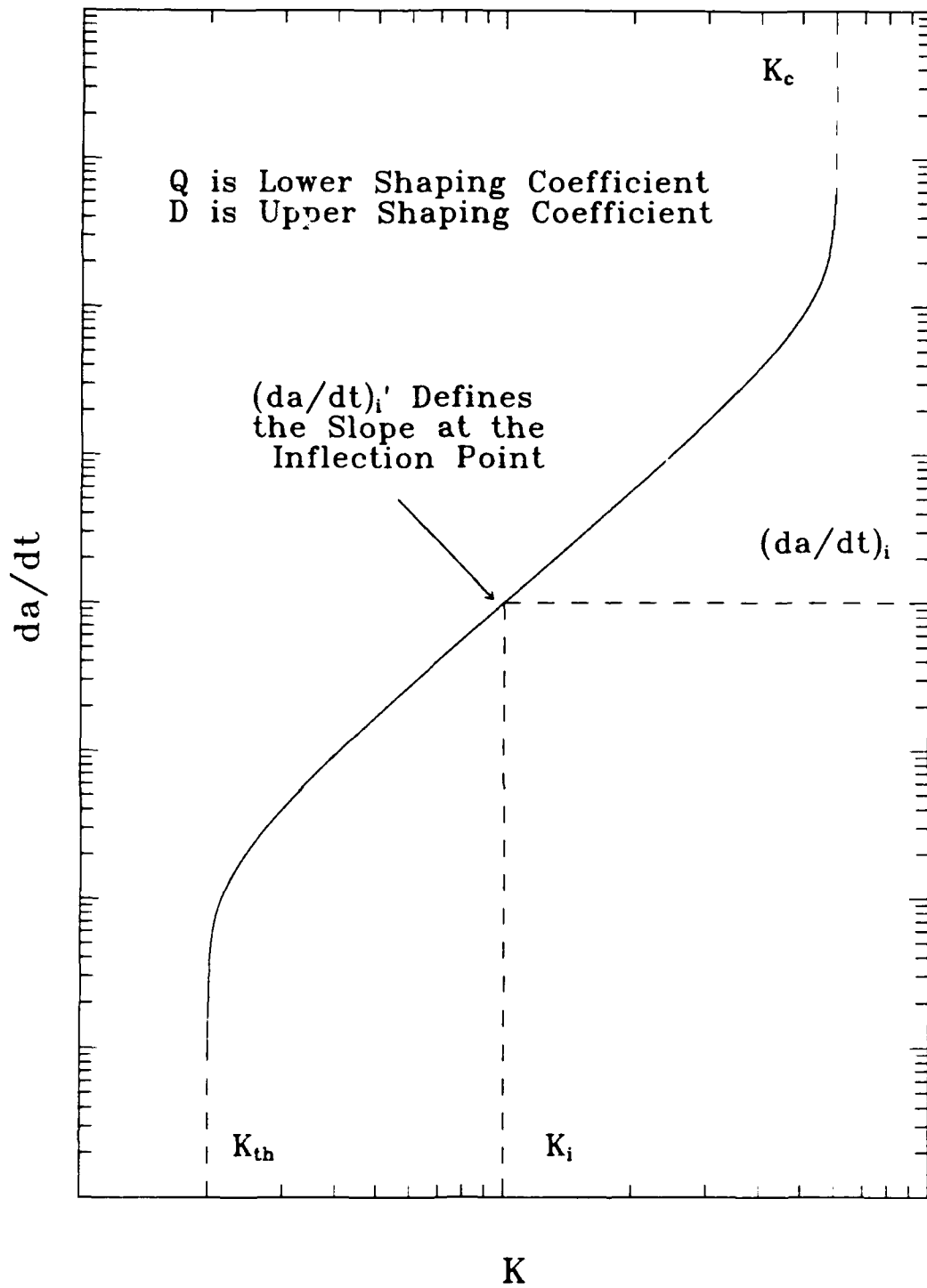
Figure 5.6 Definitions of the MSE Parameters on a *da/dt* vs. *K* Plot

169

D is expressed in terms of the other parameters as shown here:

$$D = -\left[Q^{1/2}\,\frac{\ln\left(K_i/K_c\right)}{\ln\left(K_i/K_{th}\right)}\right]^2 \tag{5.48}$$

The unretarded da/dt vs. K curves are modeled as symmetric about the inflection point as were the cycle-dependent unretarded crack growth curves, such that:

$$D = -Q \tag{5.49}$$

This simplification does not restrict the capability of the equations in this case, since both asymptotic regions need not be defined. With this simplification, K_c is defined as:

$$K_c = \frac{K_i^2}{K_{th}} \tag{5.50}$$

Similar to the unretarded cycle-dependent crack growth rate contribution, the independent MSE parameters are reduced to five when using the assumption of symmetry. Q is not a function of temperature, but the other parameters are defined as functions of T as shown in the matrix expression:

$$
\begin{bmatrix}
\log(K_{th}) \\
\log(K_i) \\
\log(da/dt)_i \\
(da/dt)'_i
\end{bmatrix}
=
\begin{bmatrix}
\log(K_{th}) \\
\log(K_i) \\
\log(da/dt)_i \\
(da/dt)'_i
\end{bmatrix}_{ref}
+
\begin{bmatrix}
B_1 \\
B_2 \\
B_3 \\
B_4
\end{bmatrix}
(T - T_{ref})
\qquad (5.51)
$$

In the following discussions, the constants defined at the reference

temperature, T_{ref} , and the constants B_i in Equation (5.51) are determined.

Determination of Time-Dependent MSE Parameters

As in the case of the cycle-dependent MSE development, the threshold

and fracture toughness regions of K are not critical to this modeling effort;

therefore, the values of K_{th} and K_c that define the unretarded time-dependent

crack growth rate contribution are held constant. Equation (5.50) implies that

K_i is held constant also. These assumptions yield:

$$
B_1 = B_2 = 0 \qquad (5.52)
$$

Following a procedure similar to that of the cycle-dependent

development, an initial assumption is made that the unretarded time-

dependent crack growth curves remain parallel as temperature changes. With

this assumption:

171

$$B_4 = 0 \tag{5.53}$$

This assumption is required to simplify the iteration process, since the only value that needs to be changed is $(da/dt)_i$. Since all other parameters remain constant during the iteration of the model, the unretarded time-dependent crack growth curves retain their shape but translate vertically on the da/dt vs. K plot as $(da/dt)_i$ is varied.

After accounting for the contributions of crack growth rate retardation (the retardation parameter is discus~d in a later section of this chapter), the MSE parameters at the reference condition of 350°C are:

$$\begin{bmatrix} \log(K_{th}) \\ \log(K_t) \\ \log(da/dt)_i \\ (da/dt)_i' \end{bmatrix}_{T=350°C} = \begin{bmatrix} \log(4.00) \\ \log(50.0) \\ \log(2.85 \times 10^{-5}) \\ 2.30 \end{bmatrix} = \begin{bmatrix} 0.6021 \\ 1.6990 \\ -4.5458 \\ 2.3000 \end{bmatrix} \tag{5.54}$$

And to account for the increase in $(da/dt)_i$ with temperature, B_3 is:

$$B_3 = 5.00 \times 10^{-3} \tag{5.55}$$

Therefore the MSE parameters for the time-dependent unretarded crack growth rate are:

$$
\begin{bmatrix}
\log(K_{th}) \\
\log(K_i) \\
\log(da/dt)_i \\
(da/dt)_i'
\end{bmatrix}
=
\begin{bmatrix}
0.6021 \\
1.6990 \\
-4.5458 \\
2.30
\end{bmatrix}
+
\begin{bmatrix}
0.00 \\
0.00 \\
5.00 \times 10^{-3} \\
0.00
\end{bmatrix}
(T - 350^\circ C)
\qquad (5.56)
$$

and

$$
Q = 0.4 \qquad\qquad\qquad (5.57)
$$

The unretarded crack growth rate curves for temperatures equal to 350, 500, and 650°C are presented in Figure 5.7. For the HNH model shown in Equation (5.1), curves similar to these were obtained from sustained-load tests. In the current effort, they represent hypothetical sustained-load crack growth in the Ti-24Al-11Nb if the crack were propagating unretarded, where $\beta = 1$). Since the crack blunts and fails to propagate under a sustained load, these curves are obtained from an iteration process to fit the elevated-temperature fatigue and isothermal fatigue with superimposed hold times. The TMF test data, which are presented in Chapter VI, are used to validate this iteration process. As the retardation effects ($\beta < 1$) contribute to retardation of crack growth, the unretarded $(da/dt)_i$ are increased to compensate for the reductions imposed by β. The values shown in Equation (5.56) have been adjusted to compensate for such retardation effects. The retardation coefficient, β, used in

173
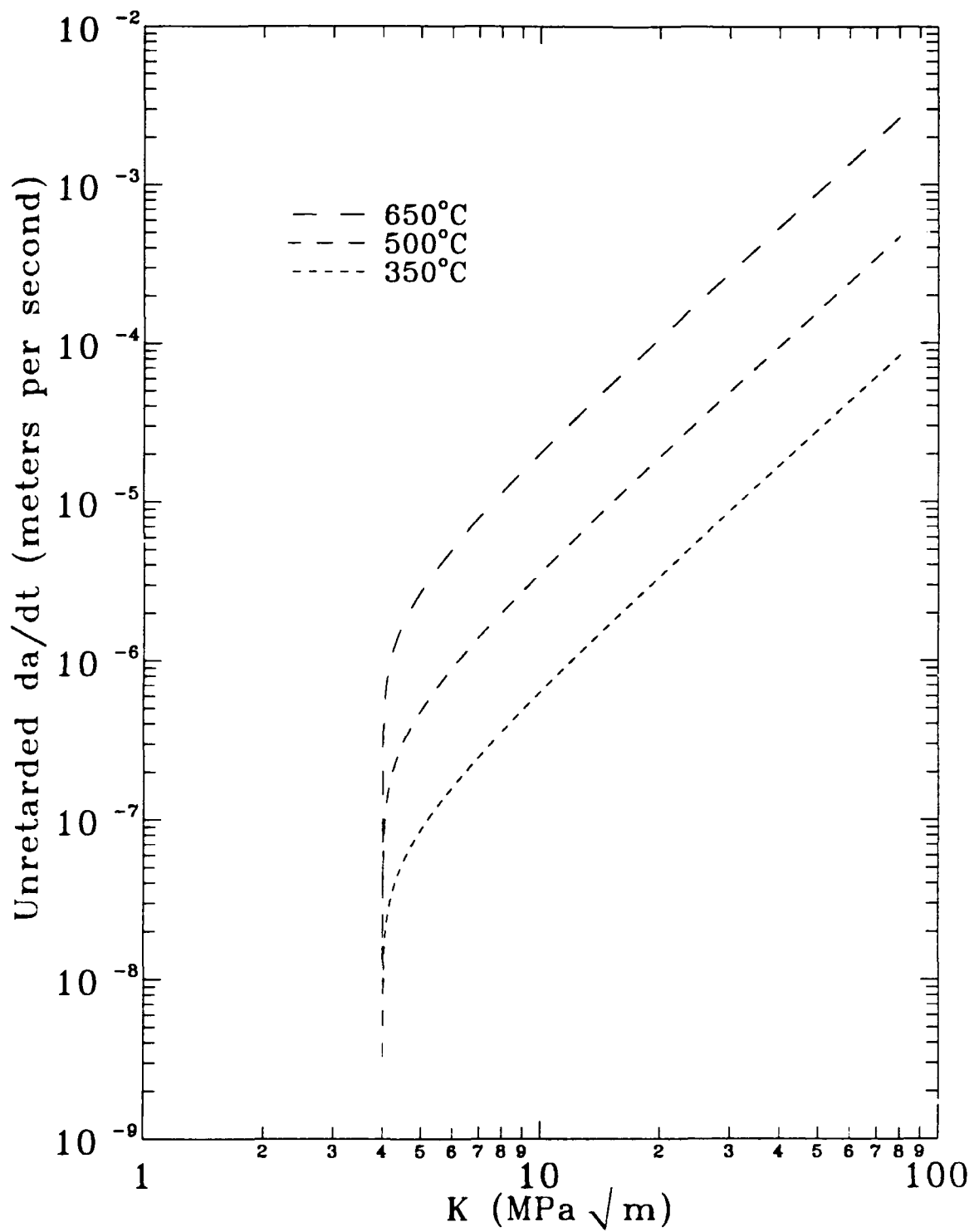
Figure 5.7 Unretarded Time-Dependent Crack Growth Curves

174

the cycle-dependent and time-dependent contributions to crack growth is the topic of the following section of this chapter.

Development of the Retardation Coefficient

Formulation of the Retardation Coefficient

The retardation coefficient, β, is used in the integrand of both the cycle-dependent and time-dependent crack growth expressions previously shown as Equations (5.17) and (5.42), respectively. This coefficient is required to account for the retardation in crack growth rates that have been observed experimentally at elevated temperatures, particularly during the hold-time experiments discussed in Chapter IV.

This retardation coefficient varies continuously with time during a TMF cycle since it is a function of both temperature and load. As discussed earlier in this chapter, it is sufficient to use an average or effective value of retardation (crack-tip blunting) over the entire cycle when considering isothermal fatigue with and without hold times. However, in the current study, the retardation coefficient, β, cannot be limited to its average value, but is required to change during a cycle as the temperature and loading conditions dictate. The capability for β to vary during a cycle is crucial in the development of a model that can be used to estimate crack growth rates during TMF cycling, since the test results indicate that retardation is a function of temperature, load, and loading frequency.

175

Before discussing the equations that are used to model the evolution (change) of β, it is helpful to understand the concept of this coefficient. β equal to unity represents a totally unretarded crack growth rate condition resulting from high-frequency fatigue. When β is less than unity, some crack growth rate retardation has occurred, and the amount of retardation is a function of temperature, load, and loading frequency. Experimental data suggest that as the temperature increases, β decreases, and as frequency decreases, β decreases. Also, β decreases more quickly for a hold at P_{max} than for a hold at P_{min}; therefore, β decreases with increasing load level. A lower limit of retardation, expressed as β_0, defines the level of retardation during steady-state sustained-load crack growth.

Since the retardation coefficient, β, changes during a cycle as a function of frequency, temperature, and load, there is no single value of β during a thermal-mechanical cycle. In fact, the rate of change of β (i.e. $d\beta/dt$) is a function of β; hence, it is not possible to determine β explicitly. But β is determined at time t during a cycle by knowing the value of β at a previous time, t_0, and integrating the rate of change (or evolution) of β from t_0 to t. This is expressed as:

$$\beta(t) = \beta(t_0) + \int_{t_0}^{t} \frac{d\beta}{dt}\, dt \qquad (5.58)$$

Thus, an evolution equation for β that satisfies the requirements defined

176

previously is developed. In functional form, the rate of change of β is
expressed as:

$$\frac{d\beta}{dt} = f(v, P/P_{max}, T, \beta) \tag{5.59}$$

where:

v is the frequency of the fatigue portion of the loading cycle,

T is the instantaneous temperature during a cycle,

P is the instantaneous load during a cycle, and

The evolution of β has two components, a increasing (crack-tip sharpening) term and a decreasing (crack-tip blunting) term; therefore, $d\beta/dt$ can be expressed as:

$$\frac{d\beta}{dt} = \left(\frac{d\beta}{dt}\right)_{inc} + \left(\frac{d\beta}{dt}\right)_{dec} \tag{5.60}$$

where $(d\beta/dt)_{inc}$ and $(d\beta/dt)_{dec}$, are respectively, the increasing and decreasing contributions to the rate of change of β with respect to time. These components represent the change in the amount (level) of retardation that is thought to be caused by the sharpening and blunting of the crack tip.

The increasing (crack-tip sharpening) contribution to Equation (5.60) is expressed as:

$$\left(\frac{d\beta}{dt}\right)_{inc} = \begin{cases} C_1(1-\beta) & ; \quad for \quad \dfrac{dP}{dt} \neq 0 \\\\ 0 & ; \quad for \quad \dfrac{dP}{dt} = 0 \end{cases} \qquad (5.61)$$

where C_1 is a function of v, which is defined later in this chapter. By definition, this increasing component must be active only during fatigue cycling; therefore, $(d\beta/dt)_{inc}$ must be equal to zero when the load is held constant (i.e. $dP/dt = 0$).

It is believed that a fatigue cycle sharpens a crack, which is reflected by an increase in $d\beta/dt$. The increasing term is constantly driving the retardation coefficient toward unity, which is the steady-state high-frequency fatigue value. If the frequency of the fatigue cycle is increased, β approaches unity faster (i.e. high frequency fatigue cycles sharpen the crack faster than lower frequency cycles). Therefore, the increasing component of $d\beta/dt$ also contains C_1 , which decreases as loading frequency increases. The expression for C_1 is determined from isothermal crack growth data obtained at different frequencies, and is discussed later.

The decreasing contribution to Equation (5.60) is expressed as:

$$\left(\frac{d\beta}{dt}\right)_{dec} = -C_2\left(\frac{P}{P_{max}}\right)(\beta - \beta_0) \qquad (5.62)$$

178

where β_0 is the value of β during steady-state sustained-load crack growth, and C_2 is a function of temperature, which is described later in this chapter. Equation (5.62) tends to drive the retardation coefficient toward β_0 when P is at its maximum value (P_{max}) for long periods of time. (Recall that β_0 is the value of β during steady-state sustained-load crack growth.) This behavior is observed when a hold time at P_{max} is superimposed on a fatigue cycle, which tends to blunt the crack tip. This condition decreases $d\beta/dt$, and the rate of decrease is determined by C_2, which increases as temperature increases. The function C_2 is determined from crack growth rate data from isothermal fatigue at different temperatures and isothermal fatigue with superimposed hold times. P/P_{max} is incorporated into Equation (5.62) to account for the effect of load on the rate of retardation. Hold times at P_{max} tend to retard growth much more than those at lower load values. This expression may not be completely accurate since very limited work has been performed with hold times other than P_{max}, but the effect is added to demonstrate the model's ability to account for this behavior.

Before discussing the procedure used to determine C_1, C_2, and β_0, an example of fatigue and hold-time loading conditions is presented to describe the behavior of β. Figure 5.8 shows how β varies during the loading and temperature conditions described in this example. Consider the case of a test specimen that previously has been cycled under very high frequency loading at low temperature; β would be equal to unity, representing a totally

179
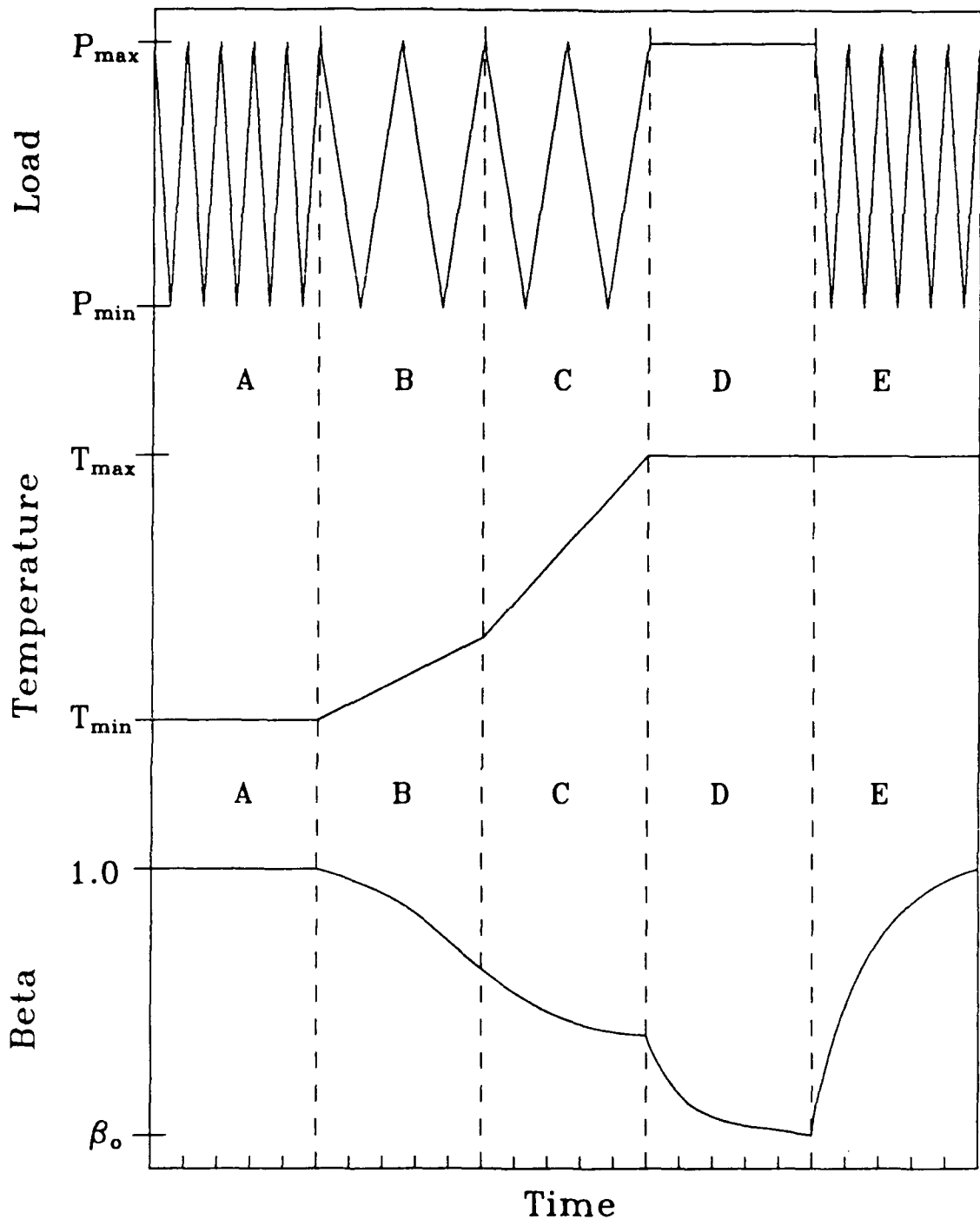
Figure 5.8 Variation of β with Frequency, Temperature, and Hold Times

180

unretarded crack growth rate condition. This condition is represented in segment "A" of Figure 5.8. The specimen then is cycled at a frequency that is not high enough to prevent any retardation (blunting), while the temperature is increased (segment "B"). This temperature is not high enough to cause a major reduction in the crack growth rate. As the temperature is increased further, the retardation effect is more pronounced and β decreases to a lower value and achieves a steady-state value at the end of segment "C". This value represents the level of retardation (condition of the crack tip) at this combination of frequency and temperature. Then the specimen is subjected to a hold at P_{max} superimposed on the fatigue cycle while still at a temperature where retardation effects take place (segment "D"). β will reduce during this hold and approach β_0 , which corresponds to sustained-load crack growth rate retardation. The rate of reduction is a function of the test temperature. The specimen then experiences a series of fatigue cycles while maintaining the elevated temperature, β starts increasing until it reaches a steady-state value somewhere in the region between β_0 and unity (segment "E"). The rate of increase, as well as the steady state value, depends on the loading frequency (the higher the frequency, the faster the increase and the higher the steady-state value of β). Note that if the temperature were lowered, the nominal (or average) value of β would increase and approach unity as the temperature at which retardation effects do not take place is approached.

181

Determination of Retardation Functions and Constants

Now that each component of the evolution equation for the retardation coefficient, β, has been discussed, the process used to determine the expressions for C_1 and C_2 and the value of β_0 is considered. This process involves the iteration of values of C_1, C_2, and β_0 to match the crack growth rate data of various isothermal and hold-time tests. For this iteration, crack growth rates for specific values of ΔK are used to simplify and speed the process, where these data are taken from constant K_{max} and constant P_{max} tests. Afterward, values of C_1, C_2, and β_0 are evaluated over the range of ΔK for the full range of temperatures and frequencies. When specific values of C_1, C_2, and β_0 produce satisfactory crack growth rate predicitions, expressions are developed for C_1 as a function of frequency and C_2 as a function of temperature. The value of $(da/dt)_i$ for the MSE that represents the unretarded time-dependent crack growth rate contribution also is changed during this process to best fit the experimental data. Recall from discussions earlier in this chapter, the values defining $(da/dt)_i$ in Equation (5.56) that are given in the previous section of this chapter are those obtained after the iterations of all the coefficients are performed. These iterations are described below.

With β_0 equal to zero and C_2 and $(da/dt)_i$ held constant, C_1 is selected to fit 650°C (T_{max} of TMF tests) isothermal data for frequencies of 0.01, 1.0, and 100.0 Hz. C_1 is varied until the predicted crack growth rate matches that of the experiment.

182

After determining values of C_1 for various frequencies, C_2 is determined to match isothermal crack growth rate data for temperatures ranging from 315 to 650°C. This is performed for 1.0 and 0.01 Hz data. Hold-time data obtained at 650°C are used to check the validity of C_2, since this parameter determines how quickly β approaches β_0, which still is equal to zero at this point in the iteration process. Appropriate adjustments are made to C_2, and then C_1 is varied to fit the frequency data as defined above. This iteration process continues until it generates satisfactory predictions of crack growth rates for the isothermal and hold-time experiments described above. Then the hold-time condition of 1000 seconds is used to define β_0, since this hold-time experiment shows a substantial increase in growth rate from the pure fatigue condition, whereas, 10 and 100 second holds show no obvious increase.

The value of $(da/dt)_i$ is varied when combinations of C_1, C_2, and β_0 cannot accurately predict the crack growth rates over all the conditions described above. After a new selection of $(da/dt)_i$ is made, the iteration process described above is repeated to check the validity of the new value of $(da/dt)_i$. This process continues until accurate predictions are made for all experimental data. The iteration process is summarized in Table 5.2.

A plot showing the values of C_1 as they vary with frequency is shown in Figure 5.9, and a plot showing the variation of C_2 is shown in Figure 5.10. The equations that describe C_1 and C_2 are plotted in Figures 5.9 and 5.10, respectively, as solid lines.

183

Table 5.2 Summary of the Iteration Process

Step	Process
1	Set $\beta_0 = 0$.
2	Set values of C_2 and $(da/dt)_i$.
3	Change values of C_1 to match 0.01, 1.0, and 100.0 Hz isothermal crack growth rates at 649°C for a single value of ΔK.
4	Change values of C_2 to match 1.0 and 0.01 Hz isothermal crack growth rate data for temperatures ranging from 315 to 650°C for a single value of ΔK.
5	650°C hold-time crack growth rate data for a single value of ΔK are used to check the values of C_2 .
6	If necessary, make adjustments to C_2 , and go to step #3. If no combination of C_1 and C_2 match data, go to step #2. If data match well, go to Step #7.
7	Set β_0 to match the 1000 second hold-time test.
8	Check $(da/dt)_i$, C_1 , C_2 , and β_0 for all isothermal fatigue and hold-time conditions for full range of ΔK. If necessary, make adjustments to C_2 and/or $(da/dt)_i$, and go to step #3. If data match well, go to step #9.
9	Develop equations to define C_1 and C_2 .
10	Check $(da/dt)_i$, C_1 , C_2 , and β_0 for all TMF conditions for full range of ΔK.

184
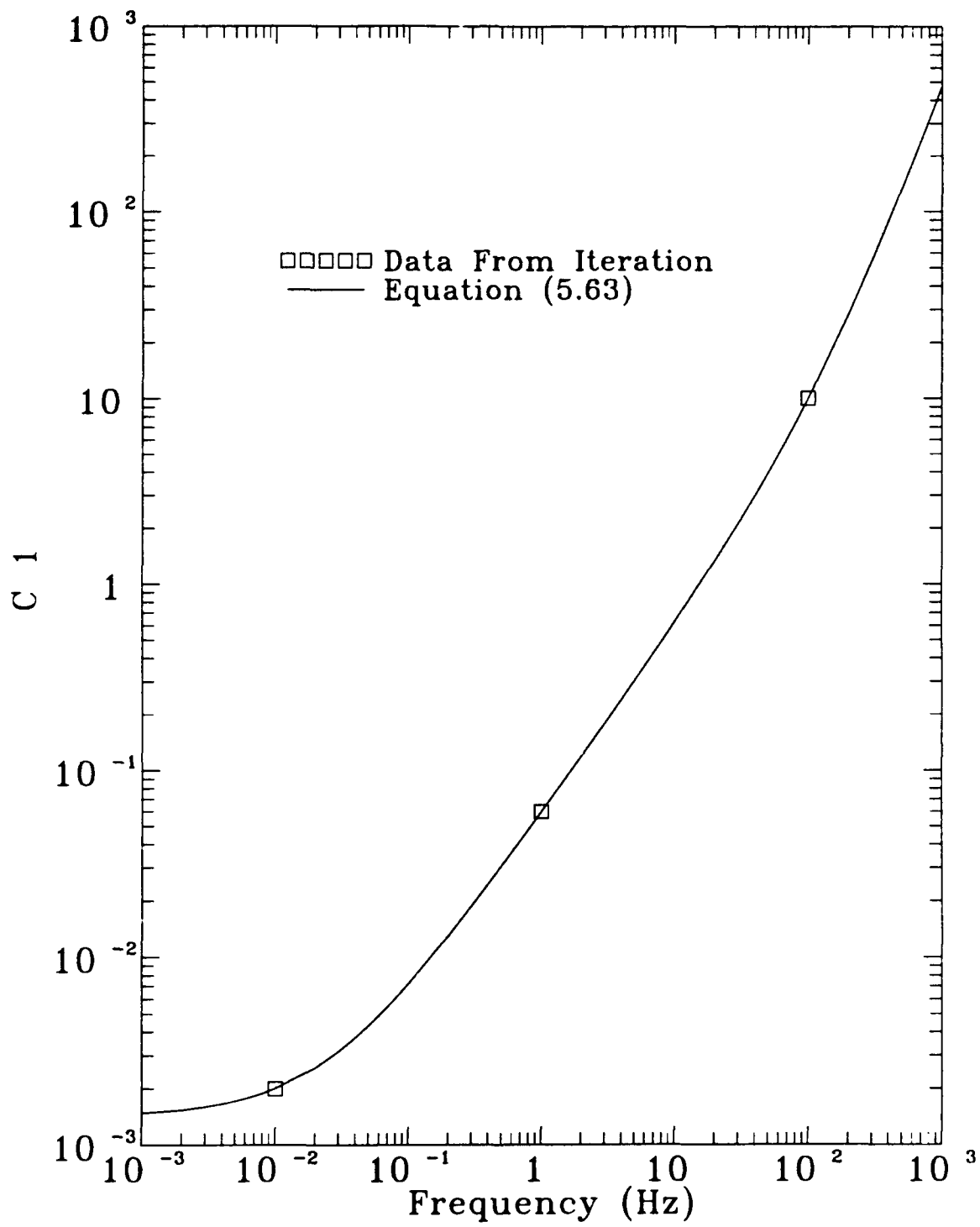
Figure 5.9 C_1 as a Function of Frequency

185
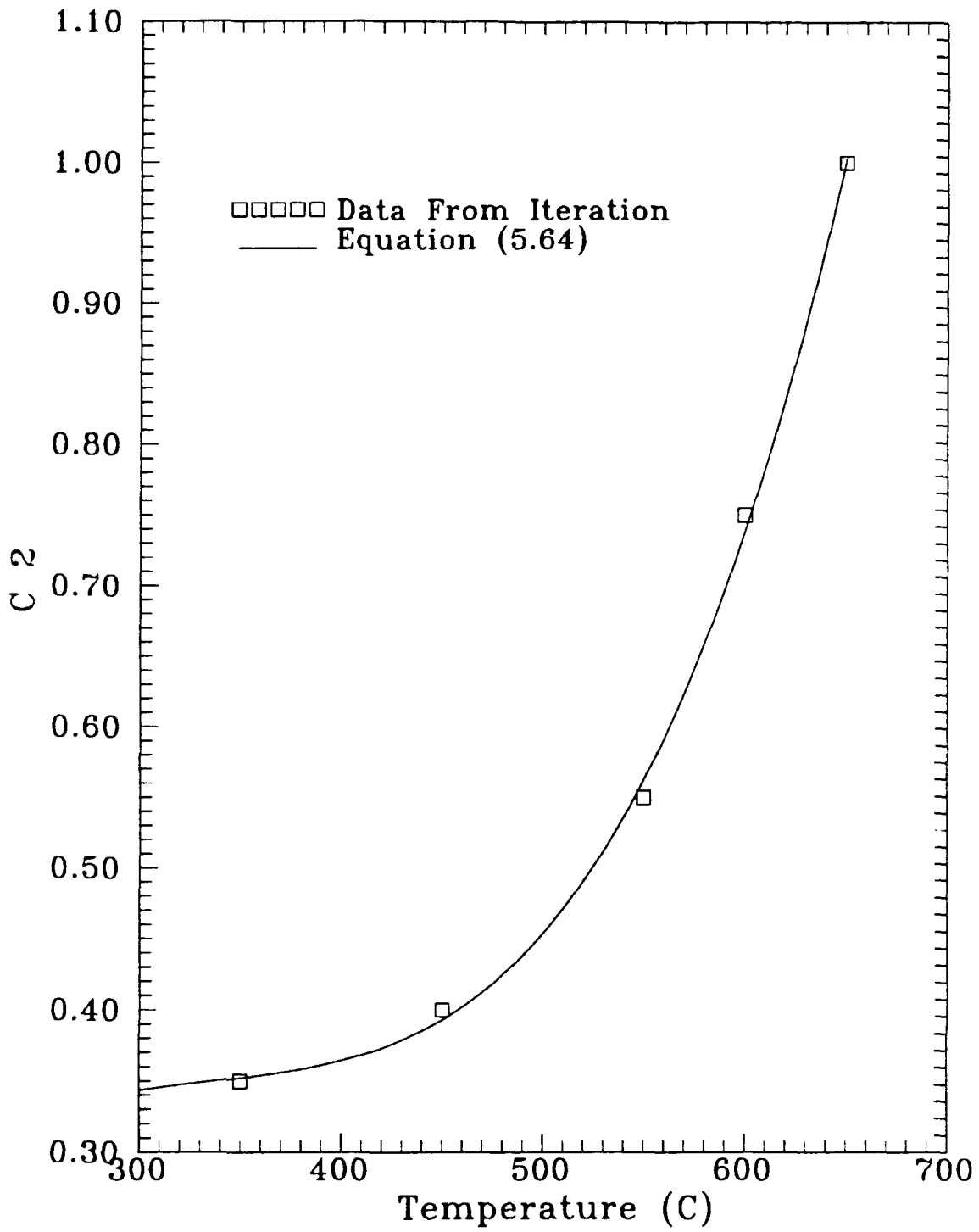
Figure 5.10 C_2 as a Function of Temperature

186

The expression for C_1 is:

$$C_1 = 1.418 \times 10^{-3} + 5.816 \times 10^{-2} v + 4.182 \times 10^{-4} v^2 \qquad (5.63)$$

where v is frequency, and the expression for C_2 is:

$$C_2 = 0.3344 - 9.889 \times 10^{-4} T + 8.463 \times 10^{-6} T^2 \\ - 2.452 \times 10^{-8} T^3 + 2.504 \times 10^{-11} T^4 \qquad (5.64)$$

where T is temperature. The value of retardation representing steady-state sustained-load crack growth, β_0, is:

$$\beta_0 = 1.0 \times 10^{-4} \qquad (5.65)$$

Using these expressions for C_1, C_2, and β_0, along with the MSE coefficients (Equations (5.39)-(5.41), (5.56), and (5.57)), the retarded cycle-dependent and retarded time-dependent crack growth rate contributions (Equations (5.17) and (5.42), respectively) is calculated. The predicted total crack growth rate is determined from the sum of the two components. This r. odel is used to predict the crack growth rates for thermal-mechanical cycling conditions, and these predictions are presented in Chapter VI. The computer program used to generate these predictions is discussed later in this chapter, but a summary of the model is presented first.

187

Summary of TMF Crack Growth Rate Model

The TMF crack growth rate model presented in this chapter can be expressed as:

$$\left(\frac{da}{dN}\right)_{tot} = \int_0^{t_{ul}} \beta(t) \left(\frac{da}{dt}\right)_{ur \atop cd} dt + \int_0^{t_{nd}} \beta(t) \left(\frac{da}{dt}\right)_{ur \atop td} dt \qquad (5.66)$$

where:

$\beta(t)$ is the retardation coefficient,

$(da/dt)_{ur\ cd}$ is the unretarded cycle-dependent crack growth rate,

$(da/dt)_{ur\ td}$ is the unretarded time-dependent crack growth rate,

t_{ul} is the uploading time, and

t_{nd} is the nondecreasing load time.

Although these terms have been defined earlier in this chapter, this section presents a summary of what these terms represent, as well as a summary of the isothermal crack growth experiments required to calculate the parameters that define $(da/dt)_{ur\ cd}$, $(da/dt)_{ur\ td}$, and β.

The retarded cycle-dependent crack growth rate contribution is determined from an integration of $[\beta(t)\ (da/dt)_{ur\ cd}]$ from $t = 0$ to $t = t_{ul}$ as shown in Equation (5.66). The term $(da/dt)_{ur\ cd}$ represents an unretarded cycle-dependent crack growth rate, which is defined in this study as 100 Hz. An unretarded crack growth rate condition exists when β is equal to unity;

188

therefore, $(da/dt)_{ur\,cd}$ can be determined directly from isothermal crack growth rate data (i.e. $(da/dN)_{ur\,cd}$) as shown in Equation (5.18).

$$\left(\frac{da}{dt}\right)_{ur\atop cd} = \frac{\left(\dfrac{da}{dN}\right)_{ur\atop cd}}{\left(\dfrac{\tau}{2}\right)} \qquad\qquad \text{(5.18)}\\ \text{repeated}$$

Where τ is the period of the isothermal fatigue test used to generate the crack growth rate data, $(da/dN)_{ur\,cd}$. These crack growth rates are expressed as a function of ΔK and six independent parameters using the modified sigmoidal equation (MSE):

$$\left(\frac{da}{dN}\right)_{ur\atop cd} = \exp(B_m)\left(\frac{\Delta K}{\Delta K_i}\right)^C \left[\ln\left(\frac{\Delta K}{\Delta K_{th}}\right)\right]^Q \left[\ln\left(\frac{\Delta K_c}{\Delta K}\right)\right]^D \qquad \text{(5.22)}\\ \text{repeated}$$

where:

   ΔK_{th} is the threshold stress intensity range,

   ΔK_c is the critical stress intensity range,

   ΔK_i is the value of ΔK at the inflection point in the da/dN vs. ΔK curve,

   Q is the lower shaping coefficient of the da/dN vs. ΔK curve, and

   D is the upper shaping coefficient of the da/dN vs. ΔK curve.

B_m is defined as:

189

$$B_m = \ln\left(\frac{da}{dN}\right)_i - Q \ln\left[\ln\left(\frac{\Delta K_i}{\Delta K_{th}}\right)\right] - D \ln\left[\ln\left(\frac{\Delta K_c}{\Delta K_i}\right)\right] \qquad \begin{matrix}(5.23)\\ \text{repeated}\end{matrix}$$

where $(da/dN)_i$ is the value of da/dN corresponding to ΔK_i , and the exponent, C, is defined as:

$$C = \left(\frac{da}{dN}\right)_i' - \frac{Q}{\ln(\Delta K_i/\Delta K_{th})} + \frac{D}{\ln(\Delta K_c/\Delta K_i)} \qquad \begin{matrix}(5.24)\\ \text{repeated}\end{matrix}$$

where $(da/dN)_i'$ is the slope of the curve at the inflection point when plotted as log (da/dN) vs. log (ΔK). In the current study, the da/dN vs. ΔK curve is modeled symmetric about the inflection point by setting:

$$D = -Q \qquad \begin{matrix}(5.27)\\ \text{repeated}\end{matrix}$$

With this symmetry, ΔK_c is expressed as a function of ΔK_i and ΔK_{th} :

$$\Delta K_c = \frac{\Delta K_i^2}{\Delta K_{th}} \qquad \begin{matrix}(5.28)\\ \text{repeated}\end{matrix}$$

The remaining independent parameters (i.e. ΔK_i , ΔK_{th} , $(da/dN)_i$, $(da/dN)_i'$, and Q) are determined from isothermal crack growth tests at frequencies high enough to obtain pure cycle-dependent crack growth. In the current study, the

190

tests used to determine the five independent parameters are summarized in

Table 5.3.

Table 5.3 Summary of Parameters that Define the Cycle-Dependent
Crack Growth Rate and the Corresponding Required Experiments

Parameter	Experiment
Q, ΔK_i, and ΔK_{th}	Selected based on isothermal crack growth rate data from the highest frequency experiment performed over the full range of ΔK (constant P_{max} crack growth tests).
$(da/dN)_i$	Obtained by matching isothermal crack growth rate data from four different temperatures at frequencies high enough that pure cycle-dependent behavior exists. (Since the da/dN vs. ΔK curves are parallel with changes in temperature, constant K_{max} data only are required.)
$(da/dN)_i'$	Obtained by averaging the slopes of crack growth curves from constant P_{max} tests (full range of ΔK) from three different frequencies and two different temperatures.

Isothermal crack growth rate data from various temperatures are

required for Ti-24Al-11Nb, since the cycle-dependent crack growth rate

contribution in this alloy is a function of temperature (see Chapter IV). This

ability of the model to account for changes in the cycle-dependent crack

growth rate with temperature is an advantage of this model over previous

191

efforts. If this model were used for a material that does not show this type of temperature dependence (i.e. the nickel-base superalloys), $(da/dt)_{ur\ cd}$ would be a function of only ΔK and R.

The retarded time-dependent crack growth rate contribution to the total crack growth rate is determined from an integration of $[\beta(t)\ (da/dt)_{ur\ td}]$ from $t = 0$ to $t = t_{nd}$ as shown in Equation (5.66). $(da/dt)_{ur\ td}$ represents an unretarded time-dependent crack growth rate condition, which is impossible to measure directly, since the retardation effects are experienced when Ti-24Al-11Nb is exposed to the temperatures at which time-dependent crack growth rate contributions occur. Therefore, $(da/dt)_{ur\ td}$ must be obtained through an iteration process. Since retardation effects occur simultaneously with the time-dependent crack growth rate contributions, the parameters that define β (summarized later in this section) must be determined simultaneously with those that define $(da/dt)_{ur\ td}$. The exact iteration procedure is discussed earlier in this chapter, but the expressions for $(da/dt)_{ur\ td}$ are discussed here.

As in the cycle-dependent case, $(da/dt)_{ur\ td}$ is expressed as a function of K and six independent parameters:

$$\left(\frac{da}{dt}\right)_{\substack{ur \\ td}} = \exp(B_m)\left(\frac{K}{K_i}\right)^C\left[\ln\left(\frac{K}{K_{th}}\right)\right]^Q\left[\ln\left(\frac{K_c}{K}\right)\right]^D \qquad \begin{array}{l}(5.45)\\ \text{repeated}\end{array}$$

where:

192

K_{th} is the threshold stress intensity,

K_c is the critical stress intensity,

K_i is the value of K at the inflection point in the da/dt vs. K curve,

Q is the lower shaping coefficient of the da/dt vs. K curve, and

D is the upper shaping coefficient of the da/dt vs. K curve.

B_m is defined as:

$$B_m = \ln\left(\frac{da}{dt}\right)_i - Q \ln\left[\ln\left(\frac{K_i}{K_{th}}\right)\right] - D \ln\left[\ln\left(\frac{K_c}{K_i}\right)\right] \qquad \begin{array}{c}(5.46)\\ \text{repeated}\end{array}$$

where $(da/dt)_i$ is the value of da/dt corresponding to K_i , and the exponent, C, is defined as:

$$C = \left(\frac{da}{dt}\right)_i' - \frac{Q}{\ln(K_i/K_{th})} + \frac{D}{\ln(K_c/K_i)} \qquad \begin{array}{c}(5.47)\\ \text{repeated}\end{array}$$

where $(da/dt)_i'$ is the slope of the curve at the inflection point when plotted as log (da/dt) vs. log (K). As for the case of the cycle-dependent case, the da/dt vs. K curve is modeled symmetric about the inflection point by setting:

$$D = -Q \qquad \begin{array}{c}(5.49)\\ \text{repeated}\end{array}$$

With this symmetry, K_c is expressed as a function of K_i and K_{th} :

$$K_c = \frac{K_i^2}{K_{th}}$$

The remaining independent parameters (i.e., K_i, K_{th}, $(da/dt)_i$, $(da/dt)_i'$, and Q) are determined from isothermal crack growth tests at frequencies low enough and temperatures high enough to obtain time-dependent contributions to the total crack growth rate. In the current study, the tests used to determine the five independent parameters are summarized in Table 5.4.

Table 5.4 Summary of Parameters that Define the Time-Dependent Crack Growth Rate and the Corresponding Required Experiments

Parameter	Experiment
Q, K_i, and K_{th}	Selected based on isothermal crack growth rate data obtained at the same frequency as the TMF experiments. (Constant P_{max} crack growth test data was used.)
$(da/dt)_i$	Obtained by matching isothermal crack growth rate data from four different temperatures at the same frequency as the baseline TMF cycles. (Since da/dN vs. ΔK curves are parallel with changes in temperature, constant K_{max} data only are required.)
$(da/dt)_i'$	Obtained from the slope of the isothermal crack growth curve obtained under constant P_{max} conditions at the same frequency as the baseline TMF tests and at the maximum temperature of the TMF cycles.

The main contribution of this modeling effort is the development of the retardation coefficient, β, which appears as a function of time in both the retarded cycle-dependent and retarded time-dependent contributions of the total crack growth rate shown in Equation (5.66). No previous modeling effort has accounted for the retardation of crack growth rates during thermal-mechanical cycling. As discussed in Chapter IV, the retardation of crack growth rates in this alloy is believed to be the result of crack-tip blunting, and the amount of crack growth rate retardation appears to be dependent upon loading frequency (v), load (P), and temperature (T); therefore, β changes continuously during a thermal-mechanical cycle.

An evolution expression (i.e., $d\beta/dt$) is developed to model the crack growth rate retardation behavior and is expressed as:

$$\frac{d\beta}{dt} = \begin{cases} C_1(1-\beta) - C_2\left(\frac{P}{P_{max}}\right)(\beta - \beta_0) & ; \ for \ \frac{dP}{dt} \neq 0 \\[4mm] - C_2\left(\frac{P}{P_{max}}\right)(\beta - \beta_0) & ; \ for \ \frac{dP}{dt} = 0 \end{cases} \tag{5.67}$$

where P is the instantaneous load during a cycle, and β_0 is the value of β during steady-state sustained-load crack growth. The expression for C_1 is:

$$C_1 = 1.418 \times 10^{-3} + 5.816 \times 10^{-2} v + 4.182 \times 10^{-4} v^2 \tag{5.63 repeated}$$

195

where ν is frequency of the fatigue portion of the loading cycle. The expression for C_2 is:

$$C_2 = 0.3344 - 9.889 \times 10^{-4} T + 8.463 \times 10^{-6} T^2$$
$$- 2.452 \times 10^{-8} T^3 + 2.504 \times 10^{-11} T^4$$

(5.64)
repeated

where T is the instantaneous temperature during a cycle.

A brief discussion of the characteristics of β is presented here. β equal to unity represents completely unretarded crack growth, and β equal to zero represents completely retarded (or no) crack growth. A lower limit of retardation, defined as β_0, represents steady-state sustained-load crack growth. If this model were used to predict crack growth rates in a material that does not exhibit growth rate retardation (i.e. the nickel-base superalloys), β would equal unity.

A summary of the parameters that define $d\beta/dt$ and the experiments required to define each are presented in Table 5.5. In addition to the tests described in Tables 5.4 and 5.5, hold-time crack growth rate data are used to check the validity of the values of $(da/dt)_i$ and C_2. Discussions of the iteration procedure used to obtain the values of these parameters is presented earlier in this chapter.

The crack growth rate predictions using this model are presented in Chapter VI. Further clarification is made between the data used to correlate the model parameters, and the data used to validate the model.

196

Table 5.5 Summary of Parameters that Define $d\beta/dt$
and the Corresponding Required Experiments

Parameter	Experiment
C_1	Obtained by matching isothermal crack growth rate data from three different frequencies at the same temperature as the maximum temperature of the TMF cycles. (Since the da/dN vs. ΔK curves are parallel with changes in frequencies, constant K_{max} data are used.)
C_2	Obtained by matching isothermal crack growth rate data from four different temperatures at the same frequency as the baseline TMF cycles. (Since the da/dN vs. ΔK curves are parallel with changes in temperature, constant K_{max} data are used.)
β_0	Obtained by matching hold-time crack growth rate data from an experiment where the hold time is three orders of magnitude larger than the length of the fatigue cycle. (Constant K_{max} test data are used.)

Computer Program for the TMF Crack Growth Rate Model

The computer program that was developed during the current study is discussed here. This program is used to compute the crack growth rates based on the model described previously in this chapter. This section of the chapter includes a description of the program and a discussion of the computations performed to obtain the crack growth rates.

Description of the Computer Program

A listing of the FORTRAN source code of the program, TMFCGR, that is used to model crack growth rates during this study is shown in the Appendix. This code consists of a main program and 17 functions and subroutines; therefore, to discuss this code more easily, the FORTRAN source code is divided into five sections: 1) the main program, 2) functions and subroutines that represent the cycle-dependent crack growth rate contribution, 3) functions and subroutines that represent the time-dependent crack growth rate contribution, 4) the subroutines that calculate the value of the retardation parameter, and 5) other subroutines consisting of primarily input and output statements. Flow charts are provided in the Appendix to describe the order of computations performed in the main program and in the more complicated subroutines and functions.

The computer program, which is written to operate on a microcomputer, is capable of calculating total crack growth rates for isothermal fatigue, isothermal fatigue with superimposed hold times at P_{max} , and thermal-mechanical cycles. The thermal-mechanical cycles include in-phase and 90°, 180°, and 270° out-of-phase cycles, as well as upper-triangular and lower-triangular-phase cycles. These cycles are shown in Figure 4.1, and a complete description of these is provided in Chapter IV. The program also can calculate growth rates for operator-defined cycles consisting of nine or less cycle segments, and further description of this capability is provided in the

Appendix in the comments written within the FORTRAN subroutine PROFILE. Crack growth rates can be computed for a single value of ΔK or an entire range of ΔK.

A brief description of the computation process is provided here. The operator selects the cycle type, maximum and minimum cycle temperatures, load ratio, and cycle time. The program establishes the temperature and load profiles associated with that cycle. The operator then inputs the integration parameters and requests the values of ΔK that will be used to calculate the crack growth rates. The retarded cycle-dependent and retarded time-dependent crack growth rate contributions are computed and summed to establish the total retarded crack growth rate for a given ΔK. The growth rates are output to disk and/or video monitor, then ΔK is incremented and the crack growth rate computations are repeated. Comments are presented throughout the FORTRAN program listing to describe the computations that are being performed.

Numerical Approximations Used in the Computer Program

The retarded cycle-dependent and retarded time-dependent integrations shown in Equations (5.17) and (5.42) are approximated using Simpson's composite rule of integration. This composite integration consists of dividing the interval of integration into subintervals and using Simpson's rule on subsequent pairs of subintervals [132]. As an example, an arbitrary function

199

of time, $f(t)$, is integrated using Simpson's rule. The integration of $f(t)$ from $t = t_a$ to $t = t_b$ is:

$$\int_{t_a}^{t_b} f(t)\, dt \approx \frac{t_b - t_a}{6} [f(t_a) + 4f(t_i) + f(t_b)] \qquad (5.68)$$

where t_a and t_b are the endpoints of integration, which must be close for Equation (5.68) to be valid, and t_i is defined as:

$$t_i = \frac{t_a + t_b}{2} \qquad (5.69)$$

Simpson's rule will yield exact integrations if $f(t)$ is a polynomial of degree three or less [132]; however, the integrands that are considered in the model (Equations (5.17) and (5.42)) are complex functions of temperature ($T(t)$), load ($P(t)$), and explicit time. When applied to thermal-mechanical cycles, this simple scheme of numerical integration could result in substantial inaccuracies. Furthermore, the limits of integration are not close, and Equation (5.68) cannot be considered valid in such a case.

To obtain a more accurate result, the interval of integration is divided into m subintervals and Simpson's rule is applied to each subsequent pair of subintervals, and then summed to approximate the integral over the entire interval. Considering the same integral as above, Simpson's composite rule of integration yields:

$$\int_{t_a}^{t_b} f(t) \ dt \approx \frac{t_b - t_a}{6m} \left[f(t_a) + 2\sum_{j=1}^{m-1} f(t_{2j}) \right.$$
$$\left. + 4\sum_{j=1}^{m} f(t_{2j-1}) + f(t_b) \right]$$

(5.70)

This integration technique is used in the functions that calculate the retarded cycle-dependent and retarded time-dependent crack growth rate contributions. These integrations are performed in functions CYCLEDEP and TIMEDEP (see Appendix) where $f(t)$ shown in Equation (5.70) is:

$$f(t) = \beta(t) \left(\frac{da}{dt} \right)_{\substack{ur \\ cd}}$$

(5.71)

for the function CYCLEDEP, and is integrated from $t = 0$ to $t = t_{ul}$ as shown previously in Equation (5.17), and $f(t)$ is:

$$f(t) = \beta(t) \left(\frac{da}{dt} \right)_{\substack{ur \\ td}}$$

(5.72)

for the function TIMEDEP, and is integrated from $t = 0$ to $t = t_{nd}$ as previously shown in Equation (5.42).

The retardation coefficient, $\beta(t)$, is determined in function TDRETARD at time t_j with the following expression:

201

$$\beta(t_j) = \beta(t_{j-1}) + (t_j - t_{j-1}) \left(\frac{\Delta\beta}{\Delta t} \right)_{t=t_{j-1}} \qquad (5.73)$$

where:

$\beta(t_{j-1})$ is the value of β at time t_{j-1} ,

t_j is the time at the j'th time step during integration,

t_{j-1} is the time at the j-1'th time step during integration, and

$(\Delta\beta/\Delta t)$ is the rate of change of β as given in Equation (5.60), where the following approximation is assumed:

$$\frac{\Delta\beta}{\Delta t} \approx \frac{d\beta}{dt} \qquad (5.74)$$

The selection of time step size, Δt, (TMSTEP in the Appendix) for the numerical integrations is discussed next. The time step size is defined as:

$$\Delta t = \frac{t_b - t_a}{m} \qquad (5.75)$$

where t_a and t_b define, respectively, the lower and upper limits of the integration interval, and m is the number of subintervals that the integration interval is divided.

For the model predictions shown in Chapter VI, m is equal to 500 for the uploading and downloading portions of all fatigue cycles, which implies

that the time step for each integration subinterval is equal to 1/500 of the total segment time. When hold times are superimposed on fatigue cycles, Δt is selected such that it is no less than 500 for all of the cycles studied. For example, if a 100 second fatigue cycle with 10 second hold is integrated, the time step size is 0.1 seconds for the ramp up to P_{max}, 0.02 seconds for the hold, and 0.1 seconds for the ramp down to P_{min}. Also, Δt is selected such that it is not less than 0.1 seconds during the hold times. For example, during the 1,000 second hold time, m is set equal to 10,000 such that Δt is equal to 0.1 seconds during the hold portion of the cycle.

The integration intervals are selected based on the following convergence study that includes a 649°C isothermal fatigue test and a 90° out-of-phase TMF test. For both cycles, the cycle time is equal to 100 seconds and the load ratio is equal to 0.1, and for the TMF test, the temperature is cycled between 315 and 649°C. The crack growth rate, da/dN, is computed for both test conditions for ΔK equal to 14.85 MPa m$^{1/2}$. Growth rates are obtained for time step size, Δt, between 2.5 to 0.025 seconds.

The crack growth rates for the isothermal test condition are plotted with respect to Δt in Figure 5.11. There is a 7.09 % increase in da/dN from Δt = 2.5 seconds to Δt = 0.25 seconds, and a 0.72 % increase in da/dN from Δt = 0.25 seconds to Δt = 0.025 seconds. For the isothermal crack growth rate predictions presented in Chapter VI, Δt = 0.10 seconds is used to speed the integrations without compromising the accuracy of the predictions. The

203
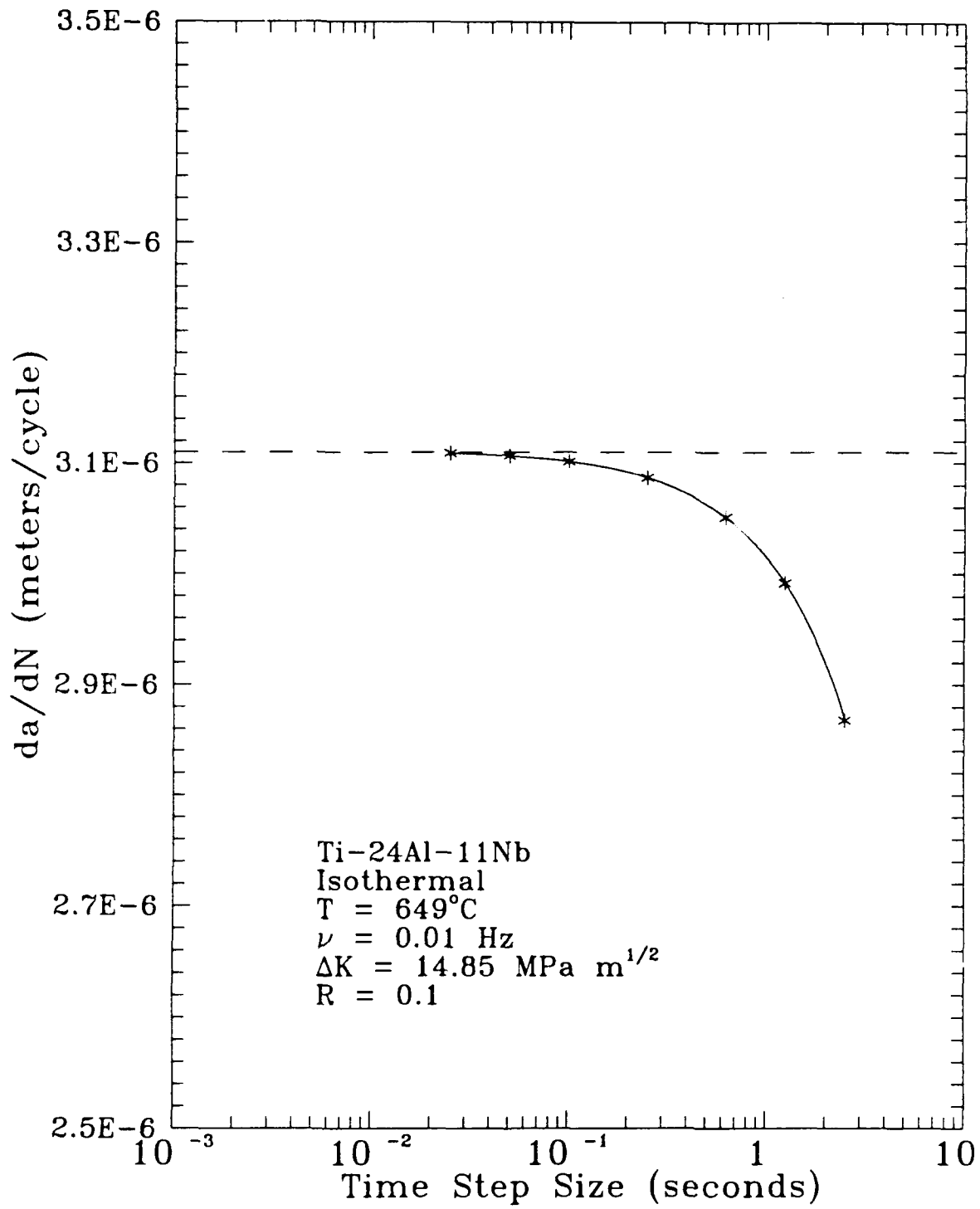
Figure 5.11 Dependence of *da/dN* on Time Step Size for a 649°C Isothermal Test

integrations using $\Delta t = 0.10$ seconds require four times the computation time as the integrations using $\Delta t = 0.025$ seconds, yet the da/dN obtained from these time steps differs by 0.25 %.

The crack growth rates for the 90° out-of-phase test condition are plotted with respect to Δt in Figure 5.12. This out-of-phase cycle is studied to determine the effect of temperature on the selection of Δt. Similar observations are made in this case. There is a 8.27 % increase in the predicted da/dN from $\Delta t = 2.5$ seconds to $\Delta t = 0.25$ seconds, and a 0.84 % increase in da/dN from $\Delta t = 0.25$ seconds to $\Delta t = 0.025$ seconds. For all the TMF crack growth rate predictions in Chapter VI, $\Delta t = 0.10$ seconds. Using $\Delta t = 0.10$ seconds instead of $\Delta t = 0.025$ seconds reduces the crack growth rate prediction by 0.29 %.
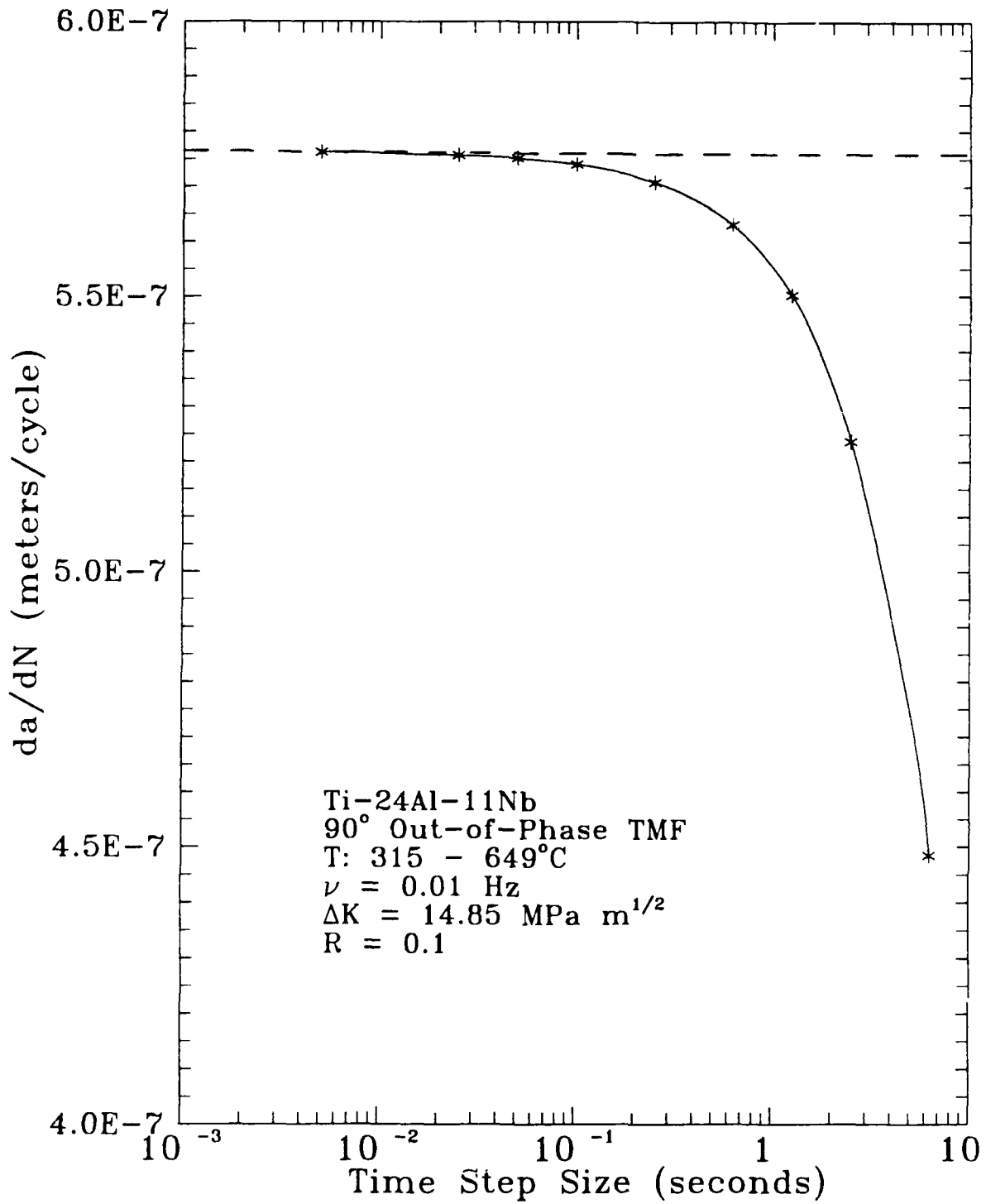
Figure 5.12 Dependence of *da/dN* on Time Step Size for
a 90° Out-of-Phase TMF Test

VI. Crack Growth Rate Model Predictions for Ti-24Al-11Nb

In this chapter, the model developed in Chapter V is used to predict the experimental crack growth rate data. There are two types of experimental data presented in Chapter IV: those required for model calibration and those employed for model verification. Isothermal data are used primarily to calibrate the model; however, there are a few used to validate the model over various ΔK values. The thermal-mechanical fatigue (TMF) crack growth rate data are used only to verify the model. There are two types of TMF crack growth rate data modeled in this study: baseline (simplified) tests and proof (complex) tests. Baseline tests have identical load and temperature cycles, but there can be a phase angle shift between them. The proof tests have different load and temperature cycles. Further discussions of these test types are presented in Chapter IV.

The crack growth rate predictions presented in this chapter include: first, isothermal fatigue and isothermal fatigue with superimposed load holds at P_{max} (hold-time tests) for single values of ΔK; second, isothermal fatigue and hold-time tests for the full range of ΔK; and third, TMF crack growth rate predictions that include both baseline and proof tests. The model predictions that are obtained during the iteration process are identified as calibration data, and all other predictions are used only to verify the model.

Data Used During Model Calibration

A complete discussion of the iteration process that determines the model parameters (model calibration) is presented in Chapter V, and a summary of this process is shown in Table 5.2. The model parameters are determined: first, by establishing the shape of the da/dN vs. ΔK curves; second, after adding the retardation effects, the crack growth rates are modeled for one value of ΔK to speed the iterations; and third, after obtaining acceptable agreement between the experimental data and model prediction, the model is applied over the range of ΔK. The crack growth rates obtained during the model calibration are present in this section.

After the functions that define C_1 and C_2, the constant β_0, and the MSE coefficients are established, the prediction of crack growth rates for different frequencies, temperatures, and hold times are made to check the validity of the functions and coefficients.

Crack Growth Rates at Various Frequencies

The predicted crack growth rates for different frequencies at 649°C for ΔK = 14.85 MPa m$^{1/2}$ are presented in Figure 6.1. The predictions do not differ from the experimental results by any significant amount. This is expected since the 0.01, 1.0, and 100.0 Hz data presented in Figure 6.1 are used primarily to calibrate the frequency dependence of the function C_1, which is given in Equation (5.63). For each of the three frequencies, values of C_1 are

208
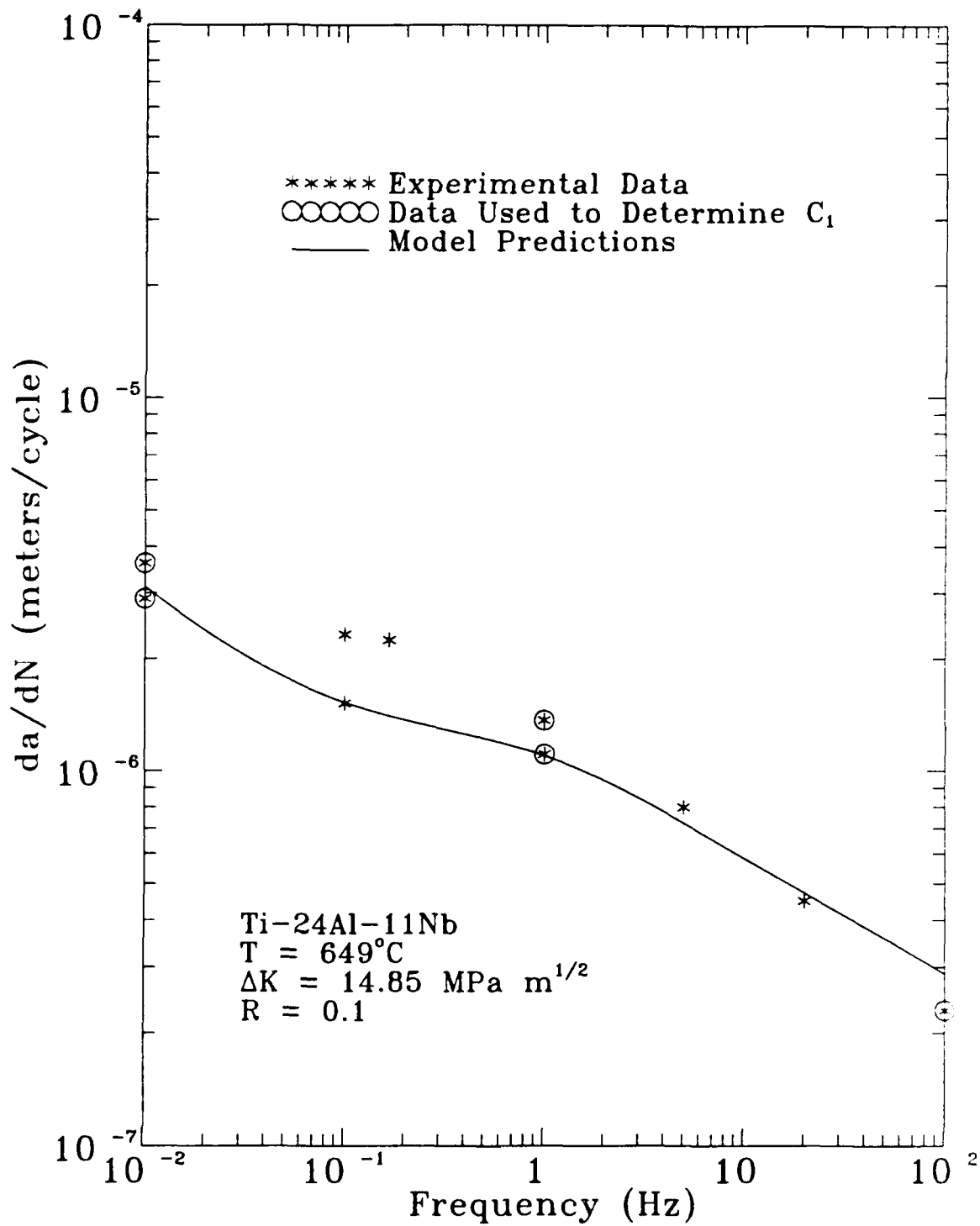
Figure 6.1 Crack Growth Rate Predictions at Different Frequencies

209

selected to match the experimental data. After adequate correlations are obtained, the expression for C_1 is developed to represent the data over the entire range of frequency.

Crack Growth Rates at Various Temperatures

The temperature effects are determined by a combination of $(da/dt)_i$ in the modified sigmoidal equation (MSE) describing unretarded time-dependent crack growth rates (Equation (5.42)), and C_2 in the equation that describes the retardation coefficient (Equation (5.62)). The crack growth rate predictions for temperatures between 315 and 649°C for frequencies of 0.01 and 1.0 Hz are shown in Figure 6.2, along with the experimental crack growth rate data. The 0.01 Hz condition is used to develop the effect of temperature; therefore, it is not surprising that this fit to the data is almost perfect. On the other hand, the 1.0 Hz crack growth rate predictions are based on both the fit to the 0.01 Hz data at different temperatures shown in Figure 6.2 and fit to the 649°C data at different frequencies shown in Figure 6.1. The only 1.0 Hz data point used during model calibration is the 649°C point, and the other 1.0 Hz crack growth rate predictions match the experimental data very well.

Figures 6.1 and 6.2 show how this modeling procedure is used for isothermal crack growth rate data at different temperatures and frequencies. Next, the hold-time crack growth rate data that are used during model parameter calibration are considered.
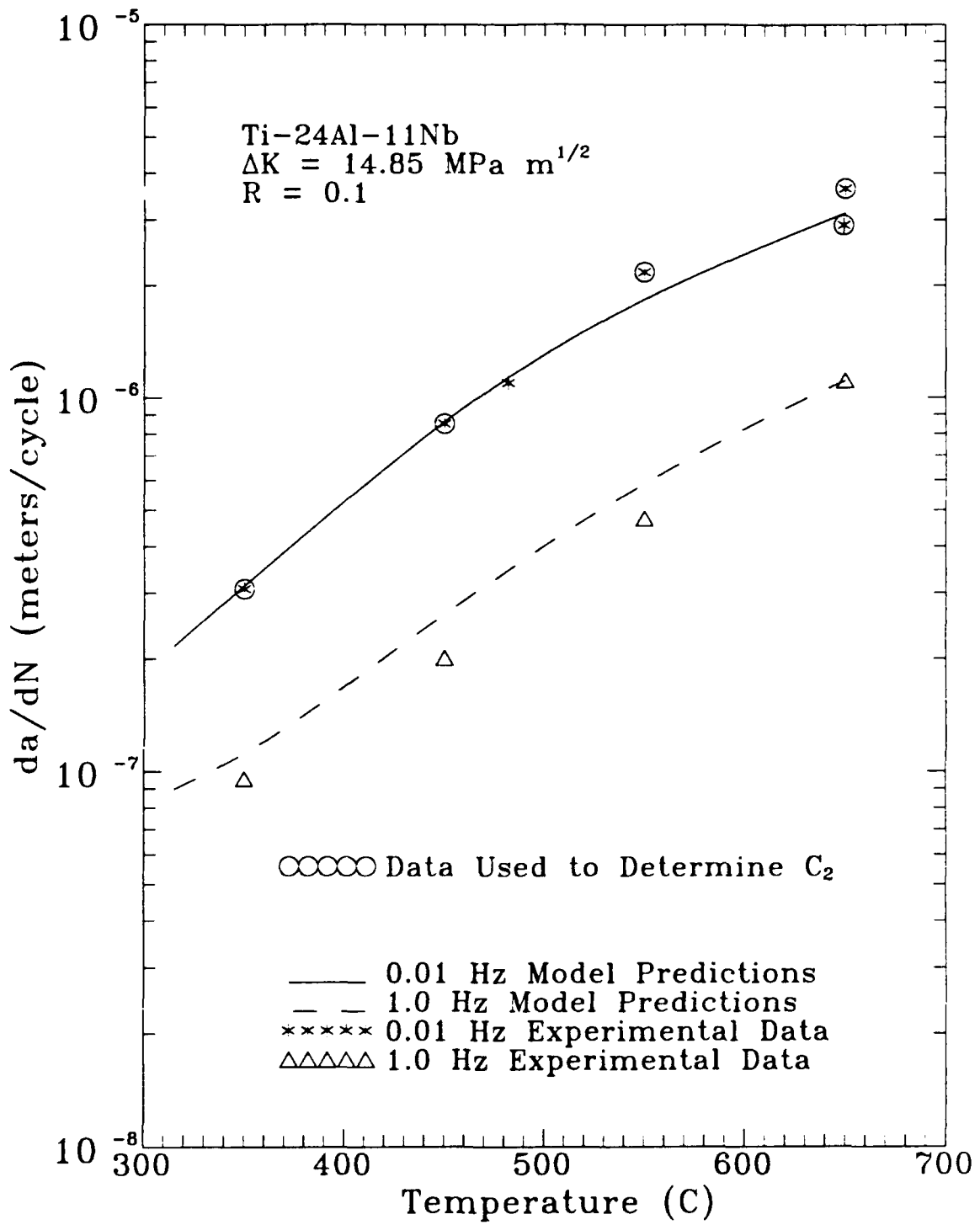
Figure 6.2 Crack Growth Rate Predictions at Different Temperatures

Crack Growth Rates at Various Hold Times

The crack growth rate predictions for hold-time tests are considered next. An infinite combination of $(da/dN)_i$ and C_2 can accurately model isothermal fatigue crack growth rates. Recall from Chapter V that if $(da/dN)_i$ is increased and C_2 is increased, the result could be no net effect, since β is reduced and decreases the effect of $(da/dt)_{ur\ td}$. But hold-time experiments identify the best combination of $(da/dN)_i$ and C_2. The crack growth rates for 1.0 second cycles with hold times of 10, 100, and 1000 seconds are shown in Figure 6.3 with the model predictions for each case. The predicted crack growth rates are somewhat high for the 10 and 100 second hold-time cases, and this may suggest either that the combination of $(da/dN)_i$ and C_2 is not the optimum, or that this is a limitation of the model. Various other combinations were attempted without success; therefore, it is most likely a model limitation. This is an aspect of the model that can be improved in future efforts. The 1000 second predicted crack growth rate matches rather well with experimental data, but this is expected since this prediction is a result of fitting β_0 to the experimental data (see Chapter V).

The crack growth rates for 100 (or 96) second cycles with hold times of 10, 48, and 100 seconds are shown in Figure 6.4 with the model predictions for each case. These predictions correlate very well with the experimental data, and this is expected since they are used during the iteration process to check the validity of $(da/dN)_i$, C_1, C_2, and β_0.

212
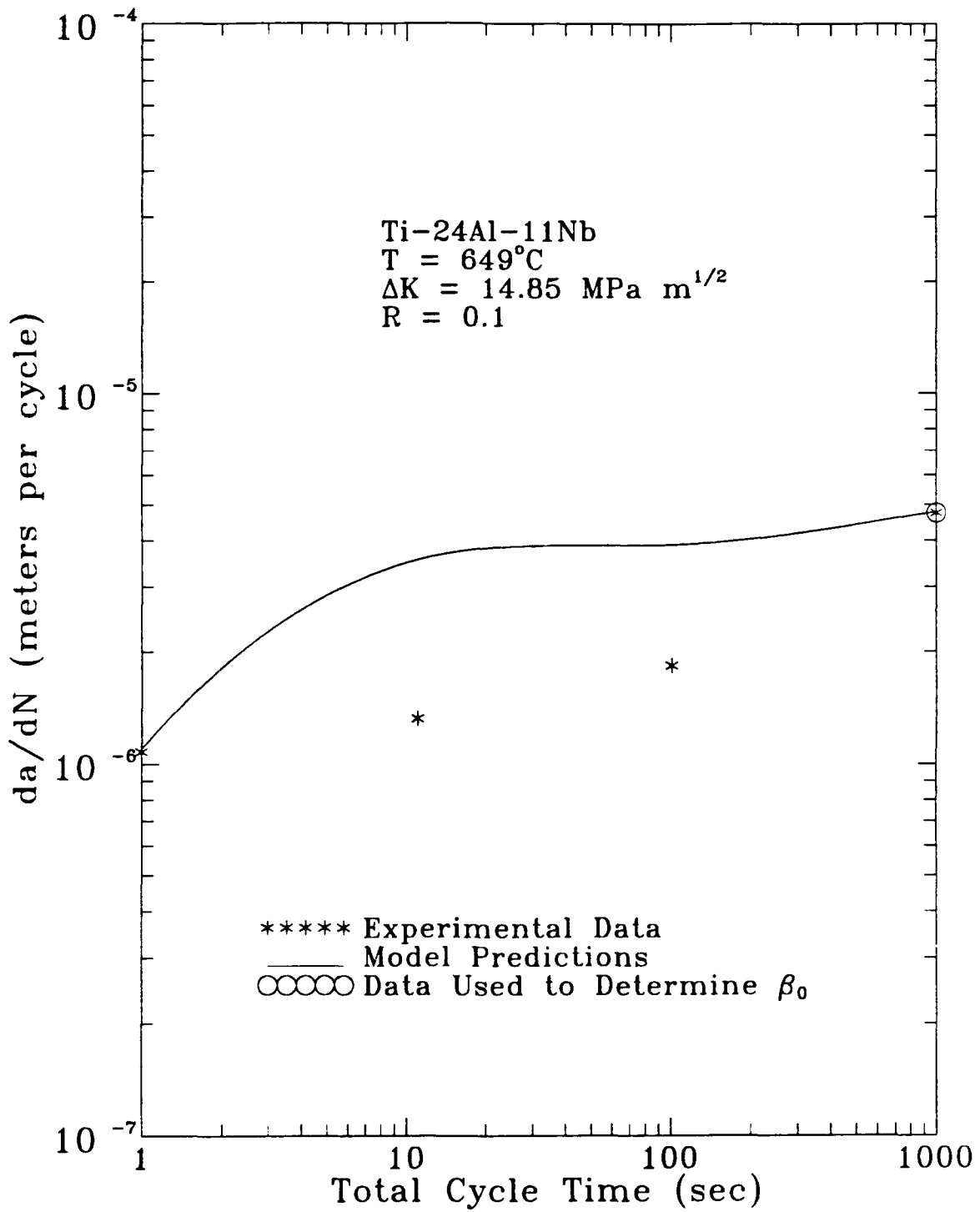
Figure 6.3 Crack Growth Predictions for 1 Second Fatigue Cycles
with Hold Times of 10, 50, 100, and 1000 Seconds

213
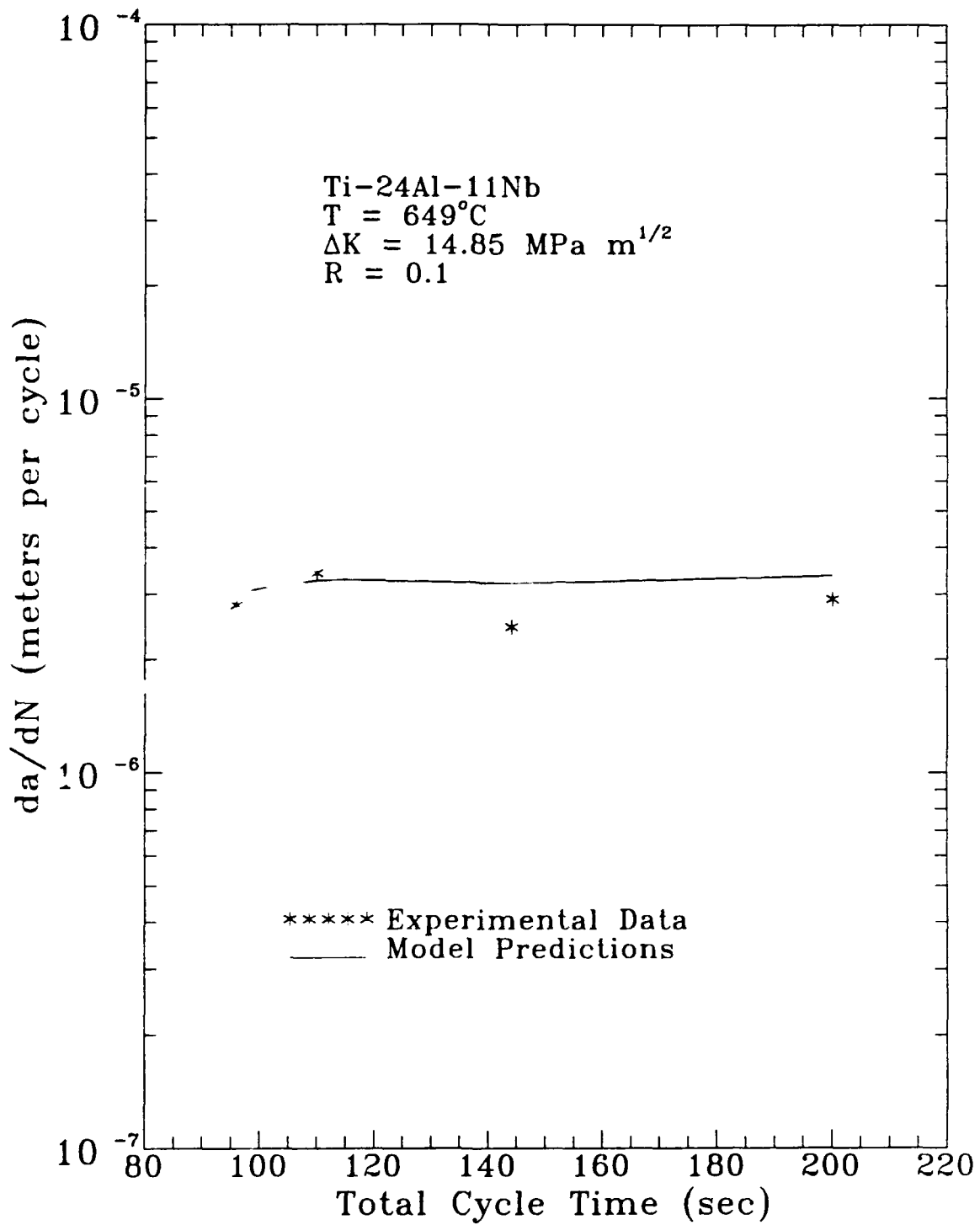
Figure 6.4 Crack Growth Predictions for 100 Second Fatigue Cycles
with Hold Times of 10, 48, 100 Seconds

214

Data Used for Model Verification

The tests used to verify the model are isothermal fatigue, isothermal fatigue with superimposed load hold times, and TMF. First, the isothermal predictions are discussed including both fatigue and hold-time conditions. Second, the TMF crack growth rate predictions are discussed, including both baseline TMF and proof TMF test cases. These results fulfill the main objective of this dissertation, which is to develop a model to predict crack growth rates in Ti-24Al-11Nb under thermal-mechanical cycling using only isothermal data for calibration.

Isothermal Crack Growth Rate Predictions

Isothermal Fatigue

Figures 6.1 and 6.2 show the predictions of crack growth rates for various frequencies and temperatures, considering a single value of ΔK. Figures 6.5 and 6.6 show crack growth rate predictions for the full range of ΔK tested. Crack growth rates for frequencies of 0.01, 0.1, and 5.0 Hz are presented in Figure 6.5. The 5.0 Hz data are used to generate the MSE coefficients that define the shape of the crack growth curve (as discussed in Chapter V), and the crack growth rates for $\Delta K = 14.85$ MPa m$^{1/2}$ from all three frequencies are used to model the frequency behavior as shown in Figure 6.1. The predictions for crack growth rates over the range of ΔK for 0.01 and 0.1 Hz compare very well with the experimental results. Similarly, the temperature

215
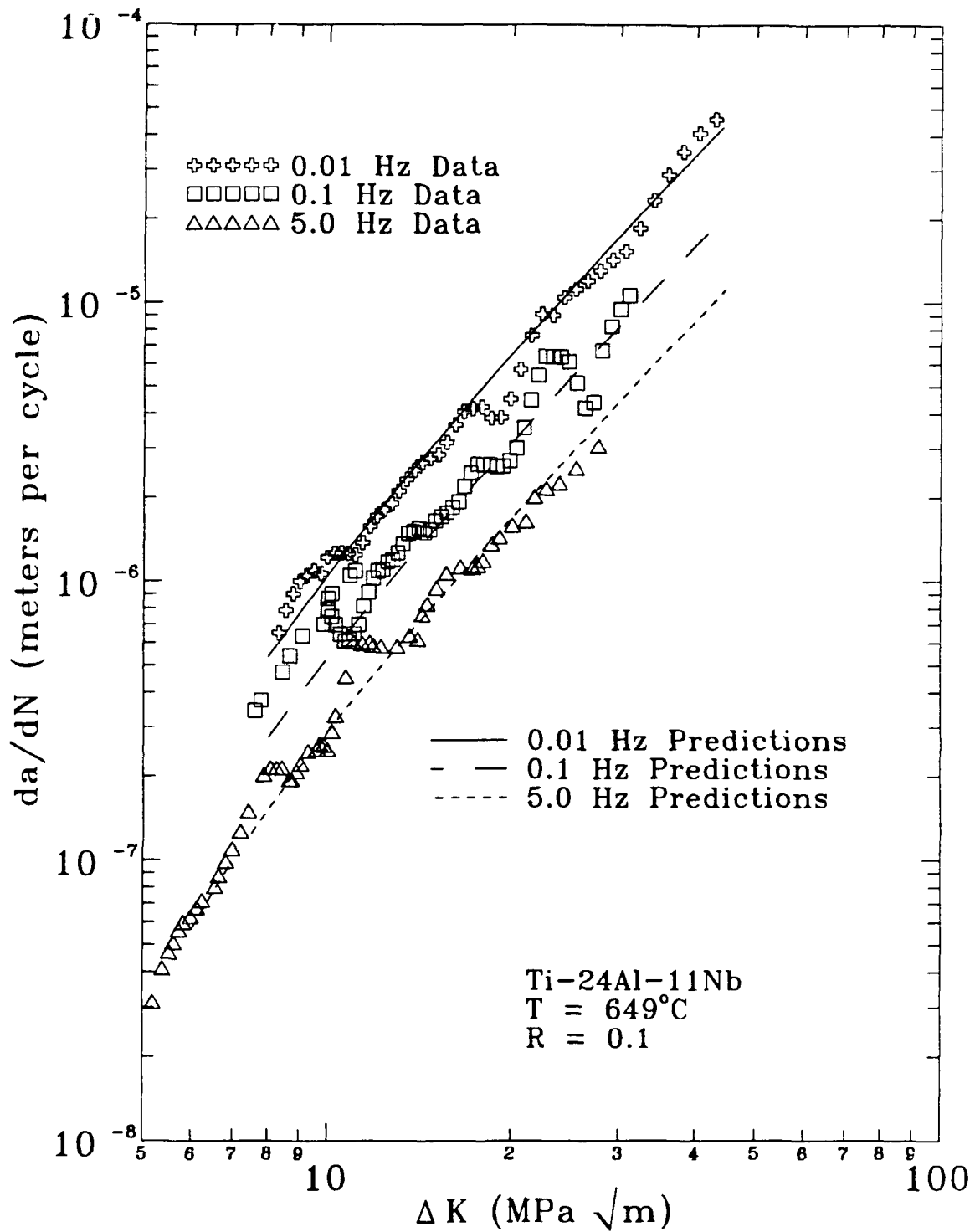
Figure 6.5 Crack Growth Rate Predictions at Different Frequencies

216
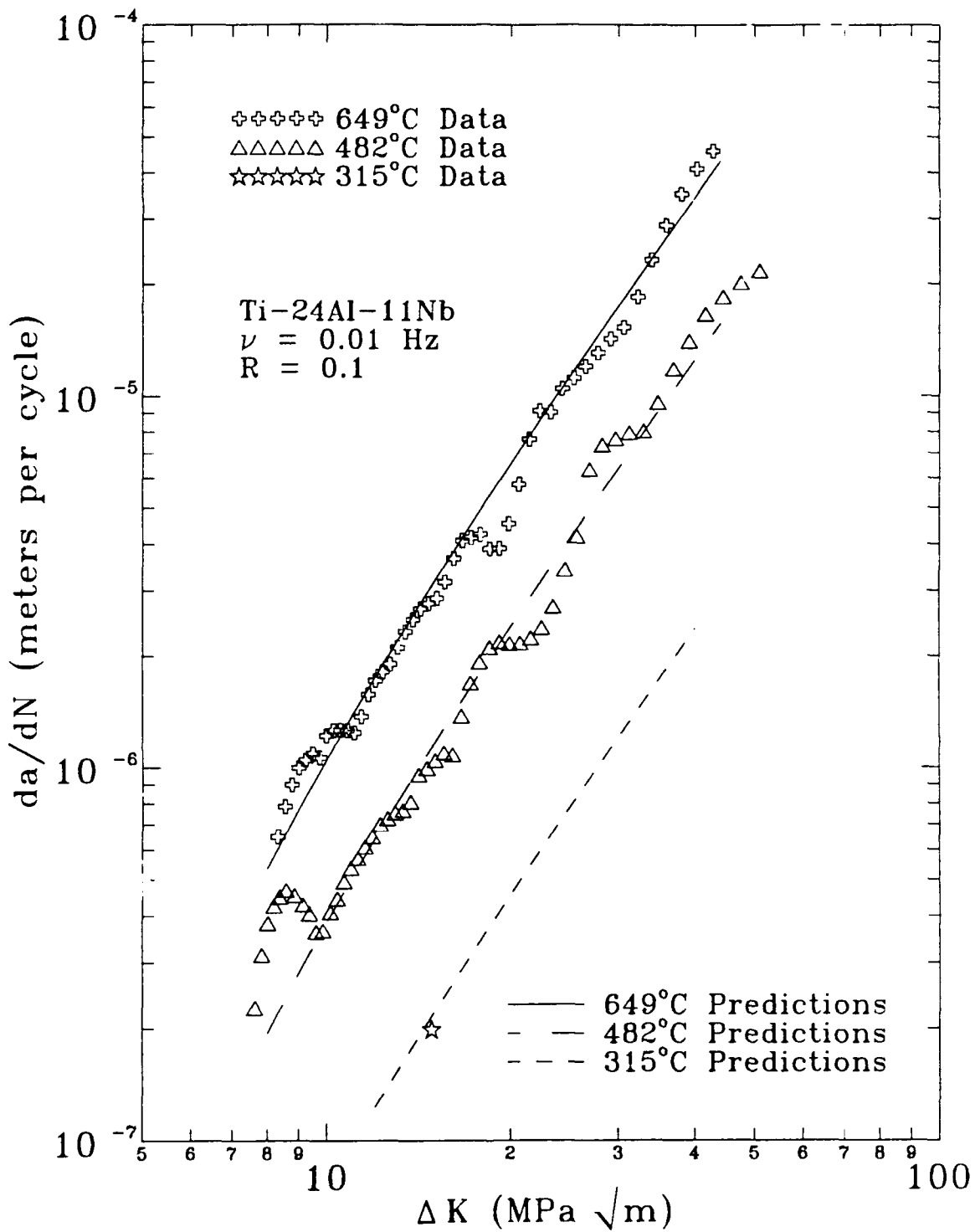
Figure 6.6 Crack Growth Rate Predictions at Different Temperatures

effect is determined from the growth rates obtained at $\Delta K = 14.85$ MPa m$^{1/2}$, and the predictions for the other values of ΔK compare well with the experimental data, as shown in Figure 6.6.

Isothermal Hold-Time Tests

The comparison of predicted and experimental crack growth rates for hold-time tests conducted at 649°C are discussed next. Recall that hold-time tests are used to validate the combination of $(da/dN)_i$ and C_2 used in the model. Figures 6.7, 6.8, and 6.9 show the crack growth predictions for fatigue cycles of 100 (or 96) seconds with superimposed load hold times of 10, 48, and 100 seconds. In each case, the predictions match the data extremely well.

It is interesting to note that the predictions do not differ dramatically between the 10, 48, and 100 second hold-time cases. However, this matches the observed behavior (experimental data) of this alloy when hold times are added to 0.01 Hz fatigue cycles. One could argue that this behavior need not be modeled since the growth rates do not change with increasing hold times, but this type of argument ignores the hold-time data with 1.0 Hz fatigue cycles. The crack growth rates become substantial as the hold time increases to orders of magnitude greater than the fatigue cycle. The model predicts this type of behavior, even for fatigue cycles of 0.01 Hz; however, experimental data of this type could not be generated for the 0.01 Hz tests, because of their long duration.

218
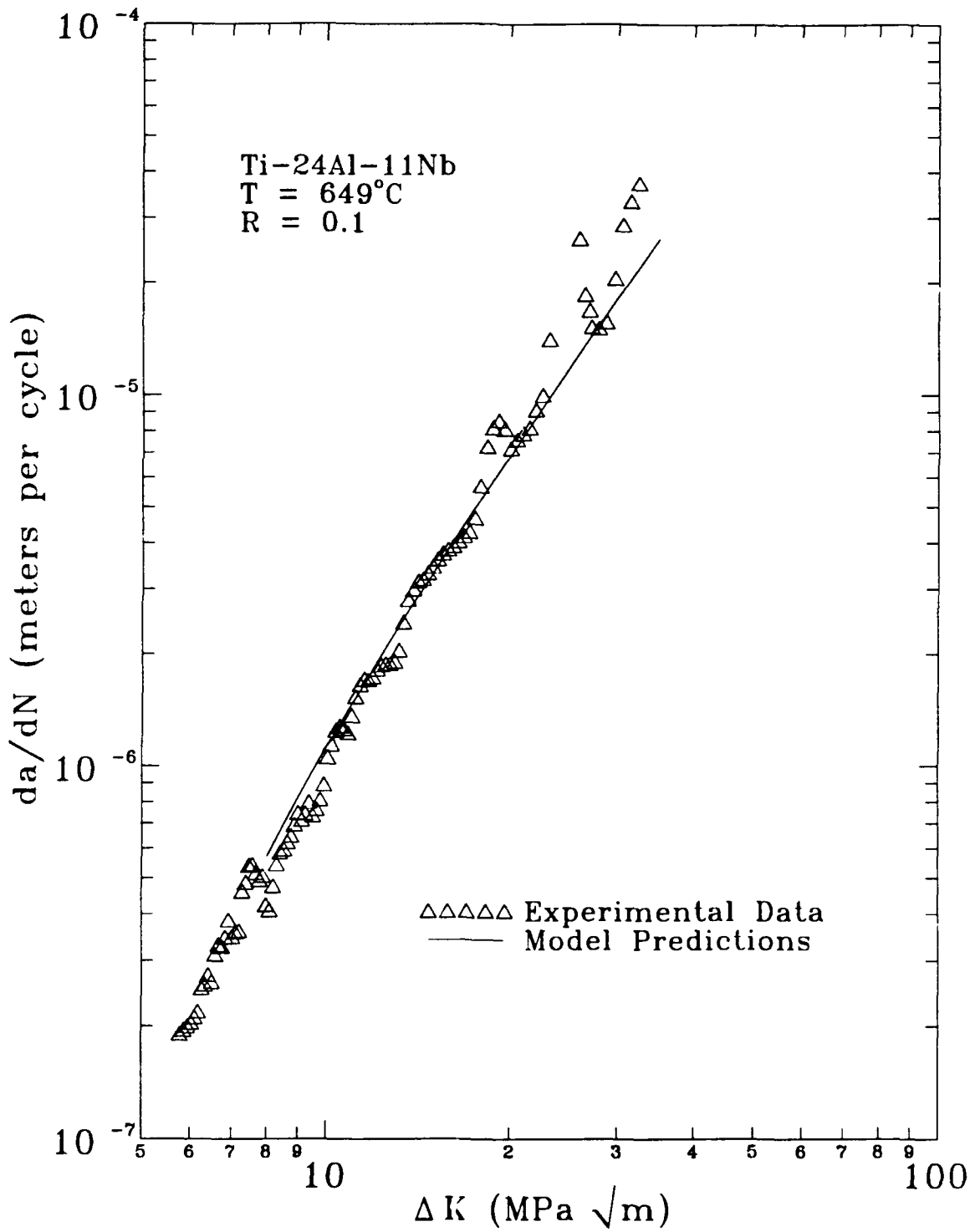
Figure 6.7 Crack Growth Rate Predictions for 100 Second Fatigue Cycle with
Superimposed 10 Second Hold Time
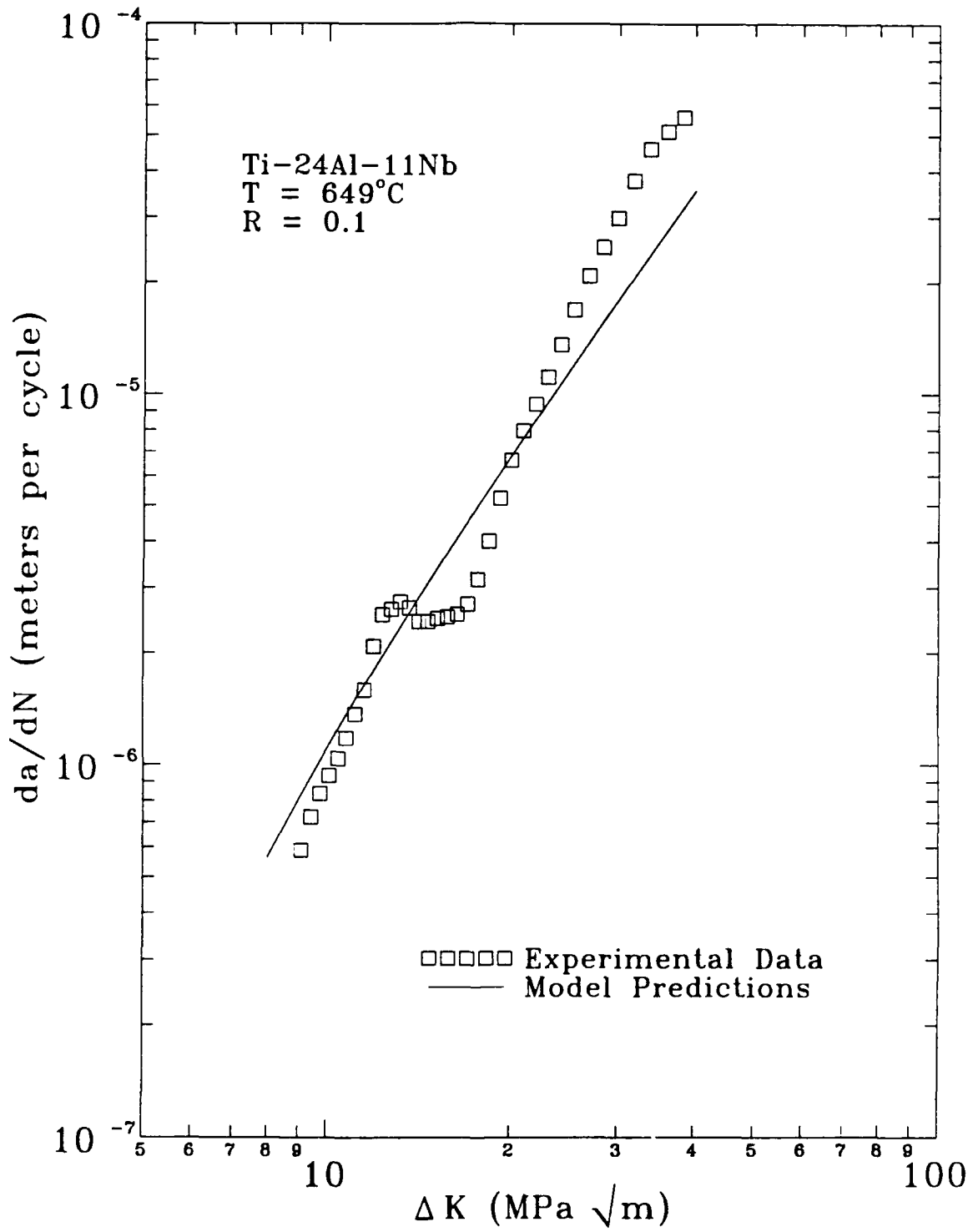
Figure 6.8 Crack Growth Rate Predictions for 96 Second Fatigue Cycle with
Superimposed 48 Second Hold Time
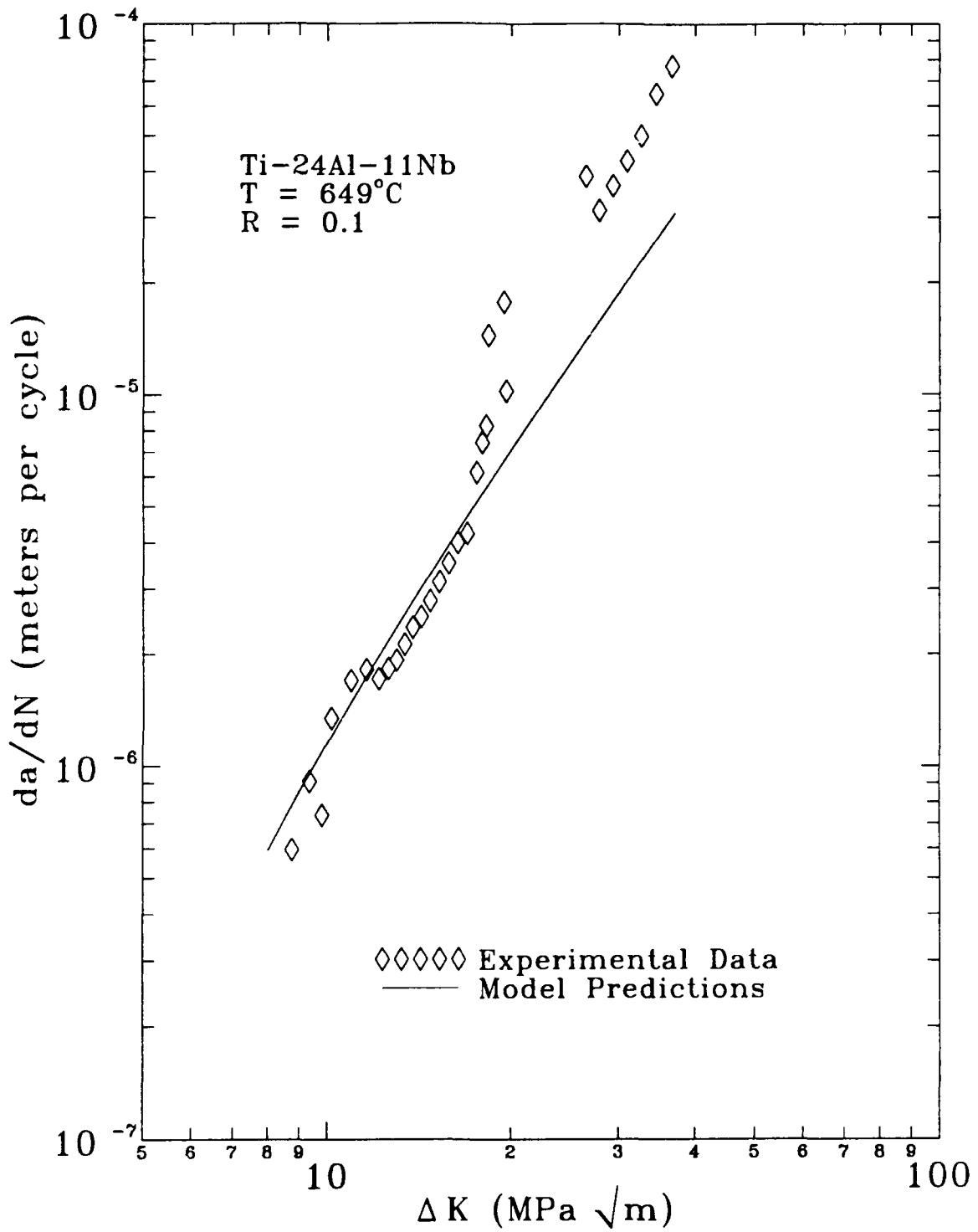
Figure 6.9 Crack Growth Rate Predictions for 100 Second Fatigue Cycle with
Superimposed 100 Second Hold Time

TMF Crack Growth Rate Predictions

The predictions for TMF crack growth rates is divided into two categories: predictions of baseline test data and predictions of proof test data. For all of the TMF tests, the temperature is cycled between 315 and 649°C.

TMF Baseline Tests

All of the baseline TMF tests are performed with 96 second triangular waveforms of load and temperature. The only difference between the baseline tests is the load-temperature phase angle. These include: in-phase, 90° out-of-phase, 180° out-of-phase, and 270° out-of-phase tests. The crack growth rate predictions for the baseline TMF tests are presented in Figures 6.10, 6.11, 6.12, and 6.13. The in-phase TMF crack growth rate predictions match the experimental data (Figure 6.10). The 90° out-of-phase TMF crack growth rate predictions are slightly lower than the experimental data for the entire range of the ΔK values studied (Figure 6.11). But the predicted crack growth rates differ from the experimental data by no more than a factor of two, which is considered to be typical specimen-to-specimen variation in data of these type. The 180° out-of-phase TMF crack growth rate predictions match the data extremely well (Figure 6.12). The 270° out-of-phase TMF crack growth rate predictions match the data at higher values of ΔK, and the predictions are slightly greater than the experimental data at the lower values of ΔK; however, these crack growth rates are within a factor of two of the data (Figure 6.13).

222
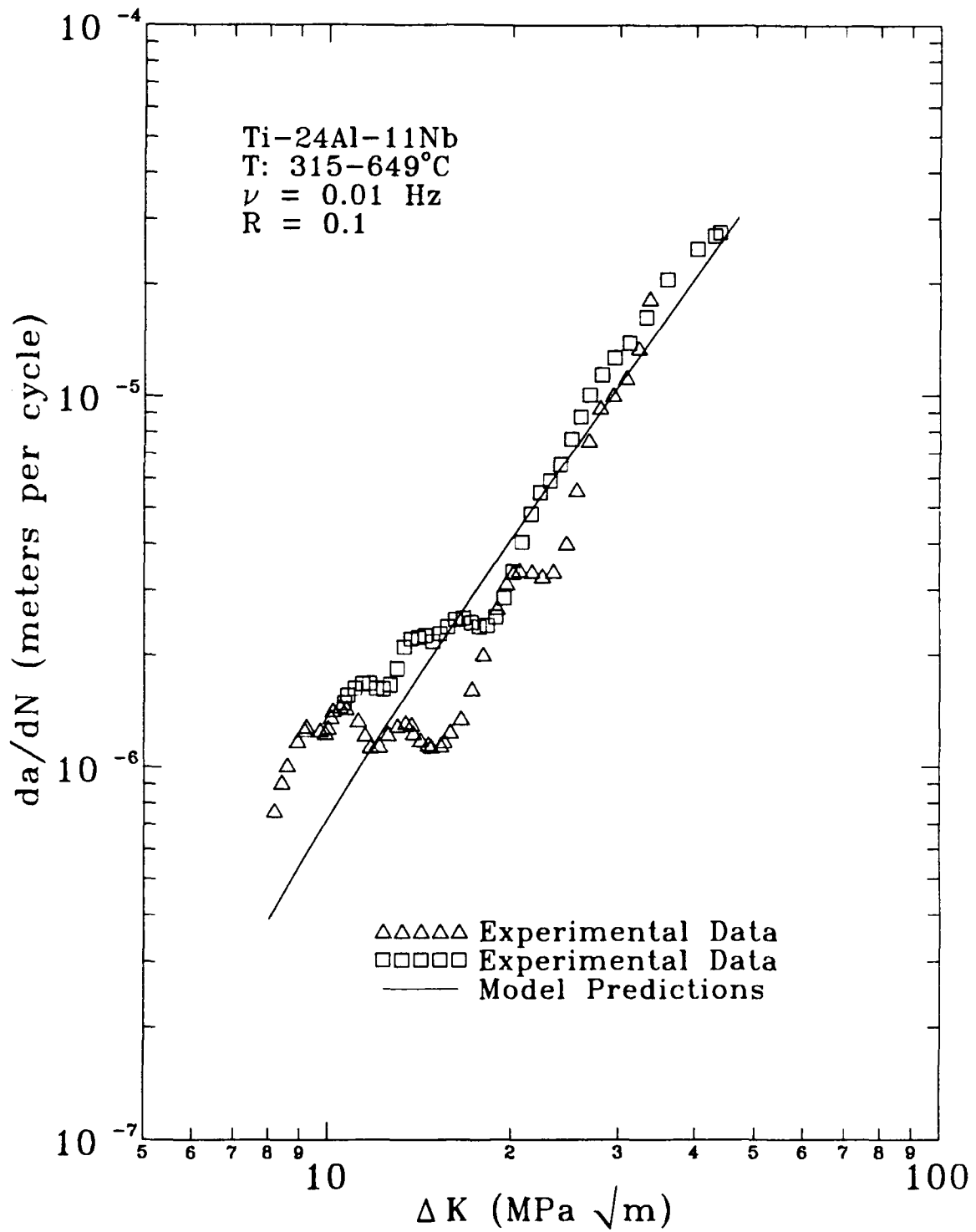
Figure 6.10 Crack Growth Rate Predictions for In-Phase TMF

223
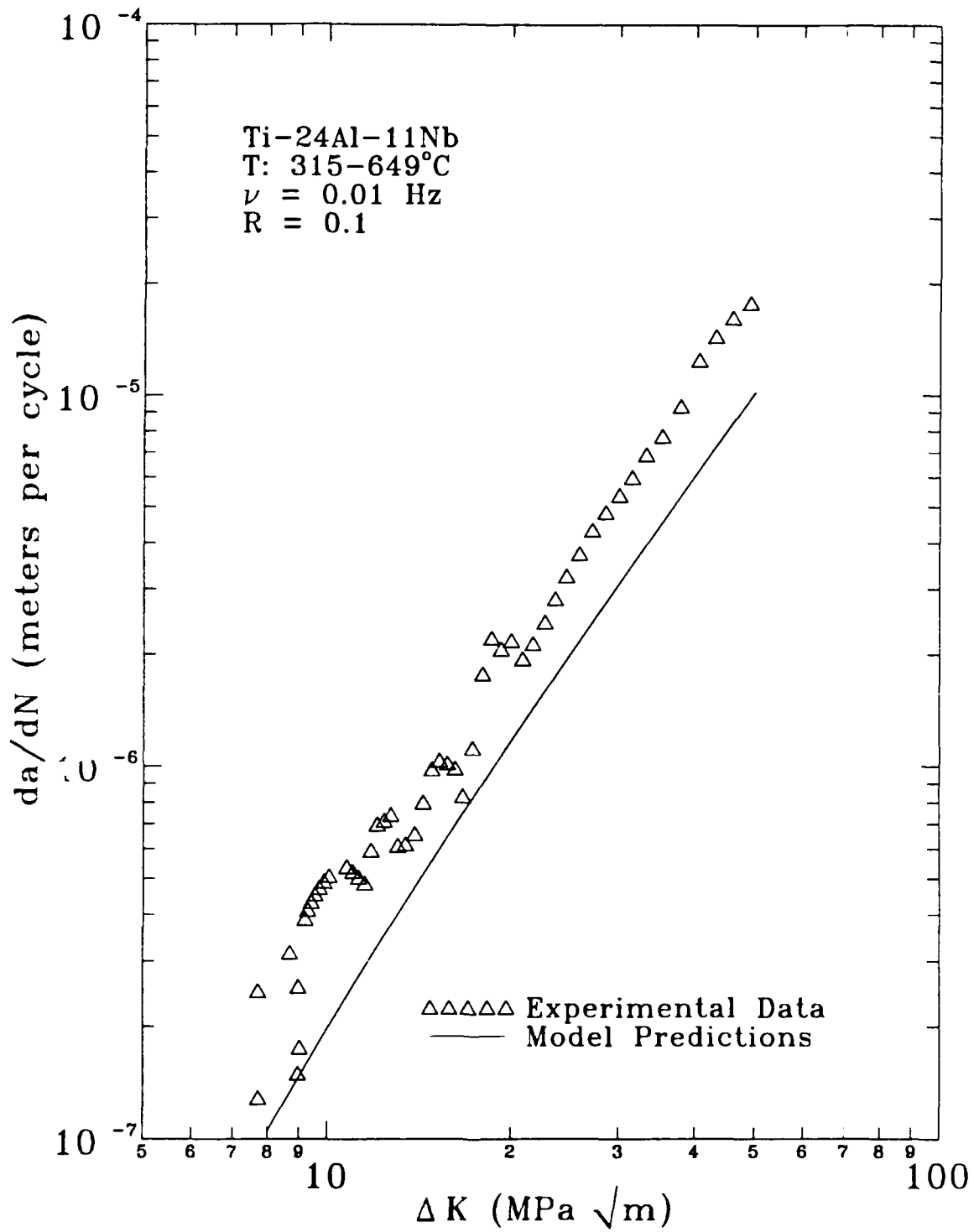
Figure 6.11 Crack Growth Rate Predictions for 90° Out-of-Phase TMF

224
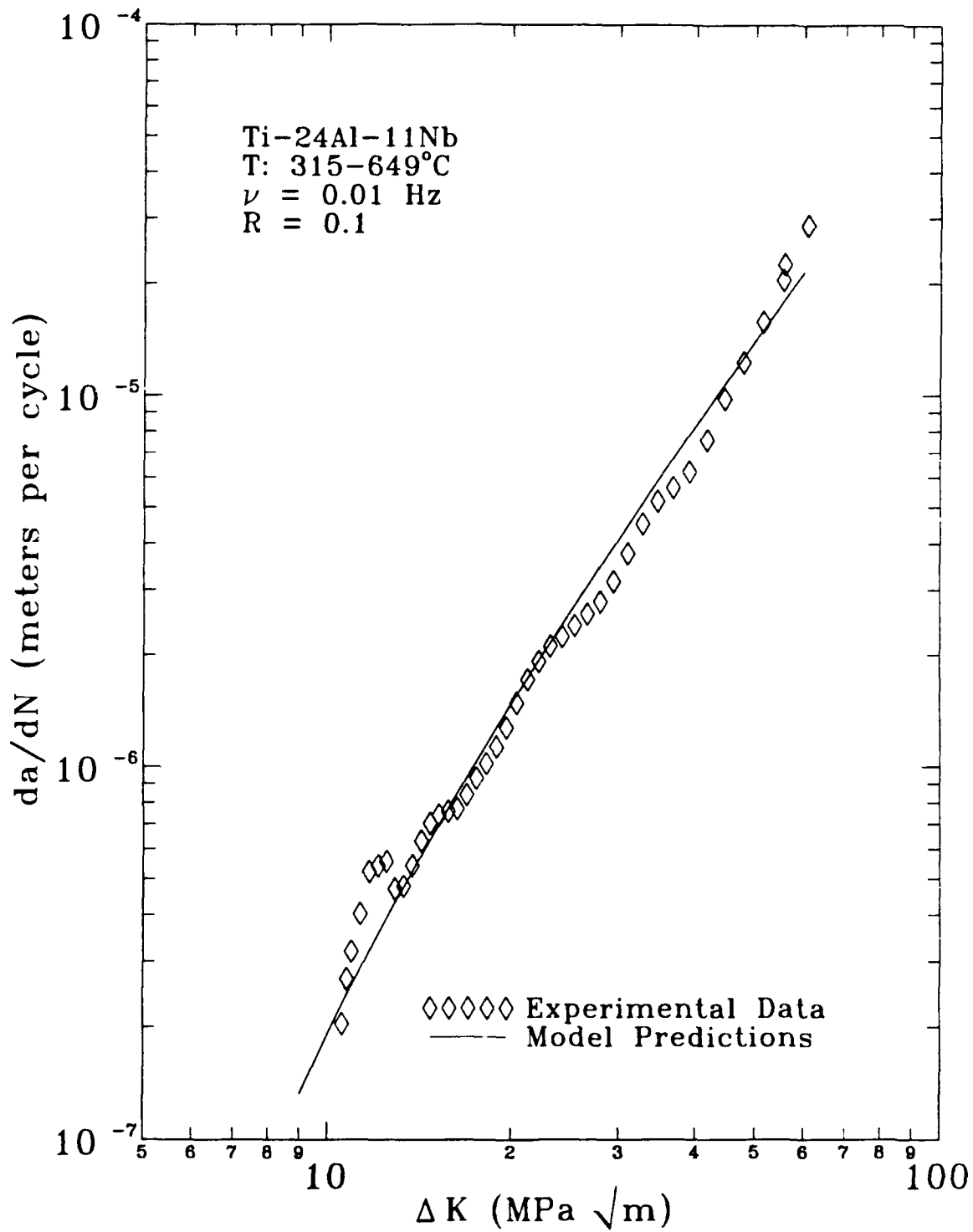
Figure 6.12 Crack Growth Rate Predictions for 180° Out-of-Phase TMF

225
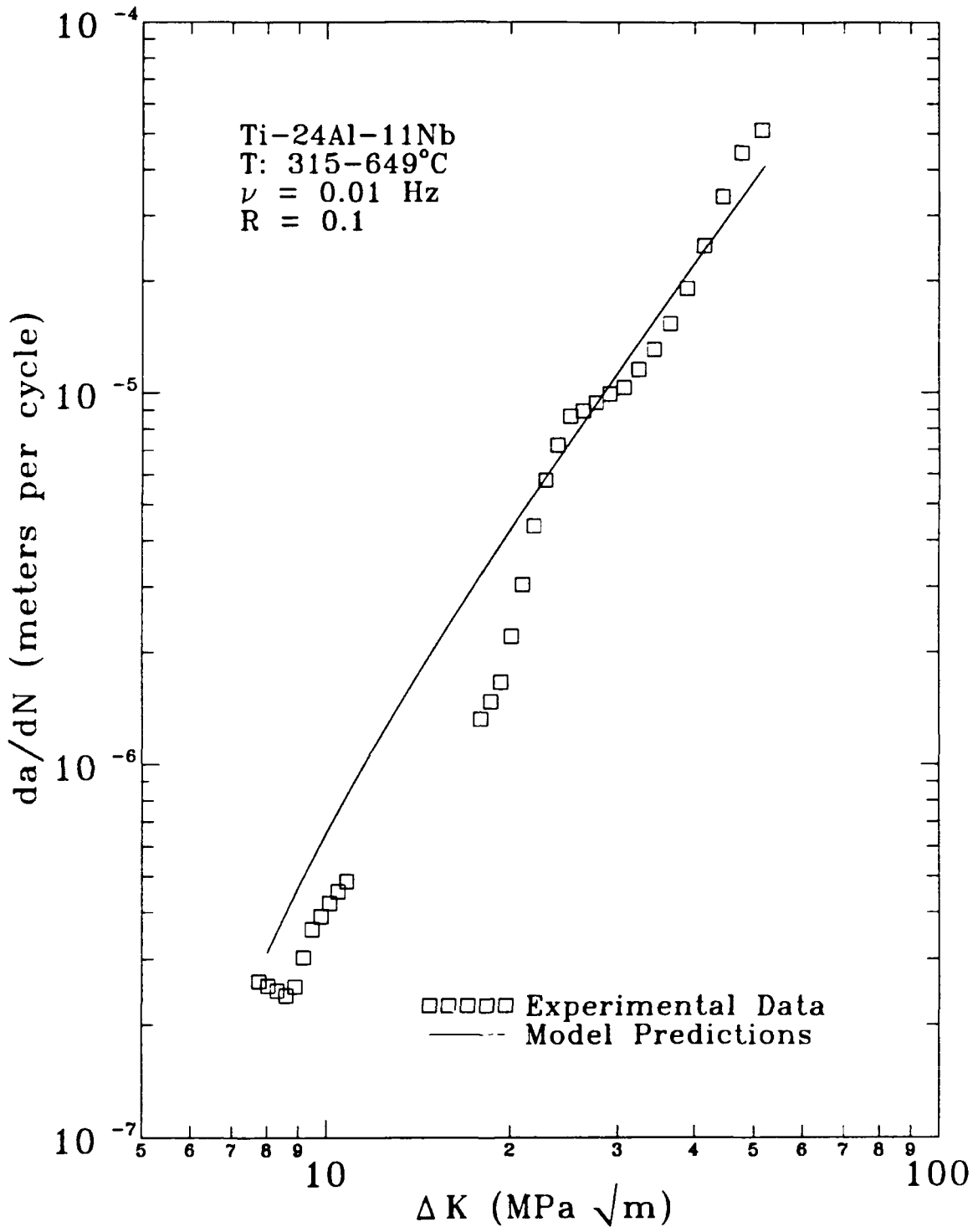
Figure 6.13 Crack Growth Rate Predictions for 270° Out-of-Phase TMF

226

TMF Proof Tests

In the TMF tests discussed previously, the load and temperature cycles are identical, but in the TMF tests discussed here, the load and temperature cycles differ. These tests are referred to as proof tests, and include the upper-triangular-phase and lower-triangular-phase TMF tests (these are defined in Chapter IV). Both of the upper and lower-triangular-phase TMF tests are performed with 48 second load and temperature ramps and 48 second load and temperature holds. These cycles are used to identify the portions of the TMF cycles where damage occurs, and also to verify the limits of integration on the retarded time-dependent calculation (Equation (5.42)). In Chapter V it is postulated that the integration is continued until the load begins to decrease, and the results presented here support these limits. (Further discussions of this are presented in Chapter V during the development of the retarded time-dependent crack growth rate contribution.)

The crack growth rate predictions for the proof TMF tests are presented in Figures 6.14 and 6.15. As shown in Figure 6.14, the upper-triangular-phase TMF crack growth rate predictions match the experimental data extremely well for the entire range of the ΔK values studied. However, the lower-triangular-phase TMF crack growth rate predictions shown in Figure 6.15 are less than the experimental crack growth rate data, but the predicted crack growth rates differ from the experimental data by no more than a factor of two.

227
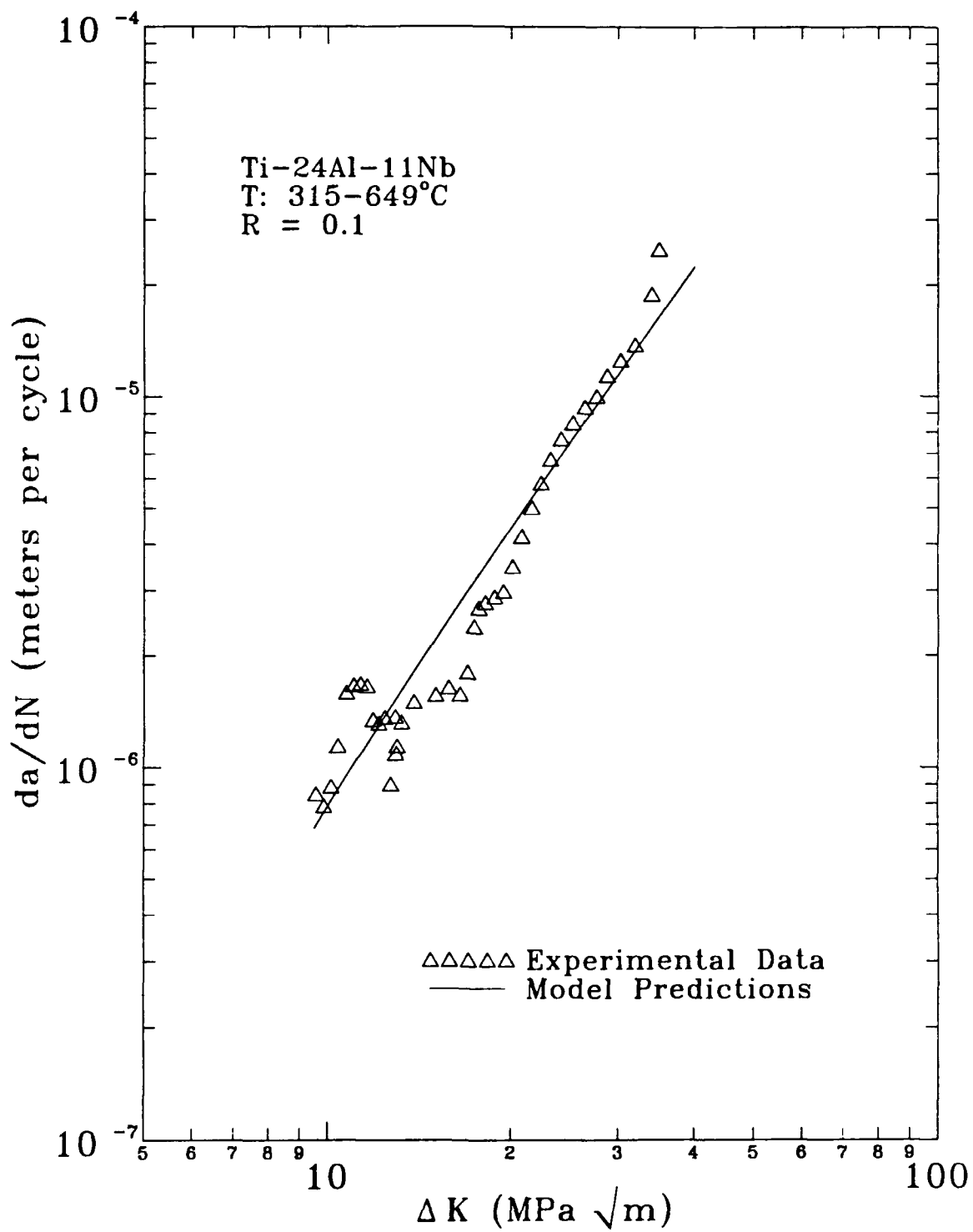
Figure 6.14 Crack Growth Rate Predictions for Upper-Triangular-Phase TMF
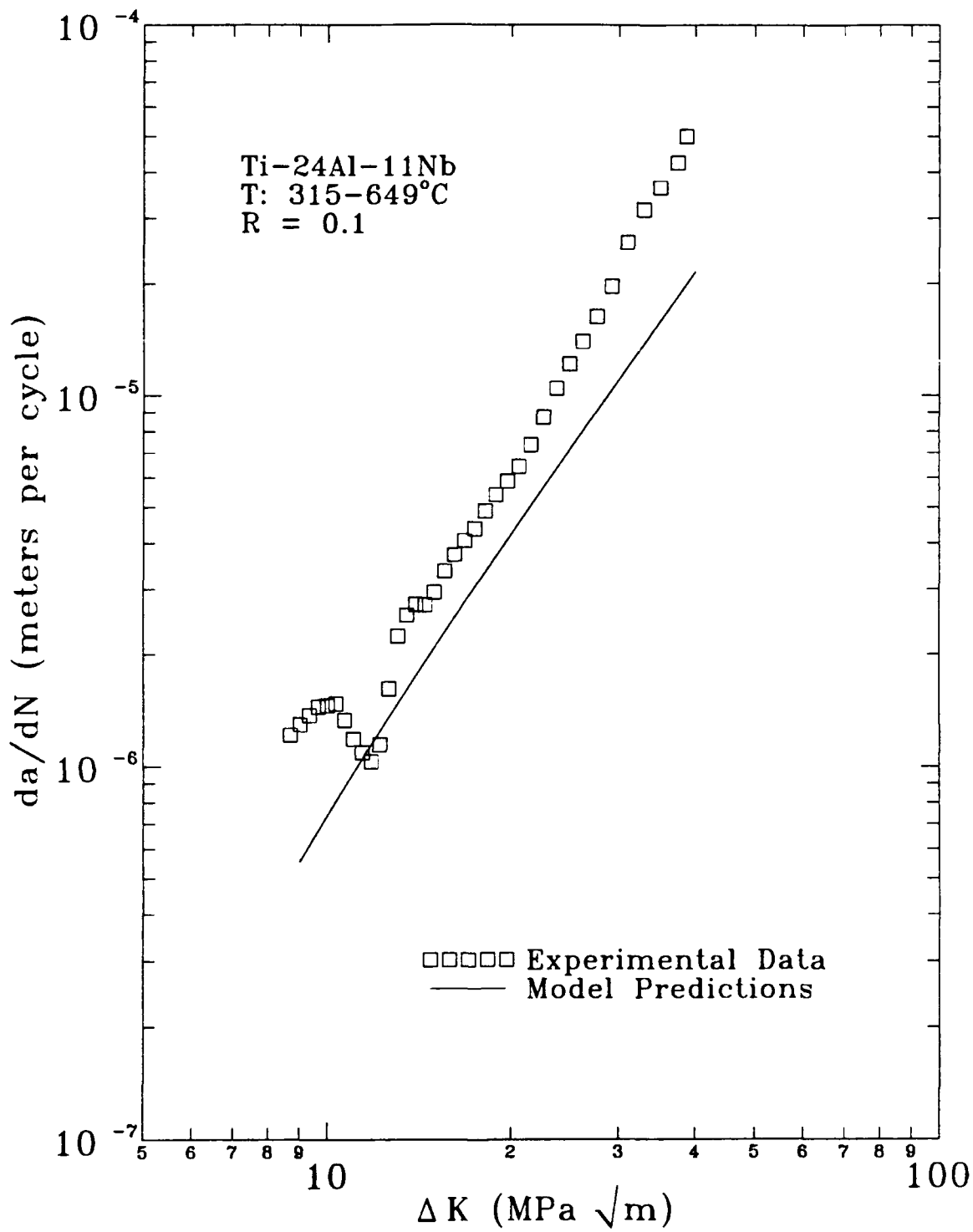
Figure 6.15 Crack Growth Rate Predictions for Lower-Triangular-Phase TMF

229

Discussion of Model Capabilities

The model presented in Chapter V predicts the crack growth rates for isothermal fatigue, isothermal fatigue with superimposed hold times at P_{max}, and thermal-mechanical fatigue of the titanium-aluminide alloy, Ti-24Al-11Nb. The two significant features of this model, which no previous efforts have addressed, are the ability to: 1) predict the cycle-dependent crack growth rate as a function of temperature, and 2) account for the retardation of crack growth rates that is attributed to creep blunting of the crack tip.

The cycle-dependent contribution to the total crack growth rate, which is shown in Equation (5.17), is presented in integral form since the reference growth rate is a function of temperature. This temperature-dependent form is a modification of the HNH model (Equation (5.1)), which expresses the cycle-dependent crack growth rate as a function of only R and K. The current modeling effort requires the dependence on temperature to model the observed cycle-dependent crack growth behavior of Ti-24Al-11Nb discussed in Chapter IV. The HNH model did not require the temperature-dependent form since the cycle-dependent crack growth rate of Inconel 718 at elevated temperatures is equal to that observed at room temperature, which is the case for most materials. The ability of the current model to account for variations in temperatures allows for use with a wider-range of materials, instead of limiting the model to materials that exhibit cycle-dependent behavior that is independent of temperature.

The model developed in this study accounts for crack growth rate retardation by introducing the coefficient β into the expressions for the cycle-dependent and time-dependent contributions to the total crack growth rate (Equations (5.17) and (5.42)). The coefficient β numerically models the experimentally-observed retardation effect that is attributed to blunting of the crack tip. The retardation coefficient, β, appears inside of the integral for both crack growth rate contributions since β changes continuously during the cycle. The expression for the evolution of β (i.e., $d\beta/dt$) is shown in Equation (5.60) as a function of v, P/P_{max}, T, and β.

With the use of this retardation coefficient, the model has the ability to predict crack growth rates for a wider range of materials than for any previous modeling effort. Since the coefficients in the expression for the evolution of β can vary with materials, β can represent the case where creep blunting dominates the crack growth rates (e.g., hold-time tests with Ti-24Al-11Nb) as well as the case where creep is not present (e.g., hold-time tests with the nickel-base superalloy, Inconel 718). For example, the model presented in this work predicts the crack growth rates for the hold-time tests for Ti-24Al-11Nb with 100 second fatigue cycles as shown in Figure 6.4. Recall in this case the growth rates show very minor increases in crack growth rates with the additions of hold times, and this represents one of the most severe cases of crack growth rate retardation. However, for the 1 second fatigue cycle with superimposed holds, Ti-24Al-11Nb shows substantial increases in growth rates

231

(Figure 6.3). In this case, the model predicts increased crack growth rates, although the predictions are somewhat higher than what is observed experimentally. For the hold-time tests described above, the model demonstrates the ability to predict no measurable increases in crack growth rates and also to predict substantial increases in crack growth rates, depending on both the time of the fatigue portion of the cycle and the time of the hold at P_{max}. The model also can predict the pure time-dependent crack growth rate behavior seen in hold-time tests with Inconel 718. This represents the extreme case where there is no crack growth rate retardation, and β is equal to unity. The model reduces to the HNH model in such a case (β =1). And as discussed in Chapter V, the HNH model predicts the crack growth rates in Inconel 718 for the same conditions that are described previously for Ti-24Al-11Nb.

VII. <u>Conclusions and Recommendations</u>

In this dissertation an empirical model is developed to predict crack growth rates during isothermal fatigue, isothermal fatigue with superimposed load hold times at maximum load, and thermal-mechanical fatigue (TMF) in the titanium-aluminide alloy, Ti-24Al-11Nb. This model requires only isothermal data to define its parameters.

In order to develop the model, the material is characterized first. This is accomplished by performing isothermal crack growth experiments at various frequencies and temperatures, and baseline (simplified) thermal-mechanical fatigur (TMF) crack growth experiments. Experimental data suggest that there are both cycle-dependent and time-dependent contributions to crack growth at elevated temperatures. The time-dependent contribution has two components: 1) an environmental degradation mechanism that enhances crack growth by oxygen diffusion, and 2) a retardation mechanism. It is speculated that this retardation is attributed to crack-tip blunting, which is observed during the experimentation.

Initial testing suggested that a linear summation model developed in an earlier study for the nickel-base superalloy, Inconel 718, could predict crack growth rates (crack growth rates) in this alloy under the various conditions discussed above. Further study of Ti-24Al-11Nb using hold-time tests prove this model is inadequate to predict the crack growth rates. The limitations of

233

the previous model are identified, and the model developed in this study addresses the issues that made the previous model inadequate for use with Ti-24Al-11Nb.

The crack growth model developed in this study uses a summation of retarded cycle-dependent and retarded time-dependent crack growth rate contributions to determine the total crack growth extension per cycle. The retardation is modeled with a retardation coefficient that is multiplied by both the unretarded cycle-dependent and time-dependent crack growth rate terms. The unretarded crack growth rates are growth rates that represent non-retarded crack growth conditions. The retardation coefficient is a function of loading frequency, load, and temperature, and these functions are material dependent. This parameter changes continuously during the cycle to estimate the amount of crack growth rate retardation for the given conditions.

The unretarded cycle-dependent crack growth rate is determined from high frequency tests over the entire temperature range studied, since no retardation is assumed to occur at high frequencies. This crack growth rate is expressed as a function of stress intensity range, load ratio, and temperature. The unretarded time-dependent crack growth rate is a hypothetical growth rate, since it represents a non-retarded crack growth rate condition. In this alloy, the crack growth rate is determined indirectly through an iteration process. First, the shape of the crack growth curve is established using a 5 Hz, 649°C test. Then the iteration involves varying the constants and functions

234

that define the unretarded time-dependent crack growth rates and retardation effects until agreement is obtained between predicted and experimental data. The unretarded time-dependent crack growth rate is expressed as a function of stress intensity and temperature.

The model is used to predict crack growth rates under pure-fatigue isothermal conditions from frequencies of 0.01 to 100.0 Hz and temperatures from 315 to 649°C. The model is used to predict crack growth rates during hold-time tests at 649°C with fatigue cycles of 1.0 and 0.01 Hz. Hold times of 1, 10, 100 and 1000 seconds are used. Also, the model predicts crack growth rates for two types of TMF tests: 0.01 Hz "baseline" TMF tests with various load-temperature phase angles and "proof" TMF tests, which have different load and temperature cycles. The baseline test phase angles include 0, 90, 180, and 270. For both types of TMF tests, the temperature is cycled between 315 and 649°C. In all cases, triangular waveforms are used for both the temperature and the load.

In most cases, the crack growth rate predictions using this model compare well the experimental data. The only predictions that do not compare well with the experimental data are the 1.0 Hz fatigue cycle with superimposed hold times of 10 and 100 seconds; hoever, in these two cases, the predictions are lower than the experimental crack growth rates by a factor of three.

The recommendations for future research include:

1) Model load ratio (R) effects. If tests with R equal to 0.5 are performed, the A_{i2} coefficients of Equation (5.29) could be determined.

2) Model TMF tests of different frequencies and temperature ranges.

3) More accurately model the behavior of the hold-time experiments with 1.0 Hz fatigue cycles when holds of 10 and 100 seconds are considered (see Figure 6.3).

4) Perform hold-time tests at different temperatures to get the proper C_2 (Equation (5.62)) and $(da/dt)_i$ (Equation (5.51)) interaction to best describe the crack growth rates over a temperature range (i.e. 315 to 649°C).

5) More accurately model the cycle-dependent behavior at 250°C. This temperature is not part of the objective of this study, but the model predicts time-dependent contributions at 250°C, which is not reflected in the crack growth rate behavior shown in Figure 4.9.

6) Attempt to use a different form of the retardation parameter. A log function may better define the observed crack growth rate behavior.

Appendix

Computer Program to Model Crack Growth Rates

This Appendix is divided into five parts: main program; cycle-dependent functions and subroutines; time-dependent functions and subroutines; retardation subroutines; and input, output, and other subroutines. The program listing contains comments (lower case text) for nearly all operations, and many of the variable names are defined in these comments. Flow charts are provided for the main program, and the more complex functions and subroutines.

Part 1 Main Program

A flow chart is shown in Figure A.1 to describe the operations in the main program.
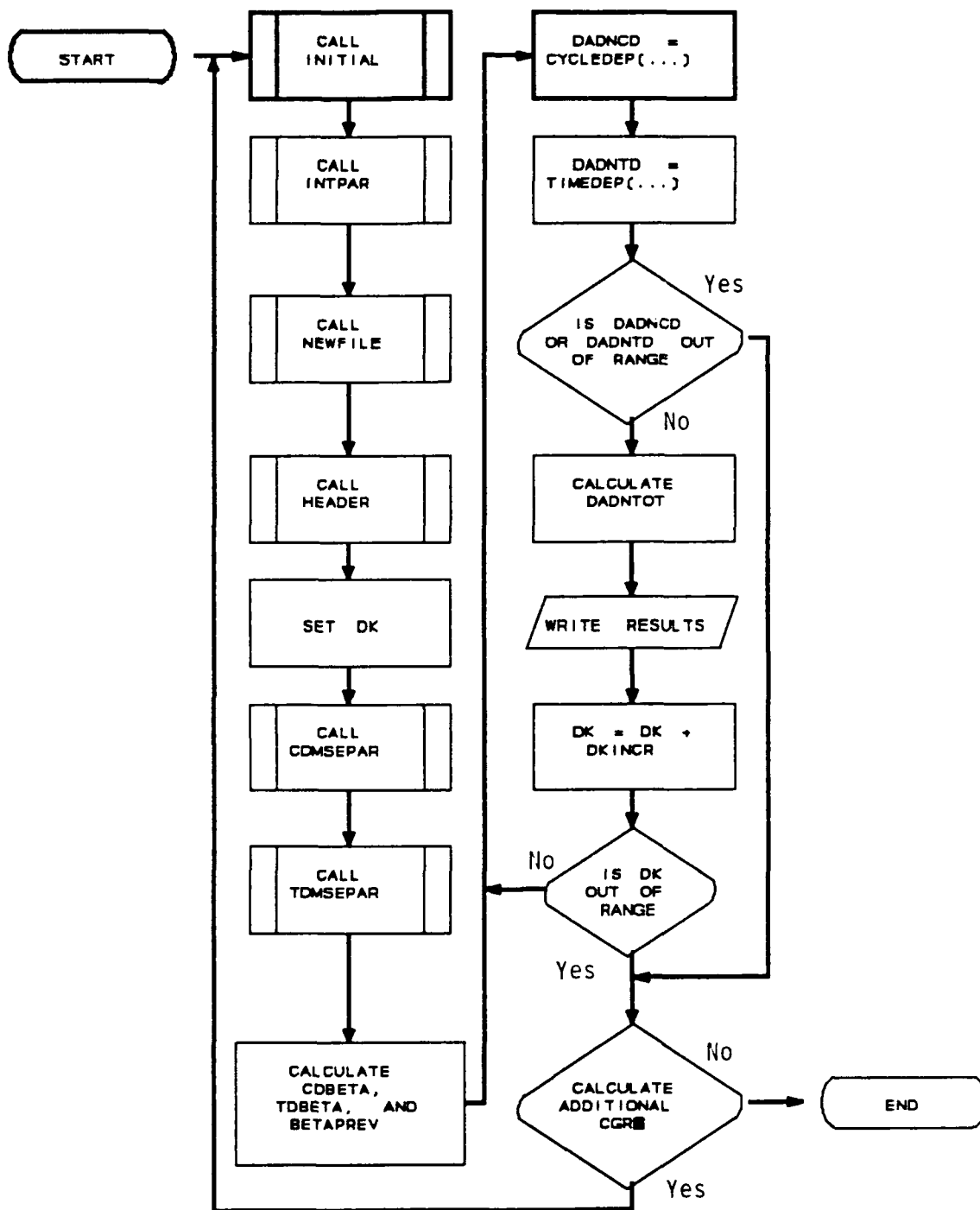
Figure A.1 Flow Chart for Main Program

238

```fortran
C      _____

C      This program predicts thermal-mechanical fatigue crack
C      growth rates in the titanium-aluminide alloy, Ti-24Al-11Nb,
C      and the nickel-base superalloy, Inconel 718.
C      The prediction scheme uses a crack growth rate model that
C      incorporates growth rate retardation effects that have been
C      observed experimentally in Ti-24Al-11Nb.  For Inconel 718,
C      the retardation effects are not used and the model reduces
C      to that used by Heil, Nicholas, and Haritos.
C      K is used as the correlating parameter for the crack
C      growth rates.  The thermal cycles range between 315 and
C      649 degrees C for Ti-24Al-11Nb and between 427 and 649
C      degrees C for Inconel 718.

       PROGRAM TMFCGR
       CHARACTER*21 NAME,BNAME,VERSION,TYPE,MATL
       INTEGER BCHECK,CHOICE,CHECK
       COMMON/BLK1/NUMMATL
       COMMON/BLK2/MATL
       COMMON/BLK3/NUMTYPE
       COMMON/BLK4/TYPE
       COMMON/BLK5/NUMDIV
       COMMON/BLK6/TIME(10),DKPERC(10),DTPERC(10)
       COMMON/BLK7/XN(10),TMSTEP(10)
       COMMON/BLK8/DKSLOPE,DTSLOPE
       COMMON/BLK9/CDBETA
       COMMON/BLK10/TDBETA
       COMMON/BLK11/BCHECK,CHECK

C      Set version number and last date of update.

       VERSION='2.24  10/06/1991'

C      Set up cycle to be analyzed.

101    CALL INITIAL(CHOICE,VERSION,TMTOT,TMUPLOAD,TMNONDEC,PA,R,
     &  TMIN,TMAX)

C      Read integration parameters from the keyboard.

       CALL INTPAR(DKINITIAL,DKFINAL,DKINCR)

C      Open the output (plot) data file.

       CALL NEWFILE(NAME,BNAME)
```

```
C     Write header to the output (plot) data file.

      CALL HEADER(VERSION,PA,TMTOT,TMUPLOAD,TMNONDEC,R,TMIN,
     &  TMAX)

C     Calculate initial temperature for CDMSEPAR and TDRETPAR.

      DT=TMAX-TMIN

      T=TMIN+DT*DTPERC(0)

C     Initialize delta K for all calculations.

      IF(DKINITIAL.NE.0)THEN

      DK=DKINITIAL

      ELSE

C     If DKINITIAL=0. then calculations start at threshold.
C     DKSTAR is the threshold delta K.
C     Subroutine CDMSEPAR contains the MSE parameters for the
C     cycle-dependent CGR calculations, and also contains the
C     threshold delta K for the given material and condition.

      CALL CDMSEPAR(R,Q,D,DKSTAR,DKI,DADNI,DADNIP,
     &  DKCRIT,DKUPPER,T)

C     Calculations start at DKSTAR + 0.001 if threshold is
C     selected as the starting value.

      DK=DKSTAR+.001

      ENDIF

C     CDBETA is the cycle-dependent retardation parameter,
C     and TDBETA is the time-dependent retardation parameter.
C
C     In this version, CDBETA = TDBETA.
C
C     Define initial value of CDBETA and TDBETA where:
C     d(CDBETA)/dt = 0 and d(TDBETA)/dt = 0, and K/KMAX = R.

C     Since CDBETA = TDBETA, USE TDRETARPAR for both.

      CALL TDRETPAR(T,C1,TMUPLOAD,C2,BETA0)

      CDBETA=(C1+C2*BETA0)/(C1+C2)
      TDBETA=(C1+C2*BETA0)/(C1+C2)
```

```fortran
C     Write to screen that calculations begin.

      WRITE(*,31)
31    FORMAT(15(/),1X,60('*'),/,12X,' CRACK GROWTH RATE',
     &  ' CALCULATIONS BEGIN',/,1X,60('*'),4(/))

C     Write header to screen, if that option was selected.

      IF(CHECK.EQ.1)THEN

      WRITE(*,32)
32    FORMAT(2(/),5X,' DELTAK',5X,' DADNTOT',5X,' DADNCD',
     &  6X,' DADNTD',4X,' % BETA ERR',/,3X,62('*'))

C     Set BETAPREV to average beta value (in this version,
C     BETAPREV = CDBETA = TDBETA, also).

      BETAPREV=(CDBETA+TDBETA)/2

      ENDIF

100   CONTINUE

C     Calculate DADNCD, the cycle dependent CGR.

      DADNCD = CYCLEDEP(DK,R,TMIN,TMAX,TMTOT,TMUPLOAD,TMNONDEC)

      IF(BCHECK.EQ.1)THEN

      WRITE(3,1010)
1010  FORMAT(/,1X,'IN BETWEEN CALLS',/)

      ENDIF

C     Output statement.

      IF(DK.GE.(DKFINAL-DKINCR/10.).AND.BCHECK.EQ.2)THEN

      BCHECK=1

      ENDIF

C     Calculate DADNTD, the time-dependent CGR.

      DADNTD = TIMEDEP(DK,R,TMIN,TMAX,TMTOT,TMUPLOAD,TMNONDEC)

C     If 1 was selected for the data print options, then da/dN
C     and delta K information is written to the screen.

      IF(CHECK.EQ.1)THEN
```

241

```fortran
          BETA=(CDBETA+TDBETA)/2

C      BERROR is the percent error in the initial value of BETA
C      for this cycle and the initial value of BETA for the
C      previous cycle.

          BERROR=((BETA-BETAPREV)/BETA)*100

C      Write output to screen.

          WRITE(*,33)DK,(DADNCD+DADNTD),DADNCD,DADNTD,BERROR
33        FORMAT(5(1X,E12.5))

          BETAPREV=BETA

          ENDIF

C      If the cycle-dependent or time-dependent CGR terms
C      come from outside the experimental data range, a flag
C      value of 10 is returned and all calculations stop.

          IF(DADNCD.EQ.10..OR.DADNTD.EQ.10.)THEN

          WRITE(*,41)DK
41         FORMAT(' OUTSIDE EXPERIMENTAL DATA RANGE AT DELTA',
     &      ' K = ',F6.2,/,' STOP CALCULATIONS,'/)

          GOTO 200

          ENDIF

C      The total crack growth is the sum of the cycle-dependent
C      and time-dependent CGRs.

          DADNTOT = DADNCD+DADNTD

C      Write to the data file.

          WRITE(2,42)DK,DADNTOT,DADNCD,DADNTD
42         FORMAT(1X,E12.5,1x,E12.5,1X,E12.5,1X,E12.5)

C      Increment delta-K for next calculation.

          DK=DK+DKINCR

C      Check to see if DELTA-K has reached the maximum value input
C      by the operator.

          IF(DK.GT.(DKFINAL+DKINCR/10.))GOTO 200
```

```
C     Return with the next value of delta-K for CGR calculations.

      GOTO 100

C     Close data file and end program.

200   CONTINUE

      REWIND(UNIT=2)
      CLOSE(UNIT=2)

      WRITE(*,51)NAME
51    FORMAT(/,' YOUR TMF DATA HAS BEEN STORED IN ',A21)

      IF(BCHECK.EQ.1)THEN

      WRITE(3,52)
52    FORMAT(1X,43('*'))

      REWIND(UNIT=3)
      CLOSE(UNIT=3)

      WRITE(*,53)BNAME
53    FORMAT(/,' YOUR BETA INFORMATION HAS BEEN STORED IN ',A21)

      ENDIF

155   WRITE(*,55)
55    FORMAT(/,' DO YOU WANT TO ...',/,/,' 1 - CALCULATE'
     &  ' MORE VALUES OR',/,' 2 - QUIT',/,/,' 1 OR 2: ',$)
      READ(*,*)CHOICE

      IF(CHOICE.NE.1.AND.CHOICE.NE.2)GOTO 155
      IF(CHOICE.EQ.1)GOTO 101

      END

C     --------------------------------------------------
```

Part 2 Cycle-Dependent Functions and Subroutines

This section includes the function CYCLEDEP, the function CDDADT, and the subroutine CDMSEPAR. Function CYCLEDEP calculates the retarded cycle-dependent crack growth rate term for given values of stress intensity range, ΔK, (DK), test load ratio (R), and temperature (T). This retarded value is obtained by multiplying an unretarded value by a retardation parameter. (Further discussions of these calculations are presented in Chapter V.) The unretarded value is expressed in terms of the modified sigmoidal equation (MSE). This retarded cycle-dependent term is independent of temperature for Inconel 718 but not for Ti-24Al-11Nb. The MSE parameters were based on the following high frequency tests: 100 Hz, 315-649°C for Ti-24Al-11Nb, and 10 Hz, 427°C for Inconel 718. A flow chart for CYCLEDEP is shown in Figure A.2.

Function CDDADT calculates the instantaneous retarded cycle-dependent crack growth rate as a function of stress intensity range, (DK), load ratio (R), temperature (T), and loading time of the cycle (TMUPLOAD) using the modified sigmoidal equation model. A flow chart for CDDADT is shown in Figure A.3.

Subroutine CDMSEPAR determines the MSE parameters for a given material and load ratio, R. These parameters are determined from low-temperature, high-frequency fatigue tests and are used to establish the

cycle-dependent contribution to crack growth (damage). This subroutine is called from the main program to establish the threshold value of delta K, DKSTAR, and is also called by the cycle-dependent damage function, CYCLEDEP.
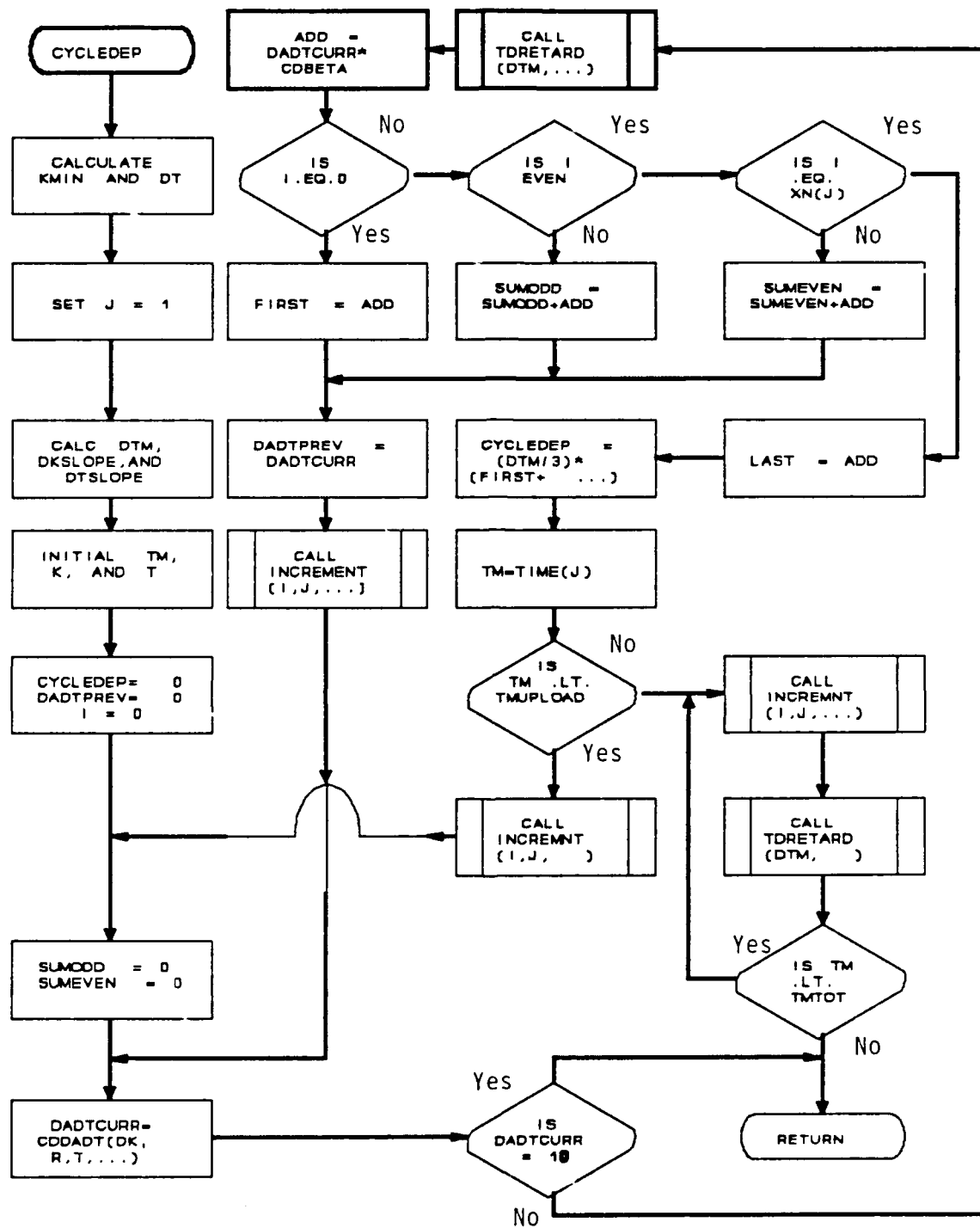
Figure A.2 Flow Chart for Function CYCLEDEP

246
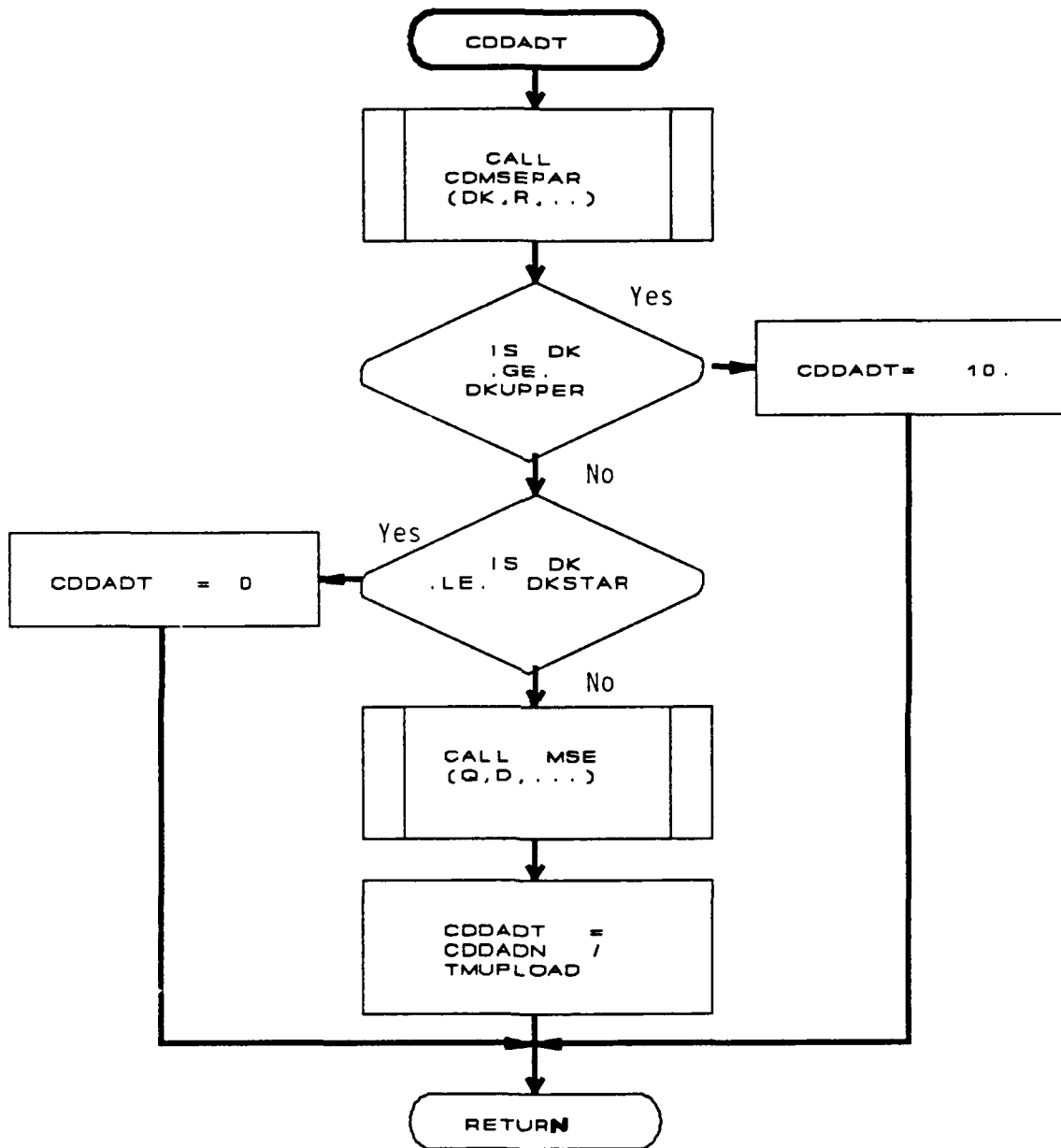
Figure A.3 Flow Chart for Function CDDADT

247

```
C       _____    _____

C       Function CYCLEDEP calculates the cycle-dependent CGR term
C       for a given delta K (DK) and test load ratio (R) using the
C       MSE model.  The cycle-dependent term is independent of
C       temperature for Inconel 718 but not for Ti-24Al-11Nb.
C       The MSE parameters were based on high frequency tests:
C       100 Hz, 315-649 degrees C for Ti-24Al-11Nb
C       10 Hz, 427 degrees C for the Inconel 718

        FUNCTION CYCLEDEP(DK,R,TMIN,TMAX,TMTOT,TMUPLOAD,TMNONDEC)
        REAL K,KMAX,KMIN,LAST
        INTEGER BCHECK
        COMMON/BLK6/TIME(10),DKPERC(10),DTPERC(10)
        COMMON/BLK7/XN(10),TMSTEP(10)
        COMMON/BLK8/DKSLOPE,DTSLOPE
        COMMON/BLK9/CDBETA
        COMMON/BLK11/BCHECK,CHECK

        IF(BCHECK.EQ.1)THEN

          WRITE(3,1051)DK
1051      FORMAT(1X,43('*'),2(/),1X,'DELTA K= ',E9.4,/)

          WRITE(3,1002)
1002      FORMAT(1X,'CYCLE DEPENDENT SUBROUTINE',/,5X,'TIME',5X,
        &      'J',6X,'I',4X,'K/KMAX',7X,'BETA')

        ENDIF

C       Define the constants for the entire cycle.

C       The minimum K of the cycle is KMIN, and the maximum K of the
C       cycle is KMAX.  The temperature range of the cycle, DT, is
C       the difference between TMAX and TMIN.

        KMAX=DK/(1.-R)
        KMIN=R*KMAX

        DT=TMAX-TMIN

C       Define the constants for the first division ( segment,
C       portion) of the cycle.

C       J is the cycle division counter.  J will vary from 1 to
C       NUMDIV, the total number of divisions in the TMF cycle.

        J=1
```

```
C     The time step size, DTM, is defined as the time of the
C     integration segment divided by the number of time step
C     increments over that segment.  The integrations are
C     typically stopped before the end of cycle is reached.

C     Note that DTM is not consistent with the use of DK or DT,
C     which both refer to ranges over the cycle.

C     Define DTM for the first portion (J=1) of the cycle.

      DTM=(TIME(1)-TIME(0))/XN(1)

C     Define the slopes of the DK vs. TM and the DT vs. TM
C     curves for the first segment of the cycle (J=1).

      DKSLOPE=DK*(DKPERC(1)-DKPERC(0))/(TIME(1)-TIME(0))
      DTSLOPE=DT*(DTPERC(1)-DTPERC(0))/(TIME(1)-TIME(0))

C     Initialize for the first segment of the cycle.

C     The initial time, stress intensity, and temperature are
C     determined.  These are set to their values at J=0, which
C     defines the first endpoint of the first cycle increment.
C     This endpoint must be defined at TM=0.

      TM=0.
      K=KMIN+DK*DKPERC(0)
      T=TMIN+DT*DTPERC(0)

C     CYCLEDEP is set equal to zero initially.  CYCLEDEP will be
C     calculated (and subsequently summed) for each division of
C     the cycle until TM reaches TMUPLOAD.

      CYCLEDEP=0.0

C     Set DADTPREV, da/dt for the previous (I-1) sample, equal
C     to zero.

      DADTPREV=0.0

C     I is the time step counter.  I is set equal to zero for the
C     first integration step of each portion of the cycle.  Here,
C     I is set equal to zero only for the first division of the
C     cycle.

C     I will vary from 0 to (TIME(J)-TIME(J-1)/DTM).

      I=0

800   CONTINUE
```

249

```
C    Initialize for the first calculation of each segment.

C    Set all odd and even (except first and last) components of
C    the Simpson's Rule summation to zero. This is required
C    since summations start at SUMODD+(1st odd value) and
C    SUMEVEN+(1st even value).

     SUMODD=0.
     SUMEVEN=0.

100  CONTINUE

     DADTCURR=CDDADT(DK,R,T,TMUPLOAD)

     IF(DADTCURR.EQ.10.)THEN

        CYCLEDEP=10.
        GOTO 500

     ENDIF

C    Use the same retardation model for cycle- and time-
C    dependent contributions of crack growth.

     CALL TDRETARD(DTM,TM,TMTOT,TMUPLOAD,TMNONDEC,T,CDBETA,K,KMAX)

     IF(BCHECK.EQ.1)THEN

        WRITE(3,1000)TM,J,I,K/KMAX,CDBETA
1000    FORMAT(1X,F9.4,2X,I3,2X,I5,4X,F6.4,4X,F10.8)

     ENDIF

     ADD=DADTCURR*CDBETA

C    Perform the Simpson's rule summations: FIRST for the
C    first term, LAST for the last term, SUMODD for the odd
C    numbered terms (except the first), and SUMEVEN for the
C    even numbered terms (except the last).

     IF(I.EQ.0)THEN
     FIRST=ADD
     GOTO 200
     ENDIF

     IF(MOD(I,2).EQ.0)THEN

C       Must end at TMUPLOAD
```

250

```fortran
      IF(I.GE.IFIX((TIME(J)-TIME(J-1))/DTM))THEN

          LAST=ADD
          GOTO 300

      ENDIF

      SUMEVEN=SUMEVEN+ADD
      GOTO 200

      ENDIF

      SUMODD=SUMODD+ADD

200   CONTINUE

      DADTPREV=DADTCURR

C     Increment the time step, the cycle division count (if
C     necessary), the time into cycle, the stress intensity
C     factor, and the temperature.

      CALL INCREMNT(I,J,TM,DTM,K,DK,KMIN,T,DT,TMIN)

C     Return with new values of I, J, TM, K, and T for next
C     calculation of Simpsons Rule integration components.

      GOTO 100

300   CONTINUE

C     Calculate the total cycle-dependent crack growth using
C     Simpson's rule.

      CYCLEDEP=(DTM/3.)*(FIRST+4.*SUMODD+2.*SUMEVEN+LAST)+CYCLEDEP


      IF(BCHECK.EQ.1)THEN

      WRITE(3,1020)
1020  FORMAT(1X,'END OF INTEGRATION SEGMENT')

      ENDIF


      TM=TIME(J)
```

```fortran
      IF(TM.LT.(TMUPLOAD-(DTM/10.)))THEN

        DTM=(TIME(J)-TIME(J-1))/XN(J)
        CALL INCREMNT(I,J,TM,DTM,K,DK,KMIN,T,DT,TMIN)
        GOTO 800

      ENDIF

      IF(BCHECK.EQ.1)THEN

        WRITE(3,1021)
1021    FORMAT(1X,'END OF INTEGRATION')

      ENDIF

400   CONTINUE

C     I,J,TM,K, and T are incremented for the rest of the
C     cycle. TDBETA is varied accordingly.

      CALL INCREMNT(I,J,TM,DTM,K,DK,KMIN,T,DT,TMIN)

      CALL TDRETARD(DTM,TM,TMTOT,TMUPLOAD,TMNONDEC,T,CDBETA,K,KMAX)

      IF(BCHECK.EQ.1)THEN

        WRITE(3,1000)TM,J,I,K/KMAX,CDBETA

      ENDIF

      IF(TM.LT.(TMTOT-(DTM/10.)))THEN

        GOTO 400

      ENDIF

500   CONTINUE

      RETURN
      END

C     ----------------------------------------------
```

```
C    ------------------------------------------------

C    Function CDDADT calculates the instantaneous cycle-
C    dependent crack growth rate as a function of stress
C    intensity range, (DK), load ratio (R), temperature (T),
C    and loading time of the cycle (TMUPLOAD) using the
C    modified sigmoidal equation model.

     FUNCTION CDDADT(DK,R,T,TMUPLOAD)

     CALL CDMSEPAR(R,Q,D,DKSTAR,DKI,DADNI,DADNIP,DKCRIT,
    &  DKUPPER,T)

C    If DK exceeds the experimental data range, set CDDADT equal
C    to a flag value of 10.

     IF(DK.GE.DKUPPER)THEN

       CDDADT=10.

C    If DK is less than the threshold value, there is no cycle-
C    dependent crack growth;  CDDADT = 0.

     ELSEIF(DK.LE.DKSTAR)THEN

       CDDADT=0.

C    If DK is greater than threshold and less than the upper
C    limit of the data range, then the cycle-dependent
C    contribution to crack growth rate is computed using the
C    modified sigmoidal equation.

     ELSE

       CALL MSE(Q,D,DKSTAR,DKI,DADNI,DADNIP,DKCRIT,DK,CDDADN)
       CDDADT=CDDADN/TMUPLOAD

     ENDIF

     RETURN
     END

C    ------------------------------------------------
```

```
C    ─────────────────────────────

C    Subroutine CDMSEPAR determines the MSE parameters for a
C    given material and load ratio, R.  These parameters are
C    determined from low-temperature, high-frequency fatigue
C    tests and are used to establish the cycle-dependent
C    contribution to crack growth (damage).  This subroutine is
C    called from the main program to establish the threshold
C    value of delta K, DKSTAR, and is also called by the cycle-
C    dependent damage function, CYCLEDEP.

     SUBROUTINE CDMSEPAR(R,Q,D,DKSTAR,DKI,DADNI,
   & DADNIP,DKCRIT,DKUPPER,T)
     COMMON/BLK1/NUMMATL

C    If NUMMATL = 1, then read the parameters for Inconel 718.

     IF(NUMMATL.EQ.1)THEN

       Q=0.4
       D=-Q
       DKSTAR=10.**(1.0866+1.0312*ALOG10(1.-R))
       DKI=10.**(1.6299+0.6068*ALOG10(1.-R))
       DADNI=10.**(-6.2244+0.7690*ALOG10(1.-R))
       DADNIP=3.5896+1.9587*ALOG10(1.-R)
       DKCRIT=(DKI**2)/DKSTAR
       DKUPPER=60.

C    If NUMMATL = 2, then read the parameters for Ti-24Al-11Nb.

     ELSE

       Q=.4
       D=-Q
       DKSTAR=4.0
       DKI=30.0
       DADNI=10.0**(-6.10+4.44E-4*(T-250))
       DADNIP=2.5
       DKCRIT=(DKI**2)/DKSTAR
       DKUPPER=65.

     ENDIF

     RETURN
     END

C    ─────────────────────────────
```

Part 3 Time-Dependent Functions and Subroutines

This section includes the function TIMEDEP, the function TDDADT, and the subroutine TDMSEPAR. Function TIMEDEP calculates the time-dependent CGR term for a given stress intensity ratio, ΔK (DK), test load ratio (R), minimum cycle temperature (TMIN), maximum cycle temperature (TMAX), phase angle between load and temperature (PA), test frequency (FREQ), and number of integration steps (XN). The function integrates the unretarded sustained-load crack growth rate (da/dt) over the loading portion of the thermal-mechanical fatigue cycle, while multiplying the unretarded values by the retardation coefficient. (See Chapter V for further information regarding these calculations.) A flow chart for TIMEDEP is shown in Figure A.4.

Function TDDADT calculates the instantaneous time-dependent crack growth rate as a function of stress intensity factor (K) and temperature (T) using the modified sigmoidal equation (MSE). A flow chart of TDDADT is shown in Figure A.5.

Subroutine TDMSEPAR determines the MSE parameters for a given material and temperature, T. These parameters are used for establishing the crack growth rates, DADT, which are integrated in the function, TIMEDEP, to establish the time-dependent contribution to the total crack growth rate. This subroutine is called from the function DADT.

255
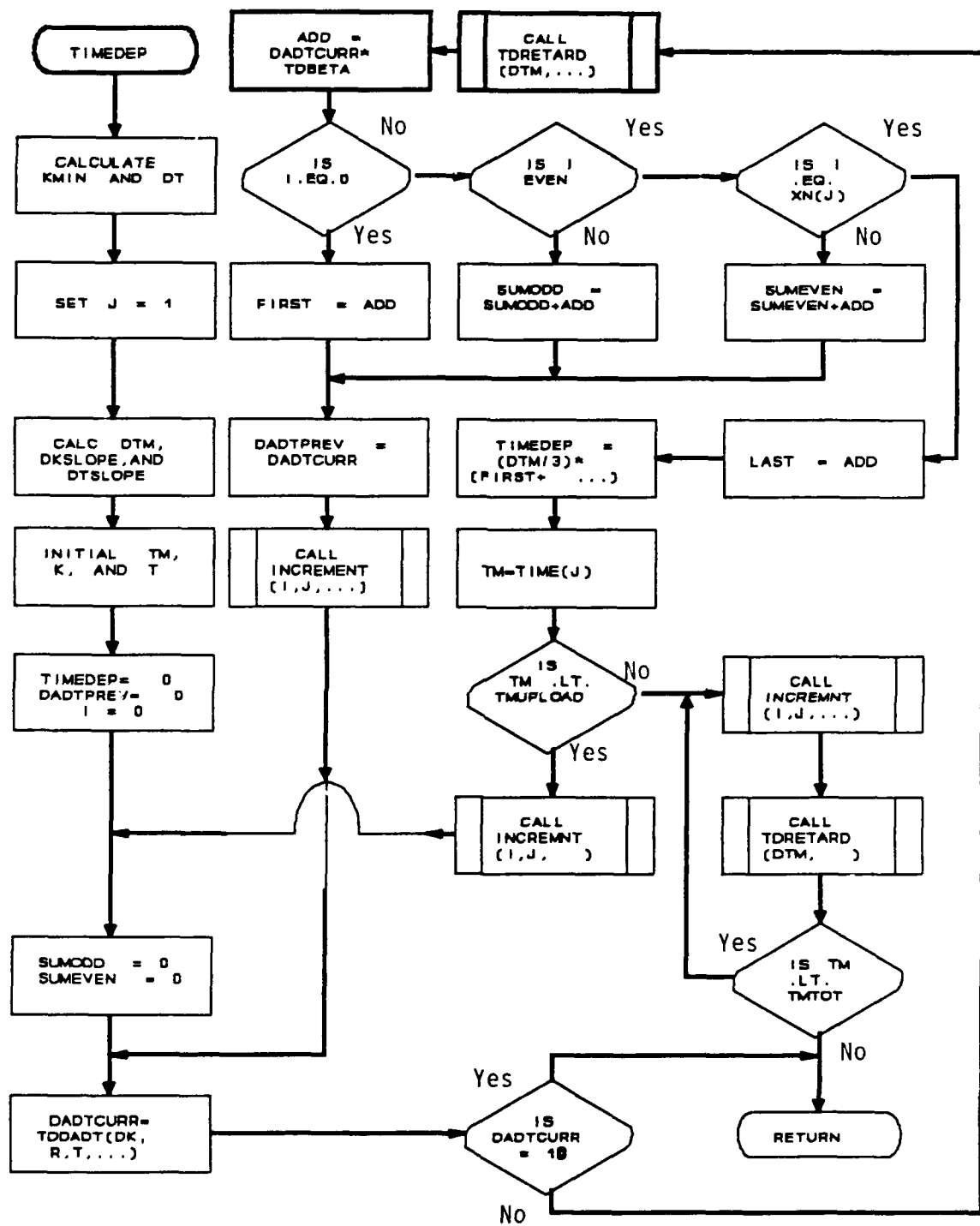
Figure A.4 Flow Chart for Function TIMEDEP

256
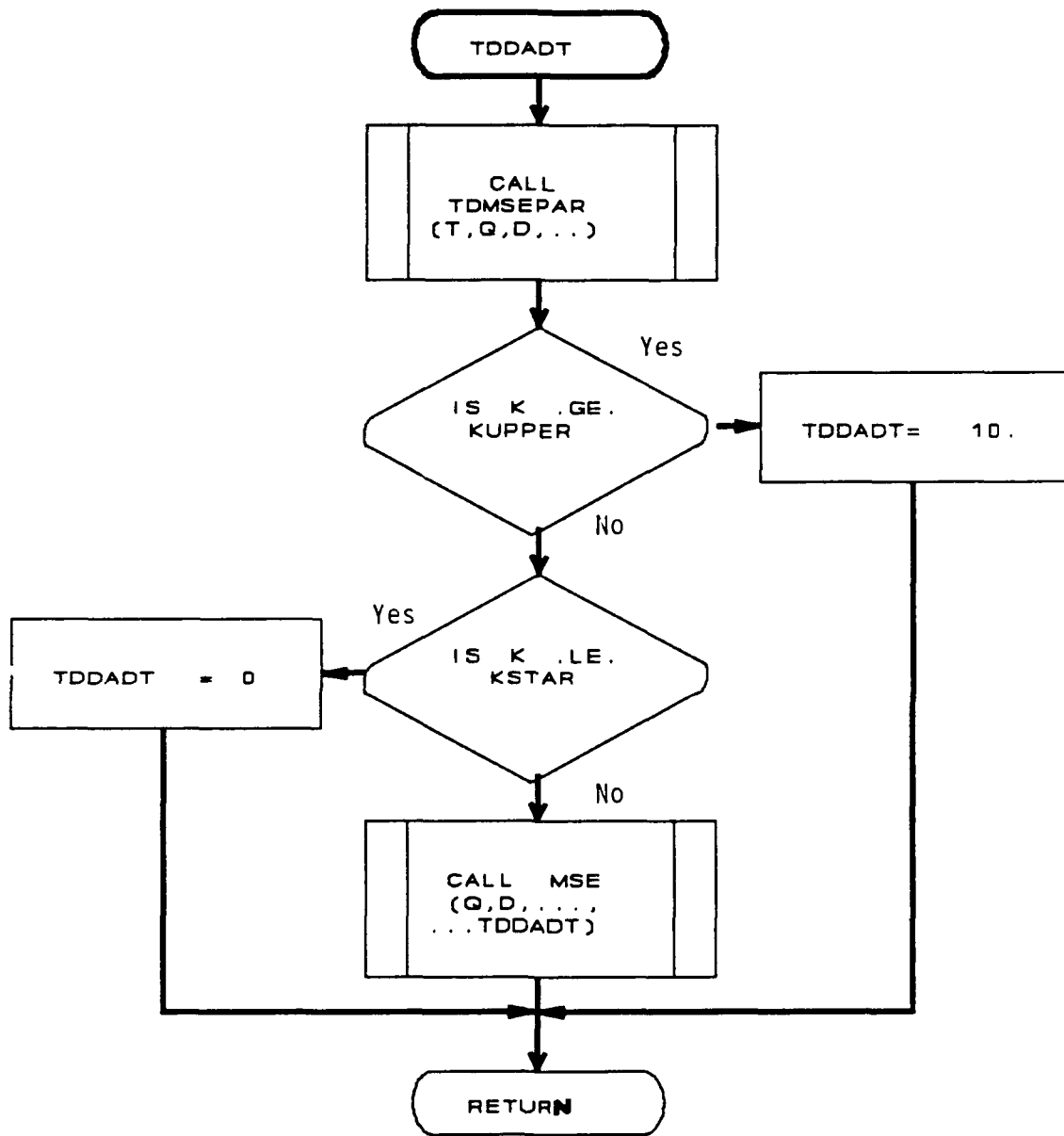
Figure A.5 Flow Chart for Function TDDADT

```
C      _____

C      Function TIMEDEP calculates the time-dependent CGR term
C      for a given delta-K (DK), test load ratio (R), minimum
C      cycle temperature (TMIN), maximum cycle temperature (TMAX),
C      phase angle between load and temperature (PA), test
C      frequency (FREQ), and number of integration steps (XN).
C      The function integrates the reference sustained-load crack
C      growth (da/dt) over the loading portion of the thermal-
C      mechanical fatigue cycle.

       FUNCTION TIMEDEP(DK,R,TMIN,TMAX,TMTOT,TMUPLOAD,TMNONDEC)
       REAL K,KMAX,KMIN,LAST
       INTEGER BCHECK
       COMMON/BLK6/TIME(10),DKPERC(10),DTPERC(10)
       COMMON/BLK7/XN(10),TMSTEP(10)
       COMMON/BLK8/DKSLOPE,DTSLOPE
       COMMON/BLK10/TDBETA
       COMMON/BLK11/BCHECK,CHECK

       IF(BCHECK.EQ.1)THEN

          WRITE(3,1002)
1002      FORMAT(1X,'TIME DEPENDENT SUBROUTINE',/,5X,'TIME',5X,
       &      'J',6X,'I',4X,'K/KMAX',7X,'BETA')

       ENDIF

C      Define the constants for the entire cycle.

C      The minimum K of the cycle is KMIN, and the maximum K of the
C      cycle is KMAX.  The temperature range of the cycle, DT, is
C      the difference between TMAX and TMIN.

       KMAX=DK/(1.-R)
       KMIN=R*KMAX

       DT=TMAX-TMIN

C      Define the constants for the first division ( segment,
C      portion) of the cycle.
C      J is the cycle division counter.  J will vary from 1 to
C      NUMDIV, the total number of divisions in the TMF cycle.

       J=1

C      The time step size, DTM, is defined as the time of the
C      integration segment divided by the number of time step
C      increments over that segment.  The integrations are
C      typically stopped before the end of cycle is reached.
```

258

```
C    Note that DTM is not consistent with the use of DK or DT,
C    which both refer to ranges over the cycle.

C    Define DTM for the first portion (J=1) of the cycle.

     DTM=(TIME(1)-TIME(0))/XN(1)

C    Define the slopes of the DK vs. TM and the DT vs. TM
C    curves for the first segment of the cycle (J=1).

     DKSLOPE=DK*(DKPERC(1)-DKPERC(0))/(TIME(1)-TIME(0))
     DTSLOPE=DT*(DTPERC(1)-DTPERC(0))/(TIME(1)-TIME(0))

C    Initialize for the first segment of the cycle.

C    The initial time, stress intensity, and temperature are
C    determined.  These are set to their values at J=0, which
C    defines the first endpoint of the first cycle increment.
C    This endpoint must be defined at TM=0.

     TM=0.
     K=KMIN+DK*DKPERC(0)
     T=TMIN+DT*DTPERC(0)

C    TIMEDEP is set equal to zero initially.  TIMEDEP will be
C    calculated (and subsequently summed) for each division of
C    the cycle until TM reaches TMNONDEC.

     TIMEDEP=0.0

C    Set DADTPREV, da/dt for the previous (I-1) sample, equal
C    to zero.

     DADTPREV=0.0

C    I is the time step counter.  I is set equal to zero for the
C    first integration step of each portion of the cycle.  Here,
C    I is set equal to zero only for the first division of the
C    cycle.

C    I will vary from 0 to (TIME(J)-TIME(J-1)/DTM).

     I=0

800  CONTINUE

C    Initialize for the first calculation of each segment.

C    Set all odd and even (except first and last) components of
C    the Simpson's Rule summation to zero.  This is required
```

```fortran
C     since summations start at SUMODD+(1st odd value) and
C     SUMEVEN+(1st even value).

      SUMODD=0.
      SUMEVEN=0.

100   CONTINUE

      DADTCURR=TDDADT(K,T)

      IF(DADTCURR.EQ.10.)THEN

        TIMEDEP=10
        GOTO 500

      ENDIF

      CALL TDRETARD(DTM,TM,TMTOT,TMUPLOAD,TMNONDEC,T,TDBETA,K,KMAX)

      IF(BCHECK.EQ.1)THEN

        WRITE(3,1000)TM,J,I,K/KMAX,TDBETA
1000    FORMAT(1X,F9.4,2X,I3,2X,I5,4X,F6.4,4X,F10.8)

      ENDIF

      ADD=DADTCURR*TDBETA

C     Perform the Simpson's rule summations: FIRST for the first
C     term, LAST for the last term, SUMODD for the odd numbered
C     terms (except the first), and SUMEVEN for the even numbered
C     terms (except the last).

      IF(I.EQ.0)THEN
      FIRST=ADD
      GOTO 200
      ENDIF

      IF(MOD(I,2).EQ.0)THEN

        IF(I.GE.(IFIX((TIME(J)-TIME(J-1))/DTM)))THEN

          IF(BCH_CK.EQ.1)THEN

          WRITE(3,1050)(IFIX((TIME(J)-TIME(J-1))/DTM))
1050      FORMAT(1X,' IFIX = ',I3)

          ENDIF
```

260

```fortran
          LAST=ADD
          GOTO 300

        ENDIF

        SUMEVEN=SUMEVEN+ADD
        GOTO 200
        ENDIF

        SUMODD=SUMODD+ADD

200     CONTINUE

        DADTPREV=DADTCURR

C       Increment the time step, the cycle division count (if
C       necessary), the time into cycle, the stress intensity
C       factor, and the temperature.

        CALL INCREMNT(I,J,TM,DTM,K,DK,KMIN,T,DT,TMIN)

C       Return with new values of I, J, TM, K, and T for next
C       calculation of Simpsons Rule integration components.

        GOTO 100

300     CONTINUE

C       Calculate the total time-dependent crack growth using
C       Simpson's rule.

        TIMEDEP=(DTM/3.)*(FIRST+4.*SUMODD+2.*SUMEVEN+LAST)+TIMEDEP

        IF(BCHECK.EQ.1)THEN

          WRITE(3,1010)
1010      FORMAT(1X,'END OF INTEGRATION SEGMENT')

        ENDIF

        TM=TIME(J)

        IF(TM.LT.(TMNONDEC-(DTM/10.)))THEN

          DTM=(TIME(J)-TIME(J-1))/XN(J)
```

```fortran
C     Increment for remainder of cycle.

      CALL INCREMNT(I,J,TM,DTM,K,DK,KMIN,T,DT,TMIN)
      GOTO 800

      ENDIF

      IF(BCHECK.EQ.1)THEN

      WRITE(3,1011)
1011    FORMAT(1X,'END OF INTEGRATION')

      ENDIF

400   CONTINUE

C     I,J,TM,K, and T are incremented for the rest of the cycle.
C     TDBETA is varied accordingly.

      CALL INCREMNT(I,J,TM,DTM,K,DK,KMIN,T,DT,TMIN)

      CALL TDRETARD(DTM,TM,TMTOT,TMUPLOAD,TMNONDEC,T,TDBETA,K,KMAX)

      IF(B' HECK.EQ.1)THEN

      WRITE(3,1000)TM,J,I,K/KMAX,TDBETA

      ENDIF

      IF(TM.LT.(TMTOT-(DTM/10.)))THEN

      GOTO 400

      ENDIF

500   CONTINUE

      IF(BCHECK.EQ.1)THEN

      WRITE(3,1111)
1111    FORMAT(/,' END OF CYCLE',2(/))

      ENDIF

      RETURN
      END

C     ------------------------------------------------
```

262

```fortran
C      ------------------------------------------------

C      Function TDDADT calculates the instantaneous time-
C      dependent crack growth rate as a function of stress
C      intensity factor (K) and temperature (T) using the
C      modified sigmoidal equation model.

       FUNCTION TDDADT(K,T)
       REAL K,KSTAR,KI,KCRIT,KUPPER

       CALL TDMSEPAR(T,Q,D,KSTAR,KI,DADTI,DADTIP,KCRIT,
     & KUPPER)

C      If K exceeds the experimental data range,
C      set TDDADT equal to a flag value of 10.

       IF(K.GE.KUPPER)THEN

          TDDADT=10.

C      If K is less than the threshold value, there is no
C      contribution to time-dependent crack growth; TDDADT = 0.

       ELSEIF(K.LE.KSTAR)THEN

          TDDADT=0.

C      If K is greater than threshold and less than the upper
C      limit of the data range, then the sustained-load crack
C      growth rate is computed using the modeified sigmoidal
C      equation.

       ELSE

          CALL MSE(Q,D,KSTAR,KI,DADTI,DADTIP,KCRIT,K,TDDADT)

       ENDIF

       RETURN
       END


C      ------------------------------------------------
```

```
C     ─────────────────────────────────

C     Subroutine TDMSEPAR determines the MSE parameters for a
C     given material and temperature, T.  These parameters are
C     used for establishing the crack growth rates, DADT, which
C     are integrated in the function, TIMEDEP, to establish the
C     time-dependent contribution to the total crack growth rate.
C     This subroutine is called from the function DADT.

      SUBROUTINE TDMSEPAR(T,Q,D,KSTAR,KI,DADTI,DADTIP,
     &  KCRIT,KUPPER)
      REAL KSTAR,KI,KCRIT,KUPPER
      COMMON/BLK1/NUMMATL

C     If NUMMATL = 1, then use the parameters for
C     Inconel 718.

      IF(NUMMATL.EQ.1)THEN

         Q=0.4
         D=-Q
         KSTAR=10.**(1.3802-9.1393E-4*(T-538.))
         KI=10.**(1.8808-9.2476E-4*(T-538.))
         DADTI=10.**(-7.1871+2.008E-2*(T-538.))
         DADTIP=1.2+1.622E-2*(T-538)
         KCRIT=(KI**2)/KSTAR
         KUPPER=KI

C     If NUMMATL = 2, then use the parameters for
C     Ti-24Al-11Nb.

      ELSE

         Q=0.4
         D=-Q
         KSTAR=4.0
         KI=50.
         DADTI=10*(10**(-5.5458+5.0E-3*(T-350)))
         DADTIP=2.3
         KCRIT=(KI**2)/KSTAR
         KUPPER=75.

      ENDIF

      RETURN
      END

C     ─────────────────────────────────
```

Part 4 <u>Retardation Subroutines</u>

This section includes the subroutine TDRETARD and the subroutine
TDRETPAR. Subroutine TDRETARD calculates the retardation to the crack
growth rate, DADT, caused by crack tip blunting. The cycle-dependent
retardation parameter is CDBETA, and the time-dependent retardation
parameter is TDBETA. Both use this subroutine to calculate the retardation
effects since CDBETA=TDBETA in this study. CDBETA=TDBETA=1.0 is the
condition of no retardation. CDBETA=TDBETA less than 1.0 is a retarded
condition of crack growth. Subroutine TDRETPAR determines the parameters
required by the subroutine TDRETARD to calculate CDBETA and TDBETA.

```
C     ———————————————————————

C     Subroutine TDRETARD calculates the retardation to the crack
C     growth rate, DADT, caused by crack tip blunting.  The time-
C     dependent retardation parameter is TDBETA.  TDBETA=1.0 is
C     the condition of no retardation. TDBETA less than 1.0 is a
C     retarded condition of crack growth.

      SUBROUTINE TDRETARD(DTM,TM,TMTOT,TMUPLOAD,TMNONDEC,T,TDBETA,
     & K,KMAX)

      REAL K,KMAX

      CALL TDRETPAR(T,C1,TMUPLOAD,C2,BETA0)

      IF(TM.LE.TMUPLOAD.OR.TM.GE.TMNONDEC)THEN

        DBETADTM=C1*(1-TDBETA)-C2*(K/KMAX)*(TDBETA-BETA0)

      ELSE

      DBETADTM=-C2*(K/KMAX)*(TDBETA-BETA0)

      ENDIF

      IF(ABS(DBETADTM*DTM).LE.1E-6)THEN

        DBETADTM=0.0

      ENDIF

      TDBETA=TDBETA+DBETADTM*DTM

      RETURN
      END

C     ———————————————————————————————
```

```fortran
C      ————————————————————————————

C      Subroutine TDRETPAR determines the parameters required
C      by the subroutine TDRETARD to calculate TDBETA.

       SUBROUTINE TDRETPAR(T,C1,TMUPLOAD,C2,BETA0)
       COMMON/BLK1/NUMMATL

       IF(NUMMATL.EQ.1)THEN

         C1=1.0
         C2=0.0
         BETA0=0.0

       ELSE

         C1=1.418E-3+((5.816E-2)*0.5/TMUPLOAD)
         C1=C1+(4.182E-4)*(0.5/TMUPLOAD)*(0.5/TMUPLOAD)

         C2=0.3344-(T*9.889E-4)+(T*T*8.463E-6)-(T*T*T*2.452E-8)
         C2=C2+(T*T*T*T*2.504E-11)

         BETA0=1.0E-5

       ENDIF

       RETURN
       END

C      ————————————————————————————
```

Part 5 Input, Output, and Other Subroutines

This section includes the subroutines: INITIAL, INTERACT, READDATA, PROFILE, INTPAR, NEWFILE, HEADER, INCREMNT, and MSE. Subroutine INITIAL initializes the program. The cycle parameters are read interactively from the keyboard using the subroutine INTERACT or from a file using the subroutine READDATA. READDATA sets the parameters for a test cycle, which is used primarily for debugging any new code. Subroutine PROFILE sets up the time-tempera' re-load profiles for all cycles. PROFILE is called from either subroutine INTERACT or subroutine READDATA. Subroutine INTPAR reads the integration parameters from the keyboard. Subroutine NEWFILE opens a plot data file, and the subroutine HEADER writes a header to that data file. Subroutine INCREMNT increments time, stress intensity, and temperature during the integrations. Subroutine MSE used the Modified Sigmoidal Equation to calculate the crack growth rate, DADN, given the intensity range, DK, and the MSE curve parameters. This subroutine can also be used to calculate DADT given the stress intensity level, K, and the appropriate MSE parameters.

```fortran
C      ──────────────────────────────────────

       SUBROUTINE INITIAL(CHOICE,VERSION,TMTOT,TMUPLOAD,TMNONDEC,
     & PA,R,TMIN,TMAX)

       CHARACTER*21 VERSION,TYPE,MATL
       INTEGER CHOICE
       COMMON/BLK1/NUMMATL
       COMMON/BLK2/MATL
       COMMON/BLK3/NUMTYPE
       COMMON/BLK4/TYPE
       COMMON/BLK5/NUMDIV
       COMMON/BLK6/TIME(10),DKPERC(10),DTPERC(10)

       IF(CHOICE.EQ.1)GOTO 104

       WRITE(*,1)VERSION
1      FORMAT(/,1X,60('*'),/,' PROGRAM TMFCG',22X,'VERSION ',
     & A21,/,1X,60('*'),/)

       WRITE(*,2)
2      FORMAT(/,' THIS PROGRAM CALCULATES CRACK GROWTH',
     & ' RATES UNDER THERMAL-',/,' MECHANICAL FATIGUE',
     & ' CONDITIONS USING A CUMULATIVE DAMAGE',/,' MODEL',
     & ' THAT CONSIDERS CRACK RETARDATION',3(/),
     & ' CURRENTLY THIS PROGRAM CAN CALCULATE GROWTH RATES',
     & ' ONLY FOR',/,' ALLOY 718 AND Ti-24Al-11Nb',10(/))

       PAUSE ' PRESS <RETURN> TO CONTINUE'

       WRITE(*,3)
3      FORMAT(15(/))

104    WRITE(*,4)
4      FORMAT(/,' DO YOU WANT TO ...',/,/,/,' 1 - READ'
     & ' PARAMETERS INTERACTIVELY OR',/,' 2 - READ'
     & ' THE TEST CYCLE PARAMETERS',/,/,' 1 OR 2: ',$)
       READ(*,*)CHOICE

C      If CHOICE = 1, read parameters interactively from the
C      keyboard.

       IF(CHOICE.EQ.1)THEN

          CALL INTERACT(TMTOT,TMUPLOAD,TMNONDEC,PA,R,TMIN,TMAX)

C      If CHOICE = 2, open the input data file and read
C      parameters from it.
```

```
        ELSEIF(CHOICE.EQ.2)THEN

            CALL READDATA(TMTOT,TMUPLOAD,TMNONDEC,PA,R,TMIN,TMAX)

C    If either 1 or 2 are not entered, return to read CHOICE
C    again.

        ELSE

            GOTO 104

        ENDIF

C    After parameters are obtained from either INTERACT or
C    READDATA, all parameters are written to the screen.

        WRITE(*,11)NUMMATL,MATL,NUMTYPE,TYPE
11      FORMAT(10(/),1X,60('*'),/,8X,' THERMAL-MECHANICAL',
     &  ' FATIGUE TEST PARAMETERS ',/,1X,60('*'),/,/,
     &  ' MATERIAL:  #',I2,' - ',A21,/,/,
     &  ' TEST TYPE:  #',I2,' - ',A21)

        IF(NUMTYPE.EQ.4)THEN

            WRITE(*,12)PA
12          FORMAT(4X,' PHASE ANGLE = ',F6.2)

        ENDIF

        WRITE(*,13)TMTOT,TMUPLOAD,TMNONDEC
13      FORMAT(/, ' TIME PARAMETERS:',/,4X,' TOTAL TIME OF',
     &  ' TMF CYCLE = ',F8.2,' SECONDS',/,4X,' TIME INTO',
     &  ' CYCLE WHEN THE',/,4X,' LOAD STOPS INCREASING  ',
     &  ' = ',F8.2,' SECONDS',/,4X,' TIME INTO',
     &  ' CYCLE WHEN THE',/,4X,' LOAD BEGINS TO DECREASE',
     &  ' = ',F8.2,' SECONDS')

        IF(NUMTYPE.EQ.2)THEN

            TMHOLD=TMTOT-2*(TMTOT-TMNONDEC)

            WRITE(*,14)TMHOLD
14          FORMAT(4X,' LENGTH OF HOLD AT P MAX = ',F8.2,
     &      ' SECONDS')

        ENDIF
```

```fortran
      WRITE(*,15)R,TMIN,TMAX
15    FORMAT(/' LOAD PARAMETER:',/,4X,' LOAD RATIO',
     &  ' = ',F4.2,2(/),' TEMPERATURE PARAMETERS:',/,4X,
     &  ' MINIMUM TEMPERATURE = ',F8.2,' DEGREES C',/,4X,
     &  ' MAXIMUM TEMPERATURE = ',F8.2,' DEGREES C',/)

      PAUSE ' PRESS <RETURN> TO CONTINUE'

      WRITE(*,21)NUMTYPE,TYPE
21    FORMAT(10(/),1X,60('*'),/,11X,' TIME-TEMPERATURE-',
     &  'LOAD PROFILE PARAMETERS',/,1X,60('*'),/,/,
     &  ' TEST TYPE:   #',I2,' - ',A21)

      IF(NUMTYPE.EQ.4)THEN

       WRITE(*,22)PA
22     FORMAT(4X,' PHASE ANGLE = ',F6.2)

      ENDIF

      WRITE(*,23)NUMDIV,(NUMDIV+1)
23    FORMAT(/,' THERE ARE',I2,' DIVISIONS OF THE TMF',
     &  ' CYCLE',/,' REQUIRING',I3,' DIVISION ENDPOINTS.',
     &  2(/),' THE DIVISION ENDPOINTS ARE: ')

      WRITE(*,24)
24    FORMAT(/,' END PT  TIME   LOAD FRACTION  TEMP',
     &  ' FRACTION',/,'  #    (SEC)   (DECIM FRACT)',
     &  '  (DECIM FRACT)')

      DO 125 J=0,NUMDIV
      WRITE(*,25)J, TIME(J),DKPERC(J),DTPERC(J)
25    FORMAT(3X,I1,3X,F8.2,7X,F5.3,11X,F5.3)
125   CONTINUE

      WRITE(*,26)
26    FORMAT(/)

      PAUSE ' PRESS <RETURN> TO CONTINUE'

      RETURN
      END

C    ------------------------------------------------
```

271

```
C    ────────────────────────────

C    Subroutine INTERACT reads all cycle parameters
C    interactively from the keyboard.

     SUBROUTINE INTERACT(TMTOT,TMUPLOAD,TMNONDEC,PA,R,
     & TMIN,TMAX)

     CHARACTER*21 TYPE,MATL
     COMMON/BLK1/NUMMATL
     COMMON/BLK2/MATL
     COMMON/BLK3/NUMTYPE
     COMMON/BLK4/TYPE

     WRITE(*,1)
1    FORMAT(13(/),1X,60("*"),/,13X,' INTERACTIVE INPUT'
     & ' OF CYCLE PARAMETERS',/,1X,60("*"),/)

102  WRITE(*,2)
2    FORMAT(/,/,' INDICATE THE MATERIAL BEING CONSIDERED',
     & 2(/),
     & ' 1 - INCONEL 718',/,' 2 - Ti-24Al-11Nb',2(/),
     & ' 1 OR 2: ',$)
     READ(*,*)NUMMATL

C    If NUMMATL does not correspond to a material, return to
C    read NUMMATL again

     IF(NUMMATL.NE.1.AND.NUMMATL.NE.2)GOTO 102

C    Set MATL equal to appropriate character constant.

     IF(NUMMATL.EQ.1)THEN

       MATL='INCONEL 718'

     ELSE

       MATL='Ti-24Al-11Nb'

     ENDIF

     WRITE(*,3)
3    FORMAT(/,' INDICATE THE TYPE OF TEST',/,/,' 1 - ISO'
     & 'THERMAL',/,' 2 - ISOTHERMAL WITH HOLD TIME IN LOAD'
     & ' CYCLE',/,' 3 - IN PHASE TMF',/,' 4 - OUT OF PHASE'
     & ' TMF',/,' 5 - UPPER TRIANGULAR PHASE TMF',/,' 6 -'
     & ' LOWER TRIANGULAR PHASE TMF',/,' 7 - USER DEFINED',
     & /,/,' 1-7: ',$)
     READ(*,*)NUMTYPE
```

272

```
C    If NUMTYPE is not equal to 1-6, then 7 is assumed.

C    Cycle time information is determined.

     WRITE(*,14)
14    FORMAT(/,' INPUT THE TOTAL CYCLE TIME',
   &  ' (IN SECONDS): ',$)
     READ(*,*)TMTOT

C    The rising portion of the loading cycle and the non-
C    decreasing load portion of the cycle are determined.

C    TMUPLOAD is the time from the initial increase in load
C    (at time = 0.) to the time when the load is no longer
C    increasing.  This value is required for the cycle-
C    dependent crack growth rate calculations.

C    TMNONDEC is the time from the initial increase of load
C    (at time = 0.) to the time when the load begins to
C    decrease.  This value is required for the time-dependent
C    crack growth rate calculations.

     IF(NUMTYPE.EQ.1)THEN

       TMUPLOAD=TMTOT/2

       TMNONDEC=TMUPLOAD

       TYPE='ISOTHERMAL'

     ELSEIF(NUMTYPE.EQ.2)THEN

       WRITE(*,15)
15      FORMAT(' INPUT THE HOLD TIME (IN SECONDS): ',$)
       READ(*,*)TMHOLD

C    The uploading portion of the hold time cycle is
C    (TMTOT-TMHOLD)/2, and the time until the load begins to
C    decrease is (TMTOT-TMHOLD)/2+TMHOLD

       TMUPLOAD=(TMTOT-TMHOLD)/2

       TMNONDEC=TMUPLOAD+TMHOLD

       TYPE='ISOTHERMAL W/ LOAD HT'

     ELSEIF(NUMTYPE.EQ.3.OR.NUMTYPE.EQ.4)THEN

       TMUPLOAD=TMTOT/2
```

273

```
        TMNONDEC=TMUPLOAD

        IF(NUMTYPE.EQ.3)THEN

          TYPE='IN PHASE TMF'

        ELSE

          TYPE='OUT OF PHASE TMF'

        ENDIF

      ELSEIF(NUMTYPE.EQ.5)THEN

        TMUPLOAD=TMTOT/3

        TMNONDEC=2*TMUPLOAD

        TYPE='UPPER TRIAN PHASE TMF'

      ELSEIF(NUMTYPE.EQ.6)THEN

        TMUPLOAD=TMTOT/3

        TMNONDEC=TMUPLOAD

        TYPE='LOWER TRIAN PHASE TMF'

      ELSE

        WRITE(*,17)
17      FORMAT(' INPUT THE TIME INTO THE CYCLE WHEN THE LOAD',
     &  ' IS NO LONGER INCREASING',/,' (IN SECONDS) : '$)
        READ(*,*)TMUPLOAD

        WRITE(*,18)
18      FORMAT(' INPUT THE TIME INTO THE CYCLE WHEN THE LOAD',
     &  ' BEGINS TO DECREASE',/,' (IN SECONDS) : '$)
        READ(*,*)TMNONDEC

        TYPE='USER DEFINED'

C    If NUMTYPE is not equal to 1-6, then 7 is assui..ed.

        NUMTYPE=7

      ENDIF

C    Load-temperature phase information is determined for the
C    basic TMF cycles.
```

274

```fortran
      IF(NUMTYPE.EQ.4)THEN

          WRITE(*,12)
12        FORMAT(/,' INPUT THE LOAD-TEMP PHASE ANGLE',
     &    ' (P LEADS T)',/,' (90, 180, OR 270): ',$)
          READ(*,*)PA

      ELSE

C     PA is set equal to zero for all other cases.

          PA=0

      ENDIF

C     Input the load information.

      WRITE(*,13)
13    FORMAT(/,' INPUT THE LOAD RATIO (R): ',$)
      READ(*,*)R

C     Input the temperature information.

      IF(NUMTYPE.EQ.1.OR.NUMTYPE.EQ.2)THEN

          WRITE(*,25)
25        FORMAT(/,' INPUT THE TEST TEMP: ',$)
          READ(*,*)TMIN

          TMAX=TMIN

      ELSE

          WRITE(*,26)
26        FORMAT(/,' INPUT THE MINIMUM TEMP: ',$)
          READ(*,*)TMIN

          WRITE(*,27)
27        FORMAT(' INPUT THE MAXIMUM TEMP: ',$)
          READ(*,*)TMAX

      ENDIF

C     Set up time-load-temperature profiles.

      CALL PROFILE(PA,TMTOT,TMHOLD)

      RETURN
      END
C     ——————————————————————————
```

```fortran
C     ------------------------------------------------

C     Subroutine READDATA sets the parameters for a test cycle
C     which is used to debug any new code.

      SUBROUTINE READDATA(TMTOT,TMUPLOAD,TMNONDEC,PA,R,TMIN,
     &  TMAX)

      CHARACTER*21 TYPE,MATL,INFILE
      COMMON/BLK1/NUMMATL
      COMMON/BLK2/MATL
      COMMON/BLK3/NUMTYPE
      COMMON/BLK4/TYPE
      COMMON/BLK5/NUMDIV
      COMMON/BLK6/TIME(10),DKPERC(10),DTPERC(10)

      WRITE(*,1)
1     FORMAT(10(/),1X,60('*'),/,13X,' INPUT OF TEST CYCLE'
     & ' PARAMETERS',/,1X,60('*'),/)

      NUMTYPE=4
      TYPE=' OUT OF PHASE TMF'
      NUMMATL=1
      MATL=' INCONEL 718'

      TMTOT=96.
      TMNONDEC=48.
      TMUPLOAD=48.
      TMHOLD=0.

      PA=270

      R=.1

      TMIN=427.
      TMAX=649.

      CALL PROFILE(PA,TMTOT,TMHOLD)

      RETURN
      END

C     ------------------------------------------------
```

276

```fortran
C     ----------------------------------

C     Subroutine PROFILE sets up the time-temperature-load
C     profiles for all TMF cycles.

      SUBROUTINE PROFILE(PA,TMTOT,TMHOLD)
      COMMON/BLK3/NUMTYPE
      COMMON/BLK5/NUMDIV
      COMMON/BLK6/TIME(10),DKPERC(10),DTPERC(10)

      IF(NUMTYPE.EQ.1)THEN

C     Isothermal cycle profile.

      NUMDIV=2

      TIME(0)=0.
      TIME(1)=TMTOT/2.
      TIME(2)=TMTOT

      DKPERC(0)=0.
      DKPERC(1)=1.
      DKPERC(2)=0.

      DTPERC(0)=1.
      DTPERC(1)=1.
      DTPERC(2)=1.

      ELSEIF(NUMTYPE.EQ.2)THEN

C     Isothermal with load hold-time cycle profile.

      NUMDIV=3

      TIME(0)=0.
      TIME(1)=(TMTOT-TMHOLD)/2.
      TIME(2)=TIME(1)+TMHOLD
      TIME(3)=TMTOT

      DKPERC(0)=0.
      DKPERC(1)=1.
      DKPERC(2)=1.
      DKPERC(3)=0.

      DTPERC(0)=1.
      DTPERC(1)=1.
      DTPERC(2)=1.
      DTPERC(3)=1.

      ELSEIF((NUMTYPE.EQ.3).OR.(NUMTYPE.EQ.4.AND.PA.EQ.0.))THEN
```

277

```
C     In-phase TMF cycle profile.

      NUMDIV=2

      TIME(0)=0.
      TIME(1)=TMTOT/2.
      TIME(2)=TMTOT

      DKPERC(0)=0.
      DKPERC(1)=1.
      DKPERC(2)=0.

      DTPERC(0)=0.
      DTPERC(1)=1.
      DTPERC(2)=0.

      ELSEIF(NUMTYPE.EQ.4.AND.PA.NE.0.)THEN

C     Out-of phase TMF cycle profiles.

      IF(PA.EQ.180.)THEN

C     180 degrees out-of-phase cycle profile.

      NUMDIV=2

      TIME(0)=0.
      TIME(1)=TMTOT/2.
      TIME(2)=TMTOT

      DKPERC(0)=0.
      DKPERC(1)=1.
      DKPERC(2)=0.

      DTPERC(0)=1.
      DTPERC(1)=0.
      DTPERC(2)=1.

      ELSEIF(PA.EQ.90..OR.PA.EQ.270.)THEN

C     90 and 270 degree TMF phases have the same time-load
C     profiles.

      NUMDIV=4

      TIME(0)=0.
      TIME(1)=TMTOT/4
      TIME(2)=TMTOT/2
      TIME(3)=3*TMTOT/4
      TIME(4)=TMTOT
```

278

```fortran
      DKPERC(0)=0.
      DKPERC(1)=.5
      DKPERC(2)=1.
      DKPERC(3)=.5
      DKPERC(4)=0.

      IF(PA.EQ.90.)THEN

C     90 degree TMF phase temperature profile.

      DTPERC(0)=.5
      DTPERC(1)=0.
      DTPERC(2)=.5
      DTPERC(3)=1.
      DTPERC(4)=.5

      ELSE

C     270 degree TMF phase temperature profile.

      DTPERC(0)=.5
      DTPERC(1)=1.
      DTPERC(2)=.5
      DTPERC(3)=0.
      DTPERC(4)=.5

      ENDIF

      ELSE

C     45, 135, 225, and 315 degree TMF cycles could fit
C     here if it is necessary to program them.  45 and 225
C     degree TMF cycles have identical load profiles, and
C     135 and 315 degree TMF cycles have identical load
C     profiles.

      ENDIF

      ELSEIF(NUMTYPE.EQ.5.OR.NUMTYPE.EQ.6)THEN

C     Upper triangular phase (UTP) and lower triangular phase
C     (LTP) TMF cycles have identical time profiles.

      NUMDIV=3

      TIME(0)=0.
      TIME(1)=TMTOT/3
      TIME(2)=2*TIME(1)
      TIME(3)=TMTOT
```

279

```
C    The load and temperature profiles differ only in
C    DKPERC(2) and DTPERC(2).

C    UTP load and temperature profiles.

     DKPERC(0)=0.
     DKPERC(1)=1.
     DKPERC(2)=1.
     DKPERC(3)=0.

     DTPERC(0)=0.
     DTPERC(1)=1.
     DTPERC(2)=0.
     DTPERC(3)=0.

C    If NUMTYPE identifies the LTP, then DKPERC(2) and
C    DTPERC(2) are reversed.

     IF(NUMTYPE.EQ.6)THEN

C    LTP TMF cycle load and temperature profile changes.

     DKPERC(2)=0.
     DTPERC(2)=1.

     ENDIF

     ELSE


C    Read time-load-temperature profile from the keyboard
C    for the user defined TMF cycle.

     WRITE(*,1)
1       FORMAT(10(/),1X,60('*'),/,10X,' THE USER DEFINED',
     &    ' TMF CYCLE WAS SELECTED',/,1X,60('*'),3(/),' THIS'
     &    ' SELECTION REQUIRES THE TIME-LOAD-TEMPERATURE'
     &    ' PROFILE',/,' INFORMATION TO BE INPUT FROM THE',
     &    ' KEYBOARD.',2(/),' NOTE:',//,' 1. TIME MUST BEGIN'
     &    ' AT 0. AND END AT TMTOT (DEFINED PREVIOUSLY)',/,
     &    ' 2. THE LOAD CYCLE MUST BEGIN ON A NON-DECREASING',
     &    ' SLOPE',/,' 3. THE INITIAL AND FINAL LOAD AND',
     &    ' TEMPERATURE FRACTIONS MUST',/,3X,' BE IDENTICAL',
     &    ' TO CLOSE THE CYCLE LOOPS.')
```

```
        WRITE(*,2)
2       FORMAT(/,' INDICATE THE NUMBER OF DIVISIONS',
     &    ' (NUMDIV) IN THE',
     &    ' TMF CYCLE',2(/),' NOTE:',/,' EACH CHANGE IN SLOPE',
     &    ' OF THE LOAD OR TEMPERATURE VS. TIME',/,' CURVES',
     &    ' REQUIRES A NEW DIVISION',2(/),
     &    ' NUMDIV CANNOT EXCEED 9',/,' NUMDIV: ',$)
        READ(*,*)NUMDIV

        WRITE(*,3)NUMDIV,(NUMDIV+1),NUMDIV
3       FORMAT(/,' THERE ARE',I2,' DIVISIONS IN THE TMF',
     &    ' CYCLE',/,' REQUIRING',I3,' DIVISION ENDPOINTS.',
     &    /,' THESE ENDPOINTS NUMBER FROM 0 TO',I2,'.',/)

        WRITE(*,4)
4       FORMAT(/,' DEFINE THE DIVISION ENDPOINTS BY',/,
     &    ' TIME (SECONDS), LOAD FRACTION, TEMPERATURE'
     &    ' FRACTION',/,
     &    ' THE FRACTIONS VARY FROM 0. TO 1. TO INDICATE',
     &    ' THE VARIATION',/,' BETWEEN MINIMUM AND MAXIMUM'
     &    ' , RESPECTIVELY.',/)

        WRITE(*,5)
5       FORMAT(/,' DEFINE THE ENDPOINTS FOR THE TMF CYCLE',
     &    ' DIVISIONS',/,' SEPARATE VALUES WITH COMMAS',/,
     &    ' ENDPT: TIME,  LOAD FRACTION,  TEMP FRACTION',
     &    /,' #    (SECS) (DECIMAL EQUIV) (DECIMAL EQUIV)',
     &    /,50('*'))

        DO 100 J=0,NUMDIV

        WRITE(*,6)J
6       FORMAT(1X,I2,':',$)
        READ(*,*)TIME(J),DKPERC(J),DTPERC(J)

100     CONTINUE

        ENDIF

        RETURN
        END
C       ------------------------------------------------
```

```fortran
C     ------------------------------------------------

C     Subroutine INTPAR reads the integration parameters from
C     the keyboard.

      SUBROUTINE INTPAR(DKINITIAL,DKFINAL,DKINCR)
      INTEGER CHOICE
      COMMON/BLK3/NUMTYPE
      COMMON/BLK5/NUMDIV
      COMMON/BLK6/TIME(10),DKPERC(10),DTPERC(10)
      COMMON/BLK7/XN(10),TMSTEP(10)

      WRITE(*,1)
1     FORMAT(10(/),1X,60('*'),/,8X,' INTERACTIVE INPUT OF',
     & ' INTEGRATION PARAMETERS',/,1X,60('*'),2(/))

100   IF(NUMTYPE.NE.2.AND.NUMTYPE.NE.7)THEN

      WRITE(*,2)NUMDIV
2     FORMAT(' THERE ARE ',I2,' DIVISIONS IN THE TMF CYCLE',
     &   2(/),' INPUT THE NUMBER OF INTEGRATION STEPS OVER EACH',
     &   /,' DIVISION OF THE TMF CYCLE',//,' NOTE:',
     &   ' THE NUMBER MUST BE EVEN',//,' NUMBER OF STEPS: '$)
      READ(*,*)IXN

      DO 200 I=1,NUMDIV

      XN(I)=IXN

200   CONTINUE

      ELSEIF(NUMTYPE.EQ.2)THEN

      WRITE(*,3)
3     FORMAT(' INPUT THE NUMBER OF INTEGRATION STEPS OVER THE',
     &   /,' UPLOADING AND DOWNLOADING PORTIONS OF THE TMF CYCLE',
     &   //,' NOTE:',
     &   ' THE NUMBER MUST BE EVEN',//,' NUMBER OF STEPS: '$)
      READ(*,*)XN(1)

      XN(3)=XN(1)

      WRITE(*,4)
4     FORMAT(' INPUT THE NUMBER OF INTEGRATION STEPS OVER THE',
     &   /,' HOLD TIME PORTION OF THE TMF CYCLE',//,' NOTE:',
     &   ' THE NUMBER MUST BE EVEN',//,' NUMBER OF STEPS: '$)
      READ(*,*)XN(2)

      ELSE
```

282

```fortran
            WRITE(*,5)NUMDIV
5           FORMAT(' THERE ARE ',I2,' DIVISIONS IN THE TMF CYCLE',
      &     2(/),' INPUT THE NUMBER OF INTEGRATION STEPS OVER EACH',
      &     /,' DIVISION OF THE TMF CYCLE',//,' NOTE:',
      &     ' EACH NUMBER MUST BE EVEN',/,/,
      &     ' DIVISION # : NUMBER OF INTEGRATION STEPS',
      &     /,40('*'))

            DO 600 J=1,NUMDIV

            WRITE(*,6)J
6           FORMAT(1X,I6,':',$)
            READ(*,*)XN(J)

600     CONTINUE

        ENDIF

            DO 700 J=1,NUMDIV

            TMSTEP(J)=(TIME(J)-TIME(J-1))/XN(J)

700     CONTINUE

108     WRITE(*,8)
8       FORMAT(/,' THE NUMBER OF INTEGRATION STEPS AND TIME STEP'
      &     ' SIZE',//,' FOR EACH DIVISION OF THE TMF CYCLE ARE: ',/,/,
      &     ' DIV',3X,' INT STEPS',3X,' STEP SIZE ',/,30('*'))

            DO 900 J=1,NUMDIV

            WRITE(*,9)J,IFIX(XN(J)),TMSTEP(J)
9           FORMAT(1X,I2,6X,I6,5X,F9.5)

900     CONTINUE

        WRITE(*,10)
10      FORMAT(/,' DO YOU WANT TO:',/,/,' 1 - CONTINUE WITH',
      &     ' THESE PARAMETERS',/,' 2 - CHANGE THEM',/,/,
      &     ' 1 OR 2: ',$)
        READ(*,*) CHOICE

        IF(CHOICE.NE.1.AND.CHOICE.NE.2)GOTO 108

        IF(CHOICE.EQ.2)GOTO 100
```

```fortran
111     WRITE(*,11)
11      FORMAT(/,/,' INPUT THE VALUE OF DELTA-K WHERE THE'
      & ' CRACK GROWTH RATE',/,' CALCULATIONS WILL BEGIN ',/,
      & ' (DELTA-K = 0. DEFINES THRESHOLD): ',$)
        READ(*,*)DKINITIAL

        WRITE(*,12)
12      FORMAT(/,' INPUT THE VALUE OF DELTA-K WHERE THE'
      & ' CRACK GROWTH RATE',/,' CALCULATIONS WILL END: ',$)
        READ(*,*)DKFINAL

        WRITE(*,13)
13      FORMAT(/,' INPUT THE INCREMENT OF DELTA-K BETWEEN'
      & ' CRACK GROWTH RATE',/,' CALCULATIONS: ',$)
        READ(*,*)DKINCR

114     WRITE(*,14)DKINITIAL,DKFINAL,DKINCR
14      FORMAT(/,' CRACK GROWTH RATE CALCULATIONS WILL:',/,
      & ' BEGIN AT DELTA-K = ',F7.3,/,' END AT DELTA-K  = ',
      & F7.3,/,' WITH INCREMENT  = ',F7.3)

        WRITE(*,15)
15      FORMAT(/,' DO YOU WANT TO:',/,/,' 1 - CONTINUE WITH',
      & ' THESE PARAMETERS',/,' 2 - CHANGE THEM',/,/,
      & ' 1 OR 2: ',$)
        READ(*,*) CHOICE

        IF(CHOICE.NE.1.AND.CHOICE.NE.2)GOTO 114

        IF(CHOICE.EQ.2)GOTO 111

        RETURN
        END

C       ------------------------------------------------
```

```
C     ---------------------------------------------------

C     Subroutine NEWFILE opens a plot data file.

      SUBROUTINE NEWFILE(NAME,BNAME)
      CHARACTER*21 NAME,BNAME
      INTEGER CHOICE,BCHECK,CHECK
      COMMON/BLK11/BCHECK,CHECK

      WRITE(*,1)
1     FORMAT(14(/),1X,60('*'),/,5X,' INTERACTIVE INPUT OF',
     & ' DATA    _OT FILE INFORMATION',/,1X,60('*'),2(/))

102   WRITE(*,2)
2     FORMAT(4(/),' DO YOU WANT RESULTS WRITTEN:',2(/),' 1 - TO',
     & ' SCREEN AND DISK',/,' 2 - ONLY TO DISK',2(/),
     & ' 1 OR 2: ',$)
      READ(*,*)CHECK

      WRITE(*,4)
4     FORMAT(2(/),' WHAT IS THE NAME OF THE OUTPUT DATA FILE?',
     & 2(/),' 21 CHARACTER STRING, MAXIMUM',2(/),' NAME: ',$)

      READ(*,5)NAME
5     FORMAT(A21)

      WRITE(*,6)
6     FORMAT(3(/),' DO YOU WANT TO... ',2(/),' 1 - CREATE A'
     & ' FILE OF BETA INFORMATION OF ALL CYCLES',/,' 2 - CREATE',
     & ' A FILE OF BETA INFORMATION OF ONLY LAST CYCLE',/,' 3 -',
     & ' NOT CREATE A BETA FILE',
     & /,/,' 1, 2, OR 3: ',$)
      READ(*,*)BCHECK

      IF (BCHECK.EQ.1.OR.BCHECK.EQ.2)THEN

      WRITE(*,7)
7     FORMAT(2(/),' WHAT IS THE NAME OF THE OUTPUT BETA FILE?',
     &    2(/),' 21 CHARACTER STRING, MAXIMUM',2(/),' NAME: ',$)

      READ(*,8)BNAME
8     FORMAT(A21)

      ENDIF

109   WRITE(*,9)
9     FORMAT(13(/))

      IF (CHECK.EQ.1.OR.CHECK.EQ.2)THEN
```

285

```fortran
      WRITE(*,10)NAME
10    FORMAT(2(/),' THE NAME OF THE OUTPUT DATA FILE IS: ',A21)

      ENDIF

      IF (BCHECK.EQ.1.OR.BCHECK.EQ.2)THEN

      WRITE(*,11)BNAME
11    FORMAT(2(/),' THE NAME OF THE OUTPUT BETA FILE IS: ',A21)

      ELSE

      WRITE(*,12)
12    FORMAT(2(/),' AN OUTPUT BETA FILE WILL NOT BE CREATED')

      ENDIF

      WRITE(*,13)
13     FORMAT(2(/),' DO YOU WANT TO:',/,/,' 1 - CONTINUE WITH',
     & ' THE FILE NAME(S) AND (OR) CHOICES',/,' 2 - CHANGE THE',
     & ' FILE NAME(S) AND (OR) CHOICES',/,/,
     & ' 1 OR 2: ',$)
      READ(*,*) CHOICE

      IF(CHOICE.NE.1.AND.CHOICE.NE.2)GOTO 109

      IF(CHOICE.EQ.2)GOTO 102

      IF (CHECK.EQ.1.OR.CHECK.EQ.2)THEN

       OPEN(UNIT=2,FILE=NAME,STATUS='UNKNOWN')

      ENDIF

      IF (BCHECK.EQ.1.OR.BCHECK.EQ.2)THEN

       OPEN(UNIT=3,FILE=BNAME,STATUS='UNKNOWN')

      ENDIF

      RETURN
      END

C     ----------------------------------------------
```

```fortran
C      ----------------------------------------

C      Subroutine HEADER writes a header to the data file.

       SUBROUTINE HEADER(VERSION,PA,TMTOT,TMUPLOAD,
     & TMNONDEC,R,TMIN,TMAX)

       CHARACTER*21 VERSION,TYPE,MATL
       COMMON/BLK1/NUMMATL
       COMMON/BLK2/MATL
       COMMON/BLK3/NUMTYPE
       COMMON/BLK4/TYPE
       COMMON/BLK5/NUMDIV
       COMMON/BLK7/XN(10),TMSTEP(10)

       WRITE(2,1)VERSION
1      FORMAT(1X,'DATA FILE FROM TMFCG VERSION ',A21,/)

       CALL GETDAT(IYR,IMON,IDAY)

       CALL GETTIM(IHR,IMIN,ISEC,I100TH)

       WRITE(2,3)IMON,IDAY,IYR,IHR,IMIN,ISEC
3      FORMAT(1X,'DATE: ',2(I2.2,'/'),I4,14X,'TIME: ',
     & 2(I2.2,':'),I2.2)

       WRITE(2,4)NUMMATL,MATL,NUMTYPE,TYPE
4      FORMAT(/,' THERMAL-MECHANICAL',
     & ' FATIGUE TEST PARAMETERS ',/,/,
     & 3X,' MATERIAL: #',I2,' - ',A21,/,
     & 3X,' TEST TYPE:  #',I2,' - ',A21)

       IF(NUMTYPE.EQ.4)THEN

       WRITE(2,5)PA
5      FORMAT(6X,' PHASE ANGLE = ',F6.2)

       ENDIF

       WRITE(2,6)TMTOT,TMUPLOAD,TMNONDEC
6      FORMAT(/,3X,
     & ' TIME PARAMETERS:',/,6X,' TOTAL TIME OF TMF CYCLE',
     & ' = ',F8.2,' SECONDS',/,6X,' TIME INTO CYCLE WHEN',
     & ' THE',/,6X,' LOAD STOPS INCREASING',2X,' = ',
     & F8.2,' SECONDS',/,6X,' TIME INTO CYCLE WHEN THE',/,
     & 6X,' LOAD BEGINS TO DECREASE = ',F8.2,' SECONDS')

       IF(NUMTYPE.EQ.2)THEN

       TMHOLD=TMTOT-2*(TMTOT-TMNONDEC)
```

287

```
      WRITE(2,7)TMHOLD
7      FORMAT(6X,' LENGTH OF HOLD AT P MAX = ',F8.2,
   &   ' SECONDS')

      ENDIF

      WRITE(2,8)R,TMIN,TMAX
8      FORMAT(/,3X,' LOAD PARAMETER:',/,6X,' LOAD RATIO',
   &   ' = ',F4.2,2(/),3X,' TEMPERATURE PARAMETERS:',/,6X,
   &   ' MINIMUM TEMPERATURE = ',F8.2,' DEGREES C',/,6X,
   &   ' MAXIMUM TEMPERATURE = ',F8.2,' DEGREES C')

      WRITE(2,9)
9      FORMAT(/,' THE NUMBER OF INTEGRATION STEPS AND TIME STEP'
   &   ' SIZE',/,' FOR EACH DIVISION OF THE TMF CYCLE ARE: ',2(/),
   &   2X,' DIV',3X,' INT STEPS',3X,' STEP SIZE (SEC)',/,
   &   3X,35('*'))

      DO 1000 J=1,NUMDIV

      WRITE(2,10)J,IFIX(XN(J)),TMSTEP(J)
10      FORMAT(3X,I2,6X,I6,6X,F9.5)

1000   CONTINUE

      WRITE(2,11)
11      FORMAT(2(/),4X,'DELTA-K',6X,'DADNTOT',7X,'DADNCD',7X,
   &   'DADNTD',/,3X,49('*'))

      RETURN
      END

C      ------------------------------------------------
```

```fortran
C      _____

       SUBROUTINE INCREMNT(I,J,TM,DTM,K,DK,KMIN,T,DT,TMIN)
       REAL K,KMIN
       COMMON/BLK6/TIME(10),DKPERC(10),DTPERC(10)
       COMMON/BLK7/XN(10),TMSTEP(10)
       COMMON/BLK8/DKSLOPE,DTSLOPE

C      Only increment the cycle divison count if the current
C      time into the cycle exceeds the maximum time of the
C      J'th cycle divison.

       IF((TM+DTM).GT.(TIME(J)+(DTM/10.)))THEN

          TM=TIME(J)

          J=J+1

          DKSLOPE=DK*(DKPERC(J)-DKPERC(J-1))/(TIME(J)-TIME(J-1))
          DTSLOPE=DT*(DTPERC(J)-DTPERC(J-1))/(TIME(J)-TIME(J-1))

          DTM=(TIME(J)-TIME(J-1))/XN(J)

          I=0

          RETURN

       ENDIF

C      Increment the time step count, and time into cycle.

       I=I+1

       TM=TIME(J-1)+DTM*I

C      Calculate K and T for the next time step.

       K=KMIN+DK*DKPERC(J-1)+(TM-TIME(J-1))*DKSLOPE
       T=TMIN+DT*DTPERC(J-1)+(TM-TIME(J-1))*DTSLOPE

       RETURN
       END

C      _____
```

289

```fortran
C     ------------------------------------------------

C     Subroutine MSE used the Modified Sigmoidal Equation
C     to calculate the crack growth rate, DADN, given the
C     intensity range, DK, and the MSE curve parameters.
C     This subroutine can also be used to calculate DADT
C     given the stress intensity level, K, and the
C     appropriate MSE parameters.

      SUBROUTINE MSE(Q,D,DKSTAR,DKI,DADNI,DADNIP,DKCRIT,
     & DK,DADN)

      CONST=ALOG(DKI/DKSTAR)
      CONST1=ALOG(DKCRIT/DKI)
      B=ALOG(DADNI)-Q*ALOG(CONST)-D*ALOG(CONST1)
      P=DADNIP-Q/CONST+D/CONST1

      DADN=EXP(B)*((DK/DKI)**P)*((ALOG(DK/DKSTAR))**Q)
     & *((ALOG(DKCRIT/DK))**D)

      RETURN
      END

C     ------------------------------------------------
```

References

1. Halford, G.R., "Low Cycle Thermal Fatigue", NASA Technical Memorandum 87225, 1986.

2. Wright, P.K., Jang, H., and Popp, H.G., "Fatigue and Fracture of Advanced Blade Materials", AFWAL-TR-84-4166, Wright-Patterson AFB OH, 1985.

3. Russel, E.S., "Practical Life Prediction Methods for TMF of Gas Turbine Buckets", Conference on Life Prediction for High Temperature Gas Turbine Materials, 1985.

4. Harris, J. A., "Engine Component Retirement For Cause: Volume I - Executive Summary", AFWAL-TR-87-4069, Wright-Patterson AFB OH, 1987.

5. Military Standard: Engine Structural Integrity Program, MIL-STD-1783 (USAF) 30 November, 1984.

6. Heil M.L., Crack Growth in Alloy 718 Under Thermal-Mechanical Cycling, PhD Dissertaion, AFIT, Wright-Patterson AFB OH, 1986.

7. Bill R.C., "Micromechanisms of Thermomechanical Fatigue - A Comparison with Isothermal Fatigue", NASA Technical Memorandum 87331, 1986.

8. Nicholas T., Heil M.L., and Haritos, G.K. "Predicting Crack Growth Under Thermo-Mechanical Cycling" International Journal of Fracture, Vol 41, 1989, pp 157-176.

9. Annis, C.G., Wallice, R.M., and Sims, D.L., "An Interpolative Model for Elevated Temperature Fatigue Crack Propagation", AFML-TR-76-176 Part I, Wright-Patterson AFB OH, 1976.

10. Wallice, R.M., Annis, C.G., and Sims, D.L., "Application of Fracture Mechanics at Elevated Temperatures", AFML-TR-76-176 Part II, Wright- Patterson AFB OH, 1977.

11. Nicholas T., Weerasooriya, T., and Ashbaugh, N.E., "A Model for Creep/ Fatigue Interactions in Alloy 718" ASTM STP 868, 1985, pp 167-180.

12. Nicholas T. and Weerasooriya, T. "Hold-Time Effects in Elevated Temperature Fatigue Crack Propagation", ASTM STP 905, 1986, pp 155-168.

13. Jordan, E.H. and Meyers, G.J., "Fracture Mechanics Applied to Nonisothermal Fatigue Crack Growth", Engineering Fracture Mechanics, Vol 23, No 2, 1986, pp 345-358.

14. Haritos, G.K., Miller, D.L., and Nicholas T.,"Sustained-Load Crack-Growth in Inconel 718 Under Nonisothermal Conditions", Journal of Engineering Materials and Technology, Vol 107, 1985, pp 172-179.

15. Heil, M.L., Nicholas, T., Haritos, G.K., "Crack Growth in Alloy 718 under Thermal-Mechanical Cycling", PVP Vol 123, 1987, pp 23-29.

16. Kerans, R.J., "Deformation in Ti Al Fatigued at Room and Elevated Temperatures", Metallurgical Transactions A, Vol 15A, Sep 1984, pp 1721-1729.

17. DeLuca, D.P., Cowles, B.A., Haake, F.K., and Holland, K.P., "Fatigue and Fracture of Titanium Aluminides", WRDC-TR-4136, Wright-Patterson AFB OH, 1990.

18. Lipsitt, H.A., "Titanium Aluminides-An Overview", Materials Research Society Symposium Proceedings, Vol 39, 1985.

19. Venkataraman, S., "Elevated Temperature Crack Growth Studies of Advanced Titanium Aluminides", AFWAL-TR-87-4103, Wright-Patterson AFB OH, 1987.

20. Balsone, S.J., "The Effect of Elevated Temperature Exposure on the Tensile and Creep Properties of Ti-24Al-11Nb", Proceedings of the Workshop on the Oxidation of High-Temperature Intermetallics held in Cleveland, OH, September, 1988, pp 22-23.

21. Mall, S., Staubs, E.A., and Nicholas, T., "Investigation of Creep/Fatigue Interaction on Crack Growth in a Titanium Aluminide Alloy", Journal of Engineering Materials and Technology, 1989, Vol 112, pp 435-441.

22. Spera, D.A., "What is Thermal Fatigue", ASTM STP 612, 1976, pp 3-9.

23. Broek D., Elementary Engineering Fracture Mechanics, Martinus Nijhoff Publishers, Dordrecht, 1986.

24. Lloyd G.J., "High Temperature Fatigue and Creep-Fatigue Propagation: Mechanisms, Mechanisms and Observed Behaviour in Structural Materials", Fatigue at High Temperatures, Applied Science Publisheres, NY, 1983.

25. Riedel H., Fracture at High Temperature, Springer-Verlag, Berlin 1987.

292

26. Sadananda, K. and Shahinian, P., "Application of Fracture Mechanics Techniques to High Temperature Crack Growth", Fracture Mechanics, University Press of Virginia, 1978, pp 159-168.

27. Sadananda, K. and Shahinian, P., "Application of Fracture Mechanics Techniques to High Temperature Crack Growth", Fracture Mechanics, University Press of Virginia, 1978, pp 685-703.

28. Sadananda, K. and Shahinian, P., "The Effect of Environment on the Creep Crack Growth Behavior of Several Structural Alloys", Materials Science and Engineering, Vol 43, 1980, pp 159-168.

29. Wareing, J., Tomkins, B., and Bretherton, I., Flow and Fracture at Elevated Temperatures, Raj, R. Ed., American Society for Metals, 1985, pp 251-278.

30. Sadananda, K. and Shahinian, P., "Review of the Fracture Mechanics Approach to Creep Crack Growth in Structural Alloys", Engineering Fracture Mechanics, Vol 3-4, 1981, pp 327-342.

31. Sadananda, K. "Theoretical Aspects of Fatigue and Creep Crack Growth", Advances in Fracture Mechanics, Proceedings of the 6th International Conference on Fracture, New Deli, India, 4-10 December 1984, pp 211-234.

32. Fine, M.E. and Wetterman, J.R.,"MicrostructuralEffects on Creep and Fatigue", Time Dependent Fracture, Krausz, A.S., Ed., 1985.

33. Riedel H., "Creep Crack Growth", Flow and Fracture at Elevated Temperatures, ASM, 1983.

34. Leckie, F.A., "The Micro- and Macromechanics of Creep Rupture", Engineering Fracture Mechanics, Vol 25, Nos 5-6, 1986, pp 505-521.

35. Ashby, M. F. and Dyson, B. F., "Creep Damage Mechanics and Micromechanisms", Advances in Fracture Mechanics, Proceedings of the 6th International Conference on Fracture, New Deli, India, 4-10 December 1984, pp 3-30.

36. Taplin, D.M.R., Tang, N.Y., and Leipholz, H.H.E., "On Fatigue-Creep-Environment Interaction and the Feasibility of Fatigue Maps", Advances in Fracture Mechanics, Proceedings of the 6th International Conference on Fracture, New Deli, India, 4-10 December 1984, pp 127-142.

293

37. Tien J.K. et al., "Creep-Fatigue Interaction in Structural Alloys", Flow and Fracture at Elevated Temperatures, ASM, 1983.

38. Raj R., "Mechanisms of Creep-Fatigue Interaction", Flow and Fracture at Elevated Temperatures, ASM, 1983.

39. VanStone, Gooden, and Krueger, "Advanced Cumulative Damage Modeling", AFWAL-TR-88-4146, Wright-Patterson AFB OH, 1988.

40. Weerasooriya, "Effect of Frequency on Fatigue Crack Growth Rate of Inconel 718 at High Temperatures", AFWAL-TR-87-4038, 1986.

41. Pedron, J.P. and Pineau, A., "The Effect of Microstructure and Environment and Environment on the Crack Growth Behavior of Inconel 718 Alloy at 650°C Under Fatigue, Creep and Combined Loading", Materials Science and Engineering, Vol 56, 1982, pp 143-156.

42. Saxena, A. and Bassani, J.L., "Time-Dependent Fatigue Crack Growth Behavior at Elevated Temperatures" ,Fracture: Interactions of Microstructure, Mechanisms and Mechanics, from Proceedings of the sysmposium sponsered by the Mechanical Metallurgical and Structural Materials Committees of the Metallurgical Society of AIME and teh Flow and Fracture Committee of the American Society for Metals, 27-29 Feb 1984, eds Wells, ,J.M. and Landes, J.D., pp 357-383.

43. Larsen J.M. and Nicholas T., "Cumulative Damage Modeling of Fatigue Crack Growth", paper presented at the Propulsion and Energetics Panel on Engine Cyclic Durability, 1984.

44. Rau C.A., Gemma, A.E., and Leverant, G.R., "Thermal-Mechanical Fatigue Crack Propagation in Nickel- and Cobalt-Base Superalloys Under Various Strain-Temperature Cycles", ASTM STP 520, 1973, pp 166-178.

45. Gemma, A.E., Langer, B.S., and Leverant, G.R., "Thermomechanical Fatigue Crack Propagation in an Anisotropic (Directionally Solidified) Nickel-Base Superalloy", Thermal Fatigue of Materials and Components, ASTM STP 612, 1976, pp 199-213.

46. Marchand N.J. and Pelloux, R.M., "A Computerized Test System for Thermal-Mechanical Fatigue Crack Growth", Journal of Testing and Evaluation, Vol 14, No 6, Nov 1986, pp 303-311.

47. Marchand N.J., Pelloux, R.M., and Ilschner, B. "Non-Isothermal Fatigue Crack Growth in Hastelloy-X", Fatigue and Fracture of Engineering Materials and Structures, Vol 10, No 1, 1987, pp 59-74.

48. Marchand N.J., Pelloux, R.M., and Ilscher, B. "A Fracture Mechanics Criterion For Thermal-Mechanical Fatigue Crack Growth of Gas Gas Turbine Materials", Engineering Fracture Mechanics, Vol 31, No 3, 1988, pp 535-551.

49. Harris, D.O., "Stress Intensity Factors for Hollow Circumferentially Notched Round Bars", Journal of Basic Engineering, March 1967, pp 49-54.

50. Gemma A.E. et al., "The Effect of Stress Dwells and Varying Mean Strain on Crack Growth During Thermal Mechanical Fatigue", Journal of Testing and Evaluation, Vol 4, 1981, pp 209-215.

51. Marchand N.J. and Pelloux, R.M., "Thermal-Mechanical Fatigue Crack Growth in Inconel X-750", Time-Dependent Fracture, Proceedings from the 11'th Canadian Fracture Conference, Ottawa, Canada, June 1984, ed Krausz, A.S., Nijhoff Publishers, 1985, pp 167-178.

52. Deluca, D.P. and Cowles, B.A., "Fatigue and Fracture of Advanced Blade Materials", AFWAL-TR-84-4167, Wright-Patterson AFB OH, 1985.

53. Wilson D.A. and Warren J.R., "Thermal Mechanical Fatigue Crack Growth", AFWAL-TR-84-4185, Wright-Patterson AFB OH, 1985.

54. Pernot, J.J., Thermal-Mechanical Fatigue Testing of a Titanium-Aluminum Alloy, Master Thesis, AFIT, Wright-Patterson AFB OH, 1987.

55. Burgess, D.G., Crack Growth of a Titanium-Aluminide Alloy under Thermal-Mechanical Fatigue, Master Thesis, AFIT, 1988.

56. Marchand, N., Parks, D.M., and Pelloux, R.M., "K Solutions for Single Edge Notch Specimens under Fixed End Displacements", International Journal of Fracture, Vol 31, 1986, pp 53-65.

57. Paris, P.C., The Growth of Fatigue Cracks Due to Variations in Load, Ph.D. Thesis, Lehigh University, 1962.

58. Broek, D. and Schijve, J., "The Influence of the Mean Stress on the Propagation of Fatigue Cracks in Aluminum Alloy Sheets", Nat. Aerospace Inst. Amsterdam TR-M-2111, 1963.

59. Erdogan, F., Crack Propagation Theories, NASA-CR-901, 1967.

60. Walker, E.K., "Effects of Environments and Complex Load History on Fatigue Life", ASTM STP 462, 1970, pp 1-14.

61. Forman, K.G., Kearney, V.E., and Engle, R.M., "Numerical Analysis of Crack Propagation in a Cyclic-Loaded Structure", Journal of Basic Engineering, Vol 89D, 1967, p 459.

62. Larsen, J.M., Schwartz, B.J., and Annis, C.G., "Cummulative Damage Fracture Mechanics Under Engine Spectra", AFML-TR-79-4159, Wright-Patterson AFB OH, 1980.

63. Sims, D.L., Annis, C.G., and Wallace, R.M., "Cummulative Damage Fracture Mechanics at Elevated Temperatures", AFML-TR-76-176, Part III, Wright-Patterson AFB OH, 1976.

64. Utah, D.A., "Crack Growth Modeling in an Advanced Powder Metallurgy Alloy", AFWAL-TR-80-4098, Wright-Patterson AFB OH, 1980.

65. Wei, R.P. and Landes, J.D., "Correlation Between Sustained-Load and Fatigue Crack Growth in High-Strength Steels", Materials Research and Standards, Vol 25, No 7, July 1969, pp 25-28.

66. Kim, Y.H. and Manning, S.D., "A Superposition Model for Corrosion-Fatigue Crack Propagation in Aluminum Alloys, Fracture Mechanics 14'th Symposium Vol 1 Theory and Analysis, ASTM STP 791, 1983, pp I-446 - I-462.

67. Gabetta, Rinaldi, and Pozzi, "A Model For Environmentally Assisted Crack Growth Rate", Environmentally Assisted Cracking: Science and Engineering, ASTM STP 1049, 1990, pp 266-282.

68. Winstone, M.R., Nikbin, K.M., and Webster, G.A., "Modes of Failure Under Creep/Fatigue Loading of a Nickel-Based Superalloy, Journal of Materials Science, Vol 20, 1985, pp 2471-2476.

69. Dimopulos, V., Nikbin, K.M., and Webster, G.A., "Influence of Cyclic to Mean Load Ratio on Creep/Fatigue Crack Growth", Metallurgical Transactions A, Vol 19A, April 1988, pp 873-880.

70. Nicholas T. and Weerasooriya, T. "Hold-Time Effects in Elevated Temperature Fatigue Crack Propagation", ASTM STP 905, 1986, pp 155-168.

71. Nicholas T., Weerasooriya, T., and Ashbaugh, N.E., "A Model for Creep/Fatigue Interactions in Alloy 718", Fracture Mechanics: Sixteenth Symposium, ASTM STP 868, 1985, pp 167-180.

72. Plumtree, A. and Nai-yong Tang, "Effect of Hold-Time damage on High temperature Behavior", Fatigue Fract. Engng Mater. Struct., Vol 12, No 5, 1989, pp 377-386.

73. Haritos, G.K., Miller, D.L., and Nicholas T.,"Sustained-Load Crack-Growth in Inconel 718 Under Nonisothermal Conditions", Journal of Engineering Materials and Technology, Vol 107, 1985, 172-179.

74. Heil M.L. et al., "Crack Growth in Alloy 718 under Thermal-Mechanical Cycling", ASME PVP Vol 123, 1987, pp 23-29.

75. Harmon, D.M, Saff, C.R., and Burns, J.G., "Thermomechanical fatigue Analysis for Monolithic materials", Elevated Temperature Crack Growth, ASME MD-Vol 18, 1990, pp 37-51.

76. Larsen, J.M., An Investigation of the Shape and Extent of Crack Tip Plastic Zones in Fatigue Crack Propagation and the Role of the Overload Plastic Zone in Retardation, Master Thesis, Vaderbilt University, 1977.

77. Hertzberg, Deformation and Fracture Mechanics of Engineering Materials, John Wiley & Sons, New York, 1976.

78. Wheeler, O.E., "Spectrum Loading and Crack Growth", Journal of Basic Engineering, March 1972, pp 181-186.

79. Willenborg, J.,Engle, R.M., and Wood, H.A., A Crack Growth Retardation Model Using an Effective Stress Concept, TM-71-1-FBR, AFFDL, Wright-Patterson AFB OH, Jan 1987.

80. Elber W., "Fatigue Crack Closure Under Cyclic Tension", Engineering Fracture Mechanics, Vol 2, 1970, 37-45.

81. Elber W., "The Significance of Fatigue Crack Closure", Damage Tolerance in Aircraft Structures, ASTM STP 486, 1971, pp 230-242.

82. Schijve, J., "Some Formulas for the Crack Opening Stress Level", Engineering Fracture Mechanics, Vol 14, 1981, pp 461-465.

83. Sehitoglu, "Characterization of Crack Closure:, Fracture Mechanics: Sixteen Symposium, ASTM STP 868, 1985, pp 361-380.

84. Newman, J.C. and Elber, W., "Summary", Mechanics of Fatigue Crack Closure, ASTM STP 982, 1988, pp 637-644.

85. McEvily, A.J., "On Crack Closure in Fatigue Crack Growth, Mechanics of Fatigue Crack Closure, ASTM STP 982, 1988, pp 35-43.

86. Hudson, C.M. and Hardrath, H.F., "Effects of Changing Stress Amplitude on the Rate of Fatigue Crack Propagation of Two Aluminium Alloys", NASA Technical Note D-960, Sept 1961.

87. Christensen, Metal Fatigue, McGraw-Hill, 1959, pp 376-412.

88. Von Euw, E.F.J., Hertzberg, R.W., and Roberts, R., "Delay Effects in Fatigue Crack Propagtion", Stress Analysis and Growth of Cracks, Proceedings of the 1971 National Symposium on Fracture Mechanics, Part I, ASTM STP 513, 1972, pp 230-259.

89. Mall, S., Nicholas, T., Burgess, D.G., and Pernot, J.J., "Crack Growth in a Titanium Aluminide Alloy Under Thermal Mechnical Cycling", Fatigue and Fracture of Engineering Materials and Structures, Vol 14, No 1, 1991, pp 79-87.

90. Lipsitt, H.A., Shechtman, D., Schafrik, R.E., "The Deformation and Fracture of Ti_3Al at Elevated Temperatures", Metallurgical Transactions A, Vol 11A, 1980, p 1369.

91. Sastry, S.M.L. and Lipsitt, H.A., "Fatigue Deformation of TiAl Base Alloys", Metallurgical Transactions A, Vol 8A, 1977, p 299.

92. Sastry, S.M.L. and Lipsitt, H.A., "Ordering Transformations and Mechanical Properties of Ti_3Al and Ti_3Al-Nb Alloys", Metallurgical Transactions A, Vol 8A, 1977, pp 1543-1552.

93. Mendiratta, M.G. and Lipsitt, H.A., "Steady-State Creep Behavior of Ti_3Al-Base Intermetallics", Journal of Material Science and Engineering, Vol 15, 1980, p 2985.

94. Shade, J.L., Preliminary Material Properties of Titanium Aluminides, Air Force Propulsion Laboratory, Wright-Patterson AFB OH, 1985.

95. Avner, S.H., Introduction to Physical Metallurgy, McGraw-Hill Book Company, New York, 1974.

96. Van Vlack, L.H., Elements of Materials Science and Engineering, Addison-Wesley Publishing Company, Reading Massachusetts, 1980.

97. "Standard Test Methoc for Measurement of Fatigue Crack Growth Rates", ASTM E 647, 1991.

98. Model 5305 Parabolic Strip Heater Rev B. Research Inc., Minneapolis MN, December 1985, pp 3.1-3.2

99. Johnson H.H., "Calibrating the Electric Potential Method for Studying Slow Crack Growth", Materials Research and Standards, Vol 5, No 9, 1965, pp 442-445.

100. Richie R.O., Garret G.G., and Knott, J.F. International Journal of Fracture Mechanics, 1971, pp 462-467

101. Halliday M.D. and Beevers, C.J., "The d.c. Electrical Potential Method for Crack Length Measurement", The Measurement of Crack Length and Shape During Fatigue, 1980, pp 85-112.

102. VanStone R.H. and Richardson T.L., "Potenti. l-Drop Monitoring of Cracks in Surface-Flawed Specimens", Automated Test Methods for Fracture and Fatigue Crack Growth, ASTM STP 877, 1985, pp 148-166.

103. Romilly, D.P., "Development of the D.C. Potential Drop Method for One- and Two-Directional Crack Growth Monitoring", Experimental Techniques, 1990, pp 22-28.

104. Hartman, G.A. and Johnson, D.A., "D-C Electric-Potential Method Applied to Thermal/Mechanical Fatigue Crack Growth", Experimental Mechanics, 1987, pp 106-112.

105. Richie, R.O. and Bathe, K.J. "On the Calibration of the Electrical Potential Technique for Monitoring Crack Growth Using Finite Element methods", International Journal of Fracture, Vol 15, No 1, 1979, pp 47-55.

106. Hicks, M.A. and Pickard A.C., "A Comparison of Theoretical and Experimental Methods of Calibrating the Electrical Poterntial Drop Technique for Crack Length Determination", International Journal of Fracture, 20, 1982, pp 91-101.

107. Catlin, W.R., Lord, D.C., Prater, T.A., and Coffin L.F., "The Reversing D-C Electrical Potential Method", Automated Test Methods for Fracture and Fatigue Crack Growth, ASTM STP 877, 1985, pp 67-85.

108. Ritchie, R.O., Garrett, G.G., and Knott, J.F., " Crack-Growth Monitoring: Optimisation of the Electrical Potential Technique using an Analogue Method", International Journal of Fracture, No 7, 1971, pp 462-467.

109. Knott, 'The Use of Analogue and Mapping Techniques with Particular Reference to Detection of Short Cracks", The Measurement of Crack Length and Shape During Fracture and Fatigue, 1980, pp 113-135.

110. University of Dayton Research Institute, Mate and Mate Modules Users Manuals - Version 2.22A Crack Growth Analysis and Test Environment, The University of Dayton, 300 College Park Drive, Dayton, OH 45469.

111. Wei, R.P. and Brazill, R.L. "An Assessment of A-C and D-C Potential Systems for Monitoring Fatigue Crack Growth", Fatigue Crack Growth Measurement and Data Analysis, ASTM STP 738, 1981, pp 103-119.

112. Larsen, J.M., "An Automated Photomicroscopic System for Monitoring the Growth of Small fatigue Cracks", Fracture Mechanics: Seventeenth Volume, ASTM STP 905, 1986, pp 226-238.

113. Larsen, J.M., Jira, J.R., and Ravichandran, K.S., "Measurement of Small Cracks by Photomicroscopy: Experiments and Analysis", Small-Crack Test Methods, ASTM STP 1149, to be published.

114. Staubs, Master Thesis, AFIT, Wright-Patterson AFB OH, 1988.

115. Balsone, S.J., Maxwell, D.C., Khobaib, M., and Nicholas, T., "Frequency Temperature, and Environmental Effects on Fatigue Crack Growth in Ti_3Al", Fatigue 90, Vol II, pp 1173-1178.

116. Parida, B.K. and Nicholas, T., "Growth of Fatigue Cracks Emanating from Notches in Titanium Aluminide", Proceedings from Joint FEFG/ICF International Conference on Fracture of Engineering materials and Structures, Singapore, 6-8 August 1991, pp 685-690.

117. Parida, B.K. and Nicholas, T., "Frequency and Hold-Time Effects on Crack Growth of Ti-24Al-11Nb at High Temperature", Proceedings from International Conference on High-Temperature Aluminides and Intermetallics, San Diego, CA, 16-19 September 1991.

118. Floreen, S. and Kane, R.H., Fatigue of Engineering Materials Materials and Structures, Vol 2, 1980, 401-412.

119. Weerasooriya, "Effect of Frequency on Fatigue Crack Growth Rate of Inconel 718 at High Temperature", Fracture Mechanics: Nineteenth Symposium, ASTM STP 969, 1988, pp 907-923.

120. James, L.A., "Stress Analysis and Growth of Cracks", Stress Analysis and Growth of Cracks, Proceedings of the 1971 National Symposium on Fracture Mechanics, Part I, ASTM STP 513, pp 218-229.

121. James L.A., "The Effect of Grain Size Upon the Fatigue-Crack Propagation Behavior of Alloy 718 Under Hold-Time Cycling at Elevated Temperatures", Engineering Fracture Mechanics, Vol 25, 1986, pp 305-314.

122. Shahinian, P. and Sadananda, K., "Crack Growth Behavior Under Creep-Fatigue Conditions in Alloy 718", 1976 ASME-MPC Symposium on Creep Fatigue Interaction, 1970, pp 365-390.

123. Smith H.H., Kullen, P.S., Michel, D.J., "Fatigue Crack Propagation Behavior of Titanium Alloys 6242S and 5621S at Elevated Temperature", Metallurgical Transactions A, Vol 19A, 1988, pp 881-885.

124. Eylon, D. and Hall, J.A., "Fatigue Behavior od Beta Processed Titanium Alloy IMI 685", Metallurgical Transactions A, Vol 8A, 1977, pp 981-990.

125. Evans, W.J. and Gostelow, C.R., "The Effect of Hold Time on the Fatigue Properties of a β-Processed Titanium Alloy", Metallurgical Transactions A, Vol 10A, 1979, pp 1837-1846.

126. Ruppen, J.A. and McEvily, A.J., "The Effect of Elevated Temperature and Environment on the Fatigue Crack Growth Characteristics of Ti-6Al-2Sn-4Zr-2Mo-0.1Si", Fatigue of Engineering Materials and Structures, Vol 2, pp 63-72.

127. Rogers, P.T. and Nicholas, T., "Micro-Mechanics of Crack Growth in Inconel 718 Under Thermo-Mechanical Fatigue", Presented at the TMS/AIME Annual Meeting, Phoenix, AZ., Jan. 1988.

128. Nicholas, T. and Mall, S., "Elevated Temperature Crack Growth in Aircracft Engine Materials", Advances in Fatigue Lifetime Predictive Techniques, ASTM STP XXX, to be published.

129. Nicholas, T., "Fatigue Crack Growth Modeling at Elevated Temperature Using Fracture Mechanics", <u>Elevated Temperature Crack Growth</u>, ASME MD-Vol 18, 1990, pp 107-112.

130. Coles, A., Johnson, R.E., and Popp, H.G., <u>Journal of Engineering Mat. Tech.</u>, 98, 1976, pp 305-315.

131. Painter, G.O., <u>Evaluation of Interpolative Modeling Concepts for Fatigue Crack Growth at Elevated Temperatures</u>, MS Thesis, AFIT, Wright-Patterson AFB OH, December 1984.

132. Burden, R.L. and Faires, J.D., <u>Numerical Analysis</u>, PWS Publishers, Boston, 1985.

Vita

Captain John J. Pernot was born on 23 June 1963 in Pittston Pennsylvania. He graduated from high school in Pittston Pennsylvania in 1981, and attended the Pennsylvania State University. He graduated in May 1986 with a Bachelor of Science in Mechanical Engineering and was commissioned in the USAF. He attended the Air Force Institute of Technology and graduated with a Master of Science in Aeronautical Engineering. In December 1987 he entered the School of Engineering, Air Force Institute of Technology.

Permanent Address: 115 Hillcrest Drive

Duryea, PA 18642

REPORT DOCUMENTATION PAGE

Public reporting burden for this collection of information is estimated to average 1 hour per response, including the time for reviewing instructions, searching existing data sources, gathering and maintaining the data needed, and completing and reviewing the collection of information. Send comments regarding this burden estimate or any other aspect of this collection of information, including suggestions for reducing this burden, to Washington Headquarters Services, Directorate for Information Operations and Reports, 1215 Jefferson Davis Highway, Suite 1204, Arlington, VA 22202-4302, and to the Office of Management and Budget, Paperwork Reduction Project (0704-0188), Washington, DC 20503.

1. AGENCY USE ONLY (Leave blank)	2 REPORT DATE December 1991	3. REPORT TYPE AND DATES COVERED Doctoral Dissertation

4. TITLE AND SUBTITLE

Crack Growth Rate Modeling of a Titanium-Aluminide Alloy Under Thermal-Mechanical Cycling

5. FUNDING NUMBERS

6. AUTHOR(S)

John J. Pernot
Captain, USAF

7. PERFORMING ORGANIZATION NAME(S) AND ADDRESS(ES)

Air Force Institute of Technology
WPAFB OH 45433-6583

8. PERFORMING ORGANIZATION REPORT NUMBER

AFIT/DS/AA/91-3

9. SPONSORING/MONITORING AGENCY NAME(S) AND ADDRESS(ES)

10. SPONSORING/MONITORING AGENCY REPORT NUMBER

11. SUPPLEMENTARY NOTES

12a. DISTRIBUTION/AVAILABILITY STATEMENT

Approved for Public Release; Distribution Unlimited

12b. DISTRIBUTION CODE

13. ABSTRACT (Maximum 200 words)

In this study, a model is developed to predict crack growth rates in a titanium-aluminide alloy under thermal-mechanical fatigue (TMF). This TMF crack growth rate prediction model, which requires only isothermal data to define its parameters, is distinguished from earlier models in two ways. First, it accounts for mechanical-fatigue and environmental crack growth rate contributions while it also considers a retardation mechanism thought to be caused by creep blunting of the crack tip. This is the first study to account for such a retardation mechanism during TMF. The second uniqueness of the model is that its general form can account for cycle-dependent crack growth rate contributions that are temperature dependent.

In addition, a series of isothermal-fatigue and hold-time tests are performed to generate the data base required for model parameters, and TMF tests are used to validate the modeling technique. The model predicts in-phase, as well as 180° and 270° out-of-phase crack growth rates extremely well, and underpredicts the 90° out-of-phase crack growth rates by a factor of two. Two other, more complex TMF cycles are studied, and the predicted crack growth rates correlate well with the experimental data.

14. SUBJECT TERMS

Thermal-Mechanical Fatigue, Thermal Fatigue, Crack Propagation Fatigue, Crack Growth Rates, Life Prediction, Damage Modeling

15. NUMBER OF PAGES

318

16. PRICE CODE

17. SECURITY CLASSIFICATION OF REPORT	18. SECURITY CLASSIFICATION OF THIS PAGE	19. SECURITY CLASSIFICATION OF ABSTRACT	20. LIMITATION OF ABSTRACT
Unclassified	Unclassified	Unclassified	UL